Characterising the iron dependence of T-cells

Megan Rhonwen Teh

Thesis submitted for the degree of

Doctor of Philosophy

Supervised by Professor Hal Drakesmith

Co-Supervised by Professor Susanna Dunachie and Dr. Andrew Armitage

Radcliffe Department of Medicine

University of Oxford

2023

Abstract

Iron is an essential micronutrient which interacts with ~400 different protein types in human cells. Meanwhile, iron deficiency remains globally prevalent affecting >1.2 billion people. Pre-clinical studies demonstrate that iron restriction impairs T-cell proliferation, activation and effector function in models of vaccination, autoimmunity and infection. However, the biochemical mechanisms underlying these effects remain undefined. In this thesis, *in silico*, *in vitro* and *in vivo* methods were used to examine T-cell iron usage and dependence. Initial mathematical modelling predicted T-cells dramatically increase iron demands post-activation. Further transcriptomic and proteomic profiling of *in vitro* activated iron deficient CD8+ T-cells revealed induction of the P53 cell cycle arrest pathway and suppression of mTORC1 and MYC signalling, together indicative of aberrant metabolic rewiring. Iron deprived CD8+ T-cells show increased mROS generation suggestive of electron transport chain dysfunction, and impaired tricarboxylic acid (TCA) cycle progression through the iron dependent enzymes aconitase 2 and succinate dehydrogenase, such that downstream metabolites α-ketoglutarate, fumarate and malate are depleted. The repressive histone mark H3K27me3 is normally removed by the iron and α-ketoglutarate dependent enzymes, KDM6A/B, but accumulates in iron deprived T-cells. Despite TCA cycle dysfunction, aspartate, which is produced downstream of the TCA cycle, was unexpectedly increased in iron restriction. Higher aspartate is proposed to be partly driven by suppressed aspartate usage by downstream iron-dependent pathways including translation and nucleotide synthesis. Interestingly, exogenous aspartate substantially rescues the proliferation of iron deprived CD8+ T-cells suggesting that endogenous aspartate sources are unusable, possibly due to trapping of aspartate within the mitochondria. Overall, this thesis demonstrates that iron deprivation impairs T-cell biochemistry at multiple nodes providing insight as to how metabolic and iron modulatory interventions could be coupled to augment or suppress immunity.

Contents for the Casual Connoisseur

The phrase “you are what you eat” correctly reflects the fact that humans are constructed from the food they consume. The proteins, sugars and fats we eat, provide the raw materials necessary to produce the cells of our bodies. Meanwhile, micronutrients including iron are only required in small amounts but are pivotal for health. While iron can be acquired from foods such as red meat, beans and green vegetables, >1.2 billion people are still iron deficient worldwide. Iron deficiency is well understood to cause anaemia, a condition where your red blood cells are unable to carry enough oxygen around the body resulting in symptoms such as fatigue. However, emerging research has begun to show that iron deficiency may also impair T-cells, a cell type important for fighting cancer and infections such as the flu. How iron deficiency negatively affects T-cells is not well understood but this thesis aims to address this.

Cells, including T-cells, are essentially little factories featuring a network of reactions similar to factory production lines. The proteins, sugars and fats from our diets enter the production line and are used to eventually generate energy and to build the equipment necessary for cells to replicate and do their jobs. For instance, T-cells respond to cancers or infections by activating, multiplying and producing molecules such as perforins which kill cancer cells or virally-infected cells by punching holes in their surface. In this thesis, we predict that T-cells need increased amounts of iron during activation and that iron deficiency causes blocks in certain production lines which require this iron. These blockages result in deficits of certain products and excess of others, preventing cells from dividing and functioning properly. Unfortunately, these breaks also cause the production of toxic molecules, not unlike the smoke which might occur if an engine breaks down, which can cause further damage. Moreover, the cell attempts (albeit unsuccessfully) to compensate for broken production lines by using alternative reactions to produce the same products. Notably, we discover that by supplementing iron deficient cells with the nutrient aspartate (originally isolated from asparagus), we can partially rescue T-cell function. By understanding iron deficiency at the cellular level, we hope to better appreciate how we can boost immunity in iron deficient patients to better combat diseases such as infection and cancer.

Natural history of an iron atom*

- *Megan Teh*

This story is quite elementary,
For iron is most necessary,
By this atom though small in size,
Life in fact is catalysed

Consumption of a ferric source,
(Beans or steak for your main course),
Sends iron on its merry way,
To help you live another day

Inside your duodenal intestine,
Iron uptake by absorption,
Moves this elemental species,
Into you and not your faeces,
Once inside an enterocyte,
Iron pauses or takes flight,
Ferroportin mediated,
To serum, iron is liberated

Another quarry to be mined,
Are red blood cells that have died,
These rotund red corpuscles,
Parcels packed with rusty metals,
Swallowed whole by macrophages,
Releasing iron from heme cages,
Thence once again, through ferroportin,
Iron to blood, is transported

From blood, transferrin tries to chelate,
Iron from its sanguineous state,
This union is most essential,
For free iron is detrimental,
Since microbes of many a kind,
Like us, for ferric ions pine,
From bids to steal the host supply,
Transferrin acts to fortify

When pathogens do invade,
And undertake an iron raid,
Another mode of self-defence,
In the liver does commence,
Hepatic hepcidin is produced,
To keep serum iron running loose,
To ferroportin it does bind,
Blocks iron export, locks ions inside

Transferrin with its iron crown,
Will quick become receptor bound,
Intake via endosome,
Brings iron to its brand new home,
Surplus stored in ferritin vaults,
In case external supply ever halts,
The rest dependant on each cell's needs,
To different pathways it does feed

For what is iron used, you ask?
Well, it's put to work at many a task,
Red cell hemoglobin claims two thirds,
And like a shepherd tries to herd,
Oxygen with all its might,
Through blood to every tissue site,
The rest is used by other cells,
In both cytosol and organelles

ONE – In DNA synthesis it plays a role,
In primases and DNA pols,
TWO – Mitochondrial metabolism,
(But try to avoid toxic oxygen radicalism),
THREE – Epigenetic regulation,
For histone and DNA demethylation,
FOUR – other roles are rather muddy,
And definitely warrants further study

In short, I hope you've come to see,
Via this peculiar poetry,
The importance of this element,
Deems work on it, time well spent

*Published as Teh, 2022, American Journal of Hematology (DOI: 10.1002/ajh.26678)

Statement of authorship

The majority of the work presented in this thesis has been completed by me, Megan Teh, under the guidance of Professor Hal Drakesmith. It should be noted that some figures and text in this thesis were previously published in either Teh *et al*, Frontiers of Immunology, 2021 (DOI: 10.3389/fimmu.2021.714613) or Frost *et al*, Science Advances, 2022 (DOI: 10.1126/sciadv.abq5384). Only sections of these publications where I was directly involved in data collection, analysis and writing are included and these sections are clearly indicated. Collaborative work has been included where experiments were jointly designed, conducted or analysed and these are also clearly indicated in the thesis. This thesis has not been submitted in part or as a whole for any other university degree at the University of Oxford or elsewhere.

Megan Teh

30/08/2023

Funding statement

This work was supported by the Clarendon Fund and the Corpus Christi College A. E. Haigh graduate scholarship to Megan Teh and the UK Medical Research Council (MRC Human Immunology Unit core funding to Hal Drakesmith, award no. MC_UU_12010/10).

Acknowledgements

It has been an absolute pleasure completing my PhD and that has in great part been due to the people who have supported me along the way. A massive thank you to:

The past and present members of the Drakesmith lab who listened to countless lab meetings, provided valuable feedback, shared their scientific expertise and were supportive from start to finish. However, a particular thank you to Joe Frost whose work provided the foundation for this project and whom along with Andrew Armitage have provided immense amounts of training, guidance and scientific conversations.

My collaborators, Linda Sinclair at the University of Dundee who provided valuable proteomics expertise and completed the protein-MS on our behalf. Sarah Dimeloe at the University of Birmingham who shared her general knowledge of T-cell immunometabolism, helped us with metabolite-MS and provided valuable career mentorship. Nancy Gudgeon, Jennie Roberts and Bryan Marzullo at the University of Birmingham who processed and ran the metabolite-MS samples. Barbara Kronsteiner-Dobramysl at the Peter Medawar Building for Pathogen Research who helped us with Seahorse assays and provided general thoughts on immunometabolism. Jan Rehwinkel at the MRC Weatherall Institute of Molecular Medicine who suggested and provided the SAMHD1-KO mouse model.

Susie Dunachie, Tom Milne, Katja Simon, Dan Tennant, David Hodson, Alex Clarke, Ana-Victoria Lechuga Vieco, and Sumana Sharma who offered valuable insights which helped this project progress. The BMS staff, particularly Roo Bhasin, Jonathon Merrill and Amy Griffin who provided training and animal husbandry essential for this project.

My family, especially my parents and grandparents who supported me throughout this PhD and who have tried valiantly to understand my work from the very beginning. Jake Burton for his love and support and the many casual scientific conversations.

Finally, my supervisor Hal Drakesmith without whose guidance this project would not have been possible. I am incredibly grateful for the generous support, mentorship, resources and freedom Hal has provided which has allowed me to develop this project in the direction that has excited me the most and has helped me to grow as a scientist and find my niche within the scientific community.

Abbreviations

2-OG – 2-oxoglutarate
2-OGDD – 2-oxoglutarate dependent dioxygenase
ACO1 – aconitase 1 (cytosolic)
ACO2 – aconitase 2 (mitochondrial)
AGC – automatic gain control
ALA – 5-aminolevulinic acid
ALB – albumin
ALL – acute lymphoblastic leukaemia
APC – antigen presenting cell
apoTf – apotransferrin
ASNS – asparagine synthetase
ASPA – Animals (Scientific Procedures) Act
ASS – argininosuccinate synthase
BCR – B-cell receptor
BMDC – bone marrow derived dendritic cell
BME – β-mercaptoethanol
bp – base pair
CAR-T-cells – chimeric antigen receptor T-cells
cDNA – complementary DNA
CI – complex I
CII – complex II
CIII – complex III
CIV – complex IV
CLP – common lymphoid progenitor
CoQ10 – coenzyme Q10
COX – cyclooxygenase
CPX – ciclopirox olamine
CRC – colorectal carcinoma
CTL – cytotoxic lymphocyte
CTV – cell trace violet
CV – complex V
CYTOF – cytometry by time of flight
DAMP – damaged associated molecular pattern
DC – dendritic cell
DDA – data dependent acquisition
DepMap – cancer dependency map
DFO – deferoxamine
DFP – deferiprone
DFX – deferasirox
DIA – data independent acquisition
diTf – diferric transferrin
DMSO – dimethyl sulfoxide
EAE – experimental autoimmune encephalitis
ECAR – extracellular acidification rate
EPO – erythropoietin
ERFE – erythroferrone
ETC – electron transport chain
FAC – ferric ammonium citrate
FBS – fetal bovine serum
FDR – false discovery rate
Fe – iron
FECH – ferrochelatase
Fe-S – iron sulfur
FH – fumarate hydratase
FISH – fluorescence in situ hybridisation
FPN – ferroportin

GDH – glutamate dehydrogenase
GEO – gene expression omnibus
GO – gene ontology
GSEA – gene set enrichment analysis
H3K27me3 – histone 3 lysine 27 trimethylation
H3K4me3 – histone 3 lysine 4 trimethylation
holoTf – holotransferrin
HPX – hemopexin
HRI – heme regulated inhibitor
ICP-MS – inductively coupled plasma mass-spectrometry
IDH – isocitrate dehydrogenase
IFN – interferon
IMM – inner mitochondrial membrane
IRE – iron response element
IREB2 – iron response element binding protein 2
IRIDA – iron refractory iron deficiency anaemia
IRP – iron regulatory protein
ISG – interferon stimulated genes
KDM – lysine demethylase
KO – knockout
LIAS – lipoic acid synthase
LPS – lipopolysaccharide
LSEC – liver sinusoidal endothelial cells
metabolite-MS – metabolite mass-spectrometry
MFN1 – mitoferrin 1
MFN2 – mitoferrin 2
mHep – minihepcidin
mLN – mesenteric lymph node
monoTf – monoferric transferrin
MPO – myeloperoxidase
mROS – mitochondrial reactive oxygen species
MS – mass-spectrometry
mtDNA – mitochondrial DNA
NAC – N-acetyl-cysteine
nDNA – nuclear DNA
NES – normalised enrichment score
NK – natural killer
NOX – NADPH oxidase
NSAID – non-steroidal anti-inflammatory drug
NTBI – non-transferrin bound iron
$O_2^{\bullet-}$ - superoxide
OCR – oxygen consumption rate
OMM – outer mitochondrial membrane
OTC – ornithine transcarbamylase
OXPHOS – oxidative phosphorylation
PAMP – Pathogen associated molecular pattern
PBS – phosphate buffered saline
PC – pyruvate carboxylase
PCR – polymerase chain reaction
PDH – pyruvate dehydrogenase
Protein-MS – protein-mass spectrometry
PRR – pathogen recognition receptor
pS6 – phospho-S6
qPCR – quantitative PCR
RBC – red blood cell
Redox – reduction-oxidation

RNA-seq – RNA-sequencing
RNR – ribonucleotide reductase
RNS – reactive nitrogen species
ROS – reactive oxygen species
RPKM – reads per kilobase of transcript per million mapped reads
SAM – S-adenosylmethionine
SCENITH – single cell energetic metabolism by profiling translation inhibition
SC-ICP-MS – single cell inductively coupled plasma mass-spectrometry
Sc-RNA-seq – single cell RNA-sequencing
SDH – succinate dehydrogenase
SEM – standard error of the mean
SLE – systemic lupus erythematosus
TCA – tricarboxylic acid
TCR – T-cell receptor
Tf – transferrin
TFA – trifluoroacetic acid
Tfh – T follicular helper cell
TfR2 – transferrin receptor 2
TFRC – transferrin receptor
TIBC – total iron binding capacity
TPM – transcripts per million
Treg – T regulatory
Tristetraprolin – TTP
TSAT – transferrin saturation
UTR – untranslated region
α-KG – α-ketoglutarate
α-KGDH – α-ketoglutarate dehydrogenase

Table of contents

Chapter 1

1 Introduction

All life is constructed from atomic building blocks. Carbon along with hydrogen, phosphorous, nitrogen, sulfur and oxygen form the skeletons of biological molecules[1]. However, these backbones that form the carbohydrates, proteins, nucleic acids, and lipids of the body are also reliant on other elemental micronutrient co-factors including iron, zinc, manganese, copper, and molybdenum[1,2]. Crucially, iron is utilised by almost all known species with the exceptions of *Borrelia burgdorferi* and *Lactobacilli*[3-5] with roles ranging from structural to enzymatic[6]. Biological systems have co-opted iron due to its ability to transiently bind gaseous ligands and to efficiently catalyse reduction-oxidation (redox) reactions necessary for cellular function[7]. However, these same redox reactions can drive the production of toxic reactive oxygen species (ROS) via Fenton reactions[8]. Meanwhile, the universality of iron usage by organisms means iron can also drive pathogen growth during infection[9]. The duality of iron as both essential and detrimental has driven the tight regulation of iron in the body at both cellular and systemic levels[7].

Within mammals, approximately 70% of iron is used by red blood cell (RBC) hemoglobin to mediate oxygen transport to tissues[7,10]. Given the necessity of iron for RBC development, it is unsurprising that iron deficiency is commonly associated with anaemia and is in fact responsible for 1.2 billion cases of anaemia worldwide with prevalence of iron deficiency without anaemia being even higher[11]. While iron deficiency classically presents with anaemia and RBC defects such as hypochromia and microcytosis[12], the requirements of all mammalian cells for iron suggests that iron deficiency may have much broader impacts across body systems. Recent literature has begun to reveal a crucial role for iron in innate and adaptive immunity[13]. For instance, iron restriction impairs B and T-cell responses in pre-clinical models of immunisation, infection and autoimmunity[14-20]. While initial studies have suggested that iron scarcity may act via impairment of metabolism in adaptive immune cells[14,15,21,22], the biochemical mechanisms of iron mediated suppression of adaptive immunity is largely uncharacterised. Further, our understanding of how and when iron is used by immune

cells remains unclear. This thesis aims to identify how T-cells utilise iron during activation and to characterise how iron deficiency impacts diverse iron requiring processes including mitochondrial metabolism and chromatin remodelling. This introduction will first provide a foundation of our current understanding of iron regulation and usage before further discussing the role of iron in the immune system.

1.1 Iron homeostasis

1.1.1 Systemic iron regulation

Humans acquire approximately 1 mg of iron daily via intestinal absorption[9]. Simultaneously, an additional approximate 25 mg of iron a day are recycled by macrophages from phagocytosed senescent RBCs (Fig. 1.1)[23]. In both contexts, egress of iron into the bloodstream from intestinal enterocytes and macrophages occurs via the sole known iron exporter, ferroportin (SLC40A1)[24-27]. Once in the blood, serum iron is typically bound by chaperone proteins, especially transferrin, which prevent the acquisition of iron by pathogens that similarly require iron for their function and in consequence their virulence[9]. At homeostasis, blood transferrin saturation (TSAT), a measure of the frequency of iron occupancy at iron binding sites across transferrin molecules (two per transferrin protein), is typically maintained at approximately 25-40%[28]. Crucially, systemic iron levels (including TSAT) are maintained via interactions between ferroportin and hepcidin, the key iron regulatory hormone[29]. Liver produced hepcidin suppresses serum iron levels by inhibiting ferroportin mediated iron export[29]. Hepcidin binds to and promotes the endocytosis and degradation of cell surface ferroportin, trapping iron within cells and blocking intestinal absorption[29]. The body is thus able to control iron levels via hepcidin in response to different stimuli[7].

Hepcidin is regulated by iron itself (Fig. 1.1). Excess iron levels can result from genetic disorders including hemochromatosis and thalassemias or from surplus iron supplementation and blood transfusions[30]. Systemic iron loading is sensed in the liver by liver sinusoidal endothelial cells (LSECs)[31]. Excess iron within LSECs drive oxidative stress and mitochondrial ROS (mROS) production via Fenton reactions[31]. ROS are in turn detected by the oxidative stress regulatory transcription factor, NRF2, which induces the production and secretion of BMP6[31]. BMP6 binds to its receptor, ALK2/3, on hepatocytes

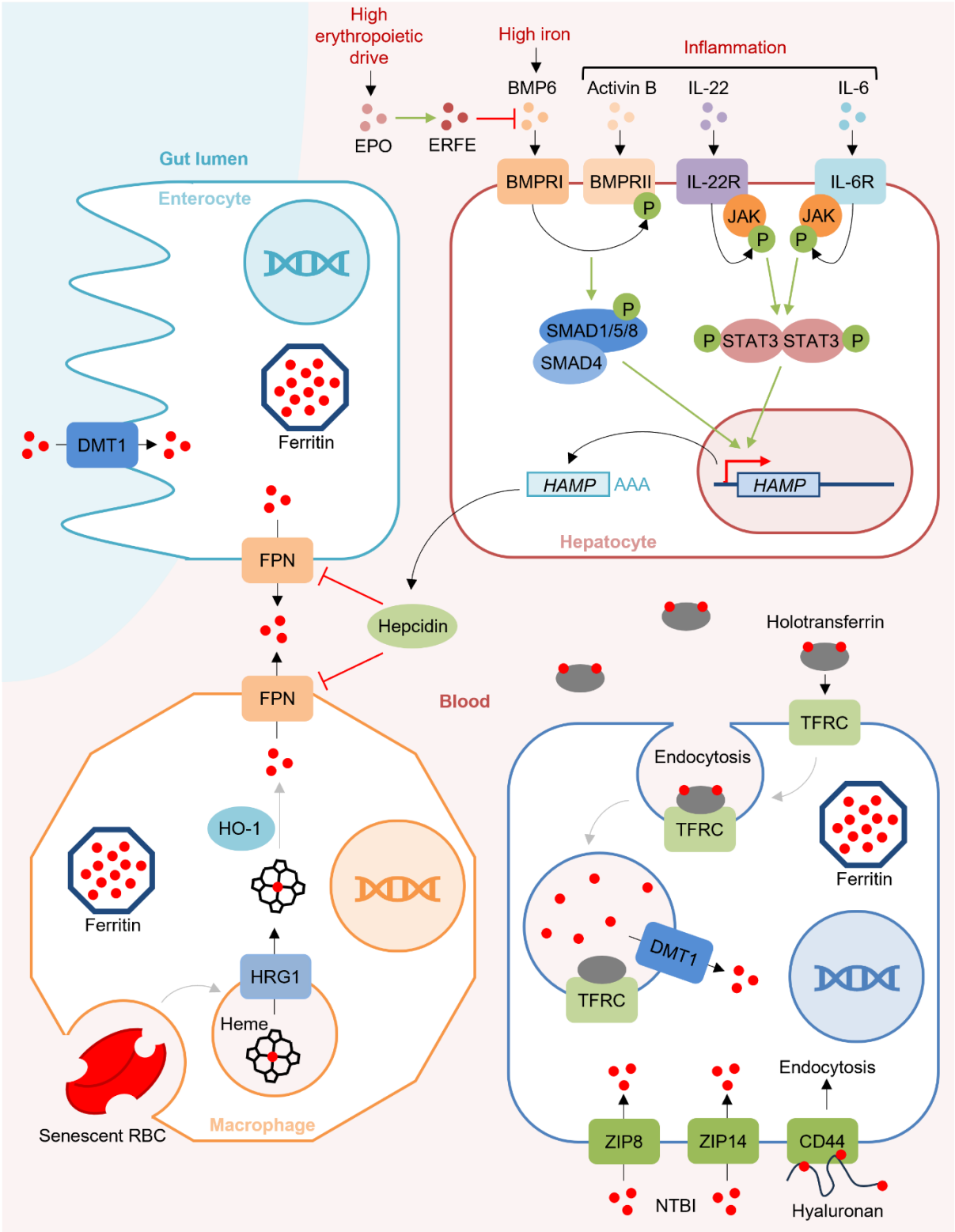

Figure 1.1. Iron homeostasis. Iron is taken up by enterocytes from the lumen of the gut by DMT1 and released into the circulation by ferroportin (FPN) or is stored in ferritin[29,32]. Macrophages recycle the iron from phagocytosed senescent RBCs[7]. RBCs are degraded and heme is released into the cytosol by HRG1[7]. HO-1 subsequently degrades heme releasing the iron ions which enter the blood via ferroportin[7,29]. Serum iron is controlled by hepatic hepcidin which inhibits iron release into the serum by ferroportin[29]. Hepcidin is induced by high iron by BMP6 and by inflammation by IL-6, IL-22 and (*Continued on next page*)

(*Continued from last page*) activin B[33-36]. IL-22 and IL-6 activate a JAK-STAT3 phosphorylation cascade to induce hepcidin upregulation[33-36]. High erythropoietic drive induces EPO and ERFE sequentially which suppresses hepcidin via BMP-6 inhibition[37-39]. BMP signalling induces SMAD1/5/8 phosphorylation and recruitment of SMAD4 to upregulate hepcidin transcription[40,41]. TFRC binding to iron bound transferrin induces endocytosis for iron uptake[42]. Endosome acidification releases the iron from transferrin and the iron can enter the cytosol via DMT1[42,43]. Non transferrin bound iron (NTBI) can also enter the cell via ZIP8 or ZIP14[44,45]. Hyaluronan bound iron can be taken up by binding of CD44 and subsequent endocytosis[46].

---

and induces SMAD1/5/8 phosphorylation[40]. The SMAD complex recruits SMAD4 and together they migrate to the nucleus to initiate hepcidin expression from the *Hamp1* loci to suppress iron absorption and promote macrophage iron sequestration[41]. Signalling and hepcidin production via the ALK2/3 receptor also requires association with hemojuvelin (HJV)[47] and ALK2/3 activity can be suppressed by HJV cleavage by the serine protease matriptase-2 (TMPRSS6)[47]. Consequently, patients with mutations in TMPRSS6 fail to suppress hepcidin which results in an iron refractory iron deficiency anaemia (IRIDA)[48]. In parallel to LSEC iron detection, hepatocytes also sense TSAT directly but the mechanism remains unclear. When TSAT is high, holotransferrin is proposed to stabilise transferrin receptor 2 (TfR2), permitting downstream signalling and hepcidin induction[7,47]. Holotransferrin may also compete for TFRC binding with the protein, HFE[47]. When TSAT is high, holotransferrin would be able to block HFE-TFRC interactions allowing HFE to promote signalling and downstream hepcidin production[47]. The specific signalling mechanism used by TfR2 and HFE to induce hepcidin are poorly understood but may act via ALK2/3-HJV or ERK-MAPK cascades[47]. Notably, mutations in genes such as HFE, TfR2 and HJV result in hemochromatosis due to inappropriate hepcidin suppression resulting in pathogenic iron loading in organs including the liver, heart and pancreas[47].

In scenarios of increased erythropoietic demand driven by stimuli such as traumatic blood loss, hypoxia, or inefficient erythropoiesis which occurs in hemoglobinopathies such as β-thalassemia, hepcidin is suppressed to allow for iron mobilisation to the bone marrow (Fig. 1.1)[37]. Reduced oxygen carriage by RBCs due to reduced cell numbers or function, induces a hypoxia response in the kidneys via HIF activation, stimulating production of erythropoietin (EPO)[38]. EPO stimulates responding erythroblasts to produce erythroferrone (ERFE), which acts as a ligand trap to sequester BMP6 and block hepcidin induction via the BMP/SMAD pathway described above[39].

Increased erythropoietic demand due to ineffective erythropoiesis in β-thalassemia patients results in hepcidin suppression via this pathway and similar to hemochromatosis can result in deleterious iron loading of the heart, liver and pancreas[49].

Many pathogens, similar to the hosts they inhabit, are also iron dependent[9]. Pathogens have developed complex mechanisms to efficiently acquire iron during infection and promote their own replication[9]. To counter pathogen iron scavenging, host inflammatory responses mediated by cytokines such as IL-6, IL-22 and activin B act on hepatocytes to stimulate hepcidin upregulation via STAT3 and subsequent suppression of blood iron concentrations (Fig. 1.1)[33-36]. While induction of hypoferremia may inhibit pathogen growth, especially of extracellular siderophilic bacteria[50-52], reduced iron availability may also impact host immune responses which also require an extracellular iron source.

1.1.2 Cellular iron uptake, storage, and trafficking

Uptake of cellular iron is canonically mediated via the transferrin receptor (TFRC, TfR1, CD71) (Fig. 1.1)[42]. Iron bound transferrin binds to TFRC inducing clathrin mediated endocytosis[42]. Acidification of the endosome releases iron from transferrin and iron is passaged into the cytosol via DMT1 (NRAMP2/SLC11A2)[42,43]. Notably, DMT1 also mediates direct dietary uptake of non-heme iron on the apical membrane of enterocytes[32]. Non-transferrin bound iron (NTBI) can enter the cell via the zinc transporters ZIP8 (SLC39A8) and ZIP14 (SLC39A14)[44,45]. More recently, iron bound to the extracellular matrix polysaccharide, hyaluronan, has been proposed to bind CD44 with the resulting complex being taken up by endocytosis[46].

Once iron enters the cell it can either be mobilised to mitochondria for heme and iron sulfur (Fe-S) cluster biosynthesis, incorporated as an ion into proteins or be stored by ferritin[53]. Ferritin is a 24 subunit cage like protein complex composed of both heavy (FTH) and light (FTL1/2) chain subunits[7]. The complex can store approximately 4300 iron atoms, thus providing substantial storage of iron[54]. Ferritin enables buffering of cellular iron by storing excess iron when iron is abundant and releasing iron when it becomes scarce[53]. Iron release is mediated by ferritin breakdown known as ferritinophagy and requires ferritin delivery to autophagosomes by NCOA4[55]. Trafficking of iron ions to ferritin and to other iron binding proteins within the cell

requires metallochaperones including PCBP1 and PCBP2[56]. Fe-S clusters and heme groups are similarly chaperoned by proteins/complexes such as GLRX3-BOLA2 and PGMRC2 respectively[56,57]. While studies have established how iron is mobilised in cell lines, how iron is trafficked during the dynamic process of T-cell activation is still unclear.

1.1.3 Intracellular iron regulation

Like the strong systemic regulation of iron by hepcidin, intracellular iron is tightly regulated. Classically, intracellular iron is regulated post-transcriptionally by the iron regulatory protein (IRP)/iron response element (IRE) system (Fig. 1.2)[53]. The IRPs, cytosolic aconitase 1 (ACO1, IRP1) and IREB2 (IRP2), are activated in the context of low cellular iron to induce iron uptake and prevent egress and storage[53]. During iron replete conditions ACO1 binds to an [4Fe-4S] cluster which enables its catalytic activity but physically obstructs its RNA-binding site[53]. Upon cellular iron deficiency, the Fe-S cluster is lost, permitting ACO1 RNA binding[53]. In contrast, IREB2 is specifically degraded in the presence of iron due to ubiquitination by the [2Fe-2S] cluster stabilised ubiquitin-ligase, FBXL5[58,59]. IRPs operate by binding to mRNA hairpin loops known as IREs that are located in the 3' untranslated regions (UTR) of mRNAs coding for proteins that promote iron uptake (TFRC and DMT1) and the 5' UTR of mRNAs encoding proteins associated with iron egress (ferroportin) and storage (FTL1/2, FTH)[53]. During iron deficiency, IRP binding to mRNAs with 3' IREs promotes mRNA stabilisation by blocking entry of RNases thus driving upregulation of iron uptake by TFRC and DMT1[53]. Meanwhile, IRP binding to 5' IRE containing mRNAs excludes ribosome binding and translation resulting in downregulation of iron egress and storage by ferroportin and ferritin respectively[53].

During iron scarcity, the IRE-IRP system also downregulates proteins associated with iron usage[60]. These include the heme synthesis regulatory protein, ALAS2[61], and the tricarboxylic acid (TCA) cycle enzyme, mitochondrial aconitase 2 (ACO2), which requires a [2Fe-2S] cluster for catalysis[62]. Presumably, downregulation of iron use by heme synthesis and the TCA cycle enables more efficient iron budgeting for use in essential pathways. Cell cycle progression and cytoskeletal reorganisation may also be directly iron regulated due to 3' IREs in the mRNAs encoding the cell cycle and cytoskeleton regulators CDC14A and MRCKα respectively[63,64].

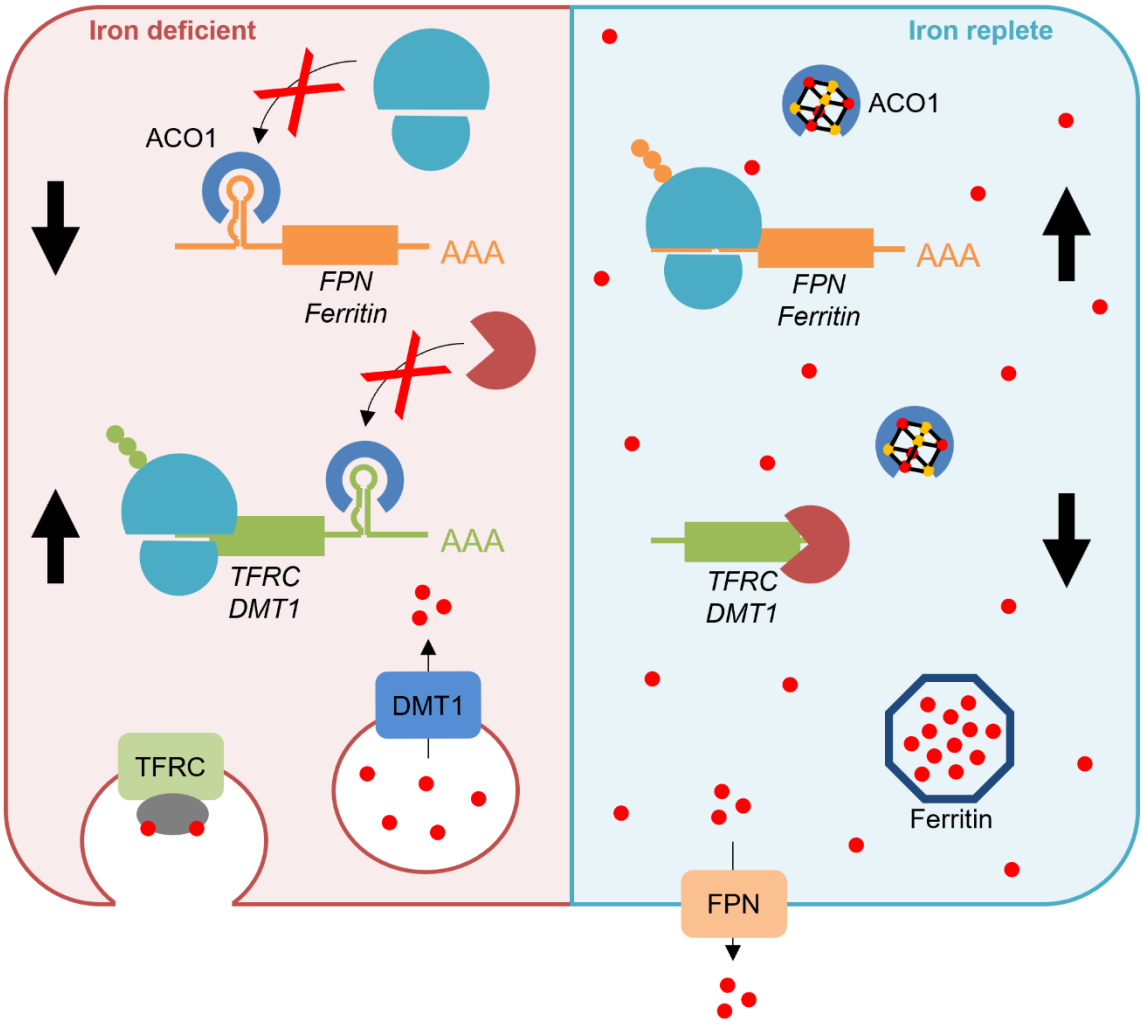

Figure 1.2. The IRP-IRE system. During iron deficient conditions, iron response proteins such as ACO1 bind to IRE mRNA structures driving an iron uptake phenotype[53]. Binding to 5' IREs in the mRNAs of ferroportin (FPN) and ferritin blocks translation and results in downregulation[53]. Binding to 3' IREs in TFRC and DMT1 mRNAs prevents degradation by RNases and allows translation[53]. Conversely, under iron replete conditions, ACO1 binding is blocked by a [4Fe-4S] cluster promoting iron sequestration and egress[53]. Ferroportin and ferritin mRNAs with 5' IREs can be translated whereas TFRC and DMT1 mRNAs with 3' IREs are degraded by RNAses[53].

While the IRP-IRE system is the canonical method of intracellular iron regulation, alternative modes of iron sensing exist. HIF proteins, key regulators of the hypoxia response, are also iron sensitive[65]. Under normoxic or iron replete conditions, PHD enzymes which are iron dependent, oxygen dependent and 2-oxoglutarate (2-OG, α-ketoglutarate (α-KG)) dependent actively hydroxylate HIFs[65]. Hydroxylation promotes ubiquitination of HIFs by the VHL proteins which marks HIF proteins for degradation[65]. Conversely, when oxygen or iron is limiting, the PHD proteins become inactive allowing for HIF stabilisation and transcriptional activity[65]. HIF has broad transcriptional activity,

but notably regulates metabolism[66]. HIF1 promotes a metabolic shift away from oxygen consumption by upregulating glycolysis and suppressing oxidative phosphorylation (OXPHOS) and fatty acid β-oxidation in part by reducing mitochondrial mass via mitophagy[66]. Interestingly, iron chelators have historically been used to study the hypoxia response due to their capacity to stabilise HIF1-α[67]. Whether the levels of iron deficiency achieved by hypoferremia results in a decrease in PHD activity sufficient to stabilise HIF in immune cells is unknown.

Tristetraprolin (TTP) has also been proposed as a regulator of the low iron response during extended iron depletion[68-70]. The IRP-IRE system largely operates by promoting iron uptake and release and preventing iron loss during iron deficiency[53]. In contrast, TTP mobilises iron to essential pathways by inhibiting non-essential but iron greedy processes[68-70]. During iron limitation, TTP is upregulated and binds to AU-rich elements in the 3' UTRs of mRNAs, promoting mRNA decay[68]. TTP targeted mRNAs include those encoding lipoic acid synthase (LIAS), ACO2, NDUFS1 and UQCRFS1, all of which are important for mitochondrial OXPHOS. Notably, OXPHOS is suggested to be "non-essential" due to the capacity of cells to switch to glycolysis for energy generation[68-70]. While TTP is clearly iron responsive, TTP's tropism and if and how TTP directly senses iron is unknown. mTOR, a crucial integrator of diverse metabolic cues including amino acid depletion, is suggested to act upstream of TTP[69]. However, how mTOR in turn detects cellular iron levels is also unclear.

While iron ions regulate HIF proteins and Fe-S cluster proteins regulate the IRP-IRE system, heme can also regulate cellular iron metabolism. Heme deficiency is sensed in RBCs by the heme regulated inhibitor (HRI, EIF2AK1)[71]. When heme is abundant, HRI binds heme which blocks HRI's kinase activity[71]. In the absence of heme, HRI becomes active and auto-phosphorylates itself and the translational initiation factor, eIF-2α[71]. eIF-2α phosphorylation blocks globin translation and prevents the accumulation of misfolded globins in the absence of heme[71]. Phosphorylation of eIF-2α simultaneously promotes the integrated stress response to promote cell survival during heme insufficiency[71]. While HRI's involvement in heme sensing is predominantly characterised in RBCs, recent work has indicated that HRI has non-erythroid roles in the responses to mitochondrial stress and cytosolic protein misfolding[72-74]. Whether HRI also plays a role in heme sensing in non-erythroid cells such as immune cells remains an open question.

Iron is tightly regulated at multiple nodes. The utility of diverse regulators is that it allows for nuanced responses to specific environmental stimuli. For instance the IRE-IRP system enables rapid responses to acute changes in cellular iron levels by increasing uptake and releasing iron stores[53]. The TTP system is instead proposed to enable cells to survive extended periods of iron scarcity where increasing iron uptake provides little benefit[68-70]. While four axes of cellular iron regulation are described (IRE-IRP, PHD-HIF, TTP and heme-HRI), it is possible that iron fluctuations could be detected and responded to by various other means with diversity across cell types.

1.2 Iron in cellular biochemistry

Within cells, iron is predicted to interact with approximately 400 different human proteins[6]. Iron interacting proteins largely utilise iron for its capacity to easily exchange electrons, thus permitting redox reactions, electron transfer and oxygen binding[7]. Iron can be bound by proteins directly as iron ions or complexed into Fe-S cluster or heme prosthetic groups[6]. These proteins operate in diverse pathways including mitochondrial function, DNA replication and repair, epigenetic regulation and nucleotide synthesis and are localised across cellular compartments[6].

1.2.1 Iron in mitochondrial metabolism

Iron interacting proteins are particularly enriched in the mitochondria with 7% of mitochondrial proteins predicted to bind iron (relative to 2% cell wide) [6]. However, how iron enters the mitochondria to furnish these proteins is not completely understood. Mitochondria have two membranes, an outer mitochondrial membrane (OMM) and an inner mitochondrial membrane (IMM) (Fig. 1.3)[75]. To cross the OMM, it has been suggested that iron may pass through large porins called VDACs on the OMM which enable uptake of metabolites such as pyruvate and ATP[76]. Others propose that iron may enter mitochondria via direct fusion of iron containing endosomes with the OMM[77] or could use an OMM localised isoform of DMT1[78,79]. Once iron has entered the intermembrane space, iron is transported into the mitochondrial matrix via mitoferrin 1 (MFN1) and mitoferrin 2 (MFN2)[80,81].

Mitochondrially localised iron can either be stored in mitochondrial ferritin[82,83], utilised for heme and Fe-S cluster biosynthesis or used by mitochondrial proteins[75].

Heme and Fe-S cluster synthesis are preferential pathways for iron usage within the cell. Failure to efficiently produce heme or Fe-S cluster cofactors due to mutations in these pathways result in mitochondrial iron overload as cells attempt to rectify the biosynthetic block by trafficking further iron into the mitochondria[75,84]. Notably, mitochondrial iron loading comes at the expense of cytosolic iron homeostasis (resulting in cytosolic iron deficiency and induction of the low iron IRP-IRE response) suggesting that mitochondrial iron takes precedence over iron in alternative compartments[84].

Heme synthesis begins with the condensation of glycine to succinyl-CoA by the rate limiting enzyme, ALAS (ALAS1 is found in all cells, ALAS2 is erythroid specific) in the mitochondrial matrix (Fig. 1.3)[75,85]. The resulting 5-aminolevulinic acid (ALA) product is passed through a chain of seven further enzymes (passing into the cytosol for steps 2-5 and returning to the mitochondria for steps 6-8) ending with the insertion of iron into porphyrin by the Fe-S cluster containing protein, ferrochelatase (FECH)[75,86]. Heme can then be used locally, for instance in complex I (CI) of the electron transport chain (ETC) or transported to the cytosol by FLVCR1b for use elsewhere in the cell[75,87].

Fe-S cluster synthesis includes both mitochondrial and cytosolic assembly pathways[88]. Mitochondrial Fe-S cluster synthesis begins with the formation of a scaffold including two each of the proteins ISCU2, NFS1, frataxin, FDX2, ISD11 and ACP1 (Fig. 1.3)[88]. This complex extracts sulfur from the amino acid cysteine and combines it with iron forming a [2Fe-2S] cluster[88]. ISCU2 transfers the [2Fe-2S] to a GLRX5 dimer with the aid of HSPA9 (HSP70) and HSP40 (HSC20)[88]. The [2Fe-2S] clusters can either be delivered to proteins by GLRX5 or fused together to form a [4Fe-4S] cluster by a complex composed of ISCA1, ISCA2 and IBA57[88]. [4Fe-4S] clusters are then inserted into their target proteins by chaperones such as NFU1, IND1, BOLA1 and BOLA3[88]. Mitochondrial Fe-S cluster targets include ACO2, LIAS and CI and complex II (CII) of the ETC [88].

Notably, while intact mitochondrial Fe-S cluster synthesis is critical for non-mitochondrial Fe-S cluster binding proteins, Fe-S clusters synthesised in the mitochondria are not believed to be capable of crossing the mitochondrial membrane[88]. Instead an uncharacterised sulfur containing factor (X-S) is thought to be produced by mitochondrial Fe-S cluster synthesis and passaged to the cytosol by ABCB7 for completion by the cytosolic Fe-S cluster synthesis pathway[88].

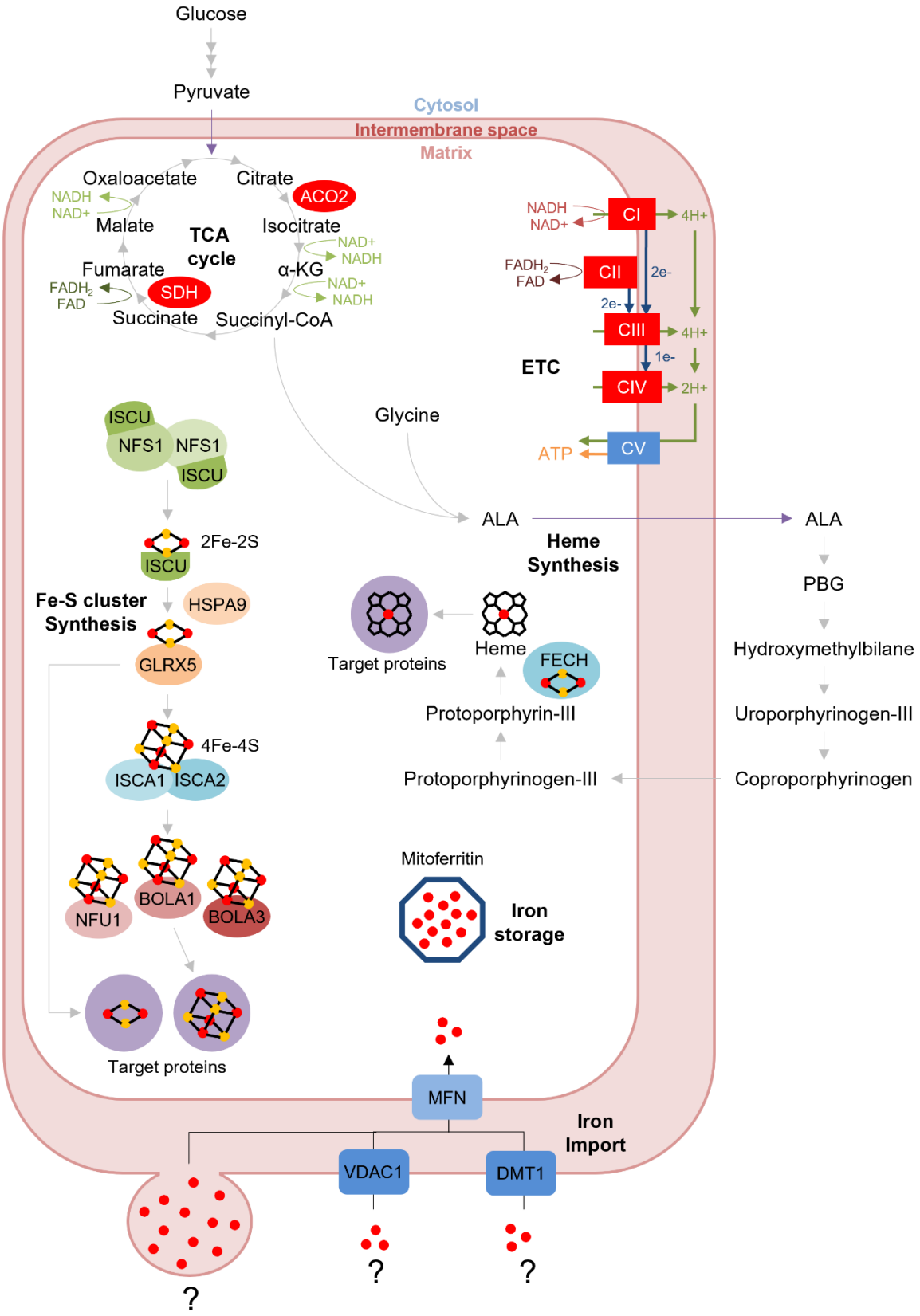

Figure 1.3. Iron in mitochondrial metabolism. Iron has been proposed to cross the outer mitochondrial membrane into the intermembrane space by direct fusion of endocytic vesicles, via VDAC1 channels or using the DMT1 transporter[76-79]. Iron then enters the matrix via mitoferrins (MFN)[80,81]. Iron in the mitochondria is used for catalysis by aconitase 2 (ACO2) and succinate (*continued on next page*)

(*continued from last page*) dehydrogenase (SDH) in the TCA cycle[88]. Iron cofactors are also necessary for electron transfer for all four complexes of the ETC[75]. Succinyl-CoA from the TCA cycle can be condensed with glycine to initiate heme synthesis[60]. Heme synthesis is a 8 step process which concludes with the deposition of iron into the porphyrin ring structure by the [2Fe-2S] cluster binding protein ferrochelatase (FECH) [6071]. Fe-S cluster synthesis begins with the formation of a [2Fe-2S] cluster on a scaffold of proteins which includes ISCU and NFS1[88]. The [2Fe-2S] cluster is transferred to GLRX5 with the help of HSPA9[88]. GLRX5 can transfer the [2Fe-2S] cluster to target proteins or two can be linked together to form a [4Fe-4S] cluster on the ISCA1/ISCA2 complex[88]. [4Fe-4S] clusters are delivered to target proteins by chaperones such as BOLA1, BOLA3 and NFU1[88].

Mitochondrial metabolism is highly iron dependent . The TCA cycle enzymes, ACO2 and succinate dehydrogenase (SDH), and the fatty acid β-oxidation protein, ETFDH, use Fe-S clusters for catalysis (Fig. 1.3)[88]. Additionally, all four complexes of the ETC rely on heme and Fe-S clusters for efficient electron transfer[75]. LIAS uses a [4Fe-4S] cluster to mediate the essential lipoylation of metabolic enzymes such as pyruvate dehydrogenase (PDH) and α-KG dehydrogenase (α-KGDH)[88]. Meanwhile FECH, uses an Fe-S cluster for the final step of heme synthesis[88]. The high dependence of the mitochondria on iron for metabolic processes, heme and Fe-S cluster synthesis suggests that iron deficiency may profoundly affect mitochondrial processes. Knock on effects on extra-mitochondrial pathways which rely on heme and Fe-S cluster cofactors would also be predicted.

1.2.2 Iron in DNA replication and repair

DNA synthesis is a complex process essential for cellular replication that requires several iron dependent enzymes[89]. DNA replication begins with the unwinding of the DNA helix by helicases including the iron dependent DNA2[90]. Once the DNA helix has been unwound, a short RNA primer must be deposited for DNA replication initiation[91]. The primer is placed by primase which consists of two subunits including iron dependent PRIM2[91]. DNA polymerases Polα, Polβ and Polε then proceed to synthesise the complementary DNA strand using their [4Fe-4S] cluster binding catalytic subunits (POLA1, POLD1 and POLE1 respectively)[89]. RRM2, a component of the ribonucleotide reductase (RNR) enzyme, also requires iron to catalyse the rate limiting step in the production of dNTPs, the subunits of DNA[92,93].

Many of the iron dependent enzymes for DNA synthesis are also involved in DNA repair[89]. For instance, DNA2 as well as the other iron dependent helicases, FANCJ, XPD and CHLR1 unwind the DNA to allow for entry to damaged DNA sites[89]. DNA glycosylase

enzymes including iron dependent MUTYH mediate the initial base removal in base excision repair where damaged or incorrect DNA bases are removed and correct bases are inserted[89,94]. The trans-lesional DNA synthesis is then completed by Polζ, which like the DNA replication polymerases, contains an iron dependent subunit, REV3L[89,95]. Notably DNA replication is a critical process during T-cell expansion while maintenance of genomic stability is necessary to avoid T-cell malignancies. How iron deficiency impacts either of these processes during T-cell activation remains unexplored.

1.2.3 Iron in oxidoreductases

Oxidoreductase enzymes catalyse redox reactions[6]. Strikingly, while 6.5% of enzymes use iron cofactors, 37% of oxidoreductases are iron dependent[6]. One of the larger classes of iron dependent oxidoreductases are the 2-OG dependent dioxygenases (2-OGDDs) which use oxygen and 2-OG as substrates to mediate hydroxylation reactions on diverse targets[96]. The PHD proteins (described in section 1.1.3) are 2-OGDDs which regulate the HIF mediated hypoxia response by marking HIF proteins for degradation via hydroxylation[96]. 2-OGDDs also arbitrate demethylation reactions where hydroxylation of methyl groups produces an unstable methyl-hydroxy intermediate which spontaneously dissociates[96]. Notably, demethylation is a critical epigenetic mechanism, acting on both methylated DNA (TET enzymes) and histones (lysine demethylase enzymes (KDMs)) to regulate transcription[96]. mRNA and tRNA hydroxylation by 2-OGDDs also play roles in mRNA stability and translational efficiency and fidelity[96].

Lipid metabolism also involves many iron dependent oxidoreductases. Cytochrome P450 monooxygenases use heme prosthetic groups in the metabolism of endogenous fatty acids, bile acids and steroids including eicosanoids and for detoxification of xenobiotics such as pharmaceuticals[97]. The cyclooxygenases (COXs) well known for being the target of non-steroidal anti-inflammatory drugs (NSAIDs) such as ibuprofen and aspirin are also heme dependent oxygenases important for prostaglandin synthesis[98]. Meanwhile, lipoxygenases use iron ions for the metabolism of unsaturated fatty acids[99]. Notably, prostaglandins and other eicosanoids are signalling molecules with immune-modulatory properties which T-cells both respond to and produce[100]. The neutrophil degranulation enzymes myeloperoxidase (MPO) and NADPH oxidases (NOXs) which produce antimicrobial ROS are also iron dependent oxygenases[101,102].

Iron's use by oxidoreductases is extensive and mediates remarkably diverse reactions, yet many iron dependent oxidoreductases remain poorly characterised[103]. However, the importance of oxidoreductases in lipid metabolism, chromatin structure and neutrophil degranulation amongst other pathways suggests that iron deficiency could have broad reaching effects on cellular biochemistry.

1.3 Experimental methods of iron modulation

While iron is clearly utilised for a myriad of cellular functions, understanding the importance of iron homeostasis and the impacts of aberrantly high or low iron availability on biology, requires experimental methods of iron modulation. Different methods have been developed that target iron handling at various steps (Table 1.1).

Low iron diets directly reduce iron availability to the whole organism and overtime result in systemic iron depletion[104]. Injected hepcidin or hepcidin analogues such as mini-hepcidin (mHep) drive macrophages and enterocytes iron sequestration resulting in functional serum iron deficiency but do not acutely deplete the whole organism of iron[29,105] (hepcidin can be used to promote ferroportin downregulation *in vitro*[106]). Iron chelators such as deferoxamine (DFO), deferiprone (DFP), deferasirox (DFX) can be used to sequester serum iron and prevent its use[107]. Notably, some chelators including DFX are cell permeable and sequester iron intracellularly[107]. Meanwhile, α-TFRC antibodies block uptake of transferrin bound iron by cells[15]. A similar effect is present in mice or cells with TFRC knockout (cell conditional as global TFRC knockout is embryonic lethal) or mutations such as $TFRC^{Y20H}$ which reduces the efficiency of TFRC endocytic cycling, preventing cells from acquiring sufficient iron[108]. Similarly, IRP1/2 double knockout cells (cell conditional as global IRP1/2 double knockout is embryonic lethal) fail to sense low intracellular iron and consequently do not upregulate the necessary iron uptake machinery resulting in intracellular iron depletion[109]. *In vitro*, iron depleted cell culture media, iron chelators and α-TFRC antibodies are all options for altering iron availability in addition to cells derived from TFRC and IRP1/2 mutant/knockout mice[14,107,108,110].

To mediate iron overload, high iron diets or bolus iron doses can be used[31]. α-BMP6 antibodies which suppress hepcidin result in acute increases in serum iron[111]. HFE knockout mice can be used to recapitulate human hereditary hemochromatosis which results in iron loading [112]. Iron supplemented media can be used *in vitro*[31].

Method	*In vitro*	*In vivo*
Hepcidin and hepcidin analogues Ex// hepcidin, mini-hepcidin	X	X
α-BMP6 antibodies		X
Iron modified diets		X
Iron chelators Ex// DFO, DFP, DFX	X	X
α-TFRC antibodies	X	X
Low iron media	X	
Genetic knockouts and mutations Ex// TFRC-KO, $TFRC^{Y20H}$, IRP1/2-DKO	X	X
Iron supplementation Ex// $FeSO_4$, Ferric ammonium citrate (FAC)	X	X

Table 1.1. Methods of iron depletion *in vivo* and *in vitro.*

1.4 Iron in immunity

The immune system responds to diverse perturbations such as infection, malignancy and tissue injury[113]. Interestingly, iron regulation has become evolutionarily entangled with immunity due to the necessity of iron for both host and pathogen[9]. Invading pathogens are initially detected by innate immune cells such as macrophages and dendritic cells (DCs) via pathogen recognition receptors (PRRs) which recognise pathogen associated molecular patterns (PAMPs) composed of microbial components including lipids, proteins and nucleic acids[114]. Tissue damage is similarly sensed by PRR binding to damage associated molecular patterns (DAMPs)[114]. PAMP or DAMP sensing promotes the production of cytokines and chemokines which induce inflammation and recruit immune cells to the local site of infection or damage[113,114]. Depending on the perturbation, the immune response activates different signalling pathways to promote particular cell types and effector functions[113]. The innate arm of immunity responds quickly to a broad range of cues[113]. In contrast, adaptive immunity is slower upon initial priming by specific antigens, but produces a more targeted response that is rapidly and more robustly induced upon re-exposure to the same antigen[113]. Due to the dynamic nature of the immune response, immune cell iron demands are not constant and shift depending on whether cells are quiescent, activated or in a primed or memory like state.

Notably, IL-6, a key inflammatory cytokine, also induces hypoferremia to prevent pathogen access to iron (described in section 1.1.1)[33]. Individuals with iron overload due to hereditary hemochromatosis have increased vulnerability to bacterial infection[115] and mice that fail to induce a hepcidin mediated hypoferremic response are highly susceptible to *Vibrio vulnificus*[50], *Yersinia enterocolitica*[51], and *Escherichia coli*[52] infection. While hypoferremia is an effective mechanism for control of extracellular bacterial species, reduced iron availability is increasingly being found to have impacts on cellular immunity.

1.4.1 Iron in innate immunity

Innate immune cells such as macrophages, neutrophils and NK cells are rapidly recruited to the local environment to control infections or perturbations[116]. Macrophages and neutrophils facilitate bacterial clearance by phagocytosis and utilise multiple iron requiring enzymes including MPO, NOX2, and COX2 (see section 1.2.3) to facilitate pathogen killing via production of toxic ROS and reactive nitrogen species (RNS)[117-120]. Intriguingly, neutrophil but not monocyte development has been demonstrated to be sensitive to iron deficiency as induction of low serum iron (hypoferremia) using the hepcidin analogue, mHep, suppresses bone marrow granulopoiesis resulting in reduced splenic and blood neutrophils but not monopoiesis[121]. Iron depleted neutrophils show defects in phagocytosis, bacterial killing and cytokine production[121]. While monocyte production does not seem to be as iron sensitive, macrophage polarisation towards classical M1 or alternative M2 phenotypes has also been associated with differential expression of key iron regulatory proteins[122]. Pro-inflammatory M1 macrophages are suggested to be more iron sequestering (reduced ferroportin, increased ferritin) while M2 macrophages associated with wound healing are described as being primed for iron export (increased ferroportin, reduced ferritin)[122]. A mouse model of wound healing demonstrated that iron loading of macrophages using iron dextran drives inflammatory TNF-α and IL-12 producing macrophages which have reduced wound healing capacity[123]. In contrast, iron deprivation induced by DFP iron chelation reduces macrophage production of inflammatory IL-1β and TNF-α in response to lipopolysaccharide (LPS)[124]. Moreover, DEF treatment in a mouse model of inflammatory crescentic glomerulonephritis attenuates macrophage mediated pathology[124].

Natural killer (NK) cells are early responding cytotoxic cells which are important for the clearance of virus infected cells and tumour killing[125]. NK cells induced by Friend retrovirus are suppressed by mHep mediated serum iron suppression with reduced expression of the activation marker CD69 and reduced IFN-γ production[126].

Conventional DCs (cDCs) link innate and adaptive immunity by carrying and presenting antigen to T-cells to mediate T-cell activation. cDCs were recently found to produce hepcidin in the intestine which is thought to aid in local iron sequestration during inflammation to promote wound healing[127,128]. Plasmacytoid DCs (pDCs) which produce large amounts of type I IFN (IFN-α and IFN-β) in the early phases of immune responses are known to express extremely high levels of TFRC suggesting high iron dependency[129]. However, the role of pDC TFRC is not understood.

1.4.2 Iron in adaptive immunity

During an immune response, naïve CD8+ and CD4+ T-cells are activated in response to T-cell receptor (TCR) binding to a specific cognate antigen presented by antigen presenting cells (APCs) on MHC-I or MHC-II respectively[130]. T-cell costimulatory molecules such as CD28 similarly bind to their cognate ligands on the APC[130]. TCR binding and co-stimulation initiates a signalling cascade via recruitment and phosphorylation of various signalling proteins and results in the activation of transcription factors such as NF-κB, AP-1 and NFAT which promote the T-cell activation program[130]. Activated T-cells proliferate rapidly with division times of approximately 6-8 hours for CD8+ T-cells and approximately 10 hours for CD4+ T-cells[131] and express activation markers such as CD69 and CD25[132]. Notably, TCR and CD28 signalling also activates the metabolic regulators MYC and mTORC1 which increase glycolysis and OXPHOS to facilitate the high biosynthetic demands of T-cell activation (the field of T-cell immunometabolism will be described in further detail in chapters 5 and 6)[133]. Moreover, T-cells dramatically shift iron handling towards uptake and retention, increasing expression of the uptake proteins TFRC, DMT1 (SLC11A2) and SLC39A14 (ZIP14) while downregulating the export protein, ferroportin (SLC40A)[14,134]. Activated T-cells also increase expression of proteins important for Fe-S cluster and heme synthesis suggesting that iron use in addition to uptake is increased (data from Howden *et al* 2019)[134].

Activated CD8+ T-cells produce perforins and granzymes to promote killing of infected and malignant cells as well as cytokines such as IL-2, TNF-α and IFN-γ[132]. CD4+ T-cells can differentiate down different axes, each with their own set of characteristics[135]. While the classical allocation of T-cells to either Th1, Th2, Th17 and T regulatory (Treg) subsets is simplistic, the association of certain pathogens, transcription factors and effector functions to each subset is helpful for understanding how different contexts may result in functionally different CD4+ T-cell responses. Th1 cells are associated with expression of the transcription factor TBET and the production of IFN-γ to promote killing of intracellular pathogens, for instance via macrophage activation[135]. Extracellular bacteria and fungi induce Th17 cells which express the transcription factor RORγt and the cytokines IL-17, IL-21, and IL-22 to promote neutrophil recruitment and production of antimicrobial peptides[135,136]. Notably, pathogenic Th17s in autoimmune disease often produce IFN-γ and GM-CSF[135]. Th2 cells characterised by GATA-3 expression, mediate responses to parasites such as helminths by producing IL-4, IL-5 and IL-13 which induce mucus production, mast and eosinophil activation and promote B-cell IgE production[135,137]. Th2 type responses are also characteristic in allergy[135]. FOXP3+ Tregs act in opposition to other T cell subsets (CD8+, Th1, Th2, Th17) to control their activation and prevent immune cell associated pathology[135]. Whether different T-cell subsets handle iron differently remains to be explored.

B-cells are similarly activated by specific antigens binding to their B cell receptors (BCRs), but also acquire additional cues by presenting antigen on MHC-II to T follicular helper cells (Tfhs)[138]. Activated B-cells can either differentiate immediately into short lived plasmablasts or enter the germinal centre where antibody class switching and somatic hypermutation occur to alter antibody effector function and increase antibody affinity respectively[138]. Antibodies in turn can neutralise viral particles and bacterial toxins, promote phagocytosis and antibody dependent cellular cytotoxicity[139]. As with T-cells, activated B-cells upregulate TFRC suggesting increased iron requirements[140].

In parallel to producing immediate effector responses, B and T-cells notably also produce memory populations which are capable of rapidly responding upon secondary stimulation with the same antigen[131,138]. Once clearance of the pathogen has occurred, effector B and T-cells undergo apoptosis in a contraction phase, but leave behind long lived memory populations[131].

The critical role of iron in adaptive immune responses is demonstrated by a combined immunodeficiency caused by a point mutation in the gene encoding TFRC ($TFRC^{Y20H}$), that reduces the efficiency of cellular iron import and results in impaired lymphocyte function and hypogammaglobulinemia[108,141]. Strikingly these patients only display mild anaemia despite the severe immunosuppression[108]. T and B-cells derived from patients or mice homozygous for the $TFRC^{Y20H}$ mutation fail to proliferate and B-cells produce less antibodies indicating a general lymphocyte dysfunction[108]. While the $TFRC^{Y20H}$ mutation is rare, the implication that reduced cellular iron availability has the capacity to dramatically impair adaptive immune responses provides rationale for investigating iron's role in adaptive immune responses especially given that iron deficiency remains the most common micronutrient deficiency worldwide[11]. Further, limited iron supply can occur not only due to reduced dietary iron intake, but also in the context of inflammation induced hypoferremia[33] and locally within iron scarce niches which may occur adjacent to iron demanding tumours[142].

The iron dependency of adaptive immune responses has been further demonstrated in a variety of contexts including immunisation, infection, and autoimmunity. Limiting serum iron availability in mice using the drug mHep suppresses adaptive T and B cell responses during immunisation with a variety of vaccine platforms[14]. Similar impairments to murine B-cell responses upon antigen immunisation have been observed during iron depletion mediated via low iron diet[16]. Meanwhile, iron supplementation increases responses to *Mycoplasma hyopneumoniae* vaccination in naturally iron depleted piglets [14] and measles vaccination in (likely iron deficient) Kenyan infants[143]. Measles vaccine antibody titres are also found to positively correlate with serum iron in human patients[16].

Beneficial immune responses to influenza virus are similarly impaired by hypoferremia, featuring reduced granzyme B (GZMB) producing T-cells, lower neutralising antibodies and increased inflammation[14]. Further, serum iron concentration and lymphocyte counts were found to be significantly lower in patients with severe vs non-severe SARS-CoV2 infections[144]. While the data cannot assign a causative relationship, the correlation between serum iron and lymphocyte counts in COVID-19 patients is at least consistent with a potential effect of serum iron deficiency suppressing appropriate immune responses in the context of human viral infection[144]. $TFRC^{Y20H/Y20H}$

mice with cellular iron restriction also fail to control infection with the malaria parasite *Plasmodium chabaudi* and feature reduced CD4+ T-cells and germinal centre B cells[17]. While low iron availability appears to be detrimental across a variety of infection settings, it should be noted that iron excess could be similarly unfavourable as high iron diet was shown to impair the differentiation of Th1 CD4+ T-cells during *Salmonella typhimurium* infection in mice[145].

Iron limitation also limits pathogenic adaptive immune responses in a variety of autoimmune models. α-TFRC antibodies which block iron uptake suppress pathogenic T-cell responses in disease models of experimental autoimmune encephalomyelitis (EAE)[19] and systemic lupus erythematosus (SLE)[15]. Likewise, mice with a CD4 specific TFRC knockout show reduced susceptibility to SLE with suppressed T and B cell responses and EAE with reduced infiltration of CD4+ T-cells into the central nervous system[15,18]. Meanwhile, the iron chelator DFX abrogates CD4+ T-cell responses and muscle damage in experimental autoimmune myositis[21]. In contrast, iron loading due to a high iron diet exacerbated CD4+ T-cell and B-cell responses in lupus mice[20].

It is evident that cellular iron restriction results in impairment of adaptive immunity *in vivo* in the context of vaccination, infection, and autoimmunity in pre-clinical models and in circumstances of rare human mutations. However, several open questions remain. Firstly, it is uncertain how translatable these observations are to more generalizable human contexts such as iron deficiency and inflammatory hypoferremia and whether iron modulation is a viable option to clinically modify immune responses for patient benefit. Secondly, the effects of iron on T and B-cell responses in other contexts such as allergy, transplantation or cancer remain unclear. Finally, how iron deficiency is modifying cellular biochemistry to exert its profound immunosuppressive effect is poorly understood.

While *in vivo* animal studies have established the necessity of iron for appropriate adaptive immune responses, *in vitro* models provide an opportunity to more closely examine the cellular processes perturbed during iron scarcity. *In vitro* T-cell iron studies began in the 1980s where α-TFRC antibodies were demonstrated to suppress T-cells in the mixed lymphocyte reaction[146-148]. Similar to the T-cells derived from $TFRC^{Y20H}$ homozygous mice and humans[108], murine CD8+ T-cells bearing dual knockouts of IRP1 and IRP2 which fail to upregulate TFRC for iron uptake show defects in activation induced

proliferation[14]. CD8+ T-cells cultured in low iron conditions also show defects in proliferation, activation measured using CD25 and GZMB production[14].

In vitro proliferation of CD4+ T-cells in unpolarised conditions has similarly been shown to be suppressed by iron chelation with DFO[22]. However, how iron limitation impacts CD4+ T-cells polarisation remains unclear with potential differences between CD4+ T-cell subsets. For instance, early work showed that Th1 T-cell clone proliferation was more sensitive to α-TFRC antibodies and DFO iron chelation suppression relative to Th2 T-cell clones[149]. Iron limitation using genetic models ($TFRC^{Y20H/Y20H}$) or iron chelation with ciclopirox olamine (CPX) or DFO has also been shown to suppress Th1 induction of IFN-γ and GM-CSF[17,18,150]. The iron sensitivity of GM-CSF was proposed to be due to GM-CSF mRNA stabilisation by the iron-binding, RNA-binding protein PCBP1 in the presence of iron[18]. Thus, in the absence of iron, PCBP1 is thought to be degraded promoting GM-CSF mRNA decay[18]. In contrast, IL-13 produced by T-cells in Th2 polarising conditions appears more resistant to iron chelation[150] reinforcing the concept that different T-cell subsets may have different iron dependencies. Similar to Th1 polarised T-cells, α-TFRC antibodies have been shown to suppress *in vitro* Th17 polarisation characterised by reduced IL-17A and GM-CSF production[19]. Suppressed IL-17A was proposed to be due to reduced binding of RORγt and RNA polymerase II to the IL-17A gene loci because of suppressed levels of the activating histone markers H3K4me3 and H3K27ac[19]. Bulk human CD4+ T-cells activated in the presence of the chelators CPX, DFX and DFO also show reductions in IFN-γ and IL-17A expression[21]. *In vitro* Tfh proliferation also appears to be abrogated by iron chelation[20]. While iron depletion of Th1 and Th17 polarised T-cells appears to be particularly detrimental, the impact of iron limitation on Treg cells may be beneficial with reports that iron scarcity increases expression of the lineage defining transcription factor FOXP3 and IL10, a tolerising cytokine in CD4+ T-cells[15,21]. It should however be noted that the existing studies of CD4+ T-cell differentiation in iron scarcity remain relatively rudimentary and largely do not explore the impacts of iron depletion beyond cytokine production. Whether iron scarcity only alters cytokine production or prevents differentiation of T-cells at an epigenetic level, or has wide transcriptional and metabolic effects, remains unclear.

B-cell function has similarly been shown to be perturbed by iron deficiency. $TFRC^{Y20H/Y20H}$ B-cells fail to divide and show impairment of antibody production and class

switching[17]. Failure of B-cells to proliferate during DFO treatment was shown to be due to an inability to remove the suppressive H3K9me2/3 methylation mark at the *Ccne1* loci which encodes the cell cycle activator, cyclin E1[16].

Due to the high dependency of mitochondrial metabolic processes on iron, alterations to metabolism during iron restriction have been proposed to be partly responsible for the observed suppression. Defects in CD8+ T-cell function during iron scarcity are accompanied by metabolic dysfunction including a reduction in pS6 expression, a downstream target of the key metabolic regulator mTORC1, reduced mitochondrial ATP production and reduced mitochondrial membrane potential[14]. Iron depleted CD4+ T-cells are similarly reported to have suppressed metabolic activity featuring suppressed pS6 and MYC, reduced mitochondrial membrane potential, mass and mROS in addition to reduced glycolysis and OXPHOS[15,21,22]. How iron deficiency exerts these effects in T-cell metabolism more generally remains unclear.

It is evident that iron depletion results in significant defects to T-cell activation, proliferation, and effector function in a variety of immunological contexts. While there are some suggestions that iron deficiency is suppressing metabolism, the specific impacts of iron scarcity on T-cell function are still largely uncharacterised. By utilising *in silico*, *in vitro* and *in vivo* methods, this thesis aims to explore the biochemical dependencies of T-cells on iron and understand how iron deficiency results in cellular dysfunction. By understanding how T-cells behave at a biochemical level during iron deficiency, it will better inform how iron modulation could be used to modify immunity in contexts such as autoimmunity, infection, and vaccination.

1.5 Aims of this study

The aims of this project:

1. Utilise existing datasets to explore how iron is used by immune cells *in silico*
2. Identify how iron scarcity affects global T-cell biochemical and metabolic signatures
3. Explore how iron deficiency impacts T-cell epigenetic and mitochondrial function
4. Modify T-cell responses to iron deficiency using nutritional, pharmacological, and genetic modulation

Each of these aims will be addressed in an independent results chapter.

1.6 References

1 Alberts, B. *et al.* in *Molecular Biology of the Cell* Ch. The Chemical Components of a Cell, (Garland Science, 2002).

2 Zoroddu, M. A. *et al.* The essential metals for humans: a brief overview. *J Inorg Biochem* **195**, 120-129 (2019). https://doi.org:10.1016/j.jinorgbio.2019.03.013

3 Archibald, F. Lactobacillus plantarum, an organism not requiring iron. *FEMS Microbiology Letters* **19**, 29-32 (1983). https://doi.org:10.1111/j.1574-6968.1983.tb00504.x

4 Posey, J. E. & Gherardini, F. C. Lack of a role for iron in the Lyme disease pathogen. *Science* **288**, 1651-1653 (2000). https://doi.org:10.1126/science.288.5471.1651

5 Sabine, D. B. & Vaselekos, J. Trace Element Requirements of Lactobacillus acidophilus. *Nature* **214**, 520-520 (1967). https://doi.org:10.1038/214520a0

6 Andreini, C., Putignano, V., Rosato, A. & Banci, L. The human iron-proteome. *Metallomics* **10**, 1223-1231 (2018). https://doi.org:10.1039/c8mt00146d

7 Ganz, T. Systemic iron homeostasis. *Physiol Rev* **93**, 1721-1741 (2013). https://doi.org:10.1152/physrev.00008.2013

8 Winterbourn, C. C. Toxicity of iron and hydrogen peroxide: the Fenton reaction. *Toxicology Letters* **82-83**, 969-974 (1995). https://doi.org:https://doi.org/10.1016/0378-4274(95)03532-X

9 Drakesmith, H. & Prentice, A. M. Hepcidin and the iron-infection axis. *Science* **338**, 768-772 (2012). https://doi.org:10.1126/science.1224577

10 Wilson, M. T. & Reeder, B. J. Oxygen-binding haem proteins. *Exp Physiol* **93**, 128-132 (2008). https://doi.org:10.1113/expphysiol.2007.039735

11 Collaborators, G. D. a. I. I. a. P. Global, regional, and national incidence, prevalence, and years lived with disability for 328 diseases and injuries for 195 countries, 1990-2016: a systematic analysis for the Global Burden of Disease Study 2016. *Lancet* **390**, 1211-1259 (2017). https://doi.org:10.1016/s0140-6736(17)32154-2

12 Pasricha, S. R., Tye-Din, J., Muckenthaler, M. U. & Swinkels, D. W. Iron deficiency. *Lancet* **397**, 233-248 (2021). https://doi.org:10.1016/s0140-6736(20)32594-0

13 Nairz, M. & Weiss, G. Iron in infection and immunity. *Mol Aspects Med* **75**, 100864 (2020). https://doi.org:10.1016/j.mam.2020.100864

14 Frost, J. N. *et al.* Hepcidin-Mediated Hypoferremia Disrupts Immune Responses to Vaccination and Infection. *Med (N Y)* **2**, 164-179.e112 (2021). https://doi.org:10.1016/j.medj.2020.10.004

15 Voss, K. *et al.* Elevated transferrin receptor impairs T cell metabolism and function in systemic lupus erythematosus. *Sci Immunol* **8**, eabq0178 (2023). https://doi.org:10.1126/sciimmunol.abq0178

16 Jiang, Y. *et al.* Iron-dependent histone 3 lysine 9 demethylation controls B cell proliferation and humoral immune responses. *Nat Commun* **10**, 2935 (2019). https://doi.org:10.1038/s41467-019-11002-5

17 Wideman, S. K. *et al.* Cellular iron governs the host response to malaria. *bioRxiv*, 2023.2002.2005.527208 (2023). https://doi.org:10.1101/2023.02.05.527208

18 Wang, Z. *et al.* Iron Drives T Helper Cell Pathogenicity by Promoting RNA-Binding Protein PCBP1-Mediated Proinflammatory Cytokine Production. *Immunity* **49**, 80-92.e87 (2018). https://doi.org:10.1016/j.immuni.2018.05.008

19 Li, L. *et al.* Iron deprivation restrains the differentiation and pathogenicity of T helper 17 cell. *J Leukoc Biol* **110**, 1057-1067 (2021). https://doi.org:10.1002/jlb.3ma0821-015r
20 Gao, X. *et al.* Iron-dependent epigenetic modulation promotes pathogenic T cell differentiation in lupus. *J Clin Invest* **132** (2022). https://doi.org:10.1172/jci152345
21 Lai, Y. *et al.* Iron controls T helper cell pathogenicity by promoting glucose metabolism in autoimmune myopathy. *Clin Transl Med* **12**, e999 (2022). https://doi.org:10.1002/ctm2.999
22 Yarosz, E. L. *et al.* Cutting Edge: Activation-Induced Iron Flux Controls CD4 T Cell Proliferation by Promoting Proper IL-2R Signaling and Mitochondrial Function. *J Immunol* **204**, 1708-1713 (2020). https://doi.org:10.4049/jimmunol.1901399
23 Knutson, M. & Wessling-Resnick, M. Iron metabolism in the reticuloendothelial system. *Crit Rev Biochem Mol Biol* **38**, 61-88 (2003). https://doi.org:10.1080/713609210
24 Donovan, A. *et al.* Positional cloning of zebrafish ferroportin1 identifies a conserved vertebrate iron exporter. *Nature* **403**, 776-781 (2000). https://doi.org:10.1038/35001596
25 McKie, A. T. *et al.* A novel duodenal iron-regulated transporter, IREG1, implicated in the basolateral transfer of iron to the circulation. *Mol Cell* **5**, 299-309 (2000). https://doi.org:10.1016/s1097-2765(00)80425-6
26 Abboud, S. & Haile, D. J. A novel mammalian iron-regulated protein involved in intracellular iron metabolism. *J Biol Chem* **275**, 19906-19912 (2000). https://doi.org:10.1074/jbc.M000713200
27 Knutson, M. D., Oukka, M., Koss, L. M., Aydemir, F. & Wessling-Resnick, M. Iron release from macrophages after erythrophagocytosis is up-regulated by ferroportin 1 overexpression and down-regulated by hepcidin. *Proc Natl Acad Sci U S A* **102**, 1324-1328 (2005). https://doi.org:10.1073/pnas.0409409102
28 Kelly, A. U., McSorley, S. T., Patel, P. & Talwar, D. Interpreting iron studies. *Bmj* **357**, j2513 (2017). https://doi.org:10.1136/bmj.j2513
29 Nemeth, E. *et al.* Hepcidin regulates cellular iron efflux by binding to ferroportin and inducing its internalization. *Science* **306**, 2090-2093 (2004). https://doi.org:10.1126/science.1104742
30 Siah, C. W., Trinder, D. & Olynyk, J. K. Iron overload. *Clin Chim Acta* **358**, 24-36 (2005). https://doi.org:10.1016/j.cccn.2005.02.022
31 Lim, P. J. *et al.* Nrf2 controls iron homeostasis in haemochromatosis and thalassaemia via Bmp6 and hepcidin. *Nat Metab* **1**, 519-531 (2019). https://doi.org:10.1038/s42255-019-0063-6
32 Canonne-Hergaux, F., Gruenheid, S., Ponka, P. & Gros, P. Cellular and subcellular localization of the Nramp2 iron transporter in the intestinal brush border and regulation by dietary iron. *Blood* **93**, 4406-4417 (1999).
33 Nemeth, E. *et al.* IL-6 mediates hypoferremia of inflammation by inducing the synthesis of the iron regulatory hormone hepcidin. *J Clin Invest* **113**, 1271-1276 (2004). https://doi.org:10.1172/jci20945
34 Armitage, A. E. *et al.* Hepcidin regulation by innate immune and infectious stimuli. *Blood* **118**, 4129-4139 (2011). https://doi.org:10.1182/blood-2011-04-351957
35 Besson-Fournier, C. *et al.* Induction of activin B by inflammatory stimuli up-regulates expression of the iron-regulatory peptide hepcidin through Smad1/5/8

signaling. *Blood* **120**, 431-439 (2012). https://doi.org:10.1182/blood-2012-02-411470

36 Verga Falzacappa, M. V. *et al.* STAT3 mediates hepatic hepcidin expression and its inflammatory stimulation. *Blood* **109**, 353-358 (2007). https://doi.org:10.1182/blood-2006-07-033969

37 Gardenghi, S., Grady, R. W. & Rivella, S. Anemia, ineffective erythropoiesis, and hepcidin: interacting factors in abnormal iron metabolism leading to iron overload in β-thalassemia. *Hematol Oncol Clin North Am* **24**, 1089-1107 (2010). https://doi.org:10.1016/j.hoc.2010.08.003

38 Shih, H. M., Wu, C. J. & Lin, S. L. Physiology and pathophysiology of renal erythropoietin-producing cells. *J Formos Med Assoc* **117**, 955-963 (2018). https://doi.org:10.1016/j.jfma.2018.03.017

39 Arezes, J. *et al.* Erythroferrone inhibits the induction of hepcidin by BMP6. *Blood* **132**, 1473-1477 (2018). https://doi.org:10.1182/blood-2018-06-857995

40 Steinbicker, A. U. *et al.* Perturbation of hepcidin expression by BMP type I receptor deletion induces iron overload in mice. *Blood* **118**, 4224-4230 (2011). https://doi.org:10.1182/blood-2011-03-339952

41 Muckenthaler, M. U., Rivella, S., Hentze, M. W. & Galy, B. A Red Carpet for Iron Metabolism. *Cell* **168**, 344-361 (2017). https://doi.org:10.1016/j.cell.2016.12.034

42 Dautry-Varsat, A. Receptor-mediated endocytosis: the intracellular journey of transferrin and its receptor. *Biochimie* **68**, 375-381 (1986). https://doi.org:10.1016/s0300-9084(86)80004-9

43 Fleming, M. D. *et al.* Nramp2 is mutated in the anemic Belgrade (b) rat: evidence of a role for Nramp2 in endosomal iron transport. *Proc Natl Acad Sci U S A* **95**, 1148-1153 (1998). https://doi.org:10.1073/pnas.95.3.1148

44 Liuzzi, J. P., Aydemir, F., Nam, H., Knutson, M. D. & Cousins, R. J. Zip14 (Slc39a14) mediates non-transferrin-bound iron uptake into cells. *Proc Natl Acad Sci U S A* **103**, 13612-13617 (2006). https://doi.org:10.1073/pnas.0606424103

45 Wang, C. Y. *et al.* ZIP8 is an iron and zinc transporter whose cell-surface expression is up-regulated by cellular iron loading. *J Biol Chem* **287**, 34032-34043 (2012). https://doi.org:10.1074/jbc.M112.367284

46 Müller, S. *et al.* CD44 regulates epigenetic plasticity by mediating iron endocytosis. *Nat Chem* **12**, 929-938 (2020). https://doi.org:10.1038/s41557-020-0513-5

47 Brissot, P. *et al.* Haemochromatosis. *Nat Rev Dis Primers* **4**, 18016 (2018). https://doi.org:10.1038/nrdp.2018.16

48 Finberg, K. E. *et al.* Mutations in TMPRSS6 cause iron-refractory iron deficiency anemia (IRIDA). *Nat Genet* **40**, 569-571 (2008). https://doi.org:10.1038/ng.130

49 Taher, A. T. & Saliba, A. N. Iron overload in thalassemia: different organs at different rates. *Hematology Am Soc Hematol Educ Program* **2017**, 265-271 (2017). https://doi.org:10.1182/asheducation-2017.1.265

50 Arezes, J. *et al.* Hepcidin-induced hypoferremia is a critical host defense mechanism against the siderophilic bacterium Vibrio vulnificus. *Cell Host Microbe* **17**, 47-57 (2015). https://doi.org:10.1016/j.chom.2014.12.001

51 Stefanova, D. *et al.* Endogenous hepcidin and its agonist mediate resistance to selected infections by clearing non-transferrin-bound iron. *Blood* **130**, 245-257 (2017). https://doi.org:10.1182/blood-2017-03-772715

52 Stefanova, D. *et al.* Hepcidin Protects against Lethal Escherichia coli Sepsis in Mice Inoculated with Isolates from Septic Patients. *Infect Immun* **86** (2018). https://doi.org:10.1128/iai.00253-18

53 Wilkinson, N. & Pantopoulos, K. The IRP/IRE system in vivo: insights from mouse models. *Front Pharmacol* **5**, 176 (2014). https://doi.org:10.3389/fphar.2014.00176

54 Fischbach, F. A. & Anderegg, J. W. An x-ray scattering study of ferritin and apoferritin. *J Mol Biol* **14**, 458-473 (1965). https://doi.org:10.1016/s0022-2836(65)80196-6

55 Mancias, J. D., Wang, X., Gygi, S. P., Harper, J. W. & Kimmelman, A. C. Quantitative proteomics identifies NCOA4 as the cargo receptor mediating ferritinophagy. *Nature* **509**, 105-109 (2014). https://doi.org:10.1038/nature13148

56 Philpott, C. C., Ryu, M. S., Frey, A. & Patel, S. Cytosolic iron chaperones: Proteins delivering iron cofactors in the cytosol of mammalian cells. *J Biol Chem* **292**, 12764-12771 (2017). https://doi.org:10.1074/jbc.R117.791962

57 Galmozzi, A. *et al.* PGRMC2 is an intracellular haem chaperone critical for adipocyte function. *Nature* **576**, 138-142 (2019). https://doi.org:10.1038/s41586-019-1774-2

58 Salahudeen, A. A. *et al.* An E3 ligase possessing an iron-responsive hemerythrin domain is a regulator of iron homeostasis. *Science* **326**, 722-726 (2009). https://doi.org:10.1126/science.1176326

59 Vashisht, A. A. *et al.* Control of iron homeostasis by an iron-regulated ubiquitin ligase. *Science* **326**, 718-721 (2009). https://doi.org:10.1126/science.1176333

60 Wang, J. & Pantopoulos, K. Regulation of cellular iron metabolism. *Biochem J* **434**, 365-381 (2011). https://doi.org:10.1042/bj20101825

61 Dandekar, T. *et al.* Identification of a novel iron-responsive element in murine and human erythroid delta-aminolevulinic acid synthase mRNA. *Embo j* **10**, 1903-1909 (1991). https://doi.org:10.1002/j.1460-2075.1991.tb07716.x

62 Gray, N. K., Pantopoulos, K., Dandekar, T., Ackrell, B. A. & Hentze, M. W. Translational regulation of mammalian and Drosophila citric acid cycle enzymes via iron-responsive elements. *Proc Natl Acad Sci U S A* **93**, 4925-4930 (1996). https://doi.org:10.1073/pnas.93.10.4925

63 Sanchez, M. *et al.* Iron regulation and the cell cycle: identification of an iron-responsive element in the 3'-untranslated region of human cell division cycle 14A mRNA by a refined microarray-based screening strategy. *J Biol Chem* **281**, 22865-22874 (2006). https://doi.org:10.1074/jbc.M603876200

64 Cmejla, R., Petrak, J. & Cmejlova, J. A novel iron responsive element in the 3'UTR of human MRCKalpha. *Biochem Biophys Res Commun* **341**, 158-166 (2006). https://doi.org:10.1016/j.bbrc.2005.12.155

65 Shah, Y. M. & Xie, L. Hypoxia-inducible factors link iron homeostasis and erythropoiesis. *Gastroenterology* **146**, 630-642 (2014). https://doi.org:10.1053/j.gastro.2013.12.031

66 Taylor, C. T. & Scholz, C. C. The effect of HIF on metabolism and immunity. *Nat Rev Nephrol* **18**, 573-587 (2022). https://doi.org:10.1038/s41581-022-00587-8

67 Cho, E. A. *et al.* Differential in vitro and cellular effects of iron chelators for hypoxia inducible factor hydroxylases. *J Cell Biochem* **114**, 864-873 (2013). https://doi.org:10.1002/jcb.24423

68 Puig, S., Askeland, E. & Thiele, D. J. Coordinated remodeling of cellular metabolism during iron deficiency through targeted mRNA degradation. *Cell* **120**, 99-110 (2005). https://doi.org:10.1016/j.cell.2004.11.032

69 Bayeva, M. *et al.* mTOR regulates cellular iron homeostasis through tristetraprolin. *Cell Metab* **16**, 645-657 (2012). https://doi.org:10.1016/j.cmet.2012.10.001

70 Sato, T. *et al.* mRNA-binding protein tristetraprolin is essential for cardiac response to iron deficiency by regulating mitochondrial function. *Proc Natl Acad Sci U S A* **115**, E6291-e6300 (2018). https://doi.org:10.1073/pnas.1804701115

71 Chen, J. J. Regulation of protein synthesis by the heme-regulated eIF2alpha kinase: relevance to anemias. *Blood* **109**, 2693-2699 (2007). https://doi.org:10.1182/blood-2006-08-041830

72 Fessler, E. *et al.* A pathway coordinated by DELE1 relays mitochondrial stress to the cytosol. *Nature* **579**, 433-437 (2020). https://doi.org:10.1038/s41586-020-2076-4

73 Guo, X. *et al.* Mitochondrial stress is relayed to the cytosol by an OMA1-DELE1-HRI pathway. *Nature* **579**, 427-432 (2020). https://doi.org:10.1038/s41586-020-2078-2

74 Abdel-Nour, M. *et al.* The heme-regulated inhibitor is a cytosolic sensor of protein misfolding that controls innate immune signaling. *Science* **365** (2019). https://doi.org:10.1126/science.aaw4144

75 Paul, B. T., Manz, D. H., Torti, F. M. & Torti, S. V. Mitochondria and Iron: current questions. *Expert Rev Hematol* **10**, 65-79 (2017). https://doi.org:10.1080/17474086.2016.1268047

76 Lane, D. J. *et al.* Cellular iron uptake, trafficking and metabolism: Key molecules and mechanisms and their roles in disease. *Biochim Biophys Acta* **1853**, 1130-1144 (2015). https://doi.org:10.1016/j.bbamcr.2015.01.021

77 Sheftel, A. D., Zhang, A. S., Brown, C., Shirihai, O. S. & Ponka, P. Direct interorganellar transfer of iron from endosome to mitochondrion. *Blood* **110**, 125-132 (2007). https://doi.org:10.1182/blood-2007-01-068148

78 Wolff, N. A., Garrick, L. M., Zhao, L., Garrick, M. D. & Thévenod, F. Mitochondria represent another locale for the divalent metal transporter 1 (DMT1). *Channels (Austin)* **8**, 458-466 (2014). https://doi.org:10.4161/19336950.2014.956564

79 Wolff, N. A. *et al.* Evidence for mitochondrial localization of divalent metal transporter 1 (DMT1). *Faseb j* **28**, 2134-2145 (2014). https://doi.org:10.1096/fj.13-240564

80 Shaw, G. C. *et al.* Mitoferrin is essential for erythroid iron assimilation. *Nature* **440**, 96-100 (2006). https://doi.org:10.1038/nature04512

81 Paradkar, P. N., Zumbrennen, K. B., Paw, B. H., Ward, D. M. & Kaplan, J. Regulation of mitochondrial iron import through differential turnover of mitoferrin 1 and mitoferrin 2. *Mol Cell Biol* **29**, 1007-1016 (2009). https://doi.org:10.1128/mcb.01685-08

82 Levi, S. *et al.* A human mitochondrial ferritin encoded by an intronless gene. *J Biol Chem* **276**, 24437-24440 (2001). https://doi.org:10.1074/jbc.C100141200

83 Arosio, P. & Levi, S. Cytosolic and mitochondrial ferritins in the regulation of cellular iron homeostasis and oxidative damage. *Biochim Biophys Acta* **1800**, 783-792 (2010). https://doi.org:10.1016/j.bbagen.2010.02.005

84 Pantopoulos, K. Iron, FRDA, and intermediary metabolism. *Blood* **137**, 1994-1995 (2021). https://doi.org:10.1182/blood.2021010835

85 Riddle, R. D., Yamamoto, M. & Engel, J. D. Expression of delta-aminolevulinate synthase in avian cells: separate genes encode erythroid-specific and nonspecific isozymes. *Proc Natl Acad Sci U S A* **86**, 792-796 (1989). https://doi.org:10.1073/pnas.86.3.792

86 Wu, C. K. *et al.* The 2.0 A structure of human ferrochelatase, the terminal enzyme of heme biosynthesis. *Nat Struct Biol* **8**, 156-160 (2001). https://doi.org:10.1038/84152

87 Chiabrando, D. *et al.* The mitochondrial heme exporter FLVCR1b mediates erythroid differentiation. *J Clin Invest* **122**, 4569-4579 (2012). https://doi.org:10.1172/jci62422

88 Lill, R. From the discovery to molecular understanding of cellular iron-sulfur protein biogenesis. *Biol Chem* **401**, 855-876 (2020). https://doi.org:10.1515/hsz-2020-0117

89 Shi, R., Hou, W., Wang, Z. Q. & Xu, X. Biogenesis of Iron-Sulfur Clusters and Their Role in DNA Metabolism. *Front Cell Dev Biol* **9**, 735678 (2021). https://doi.org:10.3389/fcell.2021.735678

90 Yeeles, J. T., Cammack, R. & Dillingham, M. S. An iron-sulfur cluster is essential for the binding of broken DNA by AddAB-type helicase-nucleases. *J Biol Chem* **284**, 7746-7755 (2009). https://doi.org:10.1074/jbc.M808526200

91 Weiner, B. E. *et al.* An iron-sulfur cluster in the C-terminal domain of the p58 subunit of human DNA primase. *J Biol Chem* **282**, 33444-33451 (2007). https://doi.org:10.1074/jbc.M705826200

92 Stubbe, J. Di-iron-tyrosyl radical ribonucleotide reductases. *Curr Opin Chem Biol* **7**, 183-188 (2003). https://doi.org:10.1016/s1367-5931(03)00025-5

93 Kolberg, M., Strand, K. R., Graff, P. & Andersson, K. K. Structure, function, and mechanism of ribonucleotide reductases. *Biochim Biophys Acta* **1699**, 1-34 (2004). https://doi.org:10.1016/j.bbapap.2004.02.007

94 McGoldrick, J. P., Yeh, Y. C., Solomon, M., Essigmann, J. M. & Lu, A. L. Characterization of a mammalian homolog of the Escherichia coli MutY mismatch repair protein. *Mol Cell Biol* **15**, 989-996 (1995). https://doi.org:10.1128/mcb.15.2.989

95 Martin, S. K. & Wood, R. D. DNA polymerase ζ in DNA replication and repair. *Nucleic Acids Res* **47**, 8348-8361 (2019). https://doi.org:10.1093/nar/gkz705

96 Islam, M. S., Leissing, T. M., Chowdhury, R., Hopkinson, R. J. & Schofield, C. J. 2-Oxoglutarate-Dependent Oxygenases. *Annu Rev Biochem* **87**, 585-620 (2018). https://doi.org:10.1146/annurev-biochem-061516-044724

97 Machalz, D., Pach, S., Bermudez, M., Bureik, M. & Wolber, G. Structural insights into understudied human cytochrome P450 enzymes. *Drug Discov Today* **26**, 2456-2464 (2021). https://doi.org:10.1016/j.drudis.2021.06.006

98 Chandrasekharan, N. V. & Simmons, D. L. The cyclooxygenases. *Genome Biol* **5**, 241 (2004). https://doi.org:10.1186/gb-2004-5-9-241

99 Mashima, R. & Okuyama, T. The role of lipoxygenases in pathophysiology; new insights and future perspectives. *Redox Biol* **6**, 297-310 (2015). https://doi.org:10.1016/j.redox.2015.08.006

100 Lone, A. M. & Taskén, K. Proinflammatory and immunoregulatory roles of eicosanoids in T cells. *Front Immunol* **4**, 130 (2013). https://doi.org:10.3389/fimmu.2013.00130

101 Ndrepepa, G. Myeloperoxidase - A bridge linking inflammation and oxidative stress with cardiovascular disease. *Clin Chim Acta* **493**, 36-51 (2019). https://doi.org:10.1016/j.cca.2019.02.022

102 Bedard, K. & Krause, K. H. The NOX family of ROS-generating NADPH oxidases: physiology and pathophysiology. *Physiol Rev* **87**, 245-313 (2007). https://doi.org:10.1152/physrev.00044.2005

103 Dunham, N. P. & Arnold, F. H. Nature's Machinery, Repurposed: Expanding the Repertoire of Iron-Dependent Oxygenases. *ACS Catal* **10**, 12239-12255 (2020). https://doi.org:10.1021/acscatal.0c03606

104 Kalisch-Smith, J. I. *et al.* Maternal iron deficiency perturbs embryonic cardiovascular development in mice. *Nat Commun* **12**, 3447 (2021). https://doi.org:10.1038/s41467-021-23660-5

105 Ramos, E. *et al.* Minihepcidins prevent iron overload in a hepcidin-deficient mouse model of severe hemochromatosis. *Blood* **120**, 3829-3836 (2012). https://doi.org:10.1182/blood-2012-07-440743

106 Drakesmith, H. *et al.* Resistance to hepcidin is conferred by hemochromatosis-associated mutations of ferroportin. *Blood* **106**, 1092-1097 (2005). https://doi.org:10.1182/blood-2005-02-0561

107 Ibrahim, O. & O'Sullivan, J. Iron chelators in cancer therapy. *Biometals* **33**, 201-215 (2020). https://doi.org:10.1007/s10534-020-00243-3

108 Jabara, H. H. *et al.* A missense mutation in TFRC, encoding transferrin receptor 1, causes combined immunodeficiency. *Nat Genet* **48**, 74-78 (2016). https://doi.org:10.1038/ng.3465

109 Ghosh, M. C., Zhang, D. L. & Rouault, T. A. Iron misregulation and neurodegenerative disease in mouse models that lack iron regulatory proteins. *Neurobiol Dis* **81**, 66-75 (2015). https://doi.org:10.1016/j.nbd.2015.02.026

110 Trowbridge, I. S. & Domingo, D. L. Anti-transferrin receptor monoclonal antibody and toxin-antibody conjugates affect growth of human tumour cells. *Nature* **294**, 171-173 (1981). https://doi.org:10.1038/294171a0

111 Petzer, V. *et al.* A fully human anti-BMP6 antibody reduces the need for erythropoietin in rodent models of the anemia of chronic disease. *Blood* **136**, 1080-1090 (2020). https://doi.org:10.1182/blood.2019004653

112 Zhou, X. Y. *et al.* HFE gene knockout produces mouse model of hereditary hemochromatosis. *Proc Natl Acad Sci U S A* **95**, 2492-2497 (1998). https://doi.org:10.1073/pnas.95.5.2492

113 Chaplin, D. D. Overview of the immune response. *J Allergy Clin Immunol* **125**, S3-23 (2010). https://doi.org:10.1016/j.jaci.2009.12.980

114 Kawasaki, T. & Kawai, T. Toll-like receptor signaling pathways. *Front Immunol* **5**, 461 (2014). https://doi.org:10.3389/fimmu.2014.00461

115 Khan, F. A., Fisher, M. A. & Khakoo, R. A. Association of hemochromatosis with infectious diseases: expanding spectrum. *Int J Infect Dis* **11**, 482-487 (2007). https://doi.org:10.1016/j.ijid.2007.04.007

116 Ni, S., Yuan, Y., Kuang, Y. & Li, X. Iron Metabolism and Immune Regulation. *Front Immunol* **13**, 816282 (2022). https://doi.org:10.3389/fimmu.2022.816282

117 Soares, M. P. & Hamza, I. Macrophages and Iron Metabolism. *Immunity* **44**, 492-504 (2016). https://doi.org:10.1016/j.immuni.2016.02.016

118 Cronin, S. J. F., Woolf, C. J., Weiss, G. & Penninger, J. M. The Role of Iron Regulation in Immunometabolism and Immune-Related Disease. *Front Mol Biosci* **6**, 116 (2019). https://doi.org:10.3389/fmolb.2019.00116

119 Arnhold, J., Furtmüller, P. G. & Obinger, C. Redox properties of myeloperoxidase. *Redox Rep* **8**, 179-186 (2003). https://doi.org:10.1179/135100003225002664

120 Vazquez-Torres, A., Jones-Carson, J., Mastroeni, P., Ischiropoulos, H. & Fang, F. C. Antimicrobial actions of the NADPH phagocyte oxidase and inducible nitric oxide synthase in experimental salmonellosis. I. Effects on microbial killing by activated peritoneal macrophages in vitro. *J Exp Med* **192**, 227-236 (2000). https://doi.org:10.1084/jem.192.2.227

121 Frost, J. N. *et al.* Plasma iron controls neutrophil production and function. *Sci Adv* **8**, eabq5384 (2022). https://doi.org:10.1126/sciadv.abq5384

122 Recalcati, S. *et al.* Differential regulation of iron homeostasis during human macrophage polarized activation. *Eur J Immunol* **40**, 824-835 (2010). https://doi.org:10.1002/eji.200939889

123 Sindrilaru, A. *et al.* An unrestrained proinflammatory M1 macrophage population induced by iron impairs wound healing in humans and mice. *J Clin Invest* **121**, 985-997 (2011). https://doi.org:10.1172/jci44490

124 Pereira, M. *et al.* Acute Iron Deprivation Reprograms Human Macrophage Metabolism and Reduces Inflammation In Vivo. *Cell Rep* **28**, 498-511.e495 (2019). https://doi.org:10.1016/j.celrep.2019.06.039

125 Glas, R. *et al.* Recruitment and activation of natural killer (NK) cells in vivo determined by the target cell phenotype. An adaptive component of NK cell-mediated responses. *J Exp Med* **191**, 129-138 (2000). https://doi.org:10.1084/jem.191.1.129

126 Littwitz-Salomon, E. *et al.* Metabolic requirements of NK cells during the acute response against retroviral infection. *Nat Commun* **12**, 5376 (2021). https://doi.org:10.1038/s41467-021-25715-z

127 Liu, K. Dendritic Cells. *Encyclopedia of Cell Biology*, 741-749 (2016). https://doi.org:10.1016/b978-0-12-394447-4.30111-0

128 Bessman, N. J. *et al.* Dendritic cell-derived hepcidin sequesters iron from the microbiota to promote mucosal healing. *Science* **368**, 186-189 (2020). https://doi.org:10.1126/science.aau6481

129 Lippitsch, A., Chukovetskyi, Y., Baal, N., Bein, G. & Hackstein, H. Unique high and homogenous surface expression of the transferrin receptor CD71 on murine plasmacytoid dendritic cells in different tissues. *Cell Immunol* **316**, 41-52 (2017). https://doi.org:10.1016/j.cellimm.2017.03.005

130 Gaud, G., Lesourne, R. & Love, P. E. Regulatory mechanisms in T cell receptor signalling. *Nat Rev Immunol* **18**, 485-497 (2018). https://doi.org:10.1038/s41577-018-0020-8

131 Kaech, S. M., Wherry, E. J. & Ahmed, R. Effector and memory T-cell differentiation: implications for vaccine development. *Nat Rev Immunol* **2**, 251-262 (2002). https://doi.org:10.1038/nri778

132 Zhang, N. & Bevan, M. J. CD8(+) T cells: foot soldiers of the immune system. *Immunity* **35**, 161-168 (2011). https://doi.org:10.1016/j.immuni.2011.07.010

133 Shyer, J. A., Flavell, R. A. & Bailis, W. Metabolic signaling in T cells. *Cell Res* **30**, 649-659 (2020). https://doi.org:10.1038/s41422-020-0379-5

134 Howden, A. J. M. *et al.* Quantitative analysis of T cell proteomes and environmental sensors during T cell differentiation. *Nat Immunol* **20**, 1542-1554 (2019). https://doi.org:10.1038/s41590-019-0495-x

135 Geginat, J. *et al.* Plasticity of human CD4 T cell subsets. *Front Immunol* **5**, 630 (2014). https://doi.org:10.3389/fimmu.2014.00630

136 Xu, S. & Cao, X. Interleukin-17 and its expanding biological functions. *Cell Mol Immunol* **7**, 164-174 (2010). https://doi.org:10.1038/cmi.2010.21

137 Walker, J. A. & McKenzie, A. N. J. T(H)2 cell development and function. *Nat Rev Immunol* **18**, 121-133 (2018). https://doi.org:10.1038/nri.2017.118

138 Cyster, J. G. & Allen, C. D. C. B Cell Responses: Cell Interaction Dynamics and Decisions. *Cell* **177**, 524-540 (2019). https://doi.org:10.1016/j.cell.2019.03.016

139 Forthal, D. N. Functions of Antibodies. *Microbiol Spectr* **2**, 1-17 (2014).

140 Futran, J., Kemp, J. D., Field, E. H., Vora, A. & Ashman, R. F. Transferrin receptor synthesis is an early event in B cell activation. *J Immunol* **143**, 787-792 (1989).

141 Aljohani, A. H. *et al.* Clinical and Immunological Characterization of Combined Immunodeficiency Due to TFRC Mutation in Eight Patients. *J Clin Immunol* **40**, 1103-1110 (2020). https://doi.org:10.1007/s10875-020-00851-1

142 Schwartz, A. J. *et al.* Hepcidin sequesters iron to sustain nucleotide metabolism and mitochondrial function in colorectal cancer epithelial cells. *Nature Metabolism* **3**, 969-982 (2021). https://doi.org:10.1038/s42255-021-00406-7

143 Stoffel, N. U. *et al.* Iron Deficiency Anemia at Time of Vaccination Predicts Decreased Vaccine Response and Iron Supplementation at Time of Vaccination Increases Humoral Vaccine Response: A Birth Cohort Study and a Randomized Trial Follow-Up Study in Kenyan Infants. *Front Immunol* **11**, 1313 (2020). https://doi.org:10.3389/fimmu.2020.01313

144 Shah, A., Frost, J. N., Aaron, L., Donovan, K. & Drakesmith, H. Systemic hypoferremia and severity of hypoxemic respiratory failure in COVID-19. *Crit Care* **24**, 320 (2020). https://doi.org:10.1186/s13054-020-03051-w

145 Pfeifhofer-Obermair, C. *et al.* Regulation of Th1 T Cell Differentiation by Iron via Upregulation of T Cell Immunoglobulin and Mucin Containing Protein-3 (TIM-3). *Front Immunol* **12**, 637809 (2021). https://doi.org:10.3389/fimmu.2021.637809

146 Takei, F. Inhibition of mixed lymphocyte response by a rat monoclonal antibody to a novel murine lymphocyte activation antigen (MALA-2). *J Immunol* **134**, 1403-1407 (1985).

147 Kemp, J. D. *et al.* Inhibition of lymphocyte activation with anti-transferrin receptor Mabs: a comparison of three reagents and further studies of their range of effects and mechanism of action. *Cell Immunol* **122**, 218-230 (1989). https://doi.org:10.1016/0008-8749(89)90162-7

148 Kemp, J. D. *et al.* Role of the transferrin receptor in lymphocyte growth: a rat IgG monoclonal antibody against the murine transferrin receptor produces highly selective inhibition of T and B cell activation protocols. *J Immunol* **138**, 2422-2426 (1987).

149 Thorson, J. A., Smith, K. M., Gomez, F., Naumann, P. W. & Kemp, J. D. Role of iron in T cell activation: TH1 clones differ from TH2 clones in their sensitivity to inhibition of DNA synthesis caused by IgG Mabs against the transferrin receptor and the iron chelator deferoxamine. *Cell Immunol* **134**, 126-137 (1991). https://doi.org:10.1016/0008-8749(91)90336-a

150 Leung, S. *et al.* Differential inhibition of inducible T cell cytokine secretion by potent iron chelators. *J Biomol Screen* **10**, 157-167 (2005). https://doi.org:10.1177/1087057104272394

Chapter 2

2 Methods[1]

2.1 Mathematical Modelling

2.1.1 Identifying iron interacting proteins

A list of human iron interacting proteins was obtained from Andreini *et al*[1]. Using the Uniprot IDs, the corresponding gene names were obtained with the Uniprot mapping tool[2]. Mouse homologues were subsequently identified using the Ensembl BioMart tool[3] selecting for comparison to the Ensembl Genes 100 database, Human genes (GRCh38.p13) dataset. Mouse homologues were identified for 88% (349/398) of the human iron interacting proteins. Manual searches were conducted where Ensembl was unable to identify murine homologues and successfully identified a further 8 matches. 23 human iron interacting proteins were found to have no corresponding mouse homologues. Poor annotation prevented the identification of matches for 18 proteins (ex// CYP2C, FAS2P1, DKFZp686G0638). Cofactor information regarding iron atom to protein stoichiometry was acquired by searching of the Uniprot database for the cofactor terms: 4Fe-4S, 3Fe-3S, 2Fe-2S, heme, Fe2+, Fe3+. It should be noted that the list of mouse iron interacting proteins is unlikely to include the full set of iron interacting proteins. The possibility exists that mouse iron interacting proteins with no human homologue or poorly annotated homologues were not identified. Conversely, it is possible that murine homologues of human iron interacting proteins may not be iron interacting.

Iron interacting proteins were identified in the Howden *et al*[4] and Rieckmann *et al*[5] proteomics datasets. To identify iron interacting proteins in these datasets, the appropriate lists of iron interacting proteins (mouse or human) were intersected with the lists of proteins detected. It should be noted the Howden *et al*[4] dataset uses the alternative name NARFL for the gene CIAO3 and therefore NARFL was added to the list of iron interacting proteins. Hemoglobin proteins (HBA1, HBB, HBD, HBG1, HBG2, HBM, HBQ1, and HBZ) were removed from the analysis as these proteins should not be

[1] Some of text in this chapter has been previously published in Teh *et al*, Frontiers of Immunology, 2021 (DOI: 10.3389/fimmu.2021.714613)

observed in immune cells and their presence is likely indicative of red blood cell contamination.

For the Howden *et al*[4] dataset, pathway enrichment for gene ontology (GO) biological processes was conducted using the gProlifer algorithm[6] designed for unranked lists. Term size was limited to 3-500 genes with a significance threshold set to a Benjamini-Hochberg false discovery rate (FDR) of <0.05.

2.1.2 Predicting immune cell iron content

Cellular iron content was predicted per cell for both the Howden *et al*[4] and Rieckmann *et al*[5] datasets. Where possible, iron atom to protein stoichiometry values were obtained from the Uniprot database under cofactor information. Where iron atoms per protein information was unavailable, conservative estimates of 1 atom for iron ion and heme interacting proteins and 2 atoms for Fe-S cluster proteins were used. Iron atom per protein values were multiplied by the protein copy number values to produce estimates of iron atoms per protein species. The total number of iron atoms per cell was calculated as the sum of iron atoms per protein species across all proteins.

$$\frac{\text{Iron atoms}}{\text{Cell}} = \sum[(\text{Protein species copy number}) \times (\frac{\text{Iron atoms}}{\text{protein}})]$$

To calculate the iron counts per cell by iron interaction, iron interaction classifications provided by Andreini *et al*[1] were used. To stratify iron counts by pathway in the Howden *et al*[4] dataset, GO terms were used: iron ion homeostasis (GO:0055072), DNA replication (GO:0006260), iron-sulfur cluster assembly (GO:0016226), oxidative phosphorylation (GO:0006119), aerobic respiration (GO:0009060), histone demethylation (GO:0016577) and DNA demethylation (GO:0080111). GO terms for oxidative phosphorylation and aerobic respiration were grouped due to discrepancies for each term. In cases where GO terms overlapped, genes were assigned to the gene set determined to be most suitable. ACO1, GLRX3, ISCU and NUBP1 were allocated to iron-sulfur cluster assembly and IREB2 was allocated to iron ion homeostasis.

For allocation of iron counts by pathway in the Rieckmann *et al*[5] dataset, GO and reactome terms were used: aerobic respiration (GO:0009060), DNA replication (GO:0006260), cellular iron ion homeostasis (GO:0006879), iron sulfur cluster assembly (GO:0016226), demethylation (GO:0070988), fatty acid metabolic process

(GO:0006631), neutrophil degranulation (R-HSA-6798695). GO terms for cellular iron ion homeostasis and iron sulfur cluster assembly were combined as a new set called "iron pathways". Where terms overlapped, proteins were assigned to pathways given the best fit given the current literature. ACO1, FTH1, FTL, FXN, IREB2, ISCU, LCN2 and SLC11A1 were assigned to iron pathways. CAT, CYP1A and CYP2D6 was assigned to neutrophil degranulation. ALOX5, GSTP1 and PTGES2 were assigned to fatty acid metabolic process.

2.1.3 Modelling iron uptake based on transferrin saturation

Transferrin saturation (TSAT) values were derived from transferrin (Tf) and serum iron concentrations using the following equations from Yamanishi *et al*[7]:

$$\text{TSAT}(\%) = \frac{[\text{Serum Fe}]\ \left(\frac{\mu\text{mol}}{\text{L}}\right)}{\text{Total iron binding capacity (TIBC)}\ \left(\frac{\mu\text{mol}}{\text{L}}\right)}$$

$$\text{TIBC}\left(\frac{\mu\text{mol}}{\text{L}}\right) = [\text{Tf, g/L}] \times \frac{1\ \text{mol Tf}}{79570\text{g Tf}} \times \frac{10^6 \mu\text{mol}}{\text{mol}} \times 2\ \text{Fe binding sites}$$

The following equations directly derived from Chasteen, *et al* and Aisen, *et al*[8,9] were used to calculate the relative proportions of the 4 Tf forms (apotransferrin (apoTf): 0 iron atoms, C terminus monoferric transferrin (monoTf): 1 iron atom, N terminus monoTf: 1 iron atom, diferric transferrin (diTf): 2 iron atoms) given any TSAT value. **It should be noted that [Fe] is a RELATIVE unitless value and thus is only useful from within this set of equations.**

Relative association constants for Fe binding to the C and N termini of Tf	
k'_{1N} = 1st atom N terminus binding	k'_{1C} = 1st atom C terminus binding
k'_{2N} = 2nd atom N terminus binding	k'_{2C} = 2nd atom C terminus binding

$$X_A = \text{mole fraction of apoTf} = \frac{1}{1 + (k'_{1N} + k'_{1C})[\text{Fe}] + k'_{1N}k'_{2C}[\text{Fe}]^2}$$

$$X_N = \text{mole fraction of N terminus monoTf} = \frac{1}{1 + \frac{k'_{1C}}{k'_{1N}} + \frac{1}{k'_{1N}[\text{Fe}]} + k'_{2C}[\text{Fe}]}$$

$$X_C = \text{mole fraction of C terminus monoTf} = \frac{1}{1 + \frac{k'_{1N}}{k'_{1C}} + \frac{1}{k'_{1C}[Fe]} + k'_{2N}[Fe]}$$

$$X_D = \text{mole fraction of diTf} = \frac{1}{1 + \frac{k'_{2C} + k'_{2N}}{k'_{2C}k'_{2N}[Fe]} + \frac{1}{k'_{1C}k'_{1N}[Fe]^2}}$$

$$\text{TSAT (\%)} = 50\,(X_N + X_C + 2X_D)$$

Each molar fraction equation was substituted into the TSAT equation as follows:

$$\text{TSAT (\%)} = 50\left[\frac{1}{1 + \frac{k'_{1C}}{k'_{1N}} + \frac{1}{k'_{1N}[Fe]} + k'_{2C}[Fe]} + \frac{1}{1 + \frac{k'_{1N}}{k'_{1C}} + \frac{1}{k'_{1C}[Fe]} + k'_{2N}[Fe]} + \frac{2}{1 + \frac{k'_{2C} + k'_{2N}}{k'_{2C}k'_{2N}[Fe]} + \frac{1}{k'_{1C}k'_{1N}[Fe]^2}}\right]$$

The following literature values for relative association constants of iron for Tf were substituted into the equation which was rearranged and solved for the value [Fe][8]:

$k'_{1N} = 1.00$	$k'_{1C} = 2.5 \pm 0.30$	$k'_{2N} = 0.66 \pm 0.07$	$k'_{2C} = 1.60 \pm 0.30$

Using the calculated [Fe] value → the values for X_A, X_N, X_C, X_D could be determined, giving the relative molar frequencies of each Tf form. Using Tf concentration ranging from 1-4g/L, estimates of actual concentrations for each Tf form were calculated[10]:

$$[\text{apoTf, mol/L}] = [\text{Tf, g/L}] \times X_A \times \frac{\text{mol}}{79570\text{g Tf}}$$

$$[\text{C terminus monoTf, mol/L}] = [\text{Tf, g/L}] \times X_C \times \frac{\text{mol}}{79570\text{g Tf}}$$

$$[\text{N terminus monoTf, mol/L}] = [\text{Tf, g/L}] \times X_N \times \frac{\text{mol}}{79570\text{g Tf}}$$

$$[\text{diTf, mol/L}] = [\text{Tf, g/L}] \times X_D \times \frac{\text{mol}}{79570\text{g Tf}}$$

To determine the relative probabilities of each Tf form binding to TFRC, literature values for association constants for Tf binding to the Tf receptor were used, substituting in the calculated concentrations for each Tf form[11].

$k_{apo} = \frac{4.6 \times 10^6}{M}$	$k_{mono\ C} = \frac{2.5 \times 10^7}{M}$	$k_{mono\ N} = \frac{2.8 \times 10^7}{M}$	$k_{di} = \frac{1.1 \times 10^8}{M}$

$$k_{apo} = \frac{4.6 \times 10^6}{M} \times [\text{apoTf, mol/L}]$$

$$k_{mono\ C} = \frac{2.5 \times 10^7}{M} \times [\text{C terminus monoTf, mol/L}]$$

$$k_{mono\ N} = \frac{2.8 \times 10^7}{M} \times [\text{N terminus monoTf, mol/L}]$$

$$k_{di} = \frac{1.1 \times 10^8}{M} \times [\text{diTf, mol/L}]$$

$$P(k_{apo}) = \frac{k_{apo}}{k_{apo} + k_{mono\ C} + k_{mono\ N} + k_{di}}$$

$$P(k_{mono\ C}) = \frac{k_{mono\ C}}{k_{apo} + k_{mono\ C} + k_{mono\ N} + k_{di}}$$

$$P(k_{mono\ N}) = \frac{k_{mono\ N}}{k_{apo} + k_{mono\ C} + k_{mono\ N} + k_{di}}$$

$$P(k_{di}) = \frac{k_{di}}{k_{apo} + k_{mono\ C} + k_{mono\ N} + k_{di}}$$

The weighted iron uptake and cycle time per TFRC protein was calculated as the probability of each Tf form binding to TFRC multiplied by the corresponding number of iron atoms or cycle time. The apoTf cycling time of 60 minutes was derived from Nuñez *et al*[12]. The diTf cycling time of 14.53 minutes was estimated as the average of cycling times described by 6 different methods in Nuñez *et al*[12] and reviewed by Mayle *et al*[13].

monoTf cycling times were assumed to fall between diTf and apoTf cycling times at an intermediate 37.265 minutes as literature values could not be found.

$$\text{iron uptake} = \left(0 \times P(k_{apo})\right) + \left(1 \times P(k_{mono\,C})\right) + \left(1 \times P(k_{mono\,N})\right) + \left(2 \times P(k_{di})\right)$$

$$\text{cycle time} = \left(60\ \text{min} \times \left(k_{apo}\right)\right) + \left(37.265\ \text{min} \times (k_{mono\,C})\right) + \left(37.265\ \text{min} \times P(k_{mono\,N})\right) + \left(14.53\ \text{min} \times P(k_{di})\right)$$

Iron need was defined as the difference in iron content estimates between 0 hours and 24 hours post-activation. The time required to uptake the calculated "iron need" was calculated using the Howden *et al* average TFRC copy-number at 24 hours, the iron uptake and cycle time values:

$$\text{iron acquired in 1h} = \text{TFRC copy number} \times \text{iron uptake} \times \left[\frac{60\ \text{min}}{\text{cycle time}}\right]$$

$$\text{Time required to meet iron need} = \frac{\text{"Iron need"}}{\text{Iron acquired in 1h}}$$

2.2 Mice

Animal work was completed under the authority of the UK home office project and personal licenses granted under the Animals (Scientific Procedures) Act (ASPA) 1986. Mice were housed in individually ventilated cages. OT-I CD45.1 mice were acquired from Vincenzo Cerundolo and Audrey Gerard, University of Oxford. SAMHD1-KO mice were obtained from Jan Rehwinkel, University of Oxford. C57BL6/J mice were purchased from Envigo. Mice were euthanised using a rising concentration of CO_2 followed by cervical dislocation.

2.3 Cell culture

2.3.1 Media

R10 media was prepared with RPMI 1640 media (Gibco, 21875034), 10% fetal bovine serum (FBS, Sigma Aldrich, 0001661628), 1% penicillin/streptomycin (Sigma, P0781-100ML) and 1% glutamine (Sigma, G7513-100ML).

Iron free media was prepared as described for R10, however, FBS was substituted with 10% panexin NTS iron free serum substitute (Pan Biotech, P04-95080). Iron free media was supplemented with set concentrations of human holotransferrin (holoTf, R&D systems, 2914-HT-001G/Sigma-Aldrich, T0665) ranging from 0.0002-0.625 mg/mL. Human apotransferrin (R&D systems, 3188-AT-001G/Sigma-Aldrich, T1147) was added to ensure a total transferrin concentration of 1.2mg/mL was maintained.

2.3.2 T-cell activation

Plates for T-cell activation were coated with 5μg/mL α-CD3 (Biolegend, 100239) in phosphate buffered saline (PBS) for approximately 2-3 hours at 37°C. Lymph nodes and spleens (inguinal, axillary, brachial, cervical and mesenteric) from mice were sterilely collected in iron free media and homogenised through 40 μm filters using EasySep buffer (Stem Cell Technologies, 20144) or an in-house alternative (PBS + 2% FBS + 1mM EDTA (Invitrogen, AM9260G)) to produce a single cell suspension. CD4+ and CD8+ T-cells were isolated from total homogenate using the EasySep Mouse Naïve CD4+ T-cell (Stem Cell Technologies, 19765) and the EasySep Mouse CD8+ T-cell (Stem Cell Technologies, 19853) isolation kits respectively using the EasyPlate EasySep magnet (Stem Cell Technologies, 18102). Provided kit protocols were followed as written. Cells were optionally stained with cell trace violet (CTV, Invitrogen, C34557) for 8 minutes at 37°C prior to culture. Cells were plated at 0.5-1x10^6 cells/mL in R10, or iron free media supplemented with defined holotransferrin concentrations (see section 2.3.1). Cells were provided with 50 μM β-mercaptoethanol (BME, Gibco, 31350-010) and 1 μg/mL α-CD28 (Biolegend, 102115) in addition to the cytokine and antibody cocktails listed in table 2.1 depending on cell type. T-cells were cultured at 37°C, 5% CO_2 for 24-120 hours.

Reagent		CD8+	CD4+ Th17
IL-2 (Biolegend, 575402)	U/mL	50	
IL-6 (Biolegend, 575702)	ng/mL		20
hTGF- β (Biolegend, 781802)	ng/mL		5
α-IL-4 (Biolegend, 504102)	μg/mL		5
α-IFN-γ (Biolegend, 505802)	μg/mL		5

Table 2.1. Polarisation cocktails by T-cell subset.

2.3.3 Nutrients/pharmacological agents for cell culture

Unless otherwise specified, nutrients/pharmacological agents were dissolved directly into cell culture media at the concentrations described in table 2.2.

Compound	Concentration		Special preparation notes
Acetate (Sigma Aldrich, 32319-500G-R)	20	mM	
Adenosine (Alfa Aesar, A10781)	20, 100	µM	Added directly into media (will not solubilise completely) and resuspended by shaking prior to adding to culture
Asparagine (MP Biomedicals, 100794)	100, 300, 1000	µM	
Aspartate (Scientific Laboratory supplies, CHE2306)	20, 40	mM	Dissolved in media by titrating in 1M NaOH (Sigma Aldrich, 30620-1KG-M) until solubilised and the pH ~7.5
CoQ10 (Cayman Chemical Company, 11506)	400	µM	
Cytodine (Sigma Aldrich, C122106-1G)	20, 100	µM	
Dimethyl α-ketoglutarate (Cayman Chemical Company, 28394)	1, 5	mM	
Dimethyl itaconate (Fluorochem, 078606)	50, 250	µM	
dNTPs (Sigma Aldrich, D7295-.2ML)	50	µM	
Doxycycline hyclate (Abcam, ab141091)	1, 3, 10	µM	
Guanosine (Alfa Aesar, A11328.14)	20, 100	µM	Added directly into media (will not solubilise completely) and resuspended by shaking prior to adding to culture
N-acetyl cysteine (Sigma Aldrich, A7250-5G)	10	mM	
Nicotinamide (Sigma, N0636-500G)	10	mM	
Nicotinamide riboside (Med Chem Express, HY-123033A)	400	µM	
Sodium pyruvate (Sigma Aldrich, P2256-5G)	5	mM	
Thymidine (Alfa Aesar, A11493.06)	20, 100	µM	
Uridine (Alfa Aesar, A15227)	100	µg/mL	

Table 2.2. Compound preparation for cell culture.

2.4 DNA

2.4.1 Mitochondrial DNA quantification

1-1.5x10^6 naïve or activated CD8+ T-cells were pelleted and snap frozen on dry ice. Pellets were lysed in 100 µL QuickExtract DNA extraction solution (Biosearch technologies, QE0905T) followed by vortexing for 15 seconds. The solution was

incubated at 65°C for 10 minutes, vortexed for 15 seconds and heated to 95°C for 5 minutes. The extracts were spun down at 17000 G for 15 minutes and the DNA containing supernatants were collected.

Mitochondrial DNA (mtDNA) and nuclear DNA (nDNA) quantification was conducted via quantitative-polymerase chain reaction (qPCR) using a protocol adapted from Rooney *et al* [14], Quiros *et al* [15] and a method kindly provided by Anna Victora Lechuga-Vieco. Sequences specific for mitochondrial and nuclear genomes were amplified in separate reactions using the primer sets (Merck) detailed in table 2.3. Primer efficiency was evaluated by testing the primer sets against a titration of DNA concentrations. If primers are adequately efficient, with each 2-fold dilution of DNA, Ct values should uniformly increase by 1. This is assessed using the following equation:

$$\% \text{ efficiency} = (10^{(-1/\text{slope})}-1)*100$$

Efficiency was found to be greater than 90% for both primer sets (Fig. 2.1).

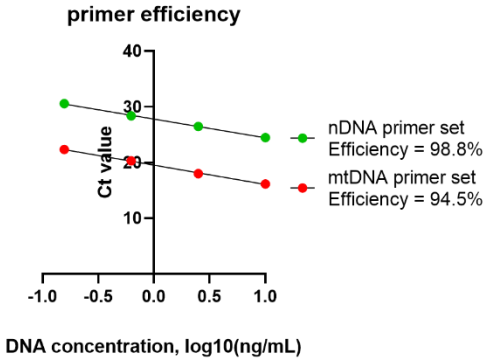

Figure 2.1. Calculating primer efficiencies for quantifying mtDNA. mtDNA and nDNA primer sets defined in table 2.3 were tested against a titration of DNA concentrations to assess efficiency.

Each reaction included 1.5 µL DNA (2.5 ng/µL) as prepared above, 5 µL Power SYBR green master mix (ThermoFisher Scientific, 4368577), 0.25 µL forward primer (10 µM), 0.25 µL reverse primer (10 µM) and 3 µL nuclease free water (Ambion, AM9937). Samples were run on the QuantStudio 7 flex real-time PCR system (Applied Biosystems, 4485701) using the following qPCR program:

1. 50°C – 2 minutes
2. 95°C – 10 minutes
3. Cycle 40X

   a. 95°C – 15 seconds
   b. 60°C – 1 minute
4. 95°C – 15 seconds
5. 60°C – 1 minutes
6. Gradual increase to 95°C

mtDNA copy number was calculated via normalisation against the nuclear genome which is assumed to have 2 copies per cell using the following equation:

$$\text{mtDNA copy number} = 2 \times 2^{(\text{nDNA Ct} - \text{mtDNA Ct})}$$

Target	Direction	Sequence (5'-3')
mtDNA	Forward	CCCAGCTACTACCATCATTCAAGT
mtDNA	Reverse	GATGGTTTGGGAGATTGGTTGATGT
nDNA (*Usf2* specific)	Forward	TGTTTATGGCGCTGGGACTAT
nDNA (*Usf2* specific)	Reverse	GCTGGCAGAGCACTTTCTTAGC

Table 2.3. Primers for mtDNA and nDNA quantification. mtDNA primers were derived from Rooney et al[14]. nDNA primers had previously been validated in the lab.

2.4.2 Samhd1-KO genotyping

DNA was extracted from mouse ear notches which were lysed in 75 µL of alkaline lysis buffer (25mM NaOH (Sigma Aldrich, 30620-1KG-M)/0.2mM EDTA (Invitrogen, AM9260G)) for 2 hours at 95°C before neutralisation with 40 mM Tris HCl (Sigma, T3253-1KG).

The PCR protocol for Samhd1-KO detection was obtained from Jan Rehwinkel[16]. Each reaction contained 12.5 µL DreamTaq green PCR master mix (ThermoScientific, K1081), 0.625 µL PJR0258 primer (20 µM), 0.625 µL PJR0259 primer (20 µM), 0.3125 µL PJR0260 primer (20 µM) and 9.9 µL nuclease free water (Ambion, AM9937).

Primer	Sequence (5'-3')
PJR0258	TCTCCTATGcagcgagccgattccgagcagTATGGATGGTTGTAAGCC
PJR0259	ACGAAGTTATATTATGTACCTGACTGAT
PJR0260	TTTGGTTCTAGGCACTCTTCTG

Table 2.4. Primers for SAMHD1-KO genotyping.

The following PCR program was used:

1. 95°C – 2 minutes
2. Cycle 30X
    a. 95°C – 30 seconds
    b. 64°C – 30 seconds
    c. 72°C – 1 minute
3. 72°C – 10 minutes
4. 4°C – hold

PCR products were run on 1.5% agarose gels (1.5% agarose (Scientific Laboratory Supplies, BIO-41025) in TAE buffer (Thermo scientific, B49) and 1:10000 gelRed nucleic acid stain (Millipore, SCT123)). Wildtype allele = 535 base pairs (bp), knockout allele = 346 bp. Heterozygotic DNA will produce both the 535 bp and 346 bp bands (Fig. 2.2).

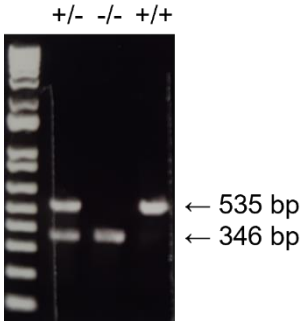

Figure 2.2. SAMHD-1 genotyping. Mutant alleles produce a 346 bp PCR product while wildtype alleles produce a 535 bp PCR product.

2.5 RNA

2.5.1 RNA extraction from CD8+ T-cells

CD8+ T-cells were collected from cell culture plates, washed twice with PBS and pellets snap frozen on dry ice. T-cell pellets were resuspended in 350 µL of RLT+ buffer from the Qiagen RNeasy plus mini kit (Qiagen, 74136) and RNA was extracted according to the manufacturer's instructions. For RNA extracted for RNA-sequencing, samples were treated on-column with the Qiagen RNase-free DNase I set (Qiagen, 79254) according to the method described in appendix D of the Qiagen RNeasy mini kit manual (Qiagen, 74104). RNA concentrations were determined using a Nanodrop one machine (Thermofisher Scientific).

2.5.2 RNA extraction from tissues

Sections (2-3 mm^3) of liver tissue, small intestine, lung and mesenteric lymph node were stored in RNAlater (Invitrogen, AM7020). Tissues were homogenised in 700 µL RLT+ buffer using a TissueRuptor (Qiagen). RNA was extracted from 350 µL of the lysate using the Qiagen RNeasy Plus Mini Kit (Qiagen, 74136). RNA concentration and quality was measured using a Nanodrop One machine (Thermofisher Scientific).

2.5.3 Complementary DNA synthesis and qPCR

Complementary DNA (cDNA) was synthesised using the High-Capacity RNA-to-cDNA kit (Applied Biosystems, 4388950) and qPCR experiments were completed on a QuantStudio 7 flex real-time PCR system (Applied Biosystems, 4485701) using the Taqman gene expression master mix (Applied Biosystems, 4369016) and appropriate Taqman Gene Expression Assays (Table 2.5). *B2m* was used as the housekeeping control for T-cells and *Hprt* was used as the housekeeping control for tissues.

Probe	Code
B2m	Mm00437762_m1
Cdkn1a	Mm04205640_g1
Dglucy	Mm01337061_m1
Hprt	Mm01545399_m1
Ifi44	Mm00505670_m1
Ifng	Mm01168134_m1
Il2	Mm00434256_m1
Isg15	Mm01705338_s1
Isg20	Mm00469585_m1
Tfrc	Mm00441941_m1

Table 2.5. Taqman probes used for qPCR.

2.5.4 RNA-sequencing

For RNA-sequencing, RNA quality was assessed using an Agilent high sensitivity RNA ScreenTape (Agilent, 5067-5579) and corresponding sample buffer (Agilent, 5067-5580) on a 4200 TapeStation system (Agilent, G2991BA). Library preparation and bulk mRNA-sequencing to a depth of 30 million paired end reads using the Illumina NovaSeq 6000 platform was conducted by Novogene.

Read alignment was conducted using RNA-star to the Mus Musculus genome (mm39) and features were annotated using FeatureCounts from the subread package. Differential gene expression analysis was conducted using EdgeR (R package) with the

thresholds of log_2|fold change| > 1.5 and an FDR <0.05 applied. Gene set enrichment analysis (GSEA) was completed using FGSEA (R package) and Hallmark pathways. ChEA3[17] was used for transcription factor footprinting and the resulting network was visualised using STRING within the Cytoscape software. gProfiler[6] GSEA was applied to transcription factors identified by the ChEA3 algorithm.

For analysis of RNA-seq data from Wang et al[18] of CPX or DMSO treated Th1 CD4+ T-cells, data was downloaded from the gene expression omnibus (GEO, GSE84702) and analysis was completed as described above.

2.5.5 Utilising the cancer dependency map (DepMap) project RNA-seq data

DGLUCY and TFRC mRNA expression data from the Expression Public 23Q2 dataset was downloaded via the DepMap portal (https://depmap.org/portal/). Correlation analysis was completed with data analysed by lineage annotated by the DepMap project.

2.6 Protein

2.6.1 Protein-mass spectrometry (protein-MS) sample preparation

48h activated CD8+ T-cells were harvested and washed twice in PBS. Cells were fixed in 2% paraformaldehyde (PFA, Thermo Scientific, 28906) for 30 minutes, washed and resuspended in PBS. Cells that were alive at the time of fixation were sorted and using forward and side scatter into PBS. Cells were pelleted and flash frozen on dry ice.

Cell pellets were processed by Linda Sinclair. Pelleted cells were lysed using the 2-step trypsin lysis protocol described by Kelly et al[19]. Cell pellets were resuspended in 200 µL TEAB digest buffer (0.1 M TEAB, 1 mM MgCl2, 1:80 benzonase, pH 8) and incubated for 20 minutes at 37°C in a thermomixer. The amount of trypsin for a 1:20 trypsin to protein (w/w) ratio was calculated and 50% of the required trypsin was added. Samples were incubated overnight at 37°C in a thermomixer. The remaining trypsin was added and samples were incubated for 60 minutes at 37°C in a thermomixer. The samples were acidified to a final concentration of 1% trifluoroacetic acid (TFA) and subjected to a C18 stage-tip desalting with the following buffers: condition (100% acetonitrile), wash (0.1% TFA), elute (66.6% acetonitrile, 0.1% TFA), ion exchange (2:1 ratio of 100% acetonitrile to 0.1% TFA). Samples were dried using a speed-vac at 65°C.

2.6.2 Data-independent acquisition MS acquisition

MS analysis was performed as described previously[20]. Peptides were analysed on a Q-Exactive-HF-X (Thermo Scientific) mass spectrometer coupled with a Dionex Ultimate 3000 RS (Thermo Scientific). LC buffers were the following: buffer A (0.1% formic acid in Milli-Q water (v/v)) and buffer B (80% acetonitrile and 0.1% formic acid in Milli-Q water (v/v)). 2 µg of each sample were loaded at 15 µL/min onto a trap column (100 µm × 2 cm, PepMap nanoViper C18 column, 5 µm, 100 Å, Thermo Scientific) equilibrated in 0.1% TFA. The trap column was washed for 3 minutes at the same flow rate with 0.1% TFA then switched in-line with a Thermo Scientific, resolving C18 column (75 µm × 50 cm, PepMap RSLC C18 column, 2 µm, 100 Å). The peptides were eluted from the column at a constant flow rate of 300 nl/minute with a linear gradient from 3% buffer B to 6% buffer B in 5 minutes, then from 6% buffer B to 35% buffer B in 115 minutes, and finally to 80% buffer B within 7 minutes. The column was then washed with 80% buffer B for 4 minutes and re-equilibrated in 3% buffer B for 15 minutes. Two blanks were run between each sample to reduce carry-over. The column was kept at a constant temperature of 50°C at all times.

The data was acquired using an easy spray source operated in positive mode with spray voltage at 1.9 kV, the capillary temperature at 250°C and the funnel RF at 60°C. The MS was operated in data-independent acquisition (DIA) mode as reported earlier with some modifications[21]. A scan cycle comprised a full MS scan (m/z range from 350–1650, with a maximum ion injection time of 20 ms, a resolution of 120,000 and automatic gain control (AGC) value of 5×10^6). MS survey scan was followed by MS/MS DIA scan events using the following parameters: default charge state of 3, resolution 30.000, maximum ion injection time 55 ms, AGC 3 × 106, stepped normalized collision energy 25.5, 27 and 30, fixed first mass 200 m/z. Data for both MS and MS/MS scans were acquired in profile mode. Mass accuracy was checked before the start of samples analysis.

2.6.3 DIA data quantification and analysis

Quantification of reporter ions was completed using Spectronaut (Biognosys; Spectronaut 14.10.201222.47784) in library-free (directDIA) mode. Minimum peptide length was set to 7, and maximum peptide length was set to 52, with a maximum of 2 missed cleavages. Trypsin was specified as the digestive enzyme used. The FDR at the precursor ion level and protein level was set at 1% (protein and precursor Q value cutoff).

The max number of variable modifications was set to 5, with protein N-terminal acetylation and glutamine and asparagine deamidation and methionine oxidation set as variable modifications. Carbamidomethylation of cysteine residues was selected as a fixed modification. Data filtering and protein copy number quantification were performed in the Perseus software package, version 1.6.6.0. Copy numbers were calculated using the proteomic ruler[22]. This method sets the summed peptide intensities of the histones to the number of histones in a typical diploid cell. The ratio between the histone peptide intensity and summed peptide intensities of all other identified proteins is then used to estimate the protein copy number per cell for all the identified proteins. Data was subsequently analysed using custom R scripts. A $\log_2|\text{fold change}| > 0.585$ (equivalent to $|\text{fold change}| > 1.5$) was used (as used in Howden et al[4]). We also applied the typical p-value threshold of <0.05 when comparing the high (0.625 mg/mL holotransferrin) and low (0.001 mg/mL holotransferrin) iron concentrations via a t-test as well as an additional threshold of p-values < 0.05 when a one-way ANOVA was conducted across all conditions. As for the RNA-seq, GSEA was conducted using FGSEA (R package) and the Hallmark pathways. For analysing mitochondrial proteins, proteins were filtered by inclusion in the MitoCarta3.0 gene set[23].

2.7 Metabolic assays

2.7.1 Metabolite-mass spectrometry (metabolite-MS)

For heavy isotope tracing experiments, CD8+ T-cells were isolated and activated as described in section 2.3. Iron free media with varying holotransferrin concentrations was prepared using phenol red free RPMI 1640 (Gibco, 11835030) as phenol red can interfere with metabolite-MS. At 24 hours prior to cell collection (24 hours post activation), cells were collected, washed and replated in media containing the heavy isotope of interest (13C6-glucose (Cambridge Isotope Laboratories, Inc., CLM-1396-1) and 13C5-glutamine (CK Isotopes, CNLM-1275)) on plates coated with α-CD3. Iron free tracing media was prepared using SILAC RPMI 1640 flex media (Gibco, A24945201) which lacks glucose, phenol red, glutamine, arginine and lysine. Argine (MP Biomedicals, 194626) and lysine hydrochloride (MP Biomedicals, 194697) were supplemented at standard RPMI 1640 concentrations of 1.2 mM and 0.2 mM respectively. For 13C6-glucose tracing, glutamine (Sigma, G7513-100ML) was added at 2 mM and 13C6-glucose at 11.1 mM. For 13C5-glutamine tracing, 13C5-glutamine was added at 2 mM and glucose (Sigma Aldrich,

158968-100G) at 11.1 mM. Holotransferrin and apotransferrin as well as activation reagents (BME, α-CD28 and IL-2) were added to the iron free tracing media as described in section 2.3 at standard concentrations.

Cells were collected, counted and 2-4x10^6 cells were washed twice in ice cold 0.9% saline made with NaCl (Sigma Aldrich, 31434-500G-M) and ultrapure HPLC grade water (Alfa Aesar, 22934). Cells were pelleted and snap frozen on dry ice. Cell pellets were processed by Nancy Gudgeon and samples run by Jennie Roberts and Bryan Marzullo at the University of Birmingham. Cells were extracted in 1:1:1 pre-chilled methanol, HPLC-grade water (containing 1.75 µg/mL D6-glutaric acid) and chloroform. The extracts were shaken at 1400 rpm for 15 minutes at 4°C and centrifuged at 12,000 g for 15 minutes at 4°C. The upper aqueous phase was collected and evaporated under vacuum. Metabolite derivatization was performed using an Agilent autosampler. Dried polar metabolites were dissolved in 15 µL of 2% methoxyamine hydrochloride in pyridine (Thermo Fisher Scientific, Cat# 25104) at 55°C, followed by an equal volume of N-tert-Butyldimethylsilyl-N-methyltrifluoroacetamide with 1% tertbutyldimethylchlorosilane after 60 minutes, and incubation for a further 90 minutes at 55°C. GC-MS analysis was performed using an Agilent 6890GC equipped with a 30m DB-35 MS capillary column. The GC was connected to an Agilent 5975C MS operating under electron impact ionization at 70 eV. The MS source was held at 230°C and the quadrupole at 150°C. The detector was operated in scan mode and 1 µL of derivatised sample was injected in splitless mode. Helium was used as a carrier gas at a flow rate of 1 mL/min. The GC oven temperature was held at 80°C for 6 minutes and increased to 325°C at a rate of 10°C/minutes for 4 minutes. The run time for each sample was 59 minutes. For determination of the mass isotopomer distributions (MIDs), spectra were corrected for natural isotope abundance. Data processing was performed using MATLAB.

2.7.2 NAD+/NADH quantification

NAD+/NADH ratio measurements were made using the NAD/NADH-Glo assay (Promega, G9071) according to the manufacturer's instructions with modifications for measuring NAD+ and NADH individually (rather than pooled). Cultured T-cells were collected, washed in PBS and counted. 1x10^5 cells in 50 µL of PBS were lysed in 50 µL of 0.2 M NaOH (Sigma Aldrich, 30620-1KG-M) with 1% dodecyltrimethylammonium

bromide (DTAB, Alfa Aesar, A10761) per condition in technical duplicates. Each sample was split (50 µL) into a second tube for matched NAD+ and NADH measurements.

For measurement of NAD+, NADH was first degraded by adding 25 µL of 0.4 M HCl (Fisher Scientific, H/1111/PB17) to the first tube, heated to 60°C for 15 minutes followed by incubation at room temperature for 10 minutes. 25 µL 0.5 M TRIZMA base (Sigma Aldrich, T1503-1KG) was added to quench the HCl.

To measure NADH, NAD+ was degraded by heating the second tube to 60°C for 15 minutes followed by incubation at room temperature for 10 minutes. 50 µL of 0.2 M HCl (Fisher Scientific, H/1111/PB17) and 0.25 M TRIZMA base (Sigma Aldrich, T1503-1KG) solution was added to quench the NaOH.

The NAD/NADH-Glo detection reagent was prepared as instructed. 50 µL of each sample (either purified for NAD+ or NADH) and 50 µL of NAD/NADH-Glo detection reagent was added to a white 96 well plate and mixed gently. The plate was incubated at room temperature and luminescence was measured using a Promega GloMax multi-detection luminometer at 30, 45 and 60 minutes.

2.7.3 Seahorse assay

Seahorse was conducted using the Seahorse XF Real-Time ATP rate assay kit (Agilent, 103592-100). The day prior to the assay, the Agilent Seahorse XF96 analyser was turned on and a sensor cartridge (Agilent, 103792-100) was hydrated in Seahorse XF calibrant (Agilent, 103059-000) in a non-CO_2 incubator overnight. The day of the assay, Seahorse XF RPMI media was prepared using 1 mM pyruvate (Agilent, 103578-100), 2 mM glutamine (Agilent, 103579-100), 10 mM glucose (Agilent, 103577-100) in seahorse XF RPMI pH 7.4 RPMI (Agilent, 103576-100) and warmed to 37°C. Cells were collected, washed and $1x10^5$ cells in 50 µL of Seahorse media were plated per well on a Poly-D-lysine (Gibco, A3890401) coated XF96 microplate (Agilent, 101085-004). Plates are spun down, supernatant removed, and cells resuspended in 180 µL of Seahorse media and incubated for 45-60 minutes in a non-CO_2 incubator. Oligomycin and rotenone/antimycin A were diluted to 1.5 µM and 0.5 µM respectively. 20 µL of oligomycin and 22 µL of rotenone/antimycin A were loaded into the sensor cartridge in ports A and B. The sensor cartridge and plate were assembled, and the corresponding

assay was run on the Seahorse Analyser. Data was analysed using the Agilent Seahorse Wave software and the Seahorse XF real-time ATP rate assay report generator.

2.8 In vivo experiments

2.8.1 Immunisation

Ovalbumin EndoFit (OVA) (Invivogen, vac-pova) was dissolved in 1 mL of physiological water (0.9% saline, Invivogen, HPV-43-07) for a stock concentration of 1 mg/mL. MPLA-SM VacciGrade (MPLA) (Invivogen, vac-mpla) was solubilised in 1 mL of DMSO (Sigma Aldrich, D5879-500ML) for a stock concentration of 1 mg/mL. 200 µg OVA, 12.5 µg MPLA and 25 µg α-CD40 (2B Scientific Limited, BE0016-2-1MG) per mouse were prepared in 200 µL of physiological water and administered intraperitoneally. For control immunisations, an equivalent volume of DMSO (to account for the DMSO used to solubilise MPLA) was added to physiological water.

2.8.2 T-cell adoptive transfer

For naïve T-cell adoptive transfer, spleens from OT-I mice were macerated through 40 µm filters. Red blood cells were lysed using red cell lysis buffer (RCL buffer, tris-ammonium chloride: 17 mM TRIZMA-base (Sigma Aldrich, T1503-1KG), 140 mM NH_4Cl (Sigma, A9434-500G) with pH adjusted to 7.2 with HCl (Fisher Scientific, H/1111/PB17) for 1-2 minutes on ice. The frequency of CD8+ T-cells were determined using flow cytometry. The splenocytes were washed into PBS and adjusted to a concentration of $0.05x10^6$ CD8+ T-cells/mL. 100 µL were injected intravenously for a final transfer of 5000 OT-I CD8+ T-cells per mouse.

For activated T-cell adoptive transfer, T-cells were activated as described under T-cell activation (see section 2.3.2) in R10 media. Cells were harvested after 1-2 days and washed into PBS. Cells were diluted to a concentration of $5x10^6$ cells/mL and 200 µL containing $1x10^6$ cells were injected intravenously per mouse.

2.8.3 Mini-hepcidin (mHep)

Up to 24 doses of mHep PR73 (Ida-Thr-His-Dpa-bhPro-Arg-Cys-Arg-bhPhe-Ahx-Ida(Hexadecylamine)-NH2)(Chinese Peptide Company, 967476) were sterilely aliquoted into eppendorfs and solubilised with 80% ethanol (Sigma Aldrich, 459836-1L) and mixed with 60 mg of Purebright SL220/Sunbright DSPE-020CN (NOF) carrier drug. The

solution was vortexed thoroughly and concentrated in a vacuum concentrator at 50°C for approximately 40-45 minutes until the solution had formed a gel like consistency. The gel was resuspended in an appropriate volume of sterile water (Gibco, 15230-089) for a final concentration of 1 mM. 100 nmoles in 100 µL were injected intraperitoneally per mouse per day at a concentration of 1mM.

2.8.4 Aspartate

The appropriate mass of aspartate (Scientific Laboratory supplies, CHE2306) was solubilised via the dropwise addition of 2.5 M NaOH (Sigma Aldrich, 30620-1KG-M). Once all aspartate had dissolved, the solution was made up to the final volume with water and the pH adjusted to ~pH 7, 12.5 mMol/kg aspartate was injected intraperitoneally per mouse. Physiological water (0.9% saline, Invivogen, HPV-43-07) was used as the control.

2.9 Flow cytometry

2.9.1 Tissue/blood processing

Spleens were homogenised through 40 µm filters. Red blood cells were lysed using RCL buffer for 1-2 minutes on ice. Blood was collected in EDTA microtainer-tubes (BD biosciences, 365975). Up to 100 µL of blood were lysed in 1 mL of RCL buffer for 30 minutes on ice.

2.9.2 Standard ex vivo staining

Up to $2x10^6$ blood or spleen cells were transferred to 96 well round bottom plates and washed with PBS.

For detection of intracellular cytokines in OVA-specific OT-I T-cells, bulk cells were stimulated with SIINFEKL peptide (1:10000) (OVA 257-264, Invivogen, vac-sin) and BME (1:1000) (Gibco, 31350-010) in iron free media for 4-5 hours at 37°C/5% CO_2. 30 minutes into stimulation, brefeldin A (BFA) (Biolegend, 420601) was added at a final concentration of 5 mg/mL.

For tetramer staining, cells were resuspended in 50 µL of tetramer (1:400) (H-2K(b)-SIINFEKL-APC, NIH tetramer core) diluted in 2% FBS, 0.04% sodium azide (Sigma Aldrich, 438456-5G) in PBS and incubated for 40 minutes at room temperature. Cells were washed prior to surface staining.

For surface staining, cells were incubated in 20 µL of α-CD16/CD32 TruStain FcX (1:100) (Biolegend, 101320) and LIVE/DEAD fixable near-IR dead cell stain (1:1000) (Invitrogen, L34975) for 10 minutes on ice. 20 µL of antibody cocktail (see table 2.6) prepared at 2x concentration was added directly on top of the block/live dead cocktail and incubated for a further 20 minutes on ice.

For intracellular staining, cells were permeabilised in perm/wash buffer (Biolegend, 421002) for 20 minutes. Intracellular targets were stained with 20-30 µL of intracellular stain prepared in perm buffer for 20 minutes to overnight. Cells were resuspended in PBS and data was acquired using an Attune NxT flow cytometer (Thermofisher Scientific) or a BD Fortessa flow cytometer (BD biosciences). Data was analysed using FlowJo (BD biosciences). Gating scheme is in Figure 2.3A.

2.9.3 Standard In vitro staining

In vitro cells were transferred from cell culture plates to 96 well round bottom plates and washed with PBS.

For intracellular cytokine staining, cells were stimulated with cell activation cocktail (1:500 or 1:2500) (Biolegend, 423301), BFA (5 mg/mL) (Biolegend, 420601) and monensin (2 mM) (Biolegend, 420701) in iron free media at 37°C/5% CO_2 for 5 hours prior to staining.

Cells were stained with 20-30 µL of surface antibody cocktail (see table 2.6) with Zombie NIR fixable viability kit (1:400-1000) (Biolegend, 423105) in PBS for 20 minutes on ice. Cells were fixed with 2% PFA (Pierce, 28906) diluted in PBS or commercial fixation buffer (Biolegend, 420801) for 20 minutes on ice. For nuclear staining of markers cells were fixed in Foxp3 transcription factor fixation buffer (eBioscience, 00-5523-00) for 1 hour on ice.

Intracellular staining and data acquisition was conducted as described under ex vivo staining (section 2.9.2). Gating schemes are in Figure 2.3B-C.

2.9.4 Mitochondrial ROS staining for flow cytometry

Detection of mitochondrial reactive oxygen species (mROS) was conducted using MitoSOX dye (Invitrogen, M36008). Cells were resuspended in 200 µL of MitoSOX dye

Target	Clone	Fluorophore	Company	Product code	Dilution (1/X)
CD25	PC61	FITC	Biolegend	102005	400
CD4	GK1.5	FITC	Biolegend	100405	400
CD8a	53-6.7	FITC	Biolegend	100705	400
CD45.1	A20	FITC	Biolegend	110706	400
CD69	H1.2F3	FITC	Biolegend	104505	400
CD71	RI7217	FITC	Biolegend	113805	400
GZMB	GB11	FITC	Biolegend	515403	100
H3K27me3	C36B11	AF488	Cell Signalling	5499S	50
NFAT	D43B1	AF488	Cell Signalling	14324S	50
TNF-a	MP6-XT22	FITC	Biolegend	506603	400
CD4	GK1.5	PerCP-Cy5.5	Biolegend	100433	200
CD8a	53-6.7	PerCP-Cy5.5	Biolegend	100733	200
CD25	3C7	PerCP-Cy5.5	Biolegend	101911	200
CD45.1	A20	PerCP-Cy5.5	Biolegend	110727	200
CD90.2	53-2.1	PerCP-Cy5.5	Biolegend	140332	200
CD4	GK1.5	APC	Biolegend	100412	200
CD25	PC61	APC	Biolegend	102011	200
CD71	RI7217	APC	Biolegend	113819	200
CD98	RL388	APC	Biolegend	128211	200
IFN-γ	XMG1.2	APC	Biolegend	505809	200
IL-2	JES6-5H4	APC	Biolegend	503809	200
IL-17	TC11-18H10.1	APC	Biolegend	506915	200
pS6	D57.2.2E	AF647	Cell Signalling	14733S	50
Tbet	4B10	APC	Biolegend	644813	200
B220	RA3-6B2	APC-Cy7	Biolegend	103223	200
CD11b	M1/70	APC-Cy7	Biolegend	101226	200
TNF-α	MP6-XT22	BV421	Biolegend	506328	200
CD8a	53-6.7	PB	Biolegend	100728	400
CD8	53-6.7	BV605	Biolegend	100743	200
CD44	IM7	BV605	Biolegend	103047	200
IL2	JES6-5H4	BV605	Biolegend	503829	400
CD4	GK1.5	PE	Biolegend	100407	200
CD8a	53-6.7	PE	Biolegend	100707	200
CD71	RI7217	PE	Biolegend	113807	200
CD62L	MEL-14	PE	Biolegend	104407	200
CD98	RL388	PE	Biolegend	128207	200
HIF1a	D1S7W	PE	Cell Signalling	59370S	50
IL-2	JES6-5H4	PE	Biolegend	503807	200
Perforin	S16009B	PE	Biolegend	154405	200
RORγt	AFKJS-9	PE	Invitrogen	12-6988-82	80
TNF-α	MP6-XT22	PE	Biolegend	506305	200
CD8	53-6.7	PE-Cy7	Biolegend	100721	200
CD25	PC61	PE-Cy7	Biolegend	102015	200
CD44	IM7	PE-Cy7	Biolegend	103029	200
CD69	H1.2F3	PeCy7	Biolegend	104511	200
CD71	RI7217	PE-Cy7	Biolegend	113811	200
IFN-g	XMG1.2	PE-Cy7	Biolegend	505825	200

Table 2.6. Antibodies for flow cytometry.

diluted to 5 µM in phenol red iron free media and incubated at 37°C/5% CO_2 for 15 minutes before surface staining. Acquisition was conducted on live cells.

2.9.5 pS6 flow cytometry

For flow staining for the metabolic regulator, pS6, cells were washed once with a solution of 50% RPMI 1640, 50% HBSS (Gibco, 14025-092) and 0.5% BSA (PAN biotech, PO6-139310) before fixation in 1% PFA (Pierce, 28906) for 20 minutes. Cells were washed with PBS and optionally surface stained for fixation stable epitopes. Cells were permeabilised using 90% ice cold methanol (Sigma, 34860-1L-R) for 20 minutes at -20°C prior to permeabilization and acquisition as described in section 2.9.2.

2.9.6 Cell counting via flow cytometry

Cells were transferred into 96 well round bottom TC plates and washed once with 2% FBS in PBS (FACS buffer). Cells were resuspended in FACS buffer containing 0.5 µg/mL 7-AAD (Biolegend, 420403) and incubated on ice for 10 minutes and then acquired directly on the Attune NxT flow cytometer (Thermofisher Scientific). 50 µL of cells were acquired per well to enable accurate calculation of cell concentration and wells were resuspended using a multichannel between each column on the 96 well plate to account for cell settling effects.

2.10 Data analysis

Unless explicitly specified, data analysis was completed using Excel (Microsoft), Prism (GraphPad), FlowJo (BD biosciences) or custom scripts written in the R coding language. Statistics are specified in figure legends.

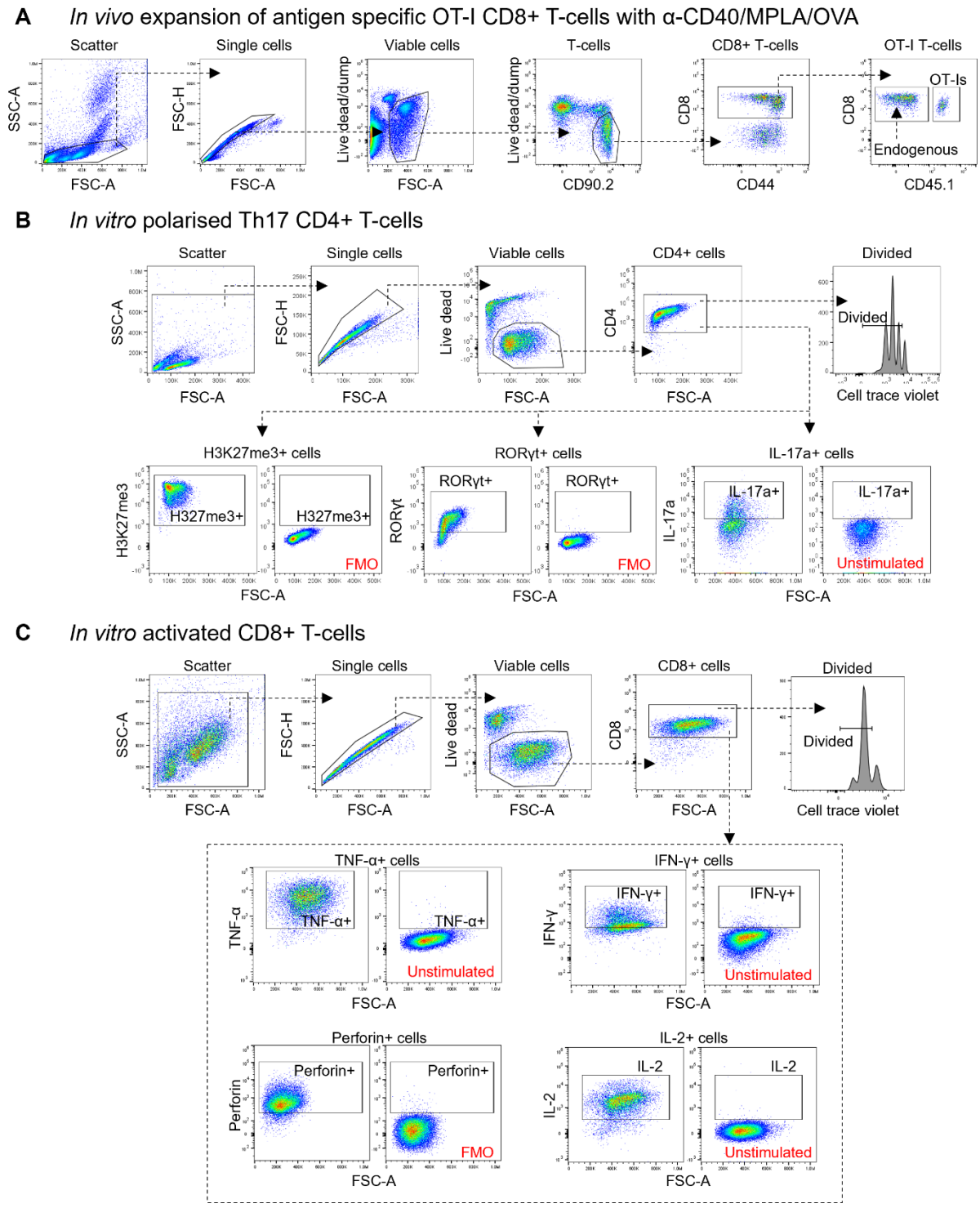

Figure 2.3. Representative gating schemes. **(A)** In vivo expanded antigen specific OT-I CD8+ T-cells from mice immunised with MPLA/α-CD40/OVA (section 2.8). Dump includes CD11b and B220. **(B)** In vitro polarised Th17 CD4+ T-cells activated as described in section 2.3. **(C)** In vitro activated CD8+ T-cells as described in section 2.3. Cells for **(B-C)** were stimulated for 4-5 hours with cell activation cocktail (PMA/ionomycin, 1:500 or 1:2500), brefeldin A (BFA, 5 mg/mL) and monensin (2 mM) to induce production and retention of cytokines. Unstimulated samples were resuspended in media lacking PMA/ionomycin/BFA/monensin. FMO = fluorescence minus one.

2.11 References

1 Andreini, C., Putignano, V., Rosato, A. & Banci, L. The human iron-proteome. *Metallomics* **10**, 1223-1231 (2018). https://doi.org:10.1039/c8mt00146d

2 UniProt: a worldwide hub of protein knowledge. *Nucleic Acids Res* **47**, D506-d515 (2019). https://doi.org:10.1093/nar/gky1049

3 Yates, A. D. *et al.* Ensembl 2020. *Nucleic Acids Res* **48**, D682-d688 (2020). https://doi.org:10.1093/nar/gkz966

4 Howden, A. J. M. *et al.* Quantitative analysis of T cell proteomes and environmental sensors during T cell differentiation. *Nat Immunol* **20**, 1542-1554 (2019). https://doi.org:10.1038/s41590-019-0495-x

5 Rieckmann, J. C. *et al.* Social network architecture of human immune cells unveiled by quantitative proteomics. *Nat Immunol* **18**, 583-593 (2017). https://doi.org:10.1038/ni.3693

6 Raudvere, U. *et al.* g:Profiler: a web server for functional enrichment analysis and conversions of gene lists (2019 update). *Nucleic Acids Research* **47**, W191-W198 (2019). https://doi.org:10.1093/nar/gkz369

7 Yamanishi, H., Iyama, S., Yamaguchi, Y., Kanakura, Y. & Iwatani, Y. Total iron-binding capacity calculated from serum transferrin concentration or serum iron concentration and unsaturated iron-binding capacity. *Clin Chem* **49**, 175-178 (2003). https://doi.org:10.1373/49.1.175

8 Chasteen, N. D. & Williams, J. The influence of pH on the equilibrium distribution of iron between the metal-binding sites of human transferrin. *Biochem J* **193**, 717-727 (1981). https://doi.org:10.1042/bj1930717

9 Aisen, P., Leibman, A. & Zweier, J. Stoichiometric and site characteristics of the binding of iron to human transferrin. *J Biol Chem* **253**, 1930-1937 (1978).

10 Kelly, A. U., McSorley, S. T., Patel, P. & Talwar, D. Interpreting iron studies. *Bmj* **357**, j2513 (2017). https://doi.org:10.1136/bmj.j2513

11 Young, S. P., Bomford, A. & Williams, R. The effect of the iron saturation of transferrin on its binding and uptake by rabbit reticulocytes. *Biochem J* **219**, 505-510 (1984). https://doi.org:10.1042/bj2190505

12 Núñez, M. T., Núñez-Millacura, C., Beltrán, M., Tapia, V. & Alvarez-Hernandez, X. Apotransferrin and holotransferrin undergo different endocytic cycles in intestinal epithelia (Caco-2) cells. *J Biol Chem* **272**, 19425-19428 (1997). https://doi.org:10.1074/jbc.272.31.19425

13 Mayle, K. M., Le, A. M. & Kamei, D. T. The intracellular trafficking pathway of transferrin. *Biochim Biophys Acta* **1820**, 264-281 (2012). https://doi.org:10.1016/j.bbagen.2011.09.009

14 Rooney, J. P. *et al.* PCR based determination of mitochondrial DNA copy number in multiple species. *Methods Mol Biol* **1241**, 23-38 (2015). https://doi.org:10.1007/978-1-4939-1875-1_3

15 Quiros, P. M., Goyal, A., Jha, P. & Auwerx, J. Analysis of mtDNA/nDNA Ratio in Mice. *Curr Protoc Mouse Biol* **7**, 47-54 (2017). https://doi.org:10.1002/cpmo.21

16 Rehwinkel, J. *et al.* SAMHD1-dependent retroviral control and escape in mice. *Embo j* **32**, 2454-2462 (2013). https://doi.org:10.1038/emboj.2013.163

17 Keenan, A. B. *et al.* ChEA3: transcription factor enrichment analysis by orthogonal omics integration. *Nucleic Acids Res* **47**, W212-w224 (2019). https://doi.org:10.1093/nar/gkz446

18 Wang, Z. *et al.* Iron Drives T Helper Cell Pathogenicity by Promoting RNA-Binding Protein PCBP1-Mediated Proinflammatory Cytokine Production. *Immunity* **49**, 80-92.e87 (2018). https://doi.org:10.1016/j.immuni.2018.05.008

19 Kelly, V., Al-Rawi, A., Lewis, D., Kustatscher, G. & Ly, T. Low Cell Number Proteomic Analysis Using In-Cell Protease Digests Reveals a Robust Signature for Cell Cycle State Classification. *Mol Cell Proteomics* **21**, 100169 (2022). https://doi.org:10.1016/j.mcpro.2021.100169

20 Reyes, L. *et al.* -------A type I IFN, prothrombotic hyperinflammatory neutrophil signature is distinct for COVID-19 ARDS. *Wellcome Open Res* **6**, 38 (2021). https://doi.org:10.12688/wellcomeopenres.16584.2

21 Muntel, J. *et al.* Surpassing 10 000 identified and quantified proteins in a single run by optimizing current LC-MS instrumentation and data analysis strategy. *Mol Omics* **15**, 348-360 (2019). https://doi.org:10.1039/c9mo00082h

22 Wiśniewski, J. R., Hein, M. Y., Cox, J. & Mann, M. A "proteomic ruler" for protein copy number and concentration estimation without spike-in standards. *Mol Cell Proteomics* **13**, 3497-3506 (2014). https://doi.org:10.1074/mcp.M113.037309

23 Rath, S. *et al.* MitoCarta3.0: an updated mitochondrial proteome now with sub-organelle localization and pathway annotations. *Nucleic Acids Res* **49**, D1541-d1547 (2021). https://doi.org:10.1093/nar/gkaa1011

Chapter 3

3 Mining published datasets to explore immune cell iron and iron interacting protein dynamics*

3.1 Introduction†

Iron is utilised by all mammalian cells. However, the dependencies of various cell types on iron and specific iron dependent processes at homeostasis, throughout development and during immunological activation is largely unexplored. Understanding the iron content of cells and how it is distributed across pathways and protein species could provide insight into how modulating iron levels could differentially alter cellular function across the immune compartment. This is an important area of investigation because iron deficiency (either absolute or functional) affects over 1.2 billion people[1], and yet the molecular mechanistic consequences of iron deprivation on cells is relatively poorly characterised.

Critically, iron is widely distributed within cells with ~2% of human protein coding genes and ~6.5% of enzymes predicted to interact with iron[2]. Protein interactions with iron can occur either directly with iron ions or via heme or iron-sulfur (Fe-S) cluster prosthetic groups[2]. Iron ion binding proteins bind iron directly and are predominantly catalytic[2]; many such proteins are 2-oxoglutarate (2-OG, also known as alpha-ketoglutarate) dependent dioxygenases which mediate hydroxylation reactions involved in processes such as oxygen sensing, histone and DNA demethylation, and collagen

* Where indicated, the text and data in this chapter has been previously published in either Teh *et al*, Frontiers of Immunology, 2021 (DOI: 10.3389/fimmu.2021.714613) or Frost *et al*, Science Advances, 2022 (DOI: 10.1126/sciadv.abq5384).

† This section (3.1) is partly derived from the text published in Teh *et al*, Frontiers of Immunology, 2021 (DOI: 10.3389/fimmu.2021.714613)

synthesis[2,3]. Meanwhile, heme cofactors consist of iron within larger porphyrin ring structures[4]. Heme proteins, including hemoglobin are well known for oxygen binding, but are also involved in mitochondrial electron transfer and oxidative reactions involved in pathways such as prostaglandin synthesis, nitric oxide production and tryptophan metabolism[4]. Finally, Fe-S clusters coordinate iron and sulfur atoms as [2Fe-2S], [3Fe-4S] or [4Fe-4S] structures in mammals[5]. Fe-S cluster interacting proteins are extremely diverse and include proteins involved in Fe-S cluster synthesis itself, mitochondrial respiration, and DNA synthesis[2,5]. The relative requirements for iron between these pathways, how distribution of iron and activity of iron-dependent pathways differ between cell types or change depending on activation or developmental state, and how iron is allocated during scarcity has not been investigated.

Understanding of cellular iron usage remains unclear predominantly because existing experimental methods for directly measuring cellular iron content remain relatively crude. The first established method for measuring cellular iron was Perl's Prussian blue stain which was first used in 1867 by Dr. Max Perl for visualising tissue iron via microscopy[6]. Prussian blue only stains Fe^{3+} iron species and thus does not allow measurements of Fe^{2+}, such as iron bound in heme cofactors[6]. Moreover, precise quantification of iron in tissue is not possible with this method. In contrast, the banthophenanthroline assay which is based on a colourimetric chemical reaction between non-heme iron with the banthophenanthroline reagent allows for more precise measurements of tissue iron, but once again fails to measure heme[7]. Further, this method lacks sensitivity and requires substantial numbers of cells. While sufficient starting material is obtainable from tissues such as liver, this method precludes iron measurements in rarer populations such as T-cells. More recently, fluorescent probes for iron detection via flow cytometry or fluorescence imaging provided promise of a more easily quantifiable metric of cellular iron at a single cell level, but in reality, suffer from being non-specific and imprecise. For instance, early iron detection probes such as calcein-AM and phen-green-SK have been shown to interact with other non iron metal ions[8]. Additionally, these dyes are "quenching" dyes meaning that their fluorescence diminishes as iron concentrations increase[8]. Given that no cell contains absolutely no iron, establishing a baseline for quantification requires treating control cells with an iron chelator and comparing the shift in fluorescence between treated and untreated cell populations, precluding true "single cell" iron measurements[8]. Next generation iron

probes include Rho-Nox1 and Rho-Nox4 (commercially available as FerroOrange) are "turn-on" dyes which unlike calcein-AM and phen-green-SK increase their fluorescence as iron levels increase[9,10]. However, these probes once again lack universality, detecting only labile Fe^{2+} and appear to be Golgi specific meaning iron in other compartments might be missed[8]. Across methods, the gold standard for total iron quantification is bulk cell inductively coupled plasma mass spectrometry (ICP-MS) which permits extremely sensitive total iron detection. However, bulk cell ICP-MS still lacks single cell resolution[11]. While single cell ICP-MS (SC-ICP-MS) methods are emerging*, they will require substantial optimisation before they will be capable of providing iron measurements with a suitable level of confidence. Further, these methods do not allow for accurate measurements of iron within multiple specific organelles or pathways.

Given the lack of easily measurable, accurate, total iron species measurements on a per cell basis, in this chapter we aimed to establish a computational method using proteomics data of iron interacting proteins to estimate cellular iron content and to examine how iron usage and distribution changes across pathways during T-cell activation and between immune cells at steady state. Further we examined the dynamics of notable iron interacting proteins and developed a mathematical model to predict how iron uptake changes as transferrin saturation, (TSAT, the source of iron for most cell types) varies.

3.1.1 Aims

This chapter aims to:

1. Identify how iron interacting protein expression shifts during T-cell activation and differentiation
2. Estimate T-cell iron content during activation and homeostatic iron content across immune cells
3. Model T-cell iron uptake dynamics as a function of changing iron availability

* I am currently collaborating with researchers at the University of Oxford Department of Earth Sciences to optimise a SC-ICP-MS method for use with leukocytes.

3.2 Results

3.2.1 Identification of iron interacting proteins during T-cell activation and differentiation*

Our analysis utilised the Howden *et al*[12] dataset which consists of quantitative protein mass spectrometry (protein-MS) data for murine CD4+ and CD8+ T-cells at 0 hours, 24 hours and 6 days post-activation. CD4+ and CD8+ T-cells cultured for 6 days were differentiated towards Th1 and cytotoxic T-lymphocytes (CTLs) respectively and protein expression data at all timepoints was reported by both copy-number and concentration[12]. Notably, total cellular protein concentration increases by two to three-fold within 24h post-activation and continues to increase at 6 days[12]. Howden *et al*[12] considered proteins with fold change values greater than 1.5 and p-values less than 0.05 as significantly differentially regulated; we also utilised these threshold values[12]. Using a computational approach, the list of iron interacting proteins provided by Andreini *et al*[2] was cross compared against the T-cell proteomic profiles from Howden *et al*[12]. Of the 9436 proteins detected in the Howden *et al*[12] dataset, 204 were identified as iron interacting proteins (Table 3.1), approximately half the number predicted by Andreini *et al*[2] as being iron-binding (398)[2]. This (204/9436) corresponds to a frequency of iron interacting proteins of 2.16% (Table 3.1), which is approximately the frequency expected given the percentage of human proteins predicted to be iron interacting[2]. This suggests that there is no apparent detection bias for or against iron interacting proteins in this dataset. However, when stratifying proteins by iron interaction type (Fe-S cluster, heme group or iron ion), heme proteins were underrepresented as assessed by a chi-squared test. While the composition of the original Andreini *et al*[2] iron interacting protein list was 48%, 35% and 18% respectively for heme, iron ion and Fe-S clusters (Table 3.1), the Howden *et al*[12] data set only contained 28% heme interacting proteins[2].

Iron interacting proteins were also identified amongst proteins considered differentially expressed by copy-number or concentration during T-cell activation (0h vs 24h) or differentiation (0h vs 6 days) for CD4+ and CD8+ T-cells (Appendix table 3.2). In all cases, approximately 2% of differentially expressed proteins were identified as iron

* This section (3.2.1) is largely derived from the text and figures published in Teh *et al*, Frontiers of Immunology, 2021 (DOI: 10.3389/fimmu.2021.714613)

interacting. When further broken down into heme, iron ion or Fe-S cluster interacting proteins, the frequencies did not deviate significantly from the frequencies observed amongst all detected iron interacting proteins (Table 3.1).

RRM2 was the most highly differentially upregulated iron interacting protein in CD4+ and CD8+ T-cells at both 24h and 6 days (Fig. 3.1A). RRM2 is also amongst the top 10 highest expressed iron interacting proteins by absolute copy-number at 6 days post-activation in CD4+ and CD8+ T-cells (Table 3.2). RRM2 is a protein subunit of the ribonucleotide reductase (RNR) which catalyses the reduction step of deoxyribonucleotide synthesis and is essential for downstream DNA synthesis[13,14]. The di-iron centre of RRM2 is critical for RNR catalytic activity and iron chelation with deferoxamine inhibits RNR activity in leukocytes[14,15]. Given the essentiality of nucleotide

			Iron interacting proteins	Heme proteins	Iron ion proteins	Fe-S cluster proteins	p-value
Andreini *et al*[2] (human)			~2%	192/398 (48.24%)	139/398 (34.92%)	70/398 (17.59%)	-
All proteins detected by Howden *et al*[12], 2019			204/9436 (2.16%)	57/204 (27.94%)	90/204 (44.12%)	60/204 (29.41%)	0.0001 †
DIFFERENTIALLY EXPRESSED (VS NAÏVE)	CD4+ 24h	copy-number	161/6842 (2.35%)	43/161 (26.71%)	71/161 (44.10%)	50/161 (31.06%)	0.8764 ‡
		concentration	154/6248 (2.46%)	39/154 (25.32%)	72/154 (46.75%)	45/154 (29.22%)	0.7241 ‡
	Th1 6 days	copy-number	175/8032 (2.18%)	46/175 (26.29%)	78/175 (44.57%)	51/175 (29.14%)	0.9122 ‡
		concentration	146/6503 (2.25%)	44/146 (30.14%)	61/146 (41.78%)	44/146 (30.14%)	0.7877 ‡
	CD8+ 24h	copy-number	174/7440 (2.34%)	44/174 (25.29%)	77/174 (44.25%)	56/174 (32.18%)	0.6327 ‡
		concentration	143/6305 (2.27%)	42/143 (29.37%)	60/143 (41.96%)	44/143 (30.77%)	0.8333 ‡
	CTL 6 days	copy-number	181/8169 (2.22%)	47/181 (25.97%)	79/181 (43.65%)	58/181 (32.04%)	0.6991 ‡
		concentration	151/6457 (2.34%)	44/151 (29.14%)	68/151 (45.03%)	42/151 (27.81%)	0.8776 ‡

Table 3.1. Frequency of iron interacting proteins in the Howden *et al*[12] dataset. Frequencies of iron interacting proteins are calculated as a fraction of total proteins detected, frequencies of individual iron interactions (heme/ions/Fe-S clusters) are calculated as a fraction of iron interacting proteins. Statistics are chi-square tests for goodness of fit for the distribution of iron ion, heme and Fe-S cluster iron interacting proteins. †The chi-square test was calculated relative to the Andreini *et al*[2] dataset. ‡Chi-square tests are calculated relative to the complete set of iron interacting proteins detected in the Howden *et al*[12] dataset.

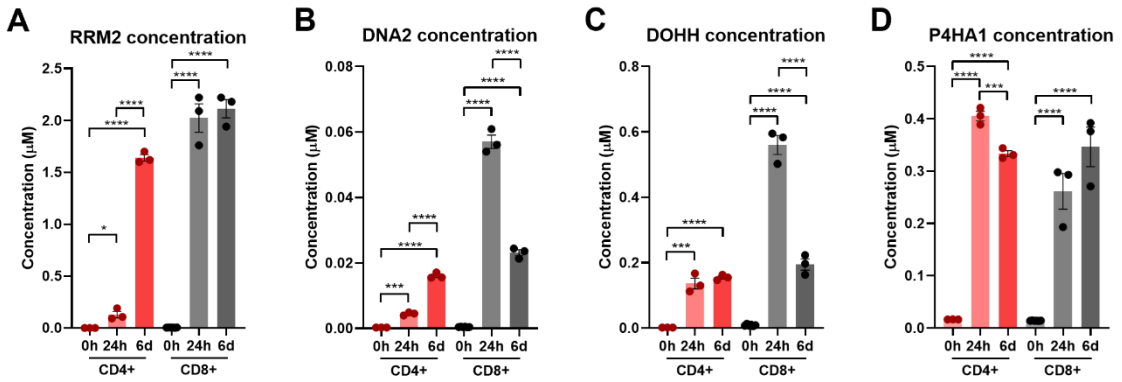

Figure 3.1. Most highly upregulated iron interacting proteins in activated T-cells. An iron interacting protein list derived from Andreini *et al*[2] was cross compared against the Howden *et al*[12] dataset consisting of protein-MS data for 0h, 24h and 6 day activated CD4+ and CD8+ T-cells. Four iron interacting protein species, RRM2, DNA2, DOHH and P4HA1, were found to have fold changes greater than 15 in all subsets. Protein concentrations derived from the Howden *et al*[12] dataset for **(A)** RRM2, **(B)** DNA2, **(C)** DOHH and **(D)** P4HA1. Data is mean ± SEM. Statistics for **(A-D)** are ordinary one-way ANOVAs with multiple comparisons using Tukey's correction within CD4+ or CD8+ T-cells. *p < 0.05; **p < 0.01; ***p<0.001; ****p < 0.0001.

synthesis for DNA replication and proliferation, RRM2 appears to be a critical target for iron usage in activated T-cells undergoing a programme of rapid proliferation.

DNA2, DOHH and P4HA1 were also amongst the most highly upregulated iron interacting proteins and were the only other upregulated iron interacting proteins with fold changes greater than 15 in all subsets (Fig. 3.1B-D). Similar to RRM2, DNA2 is involved in DNA replication and uses its Fe-S cluster to enable efficient DNA binding and mediation of helicase and nuclease activities[16]. DOHH catalyses eIF5A hypusination from polyamines, a process critical for translational efficiency[17]. DOHH knockout has been shown to dysregulate CD4+ T-cell differentiation skewing them towards a more pathogenic phenotype characterised by increased IFN-γ and IL-17A producing cells[18]. eIF5A hypusination has also been implicated in B-cell function while polyamine availability and generation is critical for T-cell proliferation, differentiation and viability[19-21]. P4HA1 is a proline hydroxylase most well-known for its role in collagen synthesis but is also known to hydroxylate other protein targets; the importance of P4H1 in T-cell function is unknown[22]. The significant upregulation of these four diverse enzymes is testament to the widespread utilisation of iron in cellular function and indicates that iron deficiency may result in complex disruption of cellular activity.

RANK	CD4+ 0h	CD4+ 24h	Th1 6 days	CD8+ 0h	CD8+ 24h	CTL 6 days
1	CYCS	ACO2	PPP1CA	HBB	PPP1CA	CYB5A
2	PPP1CA	GSTP1/2	CYB5A	GSTP1/2	GSTP1/2	PPP1CA
3	ACO2	PPP1CA	GSTP1/2	PPP1CA	CYCS	CYCS
4	CISD1	FTL1/2	CYCS	ACO2	ACO2	GSTP1/2
5	ABCE1	ADI1	BOLA2	FTL1/2	RRM2	ACO2
6	NDUFS1	CYB5A	ACO2	CYCS	FTL1/2	GLRX3
7	CISD2	GLRX3	CYB5B	CYB5A	BOLA2	BOLA2
8	SDHB	ABCE1	RRM2	CYC1	GLRX3	RRM2
9	GSTP1/2	NDUFS1	COPA	UQCRFS1	ABCE1	CYB5B
10	COPA	HBB	GLRX3	NDUFS1	PPAT	COX5A
Cumulative proportion of predicted total cellular iron content	67%	51%	41%	51%	37%	38%

Table 3.2. Top ten iron interacting proteins ranked by absolute copy-number. Colours highlight proteins commonly found in the top 10 expressed iron interacting proteins between conditions.

Many of the differentially expressed iron interacting proteins identified by our analysis were differentially regulated in both CD4+ and CD8+ T-cells, highlighting a requirement for similar iron dependent processes. Of the iron interacting proteins that were significantly upregulated 24h post-activation, 114 proteins were found to be commonly upregulated in terms of copy-number in CD4+ and CD8+ T-cells (Fig. 3.2A). 65 of these iron interacting proteins were also commonly upregulated in terms of concentration. Since the total protein content of T-cells increases upon activation and differentiation, for the concentration of these proteins to be significantly upregulated, the copy-number value must be experiencing a fold change increase greater than the fold change of total protein content. Thus, the proteins upregulated by concentration are a subset of proteins upregulated by copy-number and represent the most highly upregulated proteins. To understand if specific pathways may be particularly reliant on iron dependent proteins at 24h post T-cell activation, unranked pathway analysis using gProfiler[23] was completed on the sets of 114 iron interacting proteins upregulated by both CD4+ and CD8+ T-cells by copy-number at 24h post-activation (Fig. 3.2C). The list of upregulated iron interacting proteins was enriched for GO terms relating to demethylation, Fe-S cluster synthesis, cellular respiration and unsurprisingly, iron homeostasis. The high enrichment of these pathways with iron interacting proteins suggests that iron scarcity may disproportionately disrupt these processes.

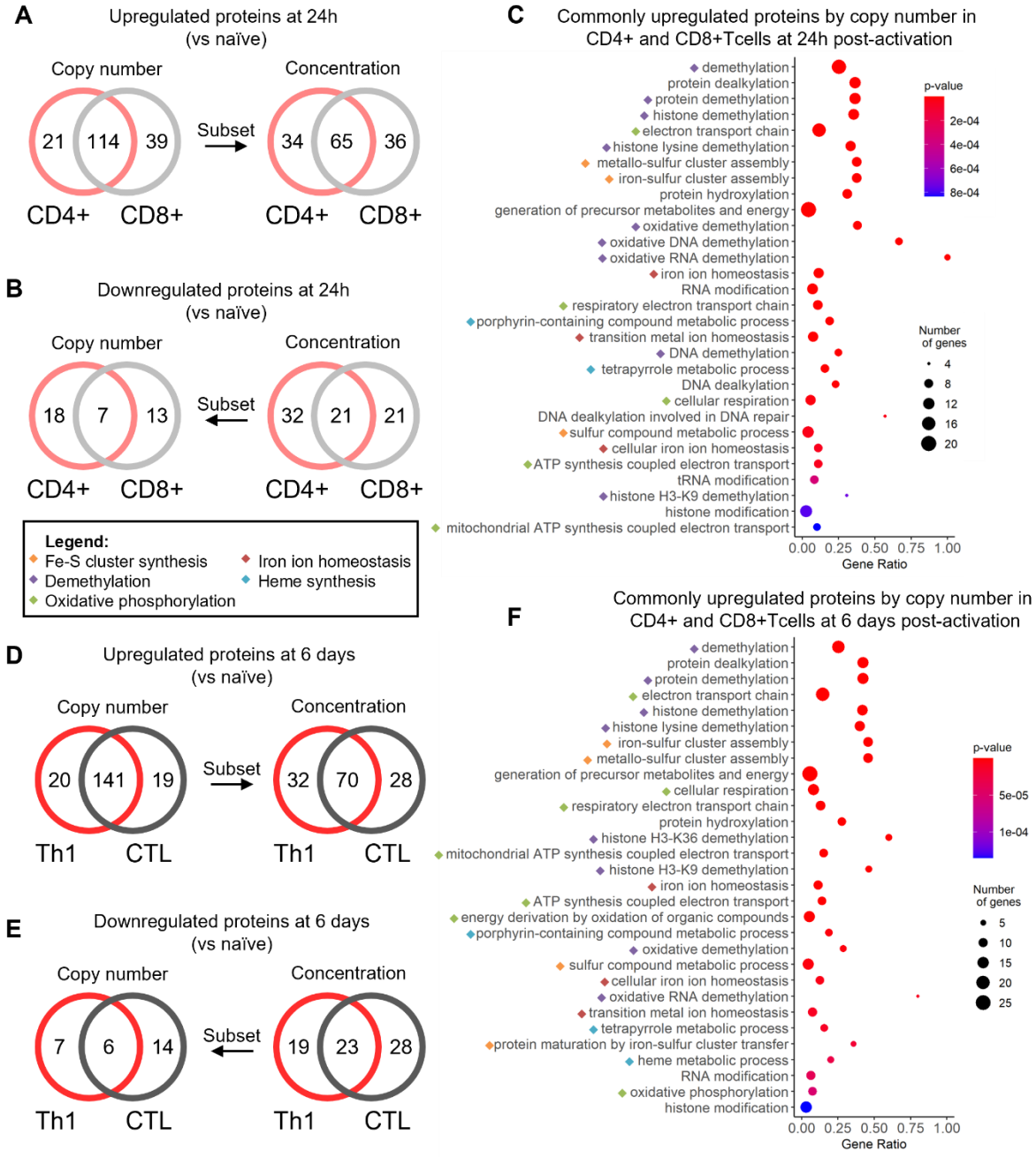

Figure 3.2. Iron interacting proteins are involved in diverse pathways during T-cell activation. Number of differentially upregulated **(A)** and downregulated **(B)** iron interacting proteins by copy-number and concentration between 0h and 24h for activated CD4+ and CD8+ T-cells. **(F)** gProfiler GO term analysis of the 114 commonly upregulated iron interacting proteins by copy-number at 24h. Gene ratios indicate the percentage of gene hits within each GO term set. Number of differentially up **(D)** and down **(E)** regulated proteins by copy number and concentration for T-cells differentiated down the Th1 and CTL lineages at 6 days post-activation compared to day 0. **(F)** gProfiler GO term analysis for the 141 commonly upregulated iron interacting proteins between Th1 and CTL subsets at 6 days.

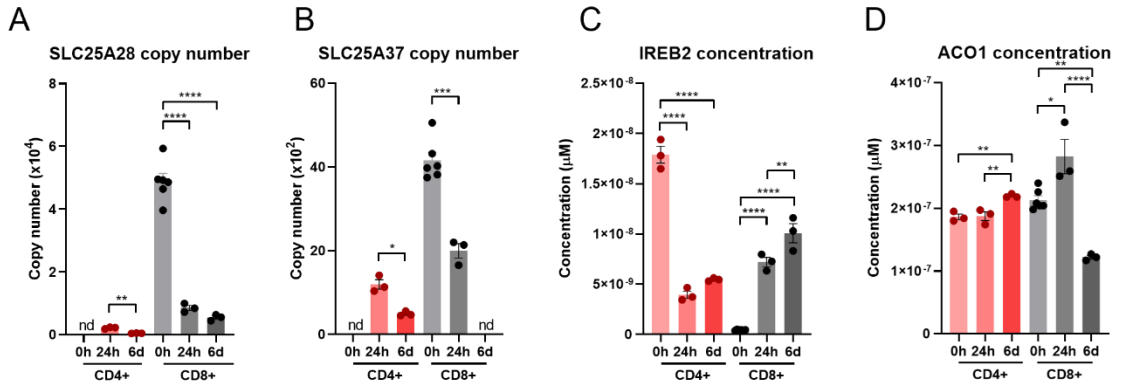

Figure 3.3. The mitochondrial iron importers, SLC25A37 and SLC25A28, and the cellular iron regulator, IREB2, show different dynamics between CD4+ and CD8+ T-cells through activation. Protein copy number for **(A)** SLC25A37 and **(B)** SLC25A28 and protein concentration for **(C)** IREB2 and **(D)** ACO1. Copy-number and concentration data is derived from the Howden *et al*[12] dataset. Data is mean ± SEM. Statistics for **(A-D)** are ordinary one-way ANOVAs with multiple comparisons using Tukey's correction within CD4+ or CD8+ T-cells. *p < 0.05; **p < 0.01; ***p<0.001; ****p < 0.0001.

At 6 days post activation, 141 proteins were commonly upregulated (from 0h) in both CD4+ and CD8+ T-cells by copy-number, of which 70 were also increased in concentration (Fig. 3.2D). Pathway analysis for the 141 upregulated iron interacting proteins by copy-number produced a very similar list of iron interacting proteins to the enrichment at 24h (Fig. 3.2F), indicating the continued necessity of iron dependent processes such as demethylation, oxidative phosphorylation (OXPHOS) and Fe-S clusters throughout T-cell activation and differentiation. Downregulated iron interacting proteins were far less common (Fig. 3.2B, E) but included iron interacting proteins such as albumin (ALB), hemopexin (HPX) and lysine demethylase 7a (KDM7A). Due to the low number of downregulated iron interacting proteins, pathway analysis on these proteins was not performed.

We were also interested in identifying iron interacting proteins that displayed extreme differences in regulation upon activation between CD4+ and CD8+ T-cells. To do so, we filtered for proteins that showed significant differences in expression upon activation in CD4+ and CD8+ T-cells but in opposite directions. Using this method, we identified three iron homeostasis proteins of interest (Fig. 3.3A-C). Prior to activation, CD4+ T-cells showed no expression of either SLC25A37 and SLC23A28 (mitoferrins 1 and 2 respectively) which govern mitochondrial iron import[24,25]. In contrast, naïve CD8+ T-cells displayed detectable expression of both importers. Upon activation, CD4+ T-cells

marginally but significantly upregulated both SLC25A28 and SLC25A37, while CD8+ T-cells dramatically downregulated both mitochondrial iron import proteins.

Iron response element binding protein 2 (IREB2) also showed divergent regulation in CD4+ and CD8+ T-cells (Fig. 3.3C). IREB2 and aconitase 1 (ACO1) are proteins that post-transcriptionally regulate iron homeostasis[26]. During cellular iron deficiency, IREB2 and ACO1 induce iron acquisition and retention by stabilising mRNAs that encode iron uptake proteins such as TFRC while blocking translation of mRNAs that encode proteins involved in iron sequestration and egress[26]. While CD8+ T-cells increase IREB2 expression upon activation, CD4+ T-cells show downregulation of IREB2. Taken alone, this data may suggest that CD4+ T-cells have a reduced ability to respond to altered environmental iron availability relative to CD8+ T-cells. However, it should be noted that the significant downregulation of IREB2 in CD4+ T-cells may be partially or completely compensated by ACO1 (functional redundancy of IREB2 and ACO1 has been reported in leukocyte populations[27]), whose concentration remains relatively constant in CD4+ T-cells at all time points (Fig. 3.3D).

3.2.2 Estimating T-cell iron content using iron interacting protein data*

To better comprehend how alterations in iron availability may impact T-cell function, it is useful to assess the cellular iron requirements during activation and differentiation. Using protein copy-number data from the Howden *et al*[12] dataset we estimated the mean iron requirement of CD4+ and CD8+ T-cells at 0h, 24h and 6d post-activation given the assumption that all iron interacting protein iron binding sites are actively occupied (Fig 3.4A). Where possible, known values of iron atoms per protein species were used based on searching the Uniprot database for iron cofactors (45% of iron interacting proteins in the Howden *et al*[12] dataset, Fig. 3.4B). In cases where exact values were not readily available, deliberate underestimations of 1 iron atom for heme or iron ion interactions or 2 iron atoms for Fe-S cluster interactions were used, to bias our estimates conservatively.

Naïve CD4+ and CD8+ T-cells had mean iron atom estimates of approximately $10x10^6$ and $16x10^6$ respectively (Fig. 3.4C). Estimates for iron requirements increase by

* This section (3.2.2) is largely derived from the text and figures published in Teh *et al*, Frontiers of Immunology, 2021 (DOI: 10.3389/fimmu.2021.714613)

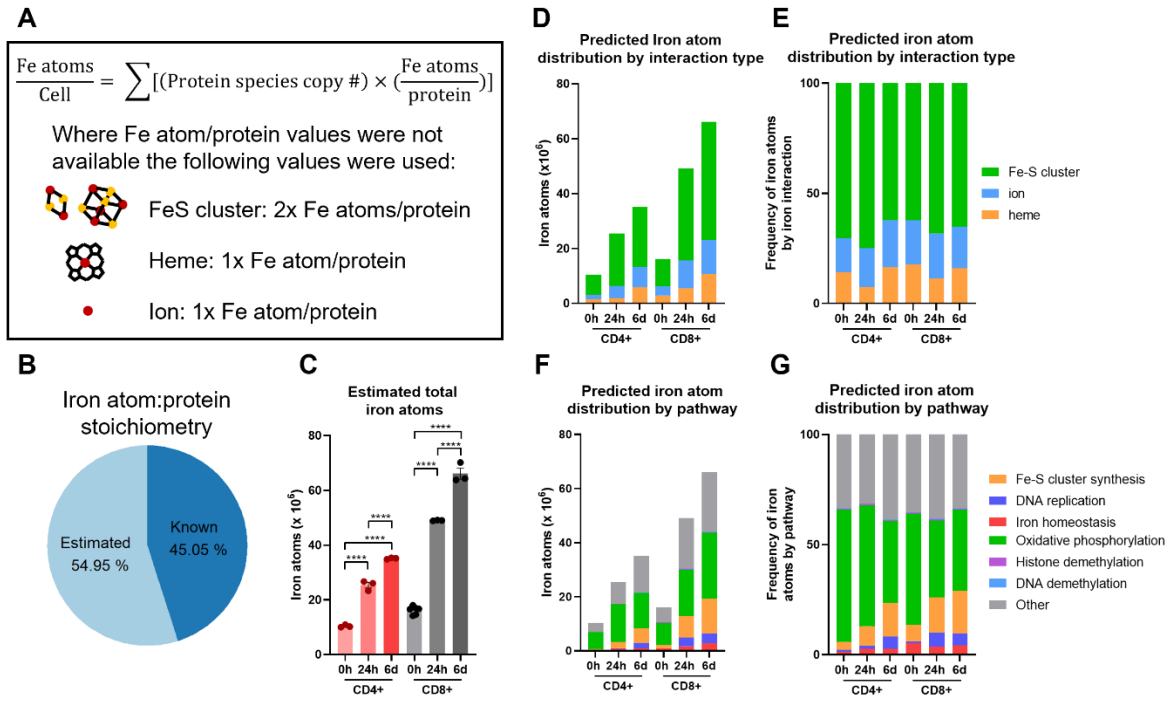

Figure 3.4. T-cells are predicted to increase total iron content upon activation. **(A)** Cellular iron atom content was estimated by assuming complete saturation of all iron binding sites by iron interacting proteins in the Howden *et al*[12] dataset. Where possible known values of iron atom:protein stoichiometry were used. If unknown, values were assumed to be 2 for Fe-S clusters, 1 for iron ions and 1 for heme groups. **(B)** Frequency of proteins for which iron atom:protein stoichiometry was known vs predicted. **(C)** Estimates for iron atom counts per cell. Estimates for iron atom **(D)** count and **(E)** frequency distribution stratified by interaction type (Fe-S cluster, iron ion, heme group). Iron interaction information was derived from Andreini *et al*[2]. Predicted iron atom **(F)** count and **(G)** frequency by pathway. Pathways were defined using GO terms (see methods). Data is mean ± SEM. Statistics for **(C)** are ordinary one-way ANOVAs with multiple comparisons using Tukey's correction within CD4+ or CD8+ T-cells. ****p < 0.0001.

approximately 2-fold for CD4+ T-cells and approximately 3-fold for CD8+ T-cells within the first 24h of activation and continue to increase at 6d post-activation. Howden *et al*[12] report a very large increase in the expression of the primary iron import protein, TFRC, throughout T-cell differentiation[12,28]. TFRC likely mediates the uptake of iron required to supply newly synthesised iron interacting proteins with their necessary iron cofactors.

While ferritin is the best characterised iron storage protein, we wanted to identify if other protein species may also make a substantial contribution to cellular iron by collectively binding high amounts of iron due to a combination of high protein expression and/or high iron interacting protein:iron atom stoichiometry and thus act as "iron sinks". We ranked iron interacting proteins by the predicted iron atoms bound by each protein

RANK	CD4+ 0h	CD4+ 24h	Th1 6 days	CD8+ 0h	CD8+ 24h	CTL 6 days
1	ACO2	ACO2	ACO2	ACO2	ACO2	ACO2
2	NDUFS1	NDUFS1	SDHB	NDUFS1	NDUFS1	NDUFS1
3	SDHB	SDHB	PPP1CA	SDHB	SDHB	SDHB
4	CYCS	GSTP1	BOLA2	HBB-BS	PPP1CA	HBB-BS
5	PPP1CA	NDUFS8	NDUFS1	GSTP1	PPAT	GSTP1
6	CISD1	PPP1CA	CYB5A	PPP1CA	NUBP2	PPP1CA
7	NDUFV1	PPAT	GSTP1	NDUFS8	BOLA2	NDUFS8
8	NDUFS2	NDUFV1	NUBP2	NDUFV1	GSTP1	NDUFV1
9	ABCE1	NUBP2	CYCS	FTL1	CYCS	FTL1
10	CISD2	GLRX3	NUBP1	CYCS	GLRX3	CYCS
Cumulative proportion of predicted total cellular iron content	73%	64%	52%	61%	48%	48%

Table 3.3. Top 10 iron interacting proteins ranked by predicted iron atoms per protein species. Colours indicate iron interacting proteins commonly predicted to be amongst the top 10 that sequester iron between conditions.

species (Table 3.3). Amongst the protein species predicted to bind the most iron are ACO2, NDUFS1, SDHB and PPP1CA which were expressed at high levels in both CD4+ and CD8+ T-cells at all time points (Table 3.3). The top 10 proteins in each cell type and differentiation state are predicted to contain 48%-73% of all non-ferritin cellular iron.

When iron atom requirements are subdivided by iron interaction, iron atoms utilised in all iron interaction types (Fe-S clusters, ions and heme groups), increase upon activation (Fig. 3.4D). At all stages of activation, >60% of iron atoms in CD4+ and CD8+ T-cells are predicted to be involved in Fe-S clusters (Fig. 3.4E). This is largely due to the nature of mammalian Fe-S clusters to contain two to four iron atoms per cluster (4Fe-4S, 3Fe-4S, 2Fe-2S) meaning that Fe-S cluster interacting proteins tend to have greater iron atom stoichiometry relative to heme or iron ion interacting proteins. We also observed enrichment of Fe-S cluster synthesis proteins detected via GO term enrichment at 24h and 6d of activation (Fig. 3.2C, F). Upregulation of Fe-S cluster synthesis machinery is likely required to facilitate the predicted high Fe-S cluster demand.

While the GO term analysis enabled us to identify the most commonly differentially regulated iron utilising pathways between T-cell subsets, it did not provide information as to the pathways that are most iron enriched. Using the gene set enrichment data, we identified GO terms of six different major iron requiring pathways and stratified our estimated iron counts per protein species by pathway (Fig. 3.4F-G). This analysis predicts

that the largest proportion of iron atoms per T-cell are being utilised within OXPHOS. In naïve T-cells, approximately 60% of iron atoms are localised in OXPHOS proteins. Following activation, the proportion of iron atoms in OXPHOS proteins, while still being the largest iron utilising pathway of the six we analysed, drops to approximately 40%. However, it should be noted that the absolute number of iron atoms in the OXPHOS pathway does increase with activation. Notably, OXPHOS contains a high number of iron interacting proteins with high stoichiometry of iron atoms per protein. For instance, NDUFS1 of CI contains 3 Fe-S clusters alone, corresponding to 10 iron atoms. The majority of the iron interactions in the electron transport chain (ETC) are with Fe-S clusters which partially accounts for the predicted high number of Fe-S cluster interactions within the cell (Fig. 3.2C and 3.2F). Given the high demand for Fe-S clusters, Fe-S cluster synthesis was unsurprisingly predicted to have the second highest proportion of iron atoms. Further, the proportion of iron atoms in this pathway increases upon activation, indicating the importance of Fe-S clusters during T-cell activation.

DNA replication was also a major hub of iron utilisation in 24h and 6d stimulated T-cells (Fig. 3.4F-G). This agrees with the observation that RRM2, DNA2 and other iron requiring DNA replication enzymes (POLE, POLA1, PRIM2) were amongst the most upregulated iron interacting proteins post-activation. In contrast, while methylation was a top hit in gene enrichment analysis, both histone and DNA methylation make minor contributions of iron atoms to total predicted cellular iron content (Fig. 3.4F). This discrepancy may be partially explained by the nature of demethylase iron interactions. While many of the enzymes involved in OXPHOS and DNA synthesis interact with Fe-S clusters containing two or more iron atoms, the JmjC KDM demethylases interact with singular iron atoms. Nevertheless, the prominence of JmjC KDM enzymes in the pathway analysis of commonly upregulated proteins is consistent with *in vitro* data (discussed in chapter 5) indicating the importance of iron for T-cell methylation remodelling.

3.2.3 Modelling T-cell iron uptake dynamics*

The iron import protein, TFRC, is critical for immunological function and is substantially upregulated upon T-cell activation (Fig 3.5A)[12,28,29]. TFRC iron uptake is facilitated via binding to the serum iron binding protein transferrin (Tf) which induces

* This section (3.2.3) is largely derived from the text and figures published in Teh *et al*, Frontiers of Immunology, 2021 (DOI: 10.3389/fimmu.2021.714613)

receptor mediated endocytosis [30]. Once internalised, acidification of the endosome promotes Tf iron release allowing for cellular use[30]. TFRC is recycled back to the cell surface to complete an endocytic cycle[30]. The $TFRC^{Y20H}$ mutation which impairs TFRC's capacity to internalise iron by approximately 50% causes severe immunodeficiency, indicating the importance of transferrin-bound iron for T-cell function[29].

Tf has two asymmetric iron binding sites located at the C and N termini of the protein with different iron binding affinities[31]. Therefore, Tf can exist in four different forms depending on iron occupancy; apotransferrin (apoTf), C or N terminus monoferric Tf (monoTf), and diferric Tf (diTf), which bind to 0, 1 and 2 iron atoms respectively[31]. Notably, all 4 forms are capable of binding and inducing endocytosis of TFRC, albeit with different affinities and endocytic cycling periods[32,33]. Since apoTf is also capable of binding and inducing endocytosis of TFRC, high levels of apoTf can effectively inhibit iron uptake via accumulation of TFRC within endosomes[32]. Using equations developed by Aisen *et al*[34], the relative proportions of each Tf form can be calculated given the overall TSAT level[31,34]. Using known association constant values for TFRC binding to each Tf form we calculated the relative probabilities of TFRC binding to each Tf form[33,35]. With the calculated relative probabilities for TFRC-Tf binding, we estimated the average iron uptake and cycling time per TFRC protein for any given TSAT value.

Using this model, the time required to obtain the calculated 24h "iron need" was determined. "Iron need" was calculated as the difference in estimated iron atoms between 0h and 24h post activation, however, it should be noted that our "iron need" predictions do not take into account intracellularly stored ferritin bound iron that may be released following activation (Fig. 3.5B-D). Ferritin levels (both light chain FTL1/2 and heavy chain FTH1) are observed to increase in T-cells post-activation but how this influences access to cellular iron in T-cells is unknown. In our model, the rate at which T-cells are capable of taking up iron is a factor of TFRC expression. While CD4+ T-cells show reduced "iron need" relative to CD8+ T-cells, since CD4+ T-cells express lower levels of TFRC, this results in an increased "iron need":TFRC ratio which is reflected in the slower iron uptake by CD4+ T-cells observed in our model (Fig. 3.5E-F). The reduced rate of iron uptake by CD4+ T-cells in this model may indicate that CD4+ T-cells may be more sensitive to iron deprivation. Given that TFRC expression is at least partially driven by iron response proteins (IREB2 and ACO1) during T-cell activation [28], the lower ability to

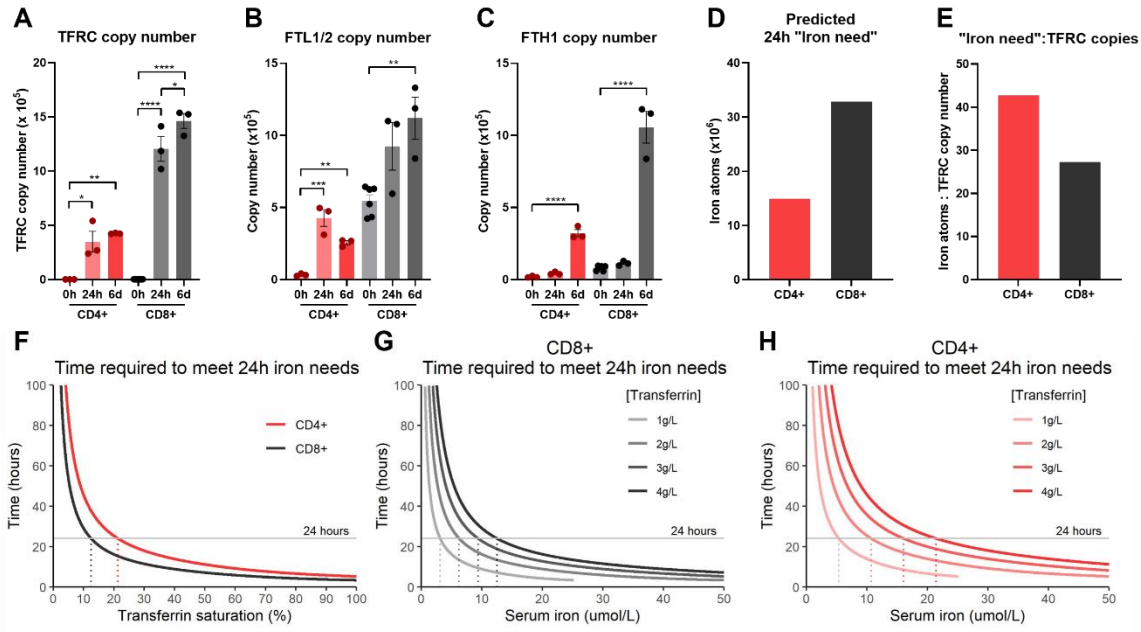

Figure 3.5. Modelling iron atom acquisition in the first 24h post-activation. **(A)** TFRC, **(B)** FTL1/2 and **(C)** FTH copy number data for CD4+ and CD8+ T-cells activated for 0h, 24h and 6 days derived from the Howden *et al*[12] dataset. **(D)** 24h "iron-need" and the **(E)** 24 "iron-need":TFRC copy ratio. 24h "iron-need" is the difference in iron atom estimates between 0h and 24h. **(F)** Model of the time required for T-cells to acquire their 24h "iron need" vs TSAT. TSAT is a function of serum iron and Tf concentration. Models of the time required for **(G)** CD8+ and **(H)** CD4+ T-cells to acquire their 24h "iron need" at different serum iron concentrations. Data is mean ± SEM. Statistics for **(A-C)** are ordinary one-way ANOVAs with multiple comparisons using Tukey's correction within CD4+ or CD8+ T-cells. *p < 0.05; **p < 0.01; ***p<0.001; ****p < 0.0001.

upregulate TFRC relative to predicted "iron need" in CD4+ T-cells may be due to the observed suppression of IREB2 in activated CD4+ T-cells relative to CD8+ T-cells.

In humans, TSAT values between 25-45% are considered normal, with TSAT values <16% defined as iron deficient by the World Health Organization[35,36]. In the context of inflammation, TSAT values <20% are often considered as consistent with "functional" iron deficiency[37]. Our model predicts that T-cells will no longer be able to meet their iron requirements (over 24 hours) at TSAT values of ~10-20% (Fig. 3.5F). This supports the idea that clinically defined iron deficiency is likely to impact on T-cell mediated immunity. Notably, our model demonstrates that the T-cells of individuals with TSAT values within the normal range should be able to easily meet iron requirements and it is unclear that there is any iron-acquisition benefit to T-cells with TSAT values greater than ~45%, for example as occurs in haemochromatosis and thalassaemia.

Given TSAT is derivable from Tf and serum iron concentrations, we were also able to model the rate of iron uptake based on these two individual factors (Fig. 3.5G-H). As Tf concentrations drop (which occurs physiologically during inflammation, because Tf is a negative acute phase protein[38]), our model predicts that the time required to meet cellular "iron need" also falls independently of serum iron concentration. This is because suppression of Tf expression while iron concentrations remain constant effectively drives up the TSAT value and increases the probability of diTf:TFRC binding. Generally, our model indicates that suppression of serum iron levels may prevent T-cells from acquiring sufficient iron for activation needs, but that sensitivity of activated T-cells to low serum iron may be more pronounced in nutritional iron deficiency (in which transferrin levels are high-normal) compared to inflammatory hypoferremia (in which transferrin is low).

3.2.4 Predicting iron content of human immune cell subtypes at steady state*

Using the model developed to examine iron content of T-cells throughout activation (Section 3.2.2, Fig. 3.4A), we sought to understand how iron requirements may differ more broadly across immune cell types using proteomics data from Rieckmann *et al*[39]. The Rieckmann *et al*[39] dataset features proteomes of 26 hematopoietic cell types sorted *via* flow cytometry from peripheral blood of healthy human donors[39]. While activation data was available for a subset of cell types, given that our main interest was to utilise immune cell iron content predictions to inform how iron demand varies between cell types during homeostatic haematopoiesis, we focused on the steady state data.

Using the same assumptions of complete occupancy of iron binding sites by iron interacting proteins and iron:protein stoichiometry values of 2 iron atoms for Fe-S cluster binding proteins and 1 iron atom for both iron ion and heme binding proteins (where known values were not available), we calculated the predicted iron content across immune cells (Fig 3.6A). Iron atom estimates per cell ranged from 27.1×10^6 iron atoms/cell for naïve B-cells to 479.4×10^6 iron atoms/cell for neutrophils. Neutrophils were estimated to contain significantly higher iron counts than all other cell types analysed with 2.5 fold higher iron counts than the next highest estimate of 191.9×10^6 iron

* This figures in this section (3.2.4) are derived from the figures previously published in Frost *et al*, Science Advances, 2022 (DOI: 10.1126/sciadv.abq5384). However, the text has been written *de novo* for this thesis.

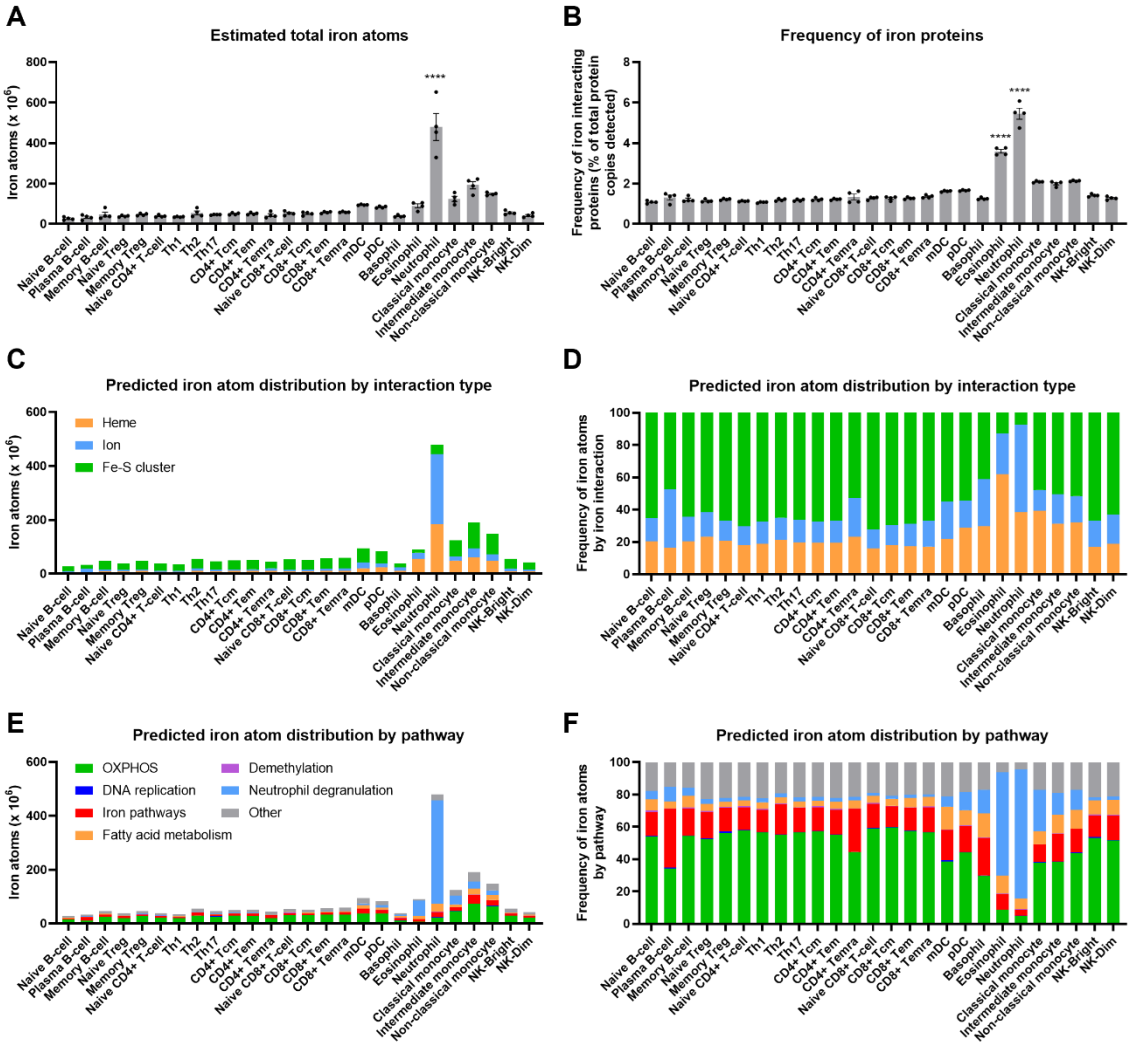

Figure 3.6. Neutrophils are predicted to have high iron requirements at steady state. Iron atom estimates were calculated using data from the Rieckmann *et al*[39] dataset using the same method as described in Fig. 3.4a where iron counts are predicted by assuming complete occupancy of iron binding sites by iron interacting proteins. Where protein:iron atom stoichiometry values were not easily accessible, values of 2, 1 and 1 iron atoms per protein were used for heme, iron ion and Fe-S cluster proteins respectively. **(A)** Iron atom estimates per cell by cell type. **(B)** Frequency of iron interacting protein copies amongst all protein copies detected. Estimated **(C)** total counts and **(D)** frequency of iron atoms stratified by interaction type (Fe-S cluster, iron ion, heme group) with interaction type information derived from Andreini *et al*[2]. Estimated **(E)** total counts and **(F)** frequency of iron atoms stratified by pathway. Pathways were defined using GO and Reactome terms. Data is mean ± SEM. Statistics for **(A-B)** are ordinary one-way ANOVAs with multiple comparisons using Dunnett's correction for multiple comparisons with comparisons made between all subsets and neutrophils for **(A)** and all subsets and neutrophils and eosinophils for **(B)**. ****p < 0.0001.

atoms/cell for intermediate monocytes. When the frequency of iron interacting protein copies amongst all protein copies detected was calculated (Fig. 3.6B), neutrophils were highlighted as having the highest levels of iron interacting proteins. Eosinophils similarly had a significantly higher iron protein content than all other immune cell types except neutrophils. The dedication of 5.5% and 3.6% of their proteomes to iron interacting proteins in neutrophils and eosinophils respectively, suggests that these cell types may have high dependencies on iron for their function. Experimental validation was conducted in Frost *et al*[40] where it was shown that serum iron suppression using the drug mini-hepcidin, decreased splenic neutrophils and eosinophils but not monocytes, dendritic cells, CD4+ T-cells, CD8+ T-cells, B-cells or NK cells[40].

Predicted iron content was stratified by interaction type (Fig. 3.6C-D) and pathway (Fig. 3.6E-F). Most cell types are predicted to largely use Fe-S cluster proteins, many of which are used in the OXPHOS pathway. In general, across immune cell types, the iron atom distributions by interaction type and pathway largely resemble one another suggesting general dependencies on iron for common "housekeeping" type pathways such energy metabolism. In contrast, neutrophils and eosinophils have much higher fractional predicted usage of heme and iron ion interacting proteins. The high predicted usage of non-Fe-S cluster binding proteins is largely explained by the high allocation of iron atoms to proteins annotated to the Reactome neutrophil degranulation protein set which includes heme and iron ion binding proteins such as myeloperoxidase (MPO), eosinophil peroxidase (EPX) and catalase (CAT) which are crucial for neutrophil and eosinophil function. This data shows that our model can be applied to varied proteomics datasets and indicates that while all cells likely require iron, the precise iron need, iron cofactors and pathways which require iron vary considerably in a cell-specific manner.

3.3 Discussion*

Using a data mining approach, we investigated the dynamics of iron and iron interacting proteins during T-cell activation and differentiation. Our analysis indicates that T-cells rapidly and substantially increase iron demands post-activation for use in diverse pathways including OXPHOS, demethylation and DNA synthesis (Fig. 3.2C, F, Fig.

* This section (3.3) is largely derived from the text published in Teh *et al*, Frontiers of Immunology, 2021 (DOI: 10.3389/fimmu.2021.714613)

3.4F-G). Similarly, we assessed iron content and usage across immune cell subsets at homeostasis and revealed particularly high predicted iron dependencies of neutrophils for use by neutrophil degranulation proteins such as MPO and EPX (Fig. 3.6E-F).

Cellular pathways which are enriched for iron interacting proteins such as DNA synthesis, OXPHOS, demethylation and Fe-S cluster biogenesis (Fig. 3.2C, F) may be particularly susceptible to dysfunction during iron deficiency. Iron atoms in Fe-S clusters seem especially important in T-cells as they make up the majority of predicted iron atoms per cell (Fig. 3.4D-E). Fe-S cluster biogenesis appeared as a top hit in pathway enrichment for activated T-cells and showed an increase in the proportion of iron atoms in that pathway during T-cell activation. Further, Fe-S cluster synthesis feeds into many pathways including OXPHOS which was predicted to be the pathway with the highest concentration of iron atoms (Fig. 3.4F-G). *In vitro* iron deprived T-cells have been shown to suppress mitochondrial ATP generation, further reinforcing the necessity of iron for T-cell OXPHOS[28].

Using our computational analysis alone, it is difficult to evaluate the degree of impairment of iron deficiency on independent processes. For instance, histone and DNA demethylation were identified as critical iron dependent processes due to the high number of individual iron interacting proteins in these pathways (Fig. 3.2C, F). But, the absolute number of iron atoms attributed to DNA and histone demethylases is relatively low compared to OXPHOS and Fe-S cluster synthesis (Fig. 3.4F-G). However, iron deprivation has been shown to impair chromatin remodelling in Th17 cells which feature elevated expression of the KDM6B target, H3K27me3 (data discussed in chapter 5)[41]. Further, while DNA synthesis did not score amongst the highest enrichment terms in pathway analysis, two critical enzymes involved in DNA synthesis, RRM2 and DNA2, were amongst the most highly differentially regulated iron interacting proteins in activated T-cells, indicating that iron dependent DNA synthesis proteins are likely critical for T-cell activation (Fig. 3.1A-B). This is in agreement with previous data showing that *in vitro* iron deprivation impairs DNA synthesis and cell-cycle progression in CD8+ T-cells[28].

It is still unclear how iron depletion affects intracellular iron distribution. Data from the Howden *et al*[12] dataset showed that Mitoferrins 1 and 2, which mediate mitochondrial iron transport, have different expression kinetics in CD4+ and CD8+ T-cells (Fig. 3.3A-B). Given that pathway analysis highlighted that iron dependent mitochondrial

pathways such as OXPHOS, Fe-S cluster synthesis and heme synthesis are commonly upregulated in both CD4+ and CD8+ T-cells, it seems counterintuitive that mitochondrial iron transporters show different kinetics of expression in these two cell types. One may speculate that CD4+ and CD8+ T-cells may differentially store and re-distribute iron throughout the cell prior and during activation. The ability of different T-cell subsets to move iron into the mitochondria could profoundly affect the nature of iron interactions in the cell as the flux of iron into mitochondrial heme and Fe-S cluster biosynthetic pathways could present a major bottleneck for cellular iron usage. The proteins and pathways from which iron is sequentially lost during iron scarcity will also be governed by factors including iron binding affinity, protein turnover and iron trafficking by intracellular iron chaperones. Proteins which have higher iron binding affinities or slow rates of turnover are more likely to retain their iron co-factors relative to weaker iron binding proteins or proteins with a high rate of turnover resulting in recycling of iron back into the cellular iron pool. Dynamics of intracellular iron usage is also controlled by iron chaperone proteins such as PCBP1 and PCBP2 which direct and regulate iron loading onto various target iron binding proteins[42]. While a specific iron-chaperone role for PCBPs has not been demonstrated in T-cells, PCBP1 was demonstrated to have iron responsive RNA binding activity in CD4+ T-cells suggesting that PCBPs could also play a role in T-cell iron distribution during iron starvation[43]. Without in depth consideration of these factors on a individual protein basis, it is difficult to predict which proteins will be left with empty iron binding sites during iron depletion. While many biological processes are iron requiring, impairment of T-cell function by iron deficiency could in principle be due to dysfunction or altered activity of a singular protein species. However, we would hypothesise that iron deficiency's impact on T-cell activation, differentiation and function will be more widespread and mediated via effects on many cellular processes.

Using protein copy-number values we estimated the total number of iron atoms per cell at various stages of activation and predicted that T-cell iron content increases 2-3-fold post-activation (Fig. 3.4C). The dramatic transition from quiescent naïve cells with relatively low estimated iron content to rapidly proliferating activated cells with elevated predicted iron content provides a rationale as to why cellular iron deficiency appears to more significantly impair activated versus naïve cells. Humans and mice carrying a TFRC mutation which impairs iron uptake have normal percentages of circulating naïve CD4+

and CD8+ T-cells, however, TFRC mutant T-cells fail to proliferate upon activation stimuli both *in vitro* and *in vivo*[28,29]. The quiescent state of naïve T-cells likely means that once adequate cellular iron is acquired, supply of iron to iron-dependent proteins can be maintained through internal turnover of iron binding proteins.

Iron content was estimated for naïve T-cells using both the Howden *et al*[12] (Fig. 3.4C) and Rieckmann *et al*[39] (Fig. 3.6A) datasets providing an opportunity to compare the method across proteomics datasets. Notably, estimates do differ by approximately 3-fold with naïve CD4+ and CD8+ T-cells estimated to contain on average $10.4x10^6$ iron atoms/cell and $16.2x10^6$ iron atoms/cell respectively based on the Howden *et al*[12] dataset and $39.3x10^6$ iron atoms/cell and $53.2x10^6$ iron atoms/cell respectively from the Rieckmann *et al*[39] dataset. This discrepancy may be partially explained by species differences between mouse (Howden *et al*[12] data) and human (Rieckmann *et al*[39] data) T-cells but is likely also due to differences in protein detection between the datasets. Measures of naïve mouse T-cell iron have also previously been evaluated using ICP-MS where iron measures for bulk T-cells were divided by the number of input cells[11]. Our predicted iron content for naïve T-cells from the Howden *et al*[12] dataset was approximately the same as the 75 percentile value for CD8+ T-cells and 1.5 fold higher than the 75 percentile value for CD4+ T-cells as measured by Konz *et al*[11]. While the iron estimates for the Howden *et al*[12] and Rieckmann *et al*[39] datasets do differ and the values from the Howden *et al*[12] dataset are on the high end of the values reported by Konz *et al*[11], the fact that the two computed values and the experimental values are of a similar magnitude gives us confidence in our methods of estimation.

Using the estimated iron counts per cell and existing kinetic data for Tf-TFRC endocytic cycling kinetics, we constructed a model to simulate T-cell iron uptake within the first 24h post-activation at various TSAT values (Fig. 3.5F-H). Our model predicts that at TSAT values between 10-20%, T-cells would no longer be able to acquire the iron they need to maintain occupancy of all iron binding sites. Low TSAT can occur either due to nutritional iron deficiency or due to inflammatory hypoferraemia caused by severe infections and/or chronic inflammation. For example, in SARS-CoV2 infection, several studies of hospitalised COVID-19 patients report average TSAT values of well below 15% with some patients with severe disease having TSAT values as low as 5%[44-47]. Our model suggests that at very low TSATs, T-cells are unlikely to be able to acquire sufficient iron

for effective activation and differentiation. Suppression of Tf concentration from normal levels (2-3.5g/L)[35] has been observed during COVID-19 infection as well as other inflammatory states such as sepsis[44,46-48]. Suppression of Tf may be a compensatory mechanism to attempt to maintain TSAT homeostasis levels to preserve a constant rate of iron availability to the host immune system during hypoferremia.

Our model further suggests that the economic theory of diminishing returns may be applicable to cellular iron nutrition: beyond a critical threshold, additional iron is unlikely to provide additional benefit. Once all iron binding proteins become saturated and are operating at peak rates, additional iron supply likely holds no advantage and may eventually become detrimental given the inherent toxicity of unchelated iron. The observation that T-cells activated in iron loaded conditions downregulate TFRC suggests that T-cells have an upper limit of desired cellular iron[41]. In support of the non-linearity of our mathematical model, previous work from our group shows that serum iron restriction mediated via administration of a mini-hepcidin analogue significantly impairs both CD8+ and CD4+ T-cell proliferation and functionality in the context of diverse vaccination models and influenza infection[28]. In contrast, increasing serum iron beyond physiological levels via an inducible hepcidin knockout mouse model, does not enhance CD8+ T-cell proliferation or GZMB expression compared to iron replete control mice[41]. Similarly, injection of wild-type mice on a standard diet with iron dextran, which increases serum iron, does not induce CD8+ T-cell proliferation beyond normal levels after immunisation[28]. Recently, it has been reported that high iron concentrations may suppress CD4+ T-cell proliferation and Th1 differentiation[49], indicating that there may be complex context-dependent effects of excess iron on CD4+ T-cells. These data indicate that while iron supplementation may be able to boost immunity in individuals with existing iron deficiency, supplementing iron in iron replete individuals may provide little benefit.

3.3.1 Limitations

One limitation to our bioinformatic approach relates to the input data. For instance, it was noted that the iron interacting protein SDHD was not detected in the Howden *et al*[12] dataset. Given that SDHD is an essential component of complex II (CII) of the ETC and all other CII proteins (SDHA, SDHB, SDHC) were detected, the absence of SDHD points to incomplete protein detection in the Howden *et al*[12] dataset.

Unfortunately, in most cases it is difficult to know whether lack of detection is due to biological or technical reasons limiting our capacity to account for undetected proteins when calculating T-cell iron content. Whether differences in the proportions of proteins involved in different types of iron interactions (heme, Fe-S cluster or iron ions) are inherent to the T-cell proteomic profiles or are due to a detection bias in the protein-MS method also remains to be determined.

When estimating cellular iron content, we used known iron atom:protein stoichiometry values where possible. However, in cases where values were not readily available, we assumed low values of 1, 1, and 2 iron atoms for each of iron ion, heme and Fe-S cluster interactions respectively to minimise the probability of overestimating iron content. While known or cautious estimates for iron content can be made for most proteins, approximations for iron bound in ferritin complexes is difficult to assess given that ferritin cages can contain anywhere from 0 to approximately 4300 iron atoms[50]. Ferritin levels do increase upon T-cell activation (Fig. 3.5B-C), however, whether the iron content of ferritin cages changes with activation is also unknown. In our analysis, FTL1/2 and FTH1 were treated similarly to all other iron ion binding proteins and were assumed to bind one iron atom per protein. Thus, each ferritin complex is assumed to contain 24 iron atoms. Again, this is likely to result in a conservatively low approximation of cellular iron content. It should be noted that the inability to properly assess ferritin iron content also impacts the predicted T-cell "iron need" as ferritin is likely to supply at least a fraction of the cellular iron requirements during activation. If naïve T-cells contain variable amounts of ferritin iron as a function of underlying iron status of the individual, this could influence the subsequent sensitivity of T-cells to extracellular iron sources following activation. Nevertheless, other evidence strongly supports a likely general dominant dependence of T-cell responses on extracellular iron. TFRC expression is upregulated over 200-fold following T-cell activation, and decreasing extracellular iron availability profoundly suppresses T-cell responses to immunization even in iron-replete animals[12,28]. Furthermore, a mutation in TFRC that reduces efficiency of extracellular iron uptake by approximately 50% causes severe immunodeficiency in children[29]. While many of our assumptions aimed to bias our estimates conservatively, we also assume complete saturation of iron binding sites, likely overestimating iron binding per protein species. Perhaps as a result of these balancing assumptions we produced iron content estimates which are of a similar magnitude to experimentally observed values[11].

When building our model for T-cell iron uptake, we assumed that TFRC values increase instantaneously from 0h levels to 24h levels, whereas this process, although very rapid, will take longer. Neither does the model account for the increased TFRC expression that would occur in response to iron deficiency at low TSAT values, nor does it account for alternative reported mechanisms for iron uptake such as via ZIP8 and ZIP14 non-transferrin bound iron (NTBI) transporters or CD44-hyaluranon-iron complexes[51-53]. While the absolute relationship between TSAT and time required to meet T-cell iron needs may be inaccurate due to the reported limitations, the shape of the relationship is likely correct as evidenced by experimental data indicating that while low serum iron severely impairs T-cell responses[28], elevated serum iron has negligible benefit[41].

3.3.2 Conclusion

In summary, using computational methods we have demonstrated the diverse nature of iron-interacting proteins in T-cell biology and across immune cell subtypes. Our analysis has highlighted that several pathways including DNA and histone demethylation, OXPHOS, DNA synthesis and Fe-S cluster synthesis may be particularly susceptible to iron deprivation in T-cells due to either high dependency on iron interacting proteins or high predicted iron atom content and provides a foundation for future experimental study. We also highlighted that neutrophils have particularly high iron requirements at steady state which was largely attributable to iron requiring degranulation proteins.

3.4 References

1 Collaborators, G. D. a. I. I. a. P. Global, regional, and national incidence, prevalence, and years lived with disability for 328 diseases and injuries for 195 countries, 1990-2016: a systematic analysis for the Global Burden of Disease Study 2016. *Lancet* **390**, 1211-1259 (2017). https://doi.org:10.1016/s0140-6736(17)32154-2

2 Andreini, C., Putignano, V., Rosato, A. & Banci, L. The human iron-proteome. *Metallomics* **10**, 1223-1231 (2018). https://doi.org:10.1039/c8mt00146d

3 Markolovic, S., Wilkins, S. E. & Schofield, C. J. Protein Hydroxylation Catalyzed by 2-Oxoglutarate-dependent Oxygenases. *J Biol Chem* **290**, 20712-20722 (2015). https://doi.org:10.1074/jbc.R115.662627

4 Poulos, T. L. Heme Enzyme Structure and Function. *Chemical Reviews* **114**, 3919-3962 (2014). https://doi.org:10.1021/cr400415k

5 Johnson, D. C., Dean, D. R., Smith, A. D. & Johnson, M. K. Structure, function, and formation of biological iron-sulfur clusters. *Annu Rev Biochem* **74**, 247-281 (2005). https://doi.org:10.1146/annurev.biochem.74.082803.133518

6 Ghio, A. J. & Roggli, V. L. Perls' Prussian Blue Stains of Lung Tissue, Bronchoalveolar Lavage, and Sputum. *J Environ Pathol Toxicol Oncol* **40**, 1-15 (2021). https://doi.org:10.1615/JEnvironPatholToxicolOncol.2020036292

7 Duarte, T. L. & Neves, J. V. Measurement of Tissue Non-Heme Iron Content using a Bathophenanthroline-Based Colorimetric Assay. *J Vis Exp* (2022). https://doi.org:10.3791/63469

8 Carter, K. P., Young, A. M. & Palmer, A. E. Fluorescent sensors for measuring metal ions in living systems. *Chem Rev* **114**, 4564-4601 (2014). https://doi.org:10.1021/cr400546e

9 Hirayama, T., Niwa, M., Hirosawa, S. & Nagasawa, H. High-Throughput Screening for the Discovery of Iron Homeostasis Modulators Using an Extremely Sensitive Fluorescent Probe. *ACS Sens* **5**, 2950-2958 (2020). https://doi.org:10.1021/acssensors.0c01445

10 Hirayama, T., Okuda, K. & Nagasawa, H. A highly selective turn-on fluorescent probe for iron(ii) to visualize labile iron in living cells. *Chemical Science* **4**, 1250-1256 (2013). https://doi.org:10.1039/C2SC21649C

11 Konz, T. *et al.* Multielemental Analysis of Low-Volume Samples Reveals Cancer-Specific Profile in Serum and Sorted Immune Cells. *Anal Chem* **92**, 8750-8758 (2020). https://doi.org:10.1021/acs.analchem.9b05643

12 Howden, A. J. M. *et al.* Quantitative analysis of T cell proteomes and environmental sensors during T cell differentiation. *Nat Immunol* **20**, 1542-1554 (2019). https://doi.org:10.1038/s41590-019-0495-x

13 Stubbe, J. Di-iron-tyrosyl radical ribonucleotide reductases. *Curr Opin Chem Biol* **7**, 183-188 (2003). https://doi.org:10.1016/s1367-5931(03)00025-5

14 Kolberg, M., Strand, K. R., Graff, P. & Andersson, K. K. Structure, function, and mechanism of ribonucleotide reductases. *Biochim Biophys Acta* **1699**, 1-34 (2004). https://doi.org:10.1016/j.bbapap.2004.02.007

15 Hoffbrand, A. V., Ganeshaguru, K., Hooton, J. W. & Tattersall, M. H. Effect of iron deficiency and desferrioxamine on DNA synthesis in human cells. *Br J Haematol* **33**, 517-526 (1976). https://doi.org:10.1111/j.1365-2141.1976.tb03570.x

16 Mariotti, L. *et al.* The iron-sulphur cluster in human DNA2 is required for all biochemical activities of DNA2. *Commun Biol* **3**, 322 (2020). https://doi.org:10.1038/s42003-020-1048-4
17 Dever, T. E., Gutierrez, E. & Shin, B.-S. The hypusine-containing translation factor eIF5A. *Critical Reviews in Biochemistry and Molecular Biology* **49**, 413-425 (2014). https://doi.org:10.3109/10409238.2014.939608
18 Puleston, D. J. *et al.* Polyamine metabolism is a central determinant of helper T cell lineage fidelity. *Cell* **184**, 4186-4202.e4120 (2021). https://doi.org:10.1016/j.cell.2021.06.007
19 Zhang, H. *et al.* Polyamines Control eIF5A Hypusination, TFEB Translation, and Autophagy to Reverse B Cell Senescence. *Mol Cell* **76**, 110-125.e119 (2019). https://doi.org:10.1016/j.molcel.2019.08.005
20 Wu, R. *et al.* De novo synthesis and salvage pathway coordinately regulate polyamine homeostasis and determine T cell proliferation and function. *Science Advances* **6**, eabc4275 (2020). https://doi.org:10.1126/sciadv.abc4275
21 Wagner, A. *et al.* Metabolic modeling of single Th17 cells reveals regulators of autoimmunity. *Cell* **184**, 4168-4185.e4121 (2021). https://doi.org:10.1016/j.cell.2021.05.045
22 Gorres, K. L. & Raines, R. T. Prolyl 4-hydroxylase. *Crit Rev Biochem Mol Biol* **45**, 106-124 (2010). https://doi.org:10.3109/10409231003627991
23 Raudvere, U. *et al.* g:Profiler: a web server for functional enrichment analysis and conversions of gene lists (2019 update). *Nucleic Acids Res* **47**, W191-w198 (2019). https://doi.org:10.1093/nar/gkz369
24 Paradkar, P. N., Zumbrennen, K. B., Paw, B. H., Ward, D. M. & Kaplan, J. Regulation of Mitochondrial Iron Import through Differential Turnover of Mitoferrin 1 and Mitoferrin 2. *Molecular and Cellular Biology* **29**, 1007 (2009). https://doi.org:10.1128/MCB.01685-08
25 Shaw, G. C. *et al.* Mitoferrin is essential for erythroid iron assimilation. *Nature* **440**, 96-100 (2006). https://doi.org:10.1038/nature04512
26 Wilkinson, N. & Pantopoulos, K. The IRP/IRE system in vivo: insights from mouse models. *Front Pharmacol* **5**, 176-176 (2014). https://doi.org:10.3389/fphar.2014.00176
27 Bonadonna, M. *et al.* Iron regulatory protein (IRP)-mediated iron homeostasis is critical for neutrophil development and differentiation in the bone marrow. *Sci Adv* **8**, eabq4469 (2022). https://doi.org:10.1126/sciadv.abq4469
28 Frost, J. N. *et al.* Hepcidin-Mediated Hypoferremia Disrupts Immune Responses to Vaccination and Infection. *Med (N Y)* **2**, 164-179.e112 (2021). https://doi.org:10.1016/j.medj.2020.10.004
29 Jabara, H. H. *et al.* A missense mutation in TFRC, encoding transferrin receptor 1, causes combined immunodeficiency. *Nature Genetics* **48**, 74-78 (2016). https://doi.org:10.1038/ng.3465
30 Dautry-Varsat, A., Ciechanover, A. & Lodish, H. F. pH and the recycling of transferrin during receptor-mediated endocytosis. *Proc Natl Acad Sci U S A* **80**, 2258-2262 (1983). https://doi.org:10.1073/pnas.80.8.2258
31 Chasteen, N. D. & Williams, J. The influence of pH on the equilibrium distribution of iron between the metal-binding sites of human transferrin. *Biochem J* **193**, 717-727 (1981). https://doi.org:10.1042/bj1930717
32 Núñez, M. T., Núñez-Millacura, C., Beltrán, M., Tapia, V. & Alvarez-Hernandez, X. Apotransferrin and holotransferrin undergo different endocytic cycles in

intestinal epithelia (Caco-2) cells. *J Biol Chem* **272**, 19425-19428 (1997). https://doi.org:10.1074/jbc.272.31.19425

33 Young, S. P., Bomford, A. & Williams, R. The effect of the iron saturation of transferrin on its binding and uptake by rabbit reticulocytes. *Biochem J* **219**, 505-510 (1984). https://doi.org:10.1042/bj2190505

34 Aisen, P., Leibman, A. & Zweier, J. Stoichiometric and site characteristics of the binding of iron to human transferrin. *J Biol Chem* **253**, 1930-1937 (1978).

35 Kelly, A. U., McSorley, S. T., Patel, P. & Talwar, D. Interpreting iron studies. *Bmj* **357**, j2513 (2017). https://doi.org:10.1136/bmj.j2513

36 WHO. Iron deficiency anaemia: assessment, prevention, and control: a guide for programme managers. (2001).

37 Lopez, A., Cacoub, P., Macdougall, I. C. & Peyrin-Biroulet, L. Iron deficiency anaemia. *The Lancet* **387**, 907-916 (2016). https://doi.org:10.1016/S0140-6736(15)60865-0

38 Gabay, C. & Kushner, I. Acute-phase proteins and other systemic responses to inflammation. *N Engl J Med* **340**, 448-454 (1999). https://doi.org:10.1056/nejm199902113400607

39 Rieckmann, J. C. *et al.* Social network architecture of human immune cells unveiled by quantitative proteomics. *Nat Immunol* **18**, 583-593 (2017). https://doi.org:10.1038/ni.3693

40 Frost, J. N. *et al.* Plasma iron controls neutrophil production and function. *Sci Adv* **8**, eabq5384 (2022). https://doi.org:10.1126/sciadv.abq5384

41 Teh, M. R., Frost, J. N., Armitage, A. E. & Drakesmith, H. Analysis of Iron and Iron-Interacting Protein Dynamics During T-Cell Activation. *Front Immunol* **12**, 714613 (2021). https://doi.org:10.3389/fimmu.2021.714613

42 Philpott, C. C., Ryu, M. S., Frey, A. & Patel, S. Cytosolic iron chaperones: Proteins delivering iron cofactors in the cytosol of mammalian cells. *J Biol Chem* **292**, 12764-12771 (2017). https://doi.org:10.1074/jbc.R117.791962

43 Wang, Z. *et al.* Iron Drives T Helper Cell Pathogenicity by Promoting RNA-Binding Protein PCBP1-Mediated Proinflammatory Cytokine Production. *Immunity* **49**, 80-92.e87 (2018). https://doi.org:10.1016/j.immuni.2018.05.008

44 Shah, A. *et al.* Systemic hypoferremia and severity of hypoxemic respiratory failure in COVID-19. *Critical Care* **24**, 320 (2020). https://doi.org:10.1186/s13054-020-03051-w

45 Bolondi, G. *et al.* Iron metabolism and lymphocyte characterisation during Covid-19 infection in ICU patients: an observational cohort study. *World J Emerg Surg* **15**, 41 (2020). https://doi.org:10.1186/s13017-020-00323-2

46 Bellmann-Weiler, R. *et al.* Prevalence and Predictive Value of Anemia and Dysregulated Iron Homeostasis in Patients with COVID-19 Infection. *J Clin Med* **9** (2020). https://doi.org:10.3390/jcm9082429

47 Hippchen, T., Altamura, S., Muckenthaler, M. U. & Merle, U. Hypoferremia is Associated With Increased Hospitalization and Oxygen Demand in COVID-19 Patients. *Hemasphere* **4**, e492 (2020). https://doi.org:10.1097/hs9.0000000000000492

48 Brandtner, A. *et al.* Linkage of alterations in systemic iron homeostasis to patients' outcome in sepsis: a prospective study. *Journal of Intensive Care* **8**, 76 (2020). https://doi.org:10.1186/s40560-020-00495-8

49 Pfeifhofer-Obermair, C. *et al.* Regulation of Th1 T Cell Differentiation by Iron via Upregulation of T Cell Immunoglobulin and Mucin Containing Protein-3 (TIM-3). *Front Immunol* **12** (2021). https://doi.org:10.3389/fimmu.2021.637809

50 Fischbach, F. A. & Anderegg, J. W. An x-ray scattering study of ferritin and apoferritin. *J Mol Biol* **14**, 458-473 (1965). https://doi.org:10.1016/s0022-2836(65)80196-6

51 Wang, C. Y. *et al.* ZIP8 is an iron and zinc transporter whose cell-surface expression is up-regulated by cellular iron loading. *J Biol Chem* **287**, 34032-34043 (2012). https://doi.org:10.1074/jbc.M112.367284

52 Liuzzi, J. P., Aydemir, F., Nam, H., Knutson, M. D. & Cousins, R. J. Zip14 (Slc39a14) mediates non-transferrin-bound iron uptake into cells. *Proc Natl Acad Sci U S A* **103**, 13612-13617 (2006). https://doi.org:10.1073/pnas.0606424103

53 Müller, S. *et al.* CD44 regulates epigenetic plasticity by mediating iron endocytosis. *Nat Chem* **12**, 929-938 (2020). https://doi.org:10.1038/s41557-020-0513-5

Chapter 4

4 Examining the impacts of iron scarcity on global T-cell biochemistry

4.1 Introduction

The efficacy of CD8+ T-cell responses depends on the integration of various environmental factors including temperature[1], pH[2] and nutritional status[3]. A growing body of literature has implicated iron as a necessary nutritional factor for induction of effective T-cell responses. Notably, iron depletion severely impairs T-cell responses in models of vaccination, viral infection and autoimmunity[4-8]. *In vitro* studies of iron starved T-cells have suggested that the functional defects may be partly explained by metabolic suppression characterised by reduced signalling by the metabolic regulator, mTORC1, reduced mitochondrial ATP generation and impaired mitochondrial membrane potential [4,6,9,10]. However, these observed metabolic changes are relatively unspecific and could be mediated by a wide range of biochemical perturbations. Thus, the specific nodes at which iron deficiency impairs T-cell metabolism and function still remain to be characterised.

With 2% of cellular proteins predicted to be iron binding[11], the scope for processes which could be impaired by iron deficiency is broad. We previously utilised published datasets (chapter 3) to explore iron interacting protein dynamics in activated T-cells to help predict the pathways that may be most impaired by T-cell iron deficiency[12]. By assessing the processes which have either the greatest upregulation of iron interacting proteins or the highest predicted iron atom content, oxidative phosphorylation (OXPHOS), DNA replication and iron homeostasis/iron-sulfur (Fe-S) cluster synthesis were suggested as pathways potentially impacted by iron deficiency due to their high dependencies on iron (Chapter 3, Fig. 3.2C, F, Fig. 3.4F-G)[12]. However, this methodology still only identifies broad biological processes and direct experimental evidence demonstrating impairment of these pathways during T-cell iron limitation is lacking.

To broadly characterise the impacts of cellular perturbations (such as iron deprivation), gene expression profiling by RNA-sequencing (RNA-seq) has become broadly utilised. Initial gene expression studies utilised the microarray, a precursor to the modern RNA-seq which was conceived in 1995[13]. Schena *et al*[13], simultaneously measured the expression of 45 *Arabidopsis thaliana* genes by hybridisation of fluorescently labelled cDNAs generated from mRNA samples to complementary DNAs affixed to a glass slide[13]. Fluorescence as a readout of gene expression was measured using a scanning laser[13]. 11 years later in 2006, the first RNA-seq paper was published, reporting detection of over 10,000 mRNAs by massively in parallel sequencing by synthesis[14]. mRNA sequencing of a single oocyte was described in 2009, giving birth to single cell RNA-seq (sc-RNA-seq)[15]. Sequencing has now become a relatively inexpensive method for assessing how different treatments or genotypes impact gene expression and typically detects 8000-16,000 protein coding genes depending on cell type[16]. While many studies use mRNA profiles as a readout of cell state, since proteins are regulated by translation, post-translational modifications, degradation and substrate availability, mRNA levels do not necessarily reflect the expression or activity of their corresponding proteins[17]. Pearson correlation coefficients calculated for paired mRNA and protein expression studies find R^2 values ranging from 0 to 0.87[18] demonstrating that mRNA expression is not always a good proxy for protein expression. Thus, while RNA-seq and protein-mass spectrometry (protein-MS) have overlapping utility (in essence both informing about gene expression), parallel RNA-seq and protein-MS could provide additional, and possibly more robust, biological insights.

Protein-MS for protein characterisation began in the 1980s. However, protein-MS for protein identification was not enabled until 1993 when methods for matching protein-MS fingerprints to existing protein datasets were developed[19-22]. In 1996, molecular mass matching algorithms together with protein-MS of yeast proteins separated using two-dimensional gel electrophoresis produced the first protein survey, identifying 150 separate proteins[23]. Since then, protein-MS has improved dramatically and is capable of comprehensively identifying cell line proteomes, with some studies detecting greater than 10,000 different proteins covering the majority of matched transcriptomes[16,24]. Single cell protein-MS has recently also become possible[25].

T-cell microarray, RNA-seq and protein-MS experiments have together helped establish the trajectory of T-cell gene and protein expression during activation. T-cells rapidly remodel transcription and translation upon activation with protein content increasing by two to three-fold within the first 24 hours post-activation [26,27]. Upregulated genes and proteins include effector molecules such as granzymes and perforins, effector T-cell transcription factors, cell adhesion molecules critical for migration, cyclins necessary for cell cycle progression, and metabolic proteins involved in glycolysis, translation and nutrient uptake[26,27]. Meanwhile, proteins which are critical for naïve T-cells but which require downregulation during early activation, such as KLF2, experience rapid protein turn over in the naïve state allowing for quick removal upon activation[28].

While metabolism appears to be a key process which is perturbed in iron restricted T-cells, whether metabolic impairment is the primary defect is unclear. In this chapter we aimed to understand how iron deficiency affects T-cell biochemistry globally by using the more unbiased approaches of RNA-seq and protein-MS. CD8+ T-cells cultured *in vitro* in low iron conditions were found to upregulate the p53 cell cycle arrest pathway and downregulate the interferon (IFN) response pathway at both the RNA and protein level in low iron conditions. Iron deprived T-cells also show suppression of signalling by the key metabolic regulators, mTORC1 and MYC, suggesting defects in metabolic rewiring. Despite reduced metabolic signalling, iron deprived T-cells show upregulation of proteins involved in mitochondrial processes such as β-oxidation and the electron transport chain (ETC). Additionally, we identified an *Dglucy* as a particular metabolic gene of interest due to its dramatic mutual upregulation at both the mRNA and protein levels.

4.1.1 Aims

This chapter aims to:

1. Characterise the gene and protein expression profile of T-cells activated under iron limiting conditions
2. Identify specific T-cell processes impacted by iron scarcity at the transcriptional and proteomic levels for future exploration

4.2 Results*

4.2.1 Iron deficiency remodels the T-cell transcriptome and proteome

To assess the global impacts of iron limitation on CD8+ T-cell biochemistry during activation, RNA-seq and protein-MS were completed. CD8+ T-cells were magnetically isolated from murine spleen and lymph nodes and activated using α-CD3, α-CD28 and IL-2 (Fig. 4.1A) as previously described[4]. To manipulate the available iron, an iron free serum substitute (rather than fetal bovine serum (FBS)) was employed, and holo-transferrin was titrated in at defined concentrations (total transferrin was kept constant at 1.2 mg/mL by adjusting apotransferrin accordingly). The highest concentration of 0.625 mg/mL holotransferrin (approximately 15.6 μmol/L of iron) was calculated to be roughly reflective of the levels of iron physiologically found in human sera (14-32 μmol/L of iron)[29]. Meanwhile, the low holotransferrin concentrations of 0.001 mg/mL are much lower than that found in plasma, but could be reflective of highly iron depleted environments such as those in the tumour microenvironment[30]. At 48 hours post-activation CD8+ T-cells were harvested and RNA-seq and protein-MS was completed.

For the RNA-seq a fold change threshold of $\log_2|\text{fold change}| > 1.5$ and a false discovery rate (FDR) threshold of <0.05 was applied (in line with previous T-cell RNA-seq studies[1,31]). 193 genes of the 11496 genes expressed at >1 count per million in at least one condition were identified as significantly differentially regulated between the high and low iron conditions (Fig. 4.1B). While cells activated in either high or low iron conditions clustered distinctly apart from their naïve counterparts, clear segregation was still observed between the two iron concentrations (Fig. 4.1C). Notably expression of the iron uptake receptor, *Tfrc*, was significantly higher in the low iron condition (Fig. 4.1D). *Tfrc* upregulation is consistent with cellular iron limitation as *Tfrc* is induced in the context of iron deficiency via the IRP-IRE system (chapter 1, section 1.1.3) to enable compensatory upregulation of iron uptake[32].

For the protein-MS data, a fold change threshold of $\log_2|\text{fold change}| > 0.585$ (equivalent to $|\text{fold change}| > 1.5$) was used (as used in Howden *et al*[26]). We applied the typical p-value threshold of <0.05 when comparing the high (0.625 mg/mL

* The protein-MS experiment described in this section (4.2) was conducted in collaboration with Linda Sinclair at the University of Dundee.

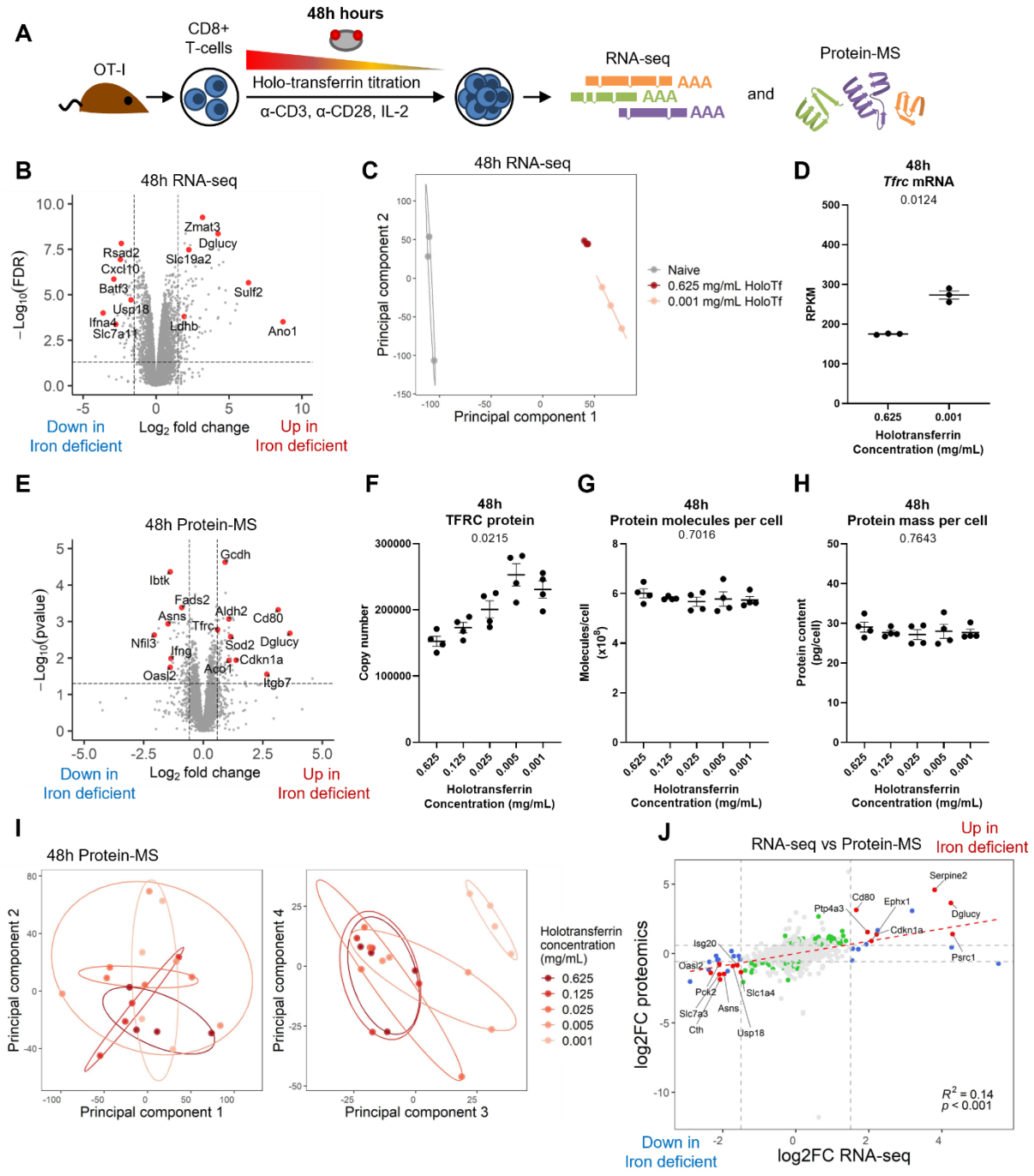

Figure 4.1. Iron deficiency alters T-cells at the transcriptional and proteomic level. **(A)** CD8+ OT-I T-cells isolated from mice were activated with 5 μg/mL plate bound α-CD3, 1 μg/mL α-CD28 and 50 U/mL IL-2 for 48h before RNA-sequencing (n = 3) or protein-mass spectrometry (n = 4). Naïve T-cells for RNA-seq were collected immediately post-isolation on day 0. **(B)** Volcano plot of RNA-seq differentially expressed genes between T-cells in high (0.625 mg/mL holotransferrin) and low (0.001 mg/mL holotransferrin) iron conditions. For the RNA-seq significance thresholds of FDR < 0.05 and $\log_2$|fold change| > 1.5 were applied. RNA-seq **(C)** principal components analysis and **(D)** *Tfrc* mRNA expression. RPKM = reads per kilobase of transcript per million mapped reads. **(E)** Volcano plot of protein-MS differentially expressed proteins between T-cells in high (0.625 mg/mL holotransferrin) and low 0.001 mg/mL (holotransferrin) iron conditions. The significance thresholds of $\log_2$|fold change| > 0.585, p-value < 0.05 (*continued on next page*)

(*continued from last page*) assessed by a t-test comparing 0.625 and 0.001 mg/mL holotransferrin and p-value < 0.05 assessed by a one-way ANOVA comparing all five iron concentrations (0.625, 0.125, 0.025, 0.005, 0.001 mg/mL holotransferrin) were applied for extra stringency. **(F)** TFRC protein expression, **(G)** protein molecules per cell, **(H)** protein mass per cell measured via protein-MS. **(I)** principal component analysis from protein-MS of T-cells in a titration of holotransferrin concentrations. **(J)** Correlation plot of the log_2|fold change| between high (0.625 mg/mL holotransferrin) and low (0.001 mg/mL holotransferrin) iron conditions by RNA-seq and protein-MS. Data is mean ± SEM. Statistics for **(D)** is a paired two-tailed t-test. Statistics for **(F-H)** are sample matched one-way ANOVAs with the Geisser-Greenhouse correction. For **(J)** a Pearson correlation R^2 value was calculated.

Gene	RNA		Protein			Pathway
	Log_2(FC)	FDR value (t-test)	Log_2(FC)	p-value (t-test)	p-value (1-way ANOVA)	
Psrc1	4.30	<0.0001	1.40	0.0297	0.0020	p53
Dglucy	4.24	<0.0001	3.64	0.0021	<0.0001	Metabolic
Serpine2	3.80	<0.0001	4.59	0.0366	<0.0001	Extracellular matrix
Cdkn1a	2.21	<0.0001	1.38	0.0114	0.0010	p53/Cell cycle
Ephx1	2.07	<0.0001	0.91	0.0155	0.0002	Metabolic
Ptp4a3	1.97	<0.0001	1.55	0.0006	0.0001	Signalling
Cd80	1.65	<0.0001	3.14	0.0005	0.0003	T-cell activation
Slc1a4	-1.51	<0.0001	-1.34	0.0118	0.0030	Metabolic
Isg20	-1.60	0.0001	-0.84	0.0020	0.0230	IFN response
Usp18	-1.72	<0.0001	-0.90	0.0168	0.0006	IFN response
Asns	-1.97	0.0011	-1.48	0.0011	0.0010	Metabolic
Cth	-2.08	<0.0001	-1.87	0.0015	0.0006	Metabolic
Slc7a3	-2.09	<0.0001	-1.50	0.0420	0.0010	Metabolic
Pck2	-2.10	<0.0001	-0.76	0.0103	0.0020	Metabolic
Oasl2	-2.33	<0.0001	-1.39	0.0181	0.0020	IFN response

Table 4.1. Mutually differentially regulated genes between the RNA-seq and protein-MS. For the RNA-seq, a threshold of Log_2|Fold Change| > 1.5 and an FDR-value < 0.05 was applied. For the protein-MS, a threshold of Log_2|Fold Change| > 0.585, a p-value < 0.05 calculated via a t-test comparing the 0.625 mg/mL and 0.001 mg/mL holotransferrin conditions and a p-value < 0.05 calculated via a one-way ANOVA for all five iron concentrations (0.625, 0.125, 0.025, 0.005, 0.001 mg/mL holotransferrin). Pink and blue denote up and downregulated genes in low iron conditions respectively. Green indicates metabolic enzymes. FC = fold change.

holotransferrin) and low (0.001 mg/mL holotransferrin) iron concentrations via a t-test. However, given we that we have data for five holotransferrin concentrations for the protein-MS, we applied an additional threshold to increase stringency of p-values < 0.05 when a one-way ANOVA was conducted across all conditions. Our analysis produced 116 differentially expressed proteins (of the 5431 proteins detected at a copy number greater than 100 in at least 1 condition) (Fig. 4.1E). As expected under conditions of iron scarcity, TFRC protein copy number increased as holotransferrin was depleted (Fig. 4.1F). Despite the differential expression of 116 proteins, no differences were observed in protein mass or protein molecules per CD8+ T-cell activated across a titration of holotransferrin conditions (Figs. 4.1G-H). Similarly, principal components analysis sees no segregation of holotransferrin conditions until principal component 3 (Fig. 4.1I). Together this suggests CD8+ T-cell iron deficiency induces relatively subtle proteomic changes despite the profound functional suppression previously reported[4].

To evaluate whether the RNA-seq and protein-MS are reflective of one another, the log2|fold change| values for the 5091 mutually detected mRNAs/proteins were compared (Fig. 4.1J). We observed a significant positive correlation between the datasets indicating some agreement between the iron deficiency phenotypes at the RNA and protein level. The R^2 value of 0.14 does suggest that iron scarcity is also inducing different alterations in the RNA and protein profiles of activated T-cells, and this was largely seen as changes at the protein but not the RNA level. However, it should be noted that many of the significantly differentially regulated genes in the RNA-seq were not

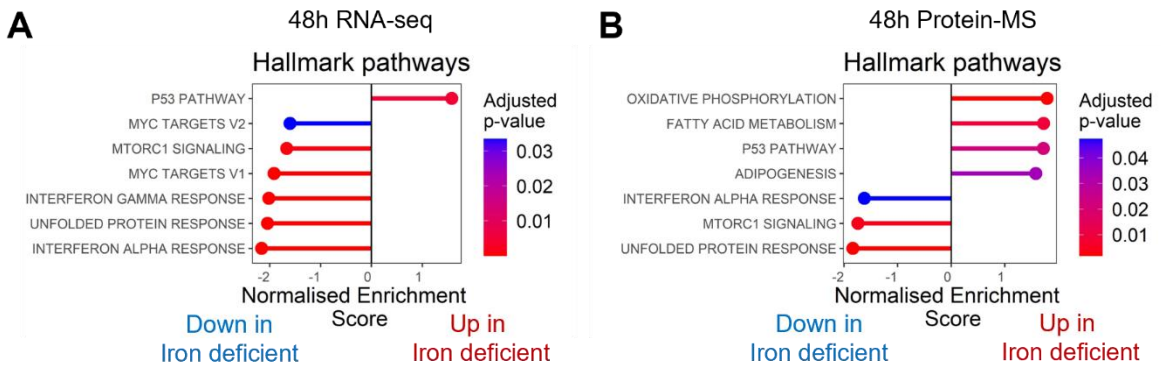

Figure 4.2. Iron restriction induces transcriptional and proteomic reprogramming. CD8+ T-cells were activated for 48h as described in figure 4.1A in varying iron concentrations. Hallmark gene set enrichment analysis (GSEA) for the **(A)** RNA-seq and **(B)** protein-MS based on comparison of samples from the high (0.625 mg/mL holotransferrin) and low (0.001 mg/mL holotransferrin) iron concentrations.

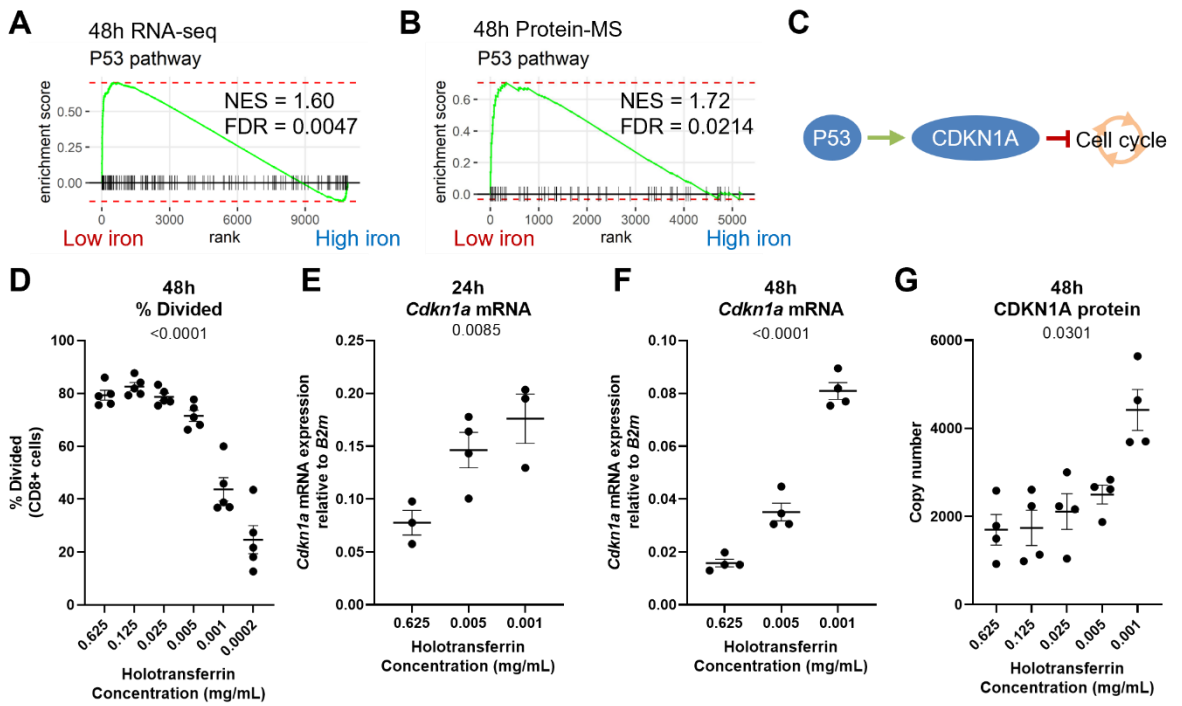

Figure 4.3. Iron scarce T-cell have a proliferative defect characterised by p53 signalling and *Cdkn1a* expression. 24-48h activated CD8+ T-cells cultured as described in figure 4.1A in varying iron concentrations. Barcode analysis for the Hallmark p53 pathway gene set for the **(A)** RNA-seq and **(B)** protein-MS, showing enrichment in the low iron condition (0.001 mg/mL holotransferrin) relative to the high iron condition (0.625 mg/mL holotransferrin). NES = Normalised enrichment score, FDR = False discovery rate. **(C)** p53 induces CDKN1A expression which inhibits the G1-S phase transition[33]. **(D)** Percentage of CD8+ T-cells that have divided as assessed using cell trace violet dye via flow cytometry. *Cdkn1a* gene expression at the mRNA level assessed by qPCR normalised to B2m expression at **(E)** 24h and **(F)** 48h. **(G)** CDKN1A protein expression at 48h. Data is mean ± SEM. Statistics for **(D-G)** are sampled matched one-way ANOVAs with the Geisser-Greenhouse correction.

detected at the protein level and thus were not considered in this analysis. Only 15 genes were found to be significantly differentially regulated at both the mRNA and protein levels (Table 4.1) with the described thresholds. Strikingly, 7/15 mutually differentially expressed genes were metabolic in nature, either acting as amino acid uptake transporters (Slc1a4, Slc7a3) or enzymes (Dglucy, Ephx1, Asns, Cth, Pck2).

4.2.2 Iron depletion induces the p53 cell cycle arrest program

Gene set enrichment analysis (GSEA) was conducted on both the RNA-seq and protein-MS datasets comparing the 0.625 mg/mL and 0.001 mg/mL iron concentrations (Fig. 4.2A-B). Amongst the top gene sets enriched in the low iron conditions was the p53 signalling pathway (Fig. 4.3A-B). Notably the p53 pathway coordinates responses to

cellular stress such as DNA damage, hypoxia, heat shock and nutrient deprivation[33]. Downstream effects of p53 signalling include cell cycle arrest, cellular senescence, apoptosis and DNA repair[33]. CDKN1A, a suppressor of the G1-S phase cell cycle transition, is a key target of p53[33] (Fig. 4.3C). In low iron conditions, we observed a profound and titratable impairment to cellular proliferation measured using the division dye, cell trace violet (CTV) at 48h (Fig. 4.3D). *Cdkn1a* expression was induced by iron deprivation at 24h, prior to the first cellular division and continued to be upregulated as CD8+ T-cells entered their proliferative phase at 48h (Fig. 4.3E-G). *Cdkn1a* was also one of the 15 mutually differentially regulated genes between the RNA-seq and protein-MS (Table 4.1). This data suggests that the proliferative defect mediated by iron starvation is driven by a p53 signalling pathway characterised by CDKN1A cell cycle suppression.

4.2.3 T-cells in low iron conditions experience metabolic rewiring

GSEA of the RNA-seq and protein-MS also identified several metabolic processes as being modified by iron scarcity in CD8+ T-cells (Fig. 4.2A-B). The mTORC1 signalling gene set was depleted at both the mRNA and protein levels (Fig. 4.4A-B) while the MYC signalling gene set was depleted in the RNA-seq alone (Fig. 4.4C). mTORC1 and MYC are metabolic regulators which are induced downstream of the T-cell receptor (TCR) and orchestrate upregulation of various biosynthetic pathways including glycolysis, amino acid and nucleotide synthesis necessary for T-cell activation (Fig. 4.4D)[34]. Suppression of mTORC1 signalling is also in line with data showing reduced phospo-S6 (pS6), a downstream target of mTORC1 signalling, in 48h iron deprived CD8+ T-cells (Fig. 4.4E; also demonstrated previously by Frost *et al*[4]). The observed depletion of proteins in the mTORC1 pathway is partially driven by suppression of proteins involved in downstream processes, such as amino acid uptake and ribosomal function (Fig. 4.4F).

In contrast to the suppression of mTORC1 and MYC signalling in low iron conditions, the protein-MS revealed an upregulation of proteins involved in metabolic pathways such as OXPHOS and fatty acid metabolism (Fig. 4.2B, 4.4G-H) which were not identified in the RNA-seq. Inspection of the proteins driving the enrichment of the fatty acid signature revealed them to be largely β-oxidation proteins involved in fatty acid and branched chain amino acid breakdown rather than fatty acid synthesis (Fig. 4.4F). ETC proteins involved in the highly iron dependent respiratory complexes I (CI), CIII and CIV

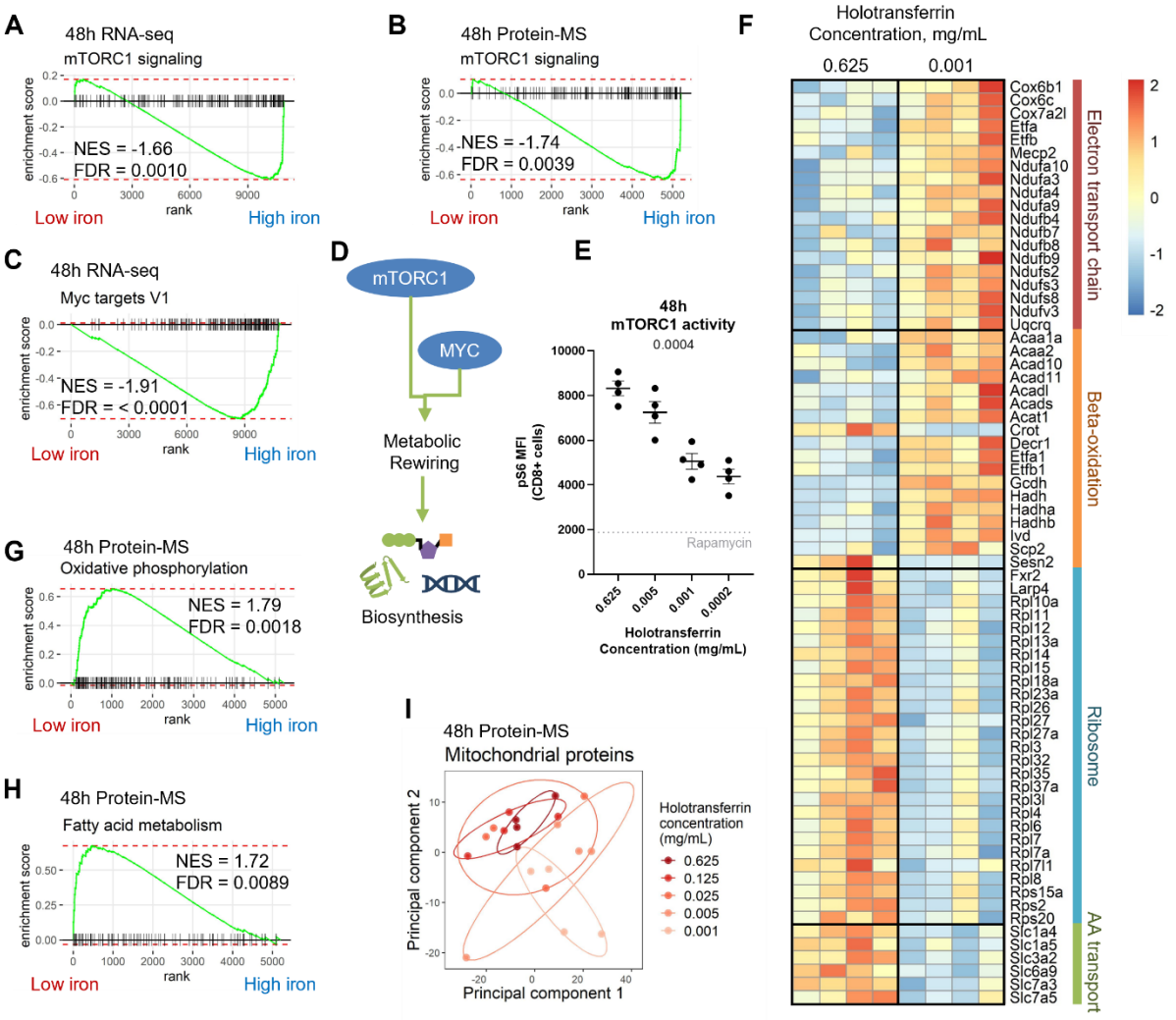

Figure 4.4. T-cell iron restriction rewires cellular metabolism. T-cells cultured for 48h in varying holotransferrin concentrations were activated as described in figure 4.1A. Barcode analysis for the Hallmark mTORC1 signalling pathway for the **(A)** RNA-seq and **(B)** proteomics. Barcode analysis for the **(C)** Hallmark MYC targets V1 gene sets for the RNA-seq. **(D)** mTORC1 and MYC are metabolic regulators that enable biosynthesis downstream of T-cell receptor stimulation. **(E)** mTORC1 activity measured via phosphorylation of its downstream target S6. Overnight treatment with the mTORC1 inhibitor, rapamycin at 1 μM, was used as a control. **(F)** Heatmap of proteins in high (0.625 mg/mL holotransferrin) or low (0.001 mg/mL holotransferrin) in selected metabolic pathways defined using GO terms where the p-value < 0.05. Electron transport chain = GO RESPIRATORY ELECTRON TRANSPORT CHAIN, beta-oxidation = GO FATTY ACID BETA OXIDATION, ribosome = GO CYTOSOLIC RIBOSOME, amino acid (AA) transport = GO AMINO ACID IMPORT. Barcode analysis for the Hallmark **(G)** oxidative phosphorylation and (**H)** fatty acid metabolism gene sets for the protein-MS. **(A-C, E-F)** show enrichment for the low iron condition (0.001 mg/mL holotransferrin) relative to the high iron condition (0.625 mg/mL holotransferrin). NES = Normalised enrichment score, FDR = False discovery rate. **(I)** Principal components analysis of the protein-MS given prior selection for proteins in the MitoCarta3.0 gene set[35]. Data is mean ± SEM. Statistics for **(E)** is a matched one-way ANOVA with the Geisser-Greenhouse correction.

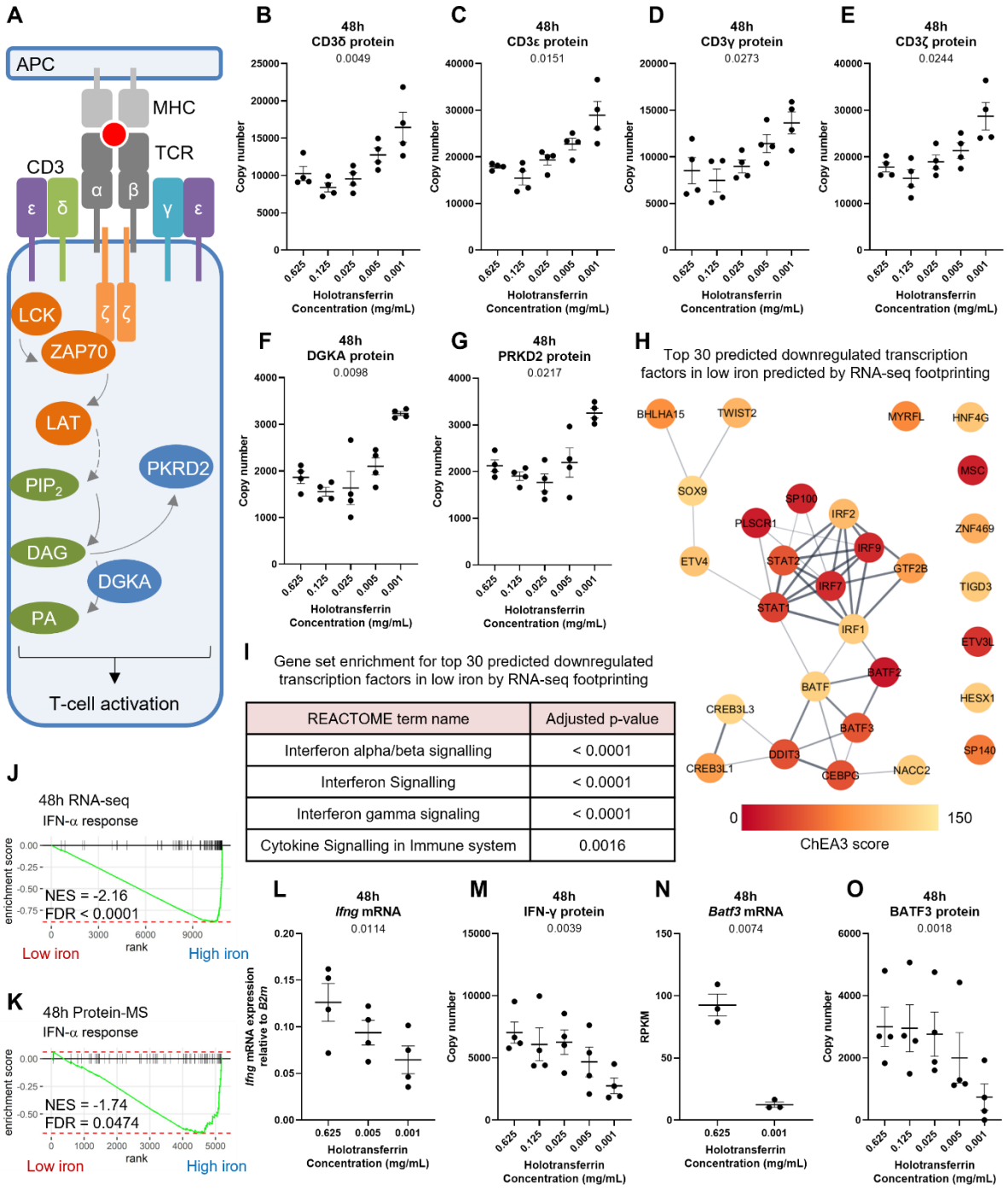

Figure 4.5. Iron deficiency alters T-cell signalling pathways and suppresses IFN related transcription. T-cells were cultured in a titration of iron conditions for 48h as described in figure 4.1A. **(A)** TCR binding to peptide-MHC induces an activation signalling cascade dependent on CD3 which is composed of CD3δ, CD3ε, CD3γ, and CD3ζ subunits. PKRD2 is activated via DAG and DGKA converts DAG to PA. Protein expression of **(B)** CD3δ, **(C)** CD3ε, **(D)** CD3γ, **(E)** CD3ζ, **(F)** DGKA, and **(G)** PRKD2. **(H)** Top 30 downregulated transcription factors in low iron conditions predicted by RNA foot printing of downregulated transcripts in the RNA-seq using the ChEA3 algorithm. Lower ChEA3 scores indicate better predictions. **(I)** Gene set enrichment of the top 30 downregulated transcription factors during iron restriction using the gProfiler algorithm. Barcode analysis for the Hallmark IFN-α response pathway for (*continued on next page*)

(*continued from last page*) the **(J)** RNA-seq and **(K)** protein-MS show depletion in the low iron condition (0.001 mg/mL holotransferrin) relative to the high iron condition (0.625 mg/mL holotransferrin). NES = Normalised enrichment score, FDR = False discovery rate. **(L)** mRNA and **(M)** protein expression of *Ifng*. **(M)** mRNA and **(N)** protein expression of *Batf3*. RPKM = reads per kilobase of transcript per million mapped reads. Data is mean ± SEM. Statistics for **(B-G, L-M, O)** are matched one-way ANOVAs with the Geisser-Greenhouse correction. Statistics for **(N)** is a paired t-test.

were also found to be upregulated (Fig. 4.4F). OXPHOS and fatty acid metabolism are largely mitochondrial processes. The accumulation of mitochondrial proteins we observed could either be driven by a compensatory feedback mechanism due to the previously observed suppression of mitochondrial ATP generation[4], or could be a defect in mitochondrial clearance, such as via mitophagy.

Mitochondrial processes were hypothesised to be particularly iron sensitive due to their high dependency on iron (chapter 3, Fig. 3.2C, F, Fig. 3.4F-G). By selecting for proteins in the MitoCarta3.0 gene set[35], we observed improved segregation within the first two principal components of CD8+ T-cells cultured in different iron concentrations (Fig. 4.4G) compared to when all proteins were analysed (Fig. 4.1I). This suggests that mitochondrial proteins are disproportionately differentially regulated relative to all proteins detected. The reduction of mTORC1 and MYC signalling pathways in conjunction with the accumulation of mitochondrial pathways suggests the iron deficiency is not simply inducing a general metabolic suppression but rather causing altered rewiring of metabolic processes.

4.2.4 Iron depletion alters CD8+ T-cell signalling and impairs IFN related pathways

Iron starvation induced upregulation of the p53 pathway and modified metabolic reprogramming. In addition to these effects, iron deprivation altered expression of key T-cell signalling proteins. Upon TCR stimulation, the CD3 complex initiates T-cell activation signalling via a LCK-ZAP70-LAT phosphorylation cascade (Fig. 4.5A) which induces a variety of intermediate mediators to activate transcription factors like NF-κB, AP-1 and NFAT[36]. Post-antigenic stimulation, CD3 is downregulated via activation of tyrosine kinases[37,38]. Notably, we observed that as iron concentrations decreased, protein expression of the CD3 components CD3δ, CD3ε, CD3γ, and CD3ζ remained high suggesting inefficient downregulation of the CD3 complex (Fig. 4.5B-E). Additionally, the protein expression of the downstream TCR signalling mediators, DGKA and PRKD2, were

similarly elevated (Fig. 4.5F-G). The failure to downregulate the TCR stimulation machinery suggests that iron deprived T-cells may inefficiently integrate activation signals resulting in impaired downstream signalling and transcriptional programs.

To understand how low iron might be impacting T-cell transcriptional reprogramming, we conducted transcription factor footprinting using the ChEA3 algorithm[39]. Transcription factor footprinting is a method of predicting the differential activity of transcription factors by assessing changes in transcriptional "footprints" measured by RNA-seq. ChEA3 predicted that iron deprivation primarily downregulates a network of transcription factors largely relating to IFN signalling (Fig. 4.5H-I). This is unsurprising given the suppression of IFN-α and IFN-γ signalling pathways observed in the GSEA of the RNA-seq and protein-MS (Fig. 4.2A-B, Fig. 4.5J-K) including suppression of well known IFN stimulated genes (ISGs) such as CXCL10, USP18 and OASL2 (Fig. 4.1B, E). However, it should be noted that there is high redundancy between the IFN-α/β and IFN-γ gene sets meaning it is not clear which pathway is impaired. We also observed that *Ifng* expression is similarly suppressed at both the mRNA and protein levels (Fig. 4.5L-M). Thus, it is possible that the reduction in IFN related pathways may be due to impaired autocrine and paracrine IFN-γ signalling. Alternatively, a reduction of IFN related pathways may be suppressing IFN-γ production.

BATF3 is an important transcription factor induced upon T-cell activation, which promotes the generation of memory T-cells[40], and was predicted to have reduced activity via transcriptional footprinting (Fig. 4.5H). *Batf3* was also found to be similarly suppressed at both the mRNA and protein levels (Fig. 4.5N-O). *In vivo* immunisation studies have found impairment of T-cell memory generation in the context of hypoferremia[4]. Whether failure to induce BATF3 may be partly responsible for the failure to generate appropriate memory T-cell responses in the context of low iron is a question for future study.

4.2.5 *Dglucy* was identified as a key upregulated gene during iron scarcity

Examination of the genes which were mutually differentially regulated between CD8+ T-cells cultured in high and low iron conditions identified *Dglucy* as one of the most upregulated genes and proteins during iron scarcity (Table 4.1, Fig. 4.6A-B). DGLUCY protein expression was highly titratable, showing substantially higher copy numbers in the 0.001 mg/mL holotransferrin than even the second lowest concentration of 0.005

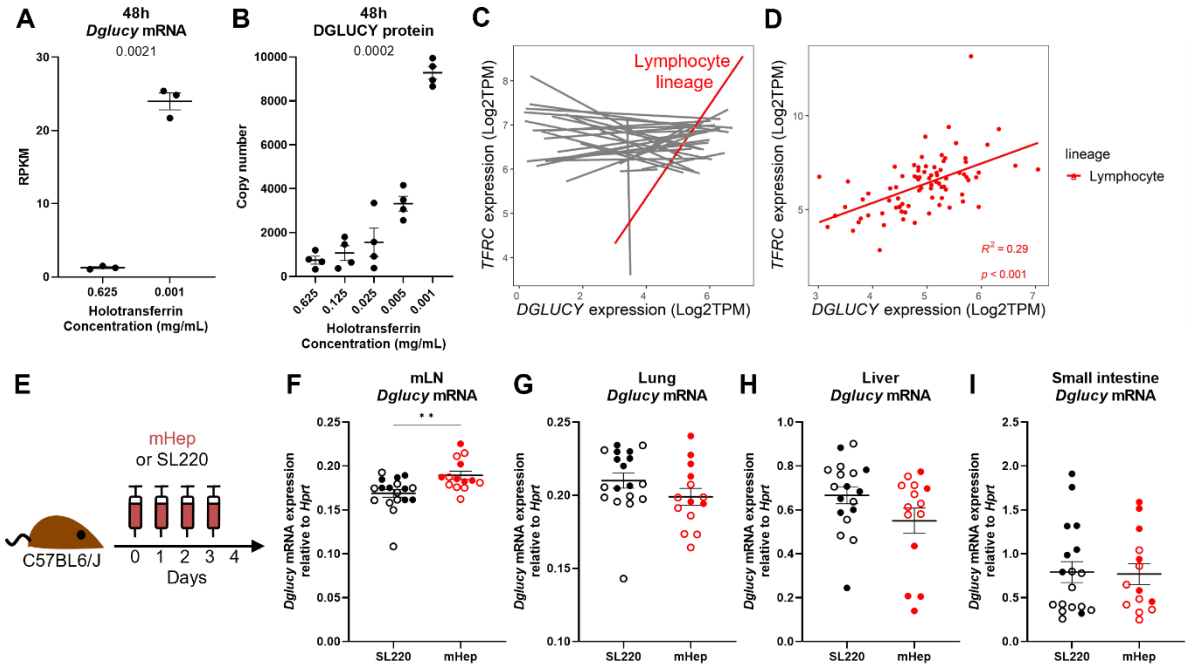

Figure 4.6. Iron scarcity induces Dglucy expression with indications of lymphoid specificity. T-cells were cultured in a titration of iron conditions for 48h as described in 4.1A. **(A)** mRNA and **(B)** protein expression of *Dglucy*. RPKM = reads per kilobase of transcript per million mapped reads. Correlation plot of *TFRC* vs *DGLUCY* mRNA expression across **(C)** all cell line lineages or in **(D)** lymphocyte cell lines in the DepMap consortium (https://depmap.org/portal/) databank. TPM = transcripts per million. **(E)** MiniHepcidin (mHep, 100 nmoles) or SL220 (control) was intraperitoneally injected for four days. qPCR analysis of Dglucy mRNA expression across **(F)** mesenteric lymph nodes (mLN), **(G)** lung, **(H)** liver, and **(I)** small intestine. Data is ± SEM. Statistics for **(A)** is a paired two-tailed t-test and statistics for **(B)** is a matched one-way ANOVA with the Geisser-Greenhouse correction. For **(D)** a Pearson correlation R^2 value was calculated. Statistics for **(F-I)** are unpaired two-tailed t-tests with Welch's correction. **p < 0.01.

mg/mL holotransferrin. The profound iron titratable effect observed with DGLUCY is stronger than even that observed with TFRC (Fig. 4.1F). *Dglucy* is an under characterised gene and was first cited in 2016 under its open reading frame designation of C14ORF159 as a locus potentially associated with body shape[41]. Since then, *Dglucy* has been characterised as a gene expressed in heart mitochondria to convert D-glutamate to 5-oxo-D-proline[42,43] and is potentially a tumour suppressor[44,45]. However, whether it plays a role in iron metabolism or immunity remains unknown.

To understand if the iron sensitivity of *Dglucy* may be generalisable, we analysed data from the DepMap Consortium which includes extensive data including gene expression (RNA-seq), gene dependency (CRISPR) and drug sensitivity of over 1000 human cell lines[46]. We assessed whether *TFRC* mRNA expression as an indicator of iron

status correlated with *DGLUCY* mRNA expression across 1406 cell lines. TFRC expression is upregulated during cellular iron deficiency and in *in vitro* CD8+ T-cells this effect is titratable with decreasing iron concentrations (Fig. 4.1F) suggesting that TFRC could be used as a proxy for cellular iron status. When looking across all cell lines, *TFRC* and *DGLUCY* gene expression did not correlate (Fig. 4.6C). However, if cell lines were stratified by lineage, lymphocyte/lymphoma cell lines showed strong correlation of *TFRC* and *DGLUCY* gene expression suggesting a potential lymphoid specific effect (Fig. 4.6D).

To assess if *Dglucy* upregulation in low iron conditions may also occur *in vivo*, mice were treated with the drug mini-hepcidin (mHep) for four consecutive days to suppress serum iron (Fig. 4.6E)*. qPCR analysis of *Dglucy* was conducted on various organs (Fig. 4.6F-I). Notably, of the organs analysed (mesenteric lymph node (mLN), lung, liver and small intestine), *Dglucy* was only significantly upregulated in the mLNs of mHep treated mice. Due to the much higher density of lymphocytes within the lymph node relative to other organs, we propose the upregulation of *Dglucy* in low iron conditions may be an immune specific affect which may be masked in other tissues due to the presence of non-responsive cells. While not conclusive, this data does provide further support that *Dglucy* may be iron responsive gene, potentially with lymphoid specificity.

4.3 Discussion

We utilised RNA-seq and protein-MS to evaluate the influence of iron deficiency on CD8+ T-cell gene expression on a global level. We identified the p53 signalling pathway as being substantially induced during iron deficiency (Fig. 4.2, Fig. 4.3) which may be responsible for the proliferative defect also observed. Iron deprived CD8+ T-cells also showed suppression of IFN signalling pathways and a reduction in the T-cell memory associated transcription factor, BATF3 (Fig. 4.2, Fig. 4.5H-O). Iron scarcity also induced profound metabolic alterations featuring reduced MYC and mTORC1 signalling but a contrasting increase in mitochondrial proteins involved in the ETC and β-oxidation (Fig. 4.2, Fig. 4.4).

* The original *in vivo* experiment was conducted by Joe Frost and banked samples were used to measure *Dglucy* mRNA expression. The assay to analyse *Dglucy* was planned by me but executed by Natasha White.

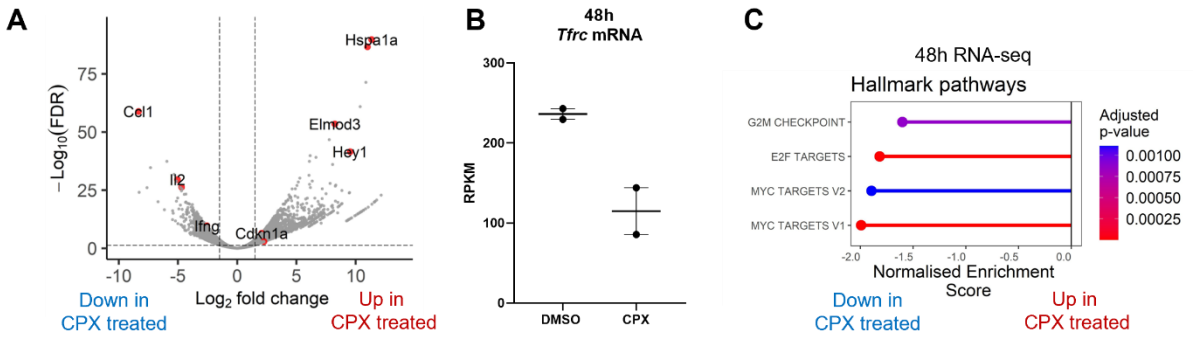

Figure 4.7. Raw data analysed from Wang *et al*[8] CD4+ T-cells were cultured in Th1 polarising conditions for 5 days and then treated with DMSO control of CPX (50 μM) for 4 hours. **(A)** Volcano plot where significance thresholds of FDR < 0.05 and $\log_2$|fold change| > 1.5 were applied. **(B)** *Tfrc* mRNA expression. RPKM = reads per kilobase of transcript per million mapped reads. **(C)** Hallmark gene set enrichment analysis. Data is mean ± SEM.

Previous studies have explored iron deficiency's impact on immune cell transcriptomes using iron chelators such as deferiprone (DEF), deferasirox (DFX) and ciclopirox olamine (CPX). We processed raw RNA-seq data from Wang *et al*[8] (not analysed in their manuscript) of Th1 polarised CD4+ T-cells treated with CPX iron chelator or dimethyl sulfoxide (DMSO) control for 4 hours. CPX treated cells showed differential expression of 3523 genes which is approximately 18-fold higher than the 193 differentially expressed genes identified in our model of low iron media (Fig. 4.7A). CPX also failed to upregulate *Tfrc* (similar to what happens at the lowest iron concentrations in low iron media) (Fig. 4.7B), suggesting that the IRP-IRE iron signalling system is no longer intact. The extreme changes in transcriptional profile observed with only 4 hours of CPX treatment relative to our 48-hour culture model in low iron media and the failure to upregulate *Tfrc* suggests that the biochemical impacts of chelators can be extremely non-physiological especially if given at high doses. Our model utilising low iron media can similarly induce profound defects in cellular proliferation (Fig. 4.3D) and function[4,8], but the level of iron deficiency is likely much more reflective of iron depleted tissues or hypoferremic sera. Care should be taken when interpreting results obtained using iron chelators as observed changes may not occur in more physiological low iron settings.

Despite the dramatic shift in overall transcriptional profile, similar to low iron media (Fig. 4.2), CPX treatment suppresses pathways associated with cell cycle (G2M checkpoint) and metabolic reprogramming (MYC targets). Human CD4+ T-cells treated with DFX iron chelator for 72 hours also show induction of the p53 pathway, but unlike

iron limiting media, DFX suppresses genes involved in glycolytic pathways[9]. Treatment of human macrophages with the DEF iron chelator impairs cell cycle progression and OXPHOS associated genes and but induces expression of genes involved in the P53 pathway, IFN signalling, and glycolysis[47]. Across studies iron limitation appears to have a generalisable repression of cell cycle progression and the capacity to modify cellular metabolism. However, the metabolic consequences of iron limitation appear context and cell specific. For instance, iron chelators suppressed glycolytic gene expression in CD4+ T-cells[9] but induced glycolytic genes in macrophages[47].

In the experiments conducted here, iron depletion strongly induced genes involved in the p53 signalling pathway including the dramatic upregulation of CDKN1A, an inhibitor of the G1-S phase cell cycle transition (Fig. 4.2, Fig. 4.3). Iron chelation has been well described to induce the p53 pathway, both in cell lines as well as in macrophages and CD4+ T-cells[9,47-49]. Iron chelation is understood to activate the p53 pathway via HIF-1α stabilisation due to impaired activity of the iron dependent PHD proteins (chapter 1, section 1.1.3)[49]. Whether the p53 pathway is induced via HIF-1α in CD8+ T-cells during more physiological iron starvation is unknown. p53 integrates a diversity of stress signals such as hypoxia, but also DNA damage and nutrient starvation which present alternative means through which iron scarcity could be sensed[33]. T-cell proliferation requires efficient and rapid DNA replication, while inefficient DNA synthesis can result in replication fork stalling and collapse which can induce p53[50]. Iron is used by DNA synthesis and repair machinery and for nucleotide production (chapter 1, section 1.2.2)[51]. However, whether iron deficiency impairs DNA synthesis to a degree that results in genome instability is unknown but presents another means through which iron starvation could activate p53. Genomic instability could be initially assessed by fluorescent labelling of the histone variant H2AX which is associated with double stranded DNA breaks which can occur during replication fork collapse[52]. Nutrient or metabolic status can also be signalled to p53 via an AMPK/mTOR axis[53]. AMPK senses low energy status such as during glucose limitation and glycolytic suppression via increased ratios of AMP to ATP[53]. AMPK activation in turn can induce p53. In contrast, mTOR represses p53 activity during nutrient abundance[53]. However, upon amino acid starvation or nutrient stress, mTOR is inactivated and p53 repression is lifted[53]. Notably, during CD8+ T-cell iron limitation, mTOR activity is reduced and ATP levels drop, in theory increasing AMP levels and activating AMPK[53]. The coordinated activation of AMPK

and impairment of mTOR during iron scarcity provides another avenue through which p53 could be induced[53]. These different alternatives for p53 induction are not mutually exclusive, and potentially all could be operative.

We observed significant downregulation of genes and proteins involved in the MYC and mTORC1 signalling pathways in iron deprived CD8+ T-cells (Fig. 4.2, Fig. 4.4) which was partly characterised by a reduction in proteins involved in ribosomal function and amino acid uptake. MYC and mTORC1 induce metabolic reprogramming upon TCR stimulation to meet the biosynthetic and energy demands of activating T-cells[34]. Previous proteomics studies have examined impaired CD8+ T-cell MYC and mTORC1 signalling pathways via MYC knockout[54] or mTORC1 suppression by rapamycin[26] respectively. Impairment of either MYC or mTORC1 results in substantial losses in overall protein content[26,54]. Interestingly, iron deprivation did not alter CD8+ T-cell protein content on a per cell basis (Fig. 4.1G-H) (although the protein content of the total culture is reduced due to suppressed proliferation), suggesting that the MYC and mTORC1 impairments in iron deficiency are mild relative to genetic ablation or pharmacological suppression of these regulators. However, while the degree of mTORC1 or MYC suppression is likely much milder during iron deprivation, similar albeit weaker proteomic alterations were observed. MYC knockout CD8+ T-cells show reduced expression of amino acid transporters including SLC7A5 and SLC7A1 which were also suppressed by iron restriction[54]. Meanwhile, iron scarcity recapitulated the reduction of ribosomal proteins observed in rapamycin treated T-cells[26]. However, in contrast to the decline in mitochondrial proteins observed with rapamycin[26], we instead saw increased mitochondrial proteins indicating that iron deficiency's impact on metabolism is not simply due to suppression of mTORC1 and MYC. We hypothesise that accumulation of mitochondrial proteins in low iron conditions could be due to augmented generation of mitochondrial proteins to compensate for suppressed mitochondrial activity or impaired clearance by proteolysis or mitophagy. To assess defects in mitophagy, fluorescence systems such as the Mtphagy dye could be used[55]. The Mtphagy dye is a mitochondrially targeted dye which upon exposure to low pH following engulfment by the autophagosome, increases its fluorescence intensity[55]. Thus, the Mtphagy dye allows measurements of mitochondria specifically localised within the mitophagy pathway[55].

Iron deficient T-cells were observed to have suppressed *Batf3* mRNA and protein expression and a predicted reduction in transcriptional activity via RNA-seq footprinting (Fig. 4.5H, N-O). BATF3 is a transcription factor which is induced by T-cell activation and necessary for memory T-cell generation[40]. BATF3 knockout CD8+ T-cells show no defect in primary responses to antigen but fail to form robust memory populations[40]. Notably, *in vivo* serum iron suppression mediated via the hepcidin analogue, mHep, during primary antigenic stimulation similarly impairs memory T-cell responses to secondary challenge[4]. Incorrect transcriptional programming due to suppressed BATF3 during iron restriction could be partly responsible but should be tested in *in vivo* hypoferremia using BATF3 overexpressing T-cells.

DGLUCY was identified as an iron responsive protein which was strongly induced by iron restriction in *in vitro* activated CD8+ T-cells (Fig. 4.6A-B). Further examination of publicly accessible data and banked samples from hypoferremic mice revealed a potential lymphoid specificity of DGLUCY iron sensitivity (Fig. 4.6C-I). DGLUCY is a mitochondrial matrix protein with a putative metabolic role in the conversion of the unconventional amino acid D-glutamate (amino acids for biosynthesis are L-enantiomers) to 5-oxo-D-proline[42,43]. DGLUCY knockout mice were notably shown to be viable but to accumulate D-glutamate in heart tissue[42]. No further *in vivo* phenotype has been described. Whether DGLUCY has the capacity to mediate other cellular reactions is unknown but knockout in cell lines impairs mitochondrial membrane potential and suppresses levels of the conventional amino acids aspartate, asparagine and serine suggesting a larger role in cellular metabolism[44]. DGLUCY has also been proposed to be a tumour suppressor as DGLUCY knockout or knockdown in tumour cell lines results in enhanced proliferation, migration and invasion and is accompanied by increased metastatic gene signatures[44,45]. Interestingly, DGLUCY is thought to be a metalloenzyme interacting with magnesium, calcium, manganese and zinc; however, iron binding has not been assessed. Given the existing data, we propose that DGLUCY may be important for responding to mitochondrial stress during iron limitation, in part by suppressing unsupported proliferation. DGLUCY knockout CD8+ T-cells would be proposed to impair T-cell adaptation to iron deficiency, potentially resulting in increased sensitivity to less severe iron restriction and featuring exacerbated mitochondrial dysfunction.

4.3.1 Limitations

While we argue that the use of low iron media presents a superior iron deficiency model relative to iron chelators or α-CD71 antibodies, our *in vitro* iron deficiency T-cell culture model is still inherently non-physiological. T-cells are cultured at atmospheric oxygen (21%) which is substantially higher than those found in lymphoid tissues such as the spleen (3-4%) or bone marrow (6.4%)[56]. Meanwhile, RPMI 1640 media which provides the base of our iron free media contains supraphysiological levels of nutrients such as glucose and glutamine[57], while simultaneously lacking alternative carbon sources such as acetate, citrate and lactate[58]. T-cells cultured in physiological media show different metabolic routing compared to conventional culture conditions[58]. However, given that we control for gas concentrations and nutrient availability (excluding iron) across iron concentrations, we believe that our model still provides insights into T-cell biochemistry during iron restriction and provides a foundation for future *in vivo* work.

T-cell protein-MS has recently been conducted with detection of >9400 proteins[26]. In comparison our protein-MS only detected 5431 proteins at a reasonable level. The discrepancy of protein detection between our experiment and that conducted by Howden *et al*[26] can be explained by methodological differences. Howden *et al*[26] used data dependent acquisition (DDA) whereas we utilised data independent acquisition (DIA). DIA is faster and cheaper than DDA but has reduced proteomic depth[59]. The discrepancy in protein detection between our protein-MS data, our RNA-seq data and the data generated by Howden *et al*[26] does indicate that we have likely missed approximately 4000-6000 proteins. It should be noted that the absence of a protein in our protein-MS data does not necessarily indicate that the protein is unexpressed but rather could be due to technical limitations. Thus, while protein-MS provides a more accurate picture of gene expression than RNA-seq, RNA-seq still holds the benefit of breadth. As we have observed in this study, RNA-seq and protein-MS were largely reflective of each other in iron deficient CD8 T-cells but do provide complementary insights into cellular biology.

A multiple testing correction was not conducted for the protein-MS. Multiple testing corrections using methods such as the Benjamini-Hochberg procedure are typically conducted for large experiments with multiple parameters such as RNA-seq to reduce the probability of false positives[60]. For instance, in an RNA-seq experiment where a p-value threshold of < 0.05 without a multiple testing correction is applied, one would

expect approximately 500 false positives given detection of 10,000 genes. However, applying the Benjamini-Hochberg correction to our proteomics dataset resulted in no significantly differentially expressed proteins. This statistical phenomena has previously been reported for protein-MS data and is potentially due to factors such as smaller effect sizes in protein-MS relative to RNA-seq combined with low biological replicates due to cost[60]. While applying multiple testing in this context does limit false positives it likely also produces detrimental false negatives. With this consideration we have opted to omit a statistical multiple testing correction in line with others in the field[60].

4.3.2 Conclusion

Altogether, our data indicates that iron starvation significantly alters the CD8+ T-cell transcriptome and proteome and suggests several avenues for further study. For instance, iron starved CD8+ T-cells showed upregulation of P53 signalling featuring increased CDKN1A expression suggestive of G1-S phase cell cycle arrest. P53 induction could be mediated by multiple pathways including defects in DNA synthesis or AMPK activation due to low cellular energy balance. In parallel, low iron suppressed mTORC1 and MYC signalling in CD8+ T-cells indicating issues in metabolic rewiring. Meanwhile, many mitochondrial proteins including those involved in the ETC and β-oxidation were significantly induced by iron deprivation, potentially mediated by defects in clearance via mitophagy or due to compensatory increases. Intriguingly the mitochondrial enzyme DGLUCY was also significantly increased in low iron conditions, and we propose DGLUCY may play a lymphoid specific role in the metabolic adaptation to iron deficiency. Finally, iron deprivation significantly suppressed IFN associated signalling pathways including suppression of BATF3, a critical transcription factor for T-cell memory formation. Given the largely metabolic phenotype of iron deprived CD8+ T-cells, we have opted to more closely examine the implications of iron starvation on specific metabolic pathways with a particular focus on the highly iron dependent mitochondria.

4.4 References

1 Wang, X. *et al.* Febrile Temperature Critically Controls the Differentiation and Pathogenicity of T Helper 17 Cells. *Immunity* **52**, 328-341.e325 (2020). https://doi.org:10.1016/j.immuni.2020.01.006

2 Haas, R. *et al.* Lactate Regulates Metabolic and Pro-inflammatory Circuits in Control of T Cell Migration and Effector Functions. *PLoS Biol* **13**, e1002202 (2015). https://doi.org:10.1371/journal.pbio.1002202

3 Reina-Campos, M., Scharping, N. E. & Goldrath, A. W. CD8(+) T cell metabolism in infection and cancer. *Nat Rev Immunol* **21**, 718-738 (2021). https://doi.org:10.1038/s41577-021-00537-8

4 Frost, J. N. *et al.* Hepcidin-Mediated Hypoferremia Disrupts Immune Responses to Vaccination and Infection. *Med (N Y)* **2**, 164-179.e112 (2021). https://doi.org:10.1016/j.medj.2020.10.004

5 Li, L. *et al.* Iron deprivation restrains the differentiation and pathogenicity of T helper 17 cell. *J Leukoc Biol* **110**, 1057-1067 (2021). https://doi.org:10.1002/jlb.3ma0821-015r

6 Voss, K. *et al.* Elevated transferrin receptor impairs T cell metabolism and function in systemic lupus erythematosus. *Sci Immunol* **8**, eabq0178 (2023). https://doi.org:10.1126/sciimmunol.abq0178

7 Gao, X. *et al.* Iron-dependent epigenetic modulation promotes pathogenic T cell differentiation in lupus. *J Clin Invest* **132** (2022). https://doi.org:10.1172/jci152345

8 Wang, Z. *et al.* Iron Drives T Helper Cell Pathogenicity by Promoting RNA-Binding Protein PCBP1-Mediated Proinflammatory Cytokine Production. *Immunity* **49**, 80-92.e87 (2018). https://doi.org:10.1016/j.immuni.2018.05.008

9 Lai, Y. *et al.* Iron controls T helper cell pathogenicity by promoting glucose metabolism in autoimmune myopathy. *Clin Transl Med* **12**, e999 (2022). https://doi.org:10.1002/ctm2.999

10 Yarosz, E. L. *et al.* Cutting Edge: Activation-Induced Iron Flux Controls CD4 T Cell Proliferation by Promoting Proper IL-2R Signaling and Mitochondrial Function. *J Immunol* **204**, 1708-1713 (2020). https://doi.org:10.4049/jimmunol.1901399

11 Andreini, C., Putignano, V., Rosato, A. & Banci, L. The human iron-proteome. *Metallomics* **10**, 1223-1231 (2018). https://doi.org:10.1039/c8mt00146d

12 Teh, M. R., Frost, J. N., Armitage, A. E. & Drakesmith, H. Analysis of Iron and Iron-Interacting Protein Dynamics During T-Cell Activation. *Front Immunol* **12**, 714613 (2021). https://doi.org:10.3389/fimmu.2021.714613

13 Schena, M., Shalon, D., Davis, R. W. & Brown, P. O. Quantitative monitoring of gene expression patterns with a complementary DNA microarray. *Science* **270**, 467-470 (1995). https://doi.org:10.1126/science.270.5235.467

14 Bainbridge, M. N. *et al.* Analysis of the prostate cancer cell line LNCaP transcriptome using a sequencing-by-synthesis approach. *BMC Genomics* **7**, 246 (2006). https://doi.org:10.1186/1471-2164-7-246

15 Tang, F. *et al.* mRNA-Seq whole-transcriptome analysis of a single cell. *Nat Methods* **6**, 377-382 (2009). https://doi.org:10.1038/nmeth.1315

16 Nagaraj, N. *et al.* Deep proteome and transcriptome mapping of a human cancer cell line. *Mol Syst Biol* **7**, 548 (2011). https://doi.org:10.1038/msb.2011.81

17 Wang, X., Liu, Q. & Zhang, B. Leveraging the complementary nature of RNA-Seq and shotgun proteomics data. *Proteomics* **14**, 2676-2687 (2014). https://doi.org:10.1002/pmic.201400184

18 de Sousa Abreu, R., Penalva, L. O., Marcotte, E. M. & Vogel, C. Global signatures of protein and mRNA expression levels. *Mol Biosyst* **5**, 1512-1526 (2009). https://doi.org:10.1039/b908315d

19 Henzel, W. J. *et al.* Identifying proteins from two-dimensional gels by molecular mass searching of peptide fragments in protein sequence databases. *Proc Natl Acad Sci U S A* **90**, 5011-5015 (1993). https://doi.org:10.1073/pnas.90.11.5011

20 Mann, M., Højrup, P. & Roepstorff, P. Use of mass spectrometric molecular weight information to identify proteins in sequence databases. *Biol Mass Spectrom* **22**, 338-345 (1993). https://doi.org:10.1002/bms.1200220605

21 Pappin, D. J., Hojrup, P. & Bleasby, A. J. Rapid identification of proteins by peptide-mass fingerprinting. *Curr Biol* **3**, 327-332 (1993). https://doi.org:10.1016/0960-9822(93)90195-t

22 Yates, J. R., 3rd, Speicher, S., Griffin, P. R. & Hunkapiller, T. Peptide mass maps: a highly informative approach to protein identification. *Anal Biochem* **214**, 397-408 (1993). https://doi.org:10.1006/abio.1993.1514

23 Shevchenko, A. *et al.* Linking genome and proteome by mass spectrometry: large-scale identification of yeast proteins from two dimensional gels. *Proc Natl Acad Sci U S A* **93**, 14440-14445 (1996). https://doi.org:10.1073/pnas.93.25.14440

24 Beck, M. *et al.* The quantitative proteome of a human cell line. *Mol Syst Biol* **7**, 549 (2011). https://doi.org:10.1038/msb.2011.82

25 Schoof, E. M. *et al.* Quantitative single-cell proteomics as a tool to characterize cellular hierarchies. *Nat Commun* **12**, 3341 (2021). https://doi.org:10.1038/s41467-021-23667-y

26 Howden, A. J. M. *et al.* Quantitative analysis of T cell proteomes and environmental sensors during T cell differentiation. *Nat Immunol* **20**, 1542-1554 (2019). https://doi.org:10.1038/s41590-019-0495-x

27 Kaech, S. M., Hemby, S., Kersh, E. & Ahmed, R. Molecular and functional profiling of memory CD8 T cell differentiation. *Cell* **111**, 837-851 (2002). https://doi.org:10.1016/s0092-8674(02)01139-x

28 Wolf, T. *et al.* Dynamics in protein translation sustaining T cell preparedness. *Nat Immunol* **21**, 927-937 (2020). https://doi.org:10.1038/s41590-020-0714-5

29 Firkin, F. a. R., B. Interpretation of biochemical tests for iron deficiency: diagnostic difficulties related to limitations of individual tests. *Aust Prescr* **20**, 74-76 (1997). https://doi.org:https://doi.org/10.18773/austprescr.1997.063

30 Schwartz, A. J. *et al.* Hepcidin sequesters iron to sustain nucleotide metabolism and mitochondrial function in colorectal cancer epithelial cells. *Nature Metabolism* **3**, 969-982 (2021). https://doi.org:10.1038/s42255-021-00406-7

31 Scharping, N. E. *et al.* Mitochondrial stress induced by continuous stimulation under hypoxia rapidly drives T cell exhaustion. *Nat Immunol* **22**, 205-215 (2021). https://doi.org:10.1038/s41590-020-00834-9

32 Wilkinson, N. & Pantopoulos, K. The IRP/IRE system in vivo: insights from mouse models. *Front Pharmacol* **5**, 176 (2014). https://doi.org:10.3389/fphar.2014.00176

33 Levine, A. J., Hu, W. & Feng, Z. The P53 pathway: what questions remain to be explored? *Cell Death Differ* **13**, 1027-1036 (2006). https://doi.org:10.1038/sj.cdd.4401910

34 Shyer, J. A., Flavell, R. A. & Bailis, W. Metabolic signaling in T cells. *Cell Res* **30**, 649-659 (2020). https://doi.org:10.1038/s41422-020-0379-5

35 Rath, S. *et al.* MitoCarta3.0: an updated mitochondrial proteome now with sub-organelle localization and pathway annotations. *Nucleic Acids Res* **49**, D1541-d1547 (2021). https://doi.org:10.1093/nar/gkaa1011

36 Gaud, G., Lesourne, R. & Love, P. E. Regulatory mechanisms in T cell receptor signalling. *Nat Rev Immunol* **18**, 485-497 (2018). https://doi.org:10.1038/s41577-018-0020-8

37 Valitutti, S., Müller, S., Salio, M. & Lanzavecchia, A. Degradation of T cell receptor (TCR)-CD3-zeta complexes after antigenic stimulation. *J Exp Med* **185**, 1859-1864 (1997). https://doi.org:10.1084/jem.185.10.1859

38 van der Donk, L. E. H. *et al.* Separate signaling events control TCR downregulation and T cell activation in primary human T cells. *Immun Inflamm Dis* **9**, 223-238 (2021). https://doi.org:10.1002/iid3.383

39 Keenan, A. B. *et al.* ChEA3: transcription factor enrichment analysis by orthogonal omics integration. *Nucleic Acids Res* **47**, W212-w224 (2019). https://doi.org:10.1093/nar/gkz446

40 Ataide, M. A. *et al.* BATF3 programs CD8(+) T cell memory. *Nat Immunol* **21**, 1397-1407 (2020). https://doi.org:10.1038/s41590-020-0786-2

41 Ried, J. S. *et al.* A principal component meta-analysis on multiple anthropometric traits identifies novel loci for body shape. *Nat Commun* **7**, 13357 (2016). https://doi.org:10.1038/ncomms13357

42 Ariyoshi, M. *et al.* (D)-Glutamate is metabolized in the heart mitochondria. *Sci Rep* **7**, 43911 (2017). https://doi.org:10.1038/srep43911

43 Katane, M. *et al.* Structural and enzymatic properties of mammalian d-glutamate cyclase. *Arch Biochem Biophys* **654**, 10-18 (2018). https://doi.org:10.1016/j.abb.2018.07.005

44 Ohshima, K. *et al.* Mitochondrial matrix protein C14orf159 attenuates colorectal cancer metastasis by suppressing Wnt/β-catenin signalling. *Br J Cancer* **125**, 1699-1711 (2021). https://doi.org:10.1038/s41416-021-01582-9

45 Zhu, Y. M. *et al.* C14orf159 suppresses gastric cancer cells' invasion and proliferation by inactivating ERK signaling. *Cancer Manag Res* **11**, 1717-1723 (2019). https://doi.org:10.2147/cmar.S176771

46 Ghandi, M. *et al.* Next-generation characterization of the Cancer Cell Line Encyclopedia. *Nature* **569**, 503-508 (2019). https://doi.org:10.1038/s41586-019-1186-3

47 Pereira, M. *et al.* Acute Iron Deprivation Reprograms Human Macrophage Metabolism and Reduces Inflammation In Vivo. *Cell Rep* **28**, 498-511.e495 (2019). https://doi.org:10.1016/j.celrep.2019.06.039

48 Kim, B. M., Choi, J. Y., Kim, Y. J., Woo, H. D. & Chung, H. W. Desferrioxamine (DFX) has genotoxic effects on cultured human lymphocytes and induces the p53-mediated damage response. *Toxicology* **229**, 226-235 (2007). https://doi.org:10.1016/j.tox.2006.10.022

49 An, W. G. *et al.* Stabilization of wild-type p53 by hypoxia-inducible factor 1alpha. *Nature* **392**, 405-408 (1998). https://doi.org:10.1038/32925

50 Lindström, M. S., Bartek, J. & Maya-Mendoza, A. p53 at the crossroad of DNA replication and ribosome biogenesis stress pathways. *Cell Death Differ* **29**, 972-982 (2022). https://doi.org:10.1038/s41418-022-00999-w

51 Shi, R., Hou, W., Wang, Z. Q. & Xu, X. Biogenesis of Iron-Sulfur Clusters and Their Role in DNA Metabolism. *Front Cell Dev Biol* **9**, 735678 (2021). https://doi.org:10.3389/fcell.2021.735678

52 Alexander, J. L. & Orr-Weaver, T. L. Replication fork instability and the consequences of fork collisions from rereplication. *Genes Dev* **30**, 2241-2252 (2016). https://doi.org:10.1101/gad.288142.116

53 Humpton, T. J. & Vousden, K. H. Regulation of Cellular Metabolism and Hypoxia by p53. *Cold Spring Harb Perspect Med* **6** (2016). https://doi.org:10.1101/cshperspect.a026146

54 Marchingo, J. M., Sinclair, L. V., Howden, A. J. & Cantrell, D. A. Quantitative analysis of how Myc controls T cell proteomes and metabolic pathways during T cell activation. *Elife* **9** (2020). https://doi.org:10.7554/eLife.53725

55 Iwashita, H. *et al.* Live Cell Imaging of Mitochondrial Autophagy with a Novel Fluorescent Small Molecule. *ACS Chem Biol* **12**, 2546-2551 (2017). https://doi.org:10.1021/acschembio.7b00647

56 Zenewicz, L. A. Oxygen Levels and Immunological Studies. *Front Immunol* **8**, 324 (2017). https://doi.org:10.3389/fimmu.2017.00324

57 Leney-Greene, M. A., Boddapati, A. K., Su, H. C., Cantor, J. R. & Lenardo, M. J. Human Plasma-like Medium Improves T Lymphocyte Activation. *iScience* **23**, 100759 (2020). https://doi.org:10.1016/j.isci.2019.100759

58 Kaymak, I. *et al.* Carbon source availability drives nutrient utilization in CD8(+) T cells. *Cell Metab* **34**, 1298-1311.e1296 (2022). https://doi.org:10.1016/j.cmet.2022.07.012

59 Krasny, L. & Huang, P. H. Data-independent acquisition mass spectrometry (DIA-MS) for proteomic applications in oncology. *Mol Omics* **17**, 29-42 (2021). https://doi.org:10.1039/d0mo00072h

60 Pascovici, D., Handler, D. C., Wu, J. X. & Haynes, P. A. Multiple testing corrections in quantitative proteomics: A useful but blunt tool. *Proteomics* **16**, 2448-2453 (2016). https://doi.org:10.1002/pmic.201600044

Chapter 5

5 The metabolic and epigenetic effects of T-cell iron deprivation*

5.1 Introduction

T-cell activation induces metabolic reprogramming to meet cellular energy and biosynthetic demands to enable rapid proliferation and acquisition of effector functions[1]. Naïve T-cells are quiescent, predominantly using glucose and fatty acids to fuel oxidative phosphorylation (OXPHOS)[1]. Upon activation, T-cells dramatically upregulate aerobic glycolysis for ATP production, shunting the majority of glucose derived pyruvate to lactate production[1]. In parallel, mitochondrial glutamine oxidation (glutaminolysis) is increased to generate biosynthetic metabolites such as glutamate and aspartate[2,3]. These metabolic shifts are mediated by activation of the metabolic regulators, MYC and mTORC1, downstream of the T-cell receptor (TCR) which induce processes such as amino acid and glucose import and upregulation of glycolytic enzymes[4]. Notably, the iron uptake receptor, TFRC, is also a downstream target of MYC[5] and T-cell activation is known to strongly induce TFRC expression[6,7]. In contrast, memory T-cells adopt a metabolic state more similar to naïve T-cells, relying mostly on OXPHOS[1]. However, memory T-cells also upregulate mitochondrial mass and have increased usage of fatty acid β-oxidation[8].

Notably, studies of iron restricted T-cells using iron chelators, low iron media or α-CD71 antibodies have highlighted defects in metabolism concurrent with reduced T-cell effector function[6,9-11]. Metabolic defects include suppression of mTORC1 activity (chapter 4, Fig. 4.4E), impaired mitochondrial ATP production and reduced mitochondrial membrane potential[6,9,10]. While one study reports significant reductions in glycolysis in parallel with mitochondrial dysfunction[11], another finds no changes in

* Where indicated, the text and data in this chapter has been previously published in Teh *et al*, Frontiers of Immunology, 2021 (DOI: 10.3389/fimmu.2021.714613)

glycolytic ATP generation[6]. Meanwhile, our transcriptomic and proteomic survey of iron deprived CD8+ T-cells identified MYC and mTORC1 signalling pathways to be downregulated during iron depletion, but also highlighted an increase in mitochondrial proteins (chapter 4, Fig. 4.2, Fig. 4.4), overall suggesting altered metabolic rewiring. Mitochondrial metabolism was also predicted to be susceptible to iron scarcity due to a high number of iron atoms attributed to OXPHOS proteins in activated T-cells (chapter 3, Fig. 3.4F-G). While the impacts of iron deficiency on glycolysis appears less clear, mitochondrial alterations during iron limitation are evident across our work and others. However, the current literature remains relatively non-specific, broadly characterising mitochondrial health using metrics such as membrane potential and oxygen consumption but fails to identify the specific nodes of impairment during iron scarcity.

While glycolysis is not directly iron dependent given that none of the glycolytic enzymes utilise iron cofactors, mitochondrial metabolism is highly enriched for iron interacting proteins[12]. Both iron-sulfur (Fe-S) cluster production and heme synthesis occur in the mitochondria[12]. Further, within the tricarboxylic acid cycle (TCA) cycle, aconitase 2 (ACO2) and succinate dehydrogenase (SDH, complex II (CII)) require iron for enzymatic activity, while all four complexes of the electron transport chain (ETC, CI-IV) require iron prosthetic groups to mediate efficient electron transfer[12]. Despite activated T-cells preferentially using aerobic glycolysis for ATP generation, mitochondrial metabolism is increasingly being described as critical for T-cell function[1]. While general mitochondrial depletion of T-cells via USP30 knockout impairs T-cell cytolytic function[13], each of the iron requiring complexes of the ETC have also been determined to play crucial roles in aspects of T-cell function[14-16]. Inhibition of CI using rotenone results in proliferative defects[15]. While genetic inhibition of CII via SDHB knockout reduces T-cell proliferation and viability but intriguingly also promotes an inflammatory transcriptional state characterised by increased mRNA expression of *Il17a*, *Ifng* and *Il22*[17]. However, this is in contrast with another study which reports that CII blockade using dimethyl malonate does not impair T-cell expansion but does suppress Th1 differentiation, specifically, IFN-γ production[15]. It should be noted that this second study only treats Th1 T-cells with dimethyl malonate overnight on days 2 or 3 post-activation[15] and thus the differential effects between studies could be due to chronic loss of CII versus transient loss of CII activity. Antimycin A suppression of CIII impairs both proliferation and Th1 IFN-γ[15]. Meanwhile, knockout of the CIII protein UQCRFS1 abrogates T-cell activation and IL-2

production[14] and CIV impairment via COX10 knockout impairs all of T-cell activation, proliferation and viability[16]. Further, mitochondrial dysfunction has been implicated in immunological defects in humans. Multiple clinical reports have found that children with mitochondrial disorders have high rates of severe and recurrent infections[16,18-21]. Immunophenotyping in a case study of a single child with mitochondrial DNA depletion syndrome (MDS) and a retrospective study of 97 patients with mitochondrial disorders found correlations between mitochondrial disease, high rates of infection and immunodeficiency phenotypes such as hypoglobulinemia, reduced lymphocyte counts and impaired responses to vaccination[20,21]. Notably, the immune phenotypes observed in children with mitochondrial disorders display similarity to the phenotypes observed in children homozygous for the $TFRC^{Y20H}$ mutation (chapter 1, section 1.4.2)[22]. Given that the reduced capacity to uptake iron in patients with $TFRC^{Y20H}$ mutations results in phenotypes mirroring those found in mitochondrial disorders, it seems plausible that iron restriction may potentially be acting, in an immunological context at least, as a pseudo-mitochondrial disease.

Notably, perturbation of metabolic pathways including several mitochondrial processes can impact T-cell differentiation and function due to alterations in epigenetic remodelling[23]. The interplay between metabolism, epigenetics and differentiation is illustrated by the dramatic remodelling of T-cell methylation patterns which occur post-activation to enable effector function[24] but require substrates derived from cellular metabolic pathways[23]. Upon T-cell activation, histone 3 lysine 4 trimethylation (H3K4me3) marks typically associated with active transcription are deposited at promoters of effector genes such as *Gzmb* and *Ifng* while the repressive histone mark, H3K27me3, is removed[24]. Trimethylation of H3K4 (and other histone residues) by methyltransferases requires the 1-carbon cycle metabolite, S-adenosylmethionine (SAM), as the methyl donor[23]. 1-carbon metabolism while not a mitochondrial process is impaired by mitochondrial dysfunction[25]. Meanwhile, demethylation of H3K27me3 is mediated by lysine demethylases (KDMs) which are 2-oxoglutarate (2-OG, α-ketoglutarate (α-KG)), oxygen and iron dependent dioxygenases (2-OGDDs) (section 1.2.3)[26]. 2-OGDDs use α-KG produced via mitochondrially located glutaminolysis and the TCA cycle as a substrate[23]. In contrast, excessive levels of the TCA cycle metabolite, succinate, can competitively inhibit 2-OGDD enzymes[27]. Critically, inhibition of KDM6A/B the specific KDM which mediates H3K27me3 removal prevents acquisition of

CD8+ T-cell memory upon viral infection *in vivo*[28] or Th17 differentiation *in vitro*[29]. Given the reliance of the 2-OGDD KDMs on both efficient α-KG production via the iron dependent TCA cycle as well as iron itself, it is possible that iron limitation may cause impairment of demethylation, potentially explaining the alterations previously observed via RNA-seq as well as the functional T-cell defects in low iron conditions.

While iron deficiency induces metabolic alterations in CD8+ T-cells at the transcriptomic and proteomic level (chapter 3) and broad mitochondrial dysfunction has been previously reported[6,9,10], the specific impacts of iron scarcity on mitochondrial function remain uncharacterised. In this chapter, we aimed to use our established model of CD8+ T-cell iron restriction, to identify specific metabolic and epigenetic perturbations during iron deprivation. We show here that iron scarcity induced mitochondrial reactive oxygen species (mROS) production in CD8+ T-cells which is proposed to act as a signalling molecule to drive IL-2 and TNF-α production via NFAT1 activation. Iron deprivation also induced metabolic blocks downstream of the iron dependent enzymes ACO2 and SDH resulting in reduced α-KG, malate and fumarate abundances. In contrast, aspartate accumulated in iron depleted T-cells, potentially via partial reversal of the TCA cycle. Further, CD8+ T-cells and Th17 polarised CD4+ T-cells both show accumulation of the repressive histone mark, H3K27me3, which is typically removed by KDM6A/B which is an α-KG and iron requiring enzyme, suggesting KDM6A/B dysfunction. H3K27me3 accumulation in Th17 polarised CD4+ T-cells occurred in parallel to reduced expression of the lineage defining transcription factor, RORγt and cytokine, IL-17A.

5.1.1 Aims

This chapter aims to:

1. Characterise the metabolic dysfunction that occurs in iron deprived T-cells
2. Identify specific blocks to mitochondrial metabolism via ^{13}C6-glucose and ^{13}C5-glutamine tracing
3. Examine the implications of iron scarcity and consequent α-KG depletion on epigenetic remodelling

5.2 Results

5.2.1 Iron depletion promotes mitochondrial ROS, NFAT and IL-2 production

Iron deficiency has previously been associated with reduced mitochondrial membrane potential and suppressed mitochondrial ATP generation in CD8+ T-cells[6], overall suggesting reduced mitochondrial function. In contrast, our proteomic survey uncovered an accumulation of mitochondrial proteins in low iron conditions (chapter 4) which could potentially be due to reduced mitochondrial clearance. To assess another metric of mitochondrial health and state, mitochondrial ROS (mROS) were measured using the MitoSOX red dye in CD8+ T-cells cultured in a titration of iron concentrations for 48h using the model described in Fig. 4.1A. MitoSOX is a mitochondria matrix targeted reagent which fluoresces upon oxidation by superoxide ($O_2^{\bullet-}$)[30 31]. As iron concentrations declined, mitochondrial superoxide production increased (Fig. 5.1A). Notably, mROS can be produced from CI, CII and CIII of the ETC (Fig. 5.1B)[32], all of which are dependent on iron for efficient electron transfer[12]. Given the observed increase in ETC proteins (Fig. 4.4F), but the reduced availability of iron during iron restriction in CD8+ T-cells, it is proposed that an imbalance in the ETC protein to iron cofactor stoichiometry may impair efficient electron transfer and result in increased mROS generation.

Excessive mROS can cause oxidative damage of DNA, lipids and proteins[32]. In turn, cells have accumulated multiple antioxidant pathways to alleviate mROS associated oxidative stress[32]. mROS produced into the mitochondrial matrix by CI-III are first detoxified via conversion to H_2O_2 by the mitochondrial matrix protein SOD2[32]. H_2O_2 is then converted to H_2O by glutathione peroxidase (GPX) or catalase[32]. Notably, SOD2 protein expression was observed to be upregulated in low iron conditions (Fig. 5.1C) suggesting that iron depleted cells are actively trying to suppress mROS but at the lowest iron concentrations still fail to control them. The specific mechanism through which iron deficiency induces SOD2 upregulation in CD8+ T-cells is unclear but could be occurring downstream of the oxidative stress response via NRF2 or the hypoxia response via HIF1α which is known to be induced by iron chelation (albeit has not been demonstrated to occur in low iron conditions in our model)[33,34].

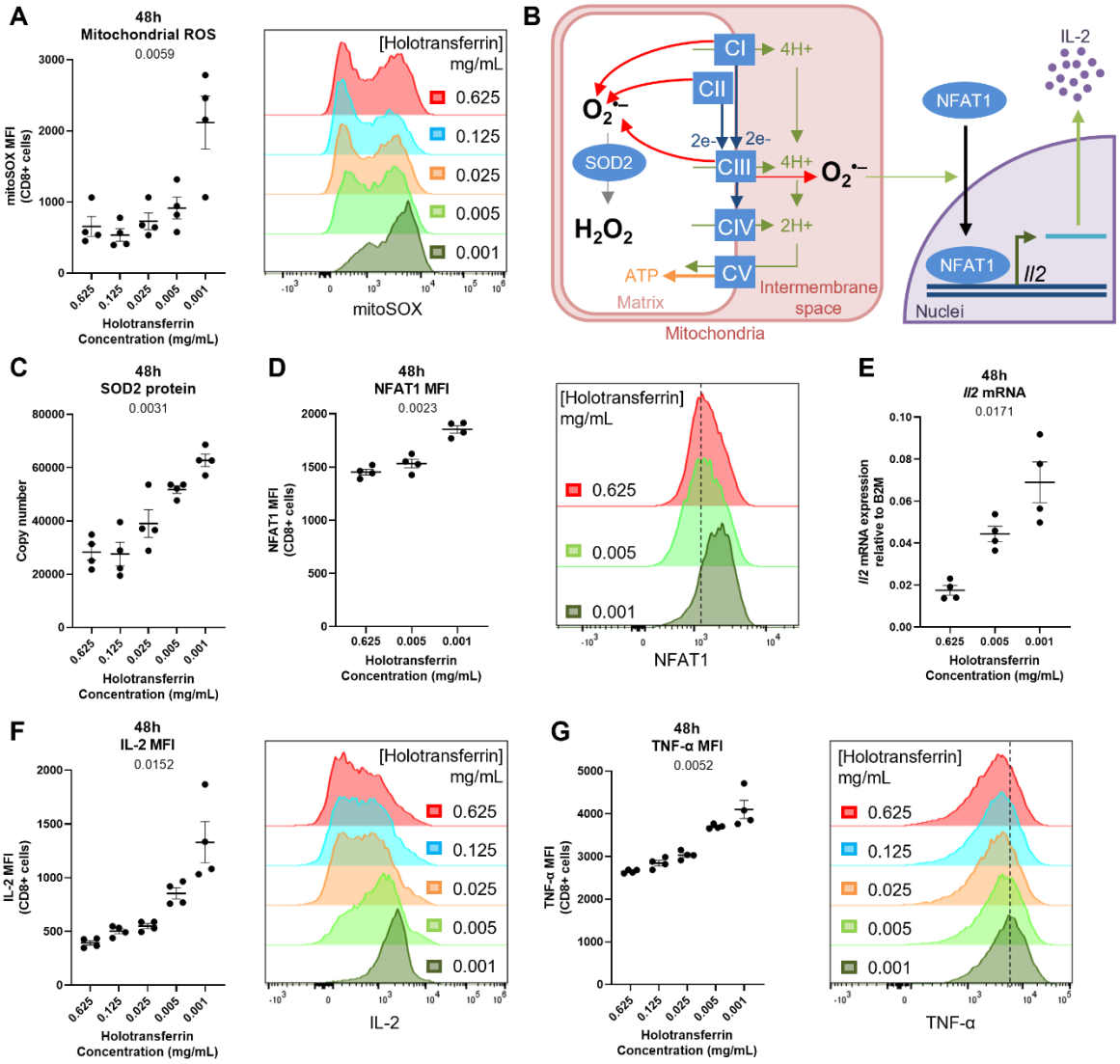

Figure 5.1. Iron restriction induces mROS, NFAT and IL-2. CD8+ T-cells were activated in a titration of iron conditions as described in figure 4.1A. **(A)** mitochondrial ROS (mROS) MFI. **(B)** mROS is proposed to be produced by iron dependent complexes I, II and III. SOD2 aids in mROS detoxification[14]. mROS can induce NFAT activation and IL-2 production[14]. **(C)** SOD2 protein expression, **(D)** NFAT1 MFI, **(E)** *Il2* mRNA expression, **(F)** IL-2 MFI and **(G)** TNF-α MFI. Data is mean ± SEM. Histograms are normalised to mode. Statistics for **(A-B)** are matched one-way ANOVAs with the Geisser-Greenhouse correction. Data for **(C-D)**, **(E)** and **(A, F-G)** representative of 1, 2 and 3 experiments, respectively.

While mROS produced from CI and CII are exclusively released into the mitochondrial matrix where they can be cleared by SOD2, CIII derived mROS are released not only into the matrix but also into the mitochondrial intermembrane space where they can play a role in cellular signalling (Fig. 5.1B)[14,35,36]. For instance, a previous study demonstrated that CIII derived mROS is necessary for NFAT1 activation and nuclear localisation and the promotion of IL-2 transcription[14]. Given the observed increase in

mROS in CD8+ T-cells activated in low iron conditions and previous reports that iron scarcity (deferoxamine (DFO) or α-CD71 mediated) can induce T-cell IL-2 production[10,37,38], it was hypothesised that mROS may similarly drive IL-2 production via NFAT1 in iron deficiency. As iron concentrations decreased, CD8+ T-cell NFAT expression increased (Fig 5.1D). Concurrent with elevated mROS and NFAT1 in low iron conditions, increased IL-2 mRNA and protein expression was also observed (Fig. 5.1E-F). Interestingly, TNF-α was also upregulated in iron deficient conditions (Fig. 5.1G). Notably, ROS (although not necessarily mROS) has also been shown to induce TNF-α downstream of NFAT1[39]. While the current data does not demonstrate a causal pathway where iron deficiency induced mROS production promotes NFAT activation and the downstream production of IL-2 and TNF-α, our observations are in line with the previously pathway described by Sena *et al*[14].

5.2.2 Iron limitation does not alter mitochondrial DNA copy number

CD8+ T-cell iron deprivation results in multiple mitochondrial alterations including the accumulation of mitochondrial proteins involved in the ETC and β-oxidation. Increased mitochondrial proteins potentially suggests defects in mitochondrial clearance or a compensatory increase in an attempt to make up for reduced mitochondrial function. Interestingly, mitochondria have their own genomes which encode 13 proteins essential for OXPHOS[40]. Unlike nuclear DNA (nDNA) which is

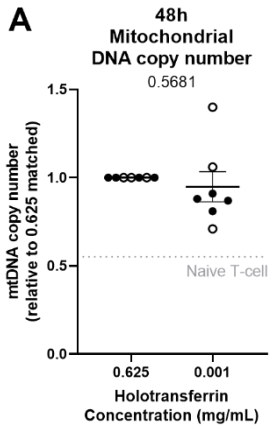

Figure 5.2. mtDNA copy number is stable during iron deficiency. CD8+ T-cells were activated in high (0.625 mg/mL) or low (0.001 mg/mL) holotransferrin for 48h as described in figure 4.1A. **(A)** mitochondrial DNA copy number normalised to nuclear DNA. Naïve T-cell samples were collected at day 0 pre-activation. Data pooled from two experiments denoted by open and closed circles. Data is mean ± SEM. Statistics for **(A)** is a paired two-tailed t-test.

typically found at two copies per cell at homeostasis, mitochondrial DNA (mtDNA) is found at high and variable copy numbers (usually 1000 to 10000 copies)[40]. An accumulation of mtDNA would support the notion of reduced mitochondrial clearance. However, the alternative could also be true, as mtDNA depletion has been associated with impaired mitochondrial function[41]. mtDNA copy numbers were measured in CD8+ T-cells activated for 48h in iron limiting conditions. Activated CD8+ T-cells increased mtDNA copies relative to naïve controls (Fig. 5.2A) as previously reported[42]. However, iron deficiency did not alter CD8+ T-cell mtDNA copy numbers suggesting that the maintenance of the mitochondrial genome is intact despite more general mitochondrial dysfunction. The equivalent mtDNA copies between iron conditions could indicate that mitophagy is not suppressed during iron deficiency. However, differences in mitophagy should be ruled out experimentally as mtDNA copy numbers do not always correlate with mitochondrial mass, demonstrated by the fact that cells completely lacking mtDNA still contain mitochondria[43].

5.2.3 Iron deprivation inhibits TCA cycle glutamine oxidation*

Given the presence of two iron requiring enzymes in the TCA cycle (ACO2 and SDH), we proposed that iron deprived CD8+ T-cells may have defective mitochondrial metabolic flux in addition to the observed reductions in membrane potential and ATP generation[44] and increased mROS. To assess the metabolic state of iron deprived CD8+ T-cells, metabolite-mass spectrometry (metabolite-MS) was conducted. CD8+ T-cells were activated for 48 hours, and ^{13}C6-glucose or ^{13}C5-glutamine were pulsed onto cells for the last 24 hours prior to harvest. Both total metabolite and 13C-labelled metabolite abundance were assayed. While minimal labelling was observed from ^{13}C6-glucose into the TCA cycle (approximately 20% into TCA cycle metabolites), ^{13}C5-glutamine was more readily incorporated into the TCA cycle, labelling 60% to 80% of TCA cycle metabolites (Fig. 5.3A). Due to the higher contribution from ^{13}C5-glutamine relative to ^{13}C-glucose to TCA cycle metabolites, ^{13}C5-glutamine date was preferentially utilised for assessing TCA metabolic flux as there was a larger dynamic range in which to observe changes.

Minimal changes in the total abundance of the glycolytic metabolites pyruvate and lactate, or the amino acids produced adjacent to glycolysis (alanine, serine and glycine)

* The metabolite-MS experiments described in this section (5.2.3) were conducted in collaboration with Sarah Dimeloe, Nancy Gudgeon, Jennie Roberts and Bryan Marzullo at the University of Birmingham.

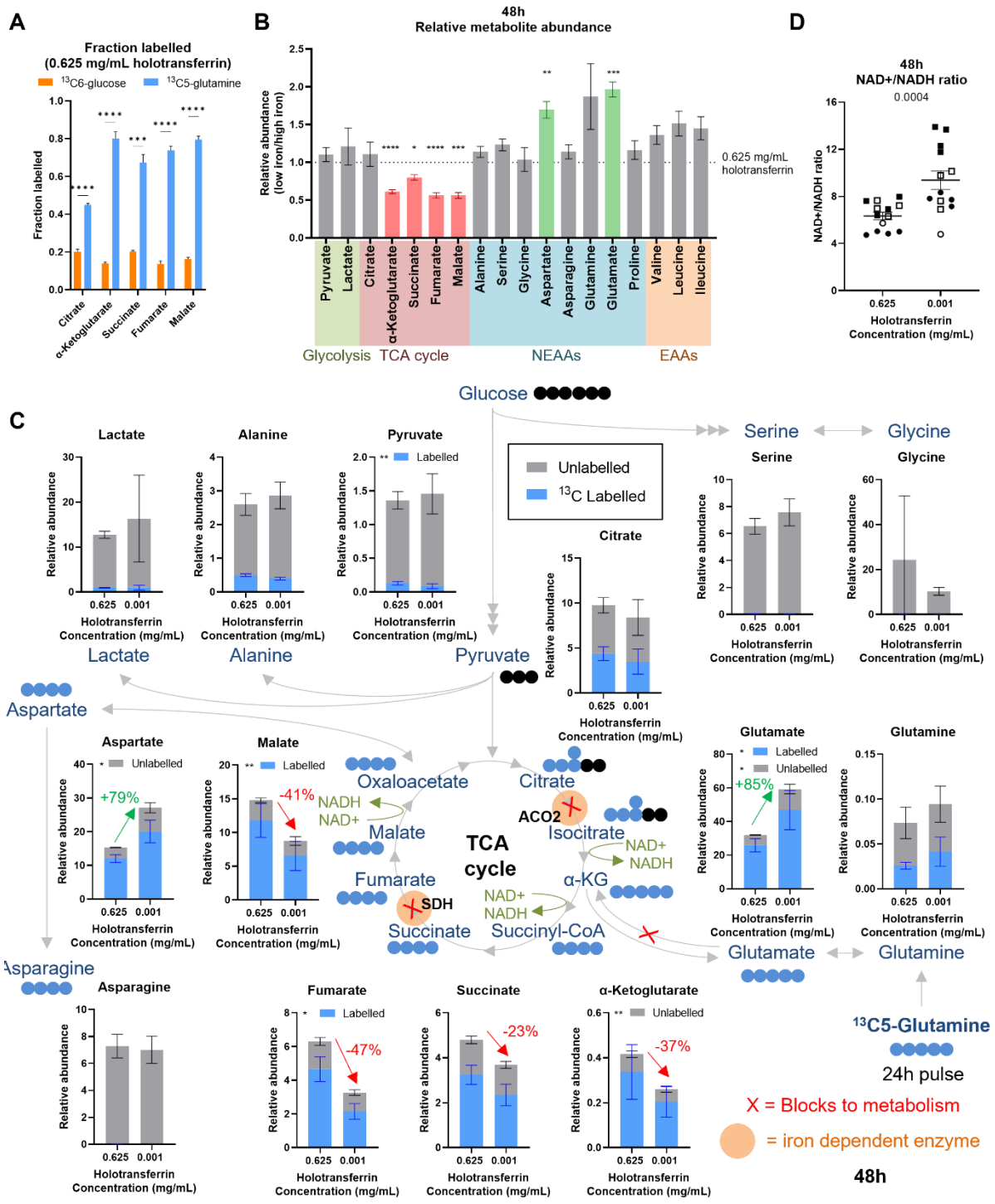

Figure 5.3. Iron scarcity impairs TCA cycle flux at the iron dependent enzymes ACO2 and SDH. T-cells were activated in iron titrations as described in figure 4.1A. For tracing experiments, T-cells were activated in standard media for 24h and then pulsed with ^{13}C6-glucose or ^{13}C5-glutamine for another 24h. **(A)** Metabolic fraction labelled by either ^{13}C6-glucose or ^{13}C5-glutamine in high iron conditions (0.625 mg/mL holotransferrin). **(B)** Relative metabolite abundance of T-cells in low iron (0.001 mg/mL holotransferrin) versus high iron (0.625 mg/mL holotransferrin) normalised to spiked in glutaric acid. Pooled relative total abundances from the ^{13}C6-glucose and ^{13}C5-glutamine experiments. NEAA = (*continued on next page*)

(*continued from last page*) non-essential amino acids, EAA = essential amino acids. **(C)** ^{13}C5-glutamine tracing. Relative abundance of labelled and unlabelled metabolites calculated as the fraction labelled multiplied by the abundance. Blue circles indicate ^{13}C labelled atoms. **(D)** NAD+/NADH ratio pooled from 4 experiments signified by the open and closed circles and squares. Data is mean ± SEM. Statistics for **(A)** is a two-way ANOVA with sample matching between metabolites but not between the two carbon tracers. Statistics for **(B-C)** are matched two-way ANOVAs with the Geisser-Greenhouse correction and the Sidak correction for multiple comparisons. Statistics for **(D)** is a paired two-tailed t-test. *p < 0.05, **p < 0.01, ***p < 0.001, ****p < 0.0001.

---

were observed suggesting no defects to the glycolytic pathway. Similarly, the TCA cycle metabolite citrate, which lies upstream of the iron dependent enzyme ACO2 showed no significant difference in either the total abundance (Fig. 5.3B) or the labelled fraction derived from ^{13}C5-glutamine (Fig. 5.3C) in iron deprived CD8+ T-cells. In contrast, α-KG, which lies downstream of ACO2 was significantly reduced in abundance and a trend in reduced ^{13}C labelling from ^{13}C5-glutamine (p-value = 0.0519) was observed suggesting impaired ACO2 activity. Succinate, similar to citrate lies upstream of an iron dependent enzyme (SDH). While succinate abundance was depressed in iron limiting conditions, succinate accumulation was observed relative to the downstream metabolites fumarate and malate suggesting reduced flux from succinate to fumarate. Further, reduced ^{13}C labelling from ^{13}C5-glutamine into fumarate and malate is also consistent with a block to metabolic flux occurring at SDH. A reduction in TCA cycle progression due to reduced ACO2 and SDH activity is in agreement with reduced NAD+ consumption and consequent increases in the NAD+/NADH ratio, which were also observed in iron scarcity (Fig. 5.3D).

Conversely, ^{13}C labelled glutamate accumulated in low iron conditions (Fig. 5.3B-C) consistent with a reduction of glutamate usage, for instance for replenishment of the TCA cycle via α-KG. The reduction of glutamate conversion to α-KG likely exacerbates α-KG depletion due to reduced ACO2 activity. The increase in unlabelled glutamate and reduction in α-KG may also be partially driven by increased breakdown of branched chain amino acids (leucine, isoleucine and valine) which produces glutamate as a by-product from α-KG[45]. Notably, branched chain amino acid degradation filters into β-oxidation, of which many proteins were upregulated in low iron conditions (chapter 4, Fig. 4.4F) including the enzyme IVD which is important for leucine breakdown suggesting increased branched chain amino acid catabolism.

5.2.4 Iron deficiency may drive aspartate generation via pyruvate carboxylase*

Aspartate, an amino acid produced downstream of the TCA cycle metabolite oxaloacetate showed increased abundance in low iron conditions despite suppression of TCA cycling (Fig. 5.3B-C). A substantial fraction of aspartate (approximately 60%) was ^{13}C labelled from ^{13}C-glutamine via oxidative TCA cycling (M4 labelling) (Fig. 5.4A) indicating that aspartate synthesis is still occurring via the oxidative TCA cycle despite significant blockades. This suggests that aspartate may be accumulating due to reduced usage by downstream pathways such as nucleotide synthesis[46], protein translation and asparagine production[47]. However, aspartate accumulation could also be partially explained by increased production via an alternative pathway, for instance via pyruvate anaplerosis to oxaloacetate via pyruvate carboxylase (PC) and reductive TCA cycling (Fig. 5.4B)[48]. Interestingly, carbon flux from $^{13}C6$-glucose through the oxidative (canonical forward cycling) TCA cycle via pyruvate dehydrogenase (PDH) results in entry of two heavy labelled carbon atoms into TCA cycle metabolites (M2 metabolites)[48]. Meanwhile, entry of carbon from $^{13}C6$-glucose to the reductive (reverse cycling) TCA cycle via PC produces M3 metabolites. During iron deficiency, significant increases in $^{13}C6$-glucose labelling into M3 TCA cycle metabolites including fumarate and malate were observed which is indicative of increased PC activity (Fig. 5.4C). PC activity evaluated as the ratio of (malate M3 – succinate M3)/pyruvate M3, as previously utilised by Elia *et al*[49], was also reduced (Fig 5.4D). Further, PC protein expression trended towards increased expression in low iron conditions (Fig. 5.4E). A reversal of TCA flux is also in agreement with the observed increase in the NAD+/NADH ratio. Together this data suggests that under iron limiting conditions, CD8+ T-cells may utilise PC and the reductive TCA cycle in an attempt to replenish the metabolites fumarate and malate which are depleted during iron deficiency while circumnavigating the use of iron dependent enzymes. Aspartate accumulation may be a byproduct of this process.

Aspartate is utilised for a wide variety of cellular processes including asparagine synthesis[47], protein translation, and nucleotide production[46]. During early T-cell activation, asparagine has been described to be predominantly obtained from

* The metabolite-MS experiments described in this section (5.2.4) were conducted in collaboration with Sarah Dimeloe, Nancy Gudgeon, Jennie Roberts and Bryan Marzullo at the University of Birmingham.

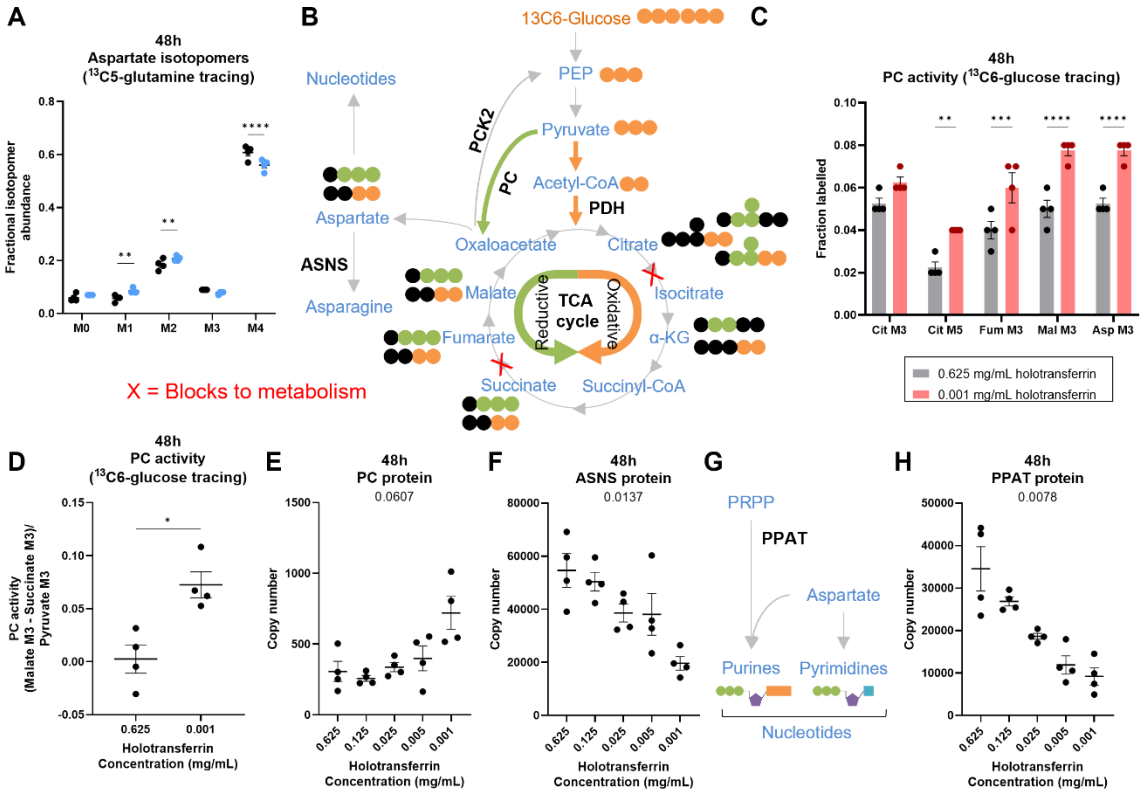

Figure 5.4. Iron deprivation induces aspartate accumulation potentially due to increased pyruvate carboxylase activity. CD8+ T-cells were activated in holotransferrin titrations as described in figure 4.1A. For the ^{13}C5-glutamine and ^{13}C6-glucose tracing experiments, T-cells were activated for 24h and then pulsed with either ^{13}C5-glutamine or ^{13}C6-glucose for a further 24h. **(A)** Aspartate isotopomers labelled from ^{13}C5-glutamine. M4 indicate isotopomers derived from oxidative TCA cycling. **(B)** Schematic of ^{13}C6-glucose tracing. Orange and green circles indicate ^{13}C labelled atoms. Orange circles show labelling expected from oxidative TCA cycling via pyruvate dehydrogenase (PDH). Green circles indicate expected labelling from reductive TCA cycling via pyruvate carboxylase (PC). Aspartate can be converted into downstream metabolites including asparagine via ASNS and nucleotides. Pyruvate carboxylase (PC) activity measured via the **(C)** fractional labelling into heavy labelled metabolites expected from reductive TCA cycling and via the **(D)** ratio of (Malate M3 – Succinate M3)/Pyruvate M3. **(E)** PC and **(F)** ASNS protein expression. **(G)** Aspartate can be incorporated into both purine and pyrimidine nucleotides. Purine synthesis requires the rate limiting enzyme PPAT. **(H)** PPAT protein expression. Data is mean ± SEM. Statistics for **(A, C)** are matched two-way ANOVA with the Sidak correction for multiple comparisons. Statistics for **(D)** is a paired two-tailed t-test. Statistics for **(E-F, H)** are one-way ANOVAs with the Geisser-Greenhouse correction.

extracellular sources rather than via aspartate[47]. By 72 hours post-activation, T-cells become competent for asparagine synthesis[47]. Consistent with this, 48h activated T-cells did not synthesise asparagine indicated by the absence of ^{13}C labelling from ^{13}C5 (Fig. 5.3C). Despite the lack of asparagine synthesis, 48h activated T-cells do express

asparagine synthetase (ASNS) which converts aspartate to asparagine, and ASNS protein levels decreased with iron deprivation (Fig. 5.4F) suggesting a reduction of future asparagine synthesis capacity. Aspartate is also essential for both purine and pyrimidine synthesis (Fig. 5.4G)[46]. Notably, PPAT, the initial enzyme of purine synthesis is significantly downregulated in iron deficiency (Fig. 5.4H). The reductions of the critical enzymes in aspartate-requiring metabolic processes, further suggests that aspartate usage may be suppressed.

5.2.5 Lysine demethylases (KDMs) are iron dependent, α-KG dependent enzymes that are induced during T-cell activation*

The KDMs are 2-OGDDs which mediate histone demethylation using an iron catalytic core (Fig. 5.5A). Using α-KG as a substrate, KDMs transfer a hydroxyl group onto methyl marks, producing an unstable intermediate which spontaneously degrades[50,51]. Given that iron deficiency reduces α-KG levels by approximately 40% (Fig. 5.5B), it was hypothesised that dual iron and α-KG depletion may impair epigenetic remodelling. Crucially, activating T-cells dramatically remodel their epigenetic landscapes to suppress

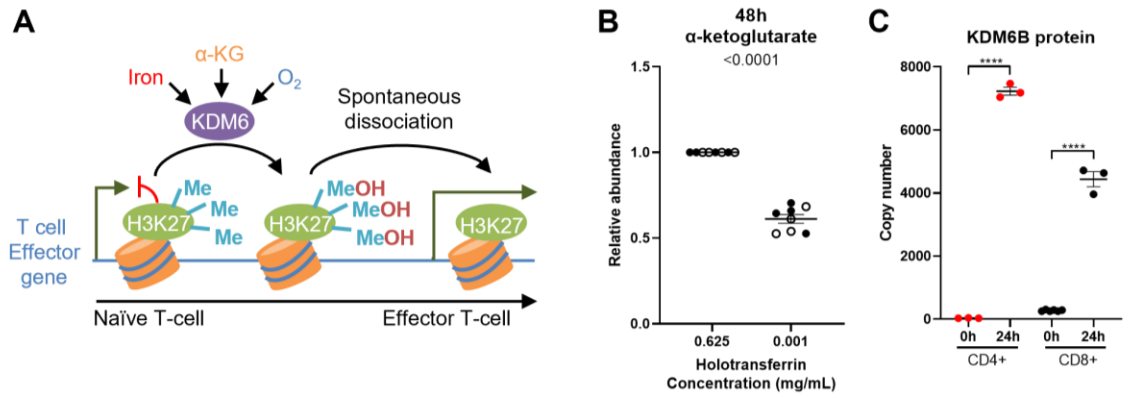

Figure 5.5. Epigenetic regulation is an iron dependent process. **(A)** KDM enzymes use iron cofactors and α-KG and oxygen substrates to mediate the hydroxylation of methyl groups which spontaneously dissociate to leave a demethylated histone[50,51]. KDM6 enzymes remove the repressive histone mark, H3K27me3, from effector gene loci upon T-cell activation[24,29]. **(B)** Relative abundance of α-KG in CD8+ T-cells activated as described in figure 4.1A in low (0.001 mg/mL holotransferrin) or high (0.625 mg/mL holotransferrin) iron conditions for 48h (as described in figure 4.1A). Data is pooled from two experiments signified by the open and closed circles. **(C)** KDM6B copy numbers from the Howden *et al*[7] dataset. Data is mean ± SEM. Statistics for **(B)** is a paired two tailed t-test. Statistics for **(C)** are unpaired t-tests. ****p < 0.0001.

* This section (5.2.5) is partly derived from the text published in Teh *et al*, Frontiers of Immunology, 2021 (DOI: 10.3389/fimmu.2021.714613)

expression of genes characteristic of naïve T-cells while permitting transcription of genes required for effector function[24,29]. Iron dependent KDMs showed dramatic changes upon T-cell activation in the Howden *et al*[7] dataset with KDM6B showed the greatest fold-change of all KDMs in CD4+ T-cells and the second greatest fold-change in CD8+ T-cells between 0h and 24h post-activation (Fig. 5.5C)[44]. KDM6B is responsible for the removal of the repressive histone mark H3K27me3, a process critical for T-cell differentiation and effector function acquisition[24,29]. Unfortunately, KDM6B was not detected in our protein-MS experiment, however, this is likely a technical issue given that KDM6B was detected in CD8+ T-cells by Howden *et al*[7] using a higher coverage protein-MS method.

5.2.6 Iron depletion results in accumulation of the repressive histone mark H3K27me3 in CD8+ T-cells

Given the importance of H3K27me3 demethylation for T-cell activation, we investigated whether H3K27me3 patterns were altered during iron scarcity in iron deprived CD8+ T-cells. In comparison to CD8+ T-cells maintained in a "naïve" like state using IL-7, *in vitro* activated CD8+ T-cells in iron replete conditions show a titratable failure to remove H3K27me3, with H3K27me3 levels remaining almost as high as IL-7 "naïve" like cells (Fig. 5.6A-B). The accumulation of H3K27me3 is consistent with the concept of reduced H3K27me3 removal by KDM6A/B during T-cell activation under iron deficient conditions. KDM6A/B enzymatic activity could also be directly assessed in the future using established commercially available colourimetric assays.

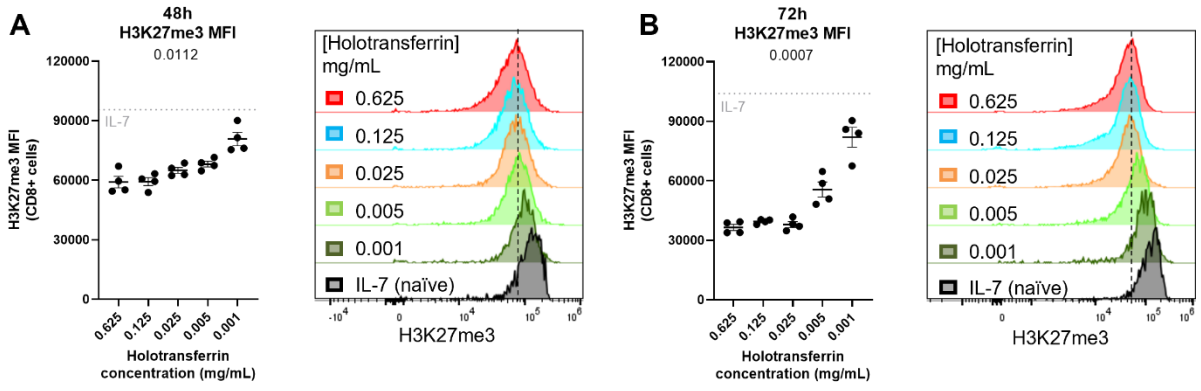

Figure 5.6. Iron deficiency results in accumulation of H3K27me3 in CD8+ T-cells. CD8+ T-cells were activated as described in figure 4.1A in a titration of iron conditions. H3K27me3 MFI measured at **(A)** 48h and **(B)** 72h post-activation. Dotted grey lines show CD8+ T-cells cultured in IL-7 (5 ng/mL) to maintain them in a naïve like state. Data is mean ± SEM. Histograms are normalised to mode. Statistics for **(A-B)** are matched one-way ANOVAs with the Geisser-Greenhouse correction.

5.2.7 Iron scarcity impairs T-cell epigenetic remodelling and differentiation in Th17 CD4+ T-cells*

Pharmacological inhibition of KDM6A/B was previously shown to attenuate Th17 CD4+ T-cell responses[29]. Given the importance of KDM6A/B for Th17 differentiation and the necessity of iron for KDM6A/B enzymatic activity, it was hypothesised that iron starvation may alter T-cell epigenetic remodelling and in consequence Th17 differentiation. To assess the impact of iron deficiency on Th17 CD4+ T-cells we used an *in vitro* iron deficiency model of Th17 polarisation (Fig. 5.7A). Similar to the *in vitro* model of CD8+ T-cell activation (Fig. 4.1A), iron is titrated into iron depleted media in the form of iron-saturated holotransferrin at set concentrations and the total transferrin concentration is maintained at 1.2 mg/mL. Th17 polarisation is induced *in vitro* by TGF-β and IL-6 in the absence of IFN-γ and IL-4 (neutralised using α-IFN-γ and α-IL-4 antibodies) which promote Th1 and Th2 differentiation respectively and inhibit Th17 differentiation[52]. *In vivo* Th17s are promoted during extracellular bacterial and fungal infection[53]. The lineage defining transcription factor, RORγt, directs differentiation down the Th17 lineage and promotes production of Th17 cytokines including IL-17A and IL-22 with downstream functions such as the production of antimicrobial peptides and neutrophil promoting and recruiting cytokines and chemokines[53,54].

As iron availability decreased, CD4+ T-cells in Th17 polarising conditions showed significantly reduced viability and proliferation (Fig. 5.7B-C). Iron depleted Th17 cells also demonstrated elevated H3K27me3 expression (Fig. 5.7D) indicating alterations in global chromatin remodelling. Elevated H3K27me3 expression in iron starved Th17 cells could be due to reduced passive loss of methylation by division dilution. However, H3K27me3 levels were similar between iron deprived T-cells that had and had not undergone division (Fig. 5.7E), supporting our hypothesis that high H3K27me3 levels may be attributed to impaired active demethylation by KDM6A/B during iron deficiency. A concurrent decrease in the percentage of cells expressing the Th17 lineage defining transcription factor, RORγt, and cytokine, IL-17A, was also observed during iron starvation (Fig. 5.7F-G). The reduction in RORγt with iron deficiency is less dramatic than that for IL-17A suggesting that RORγt induction may be less sensitive than the resulting

* This section (5.2.7) is partly derived from the text published in Teh *et al*, Frontiers of Immunology, 2021 (DOI: 10.3389/fimmu.2021.714613)

RORγt program. This data shows that iron availability influences epigenetic regulation and differentiation of Th17 cells.

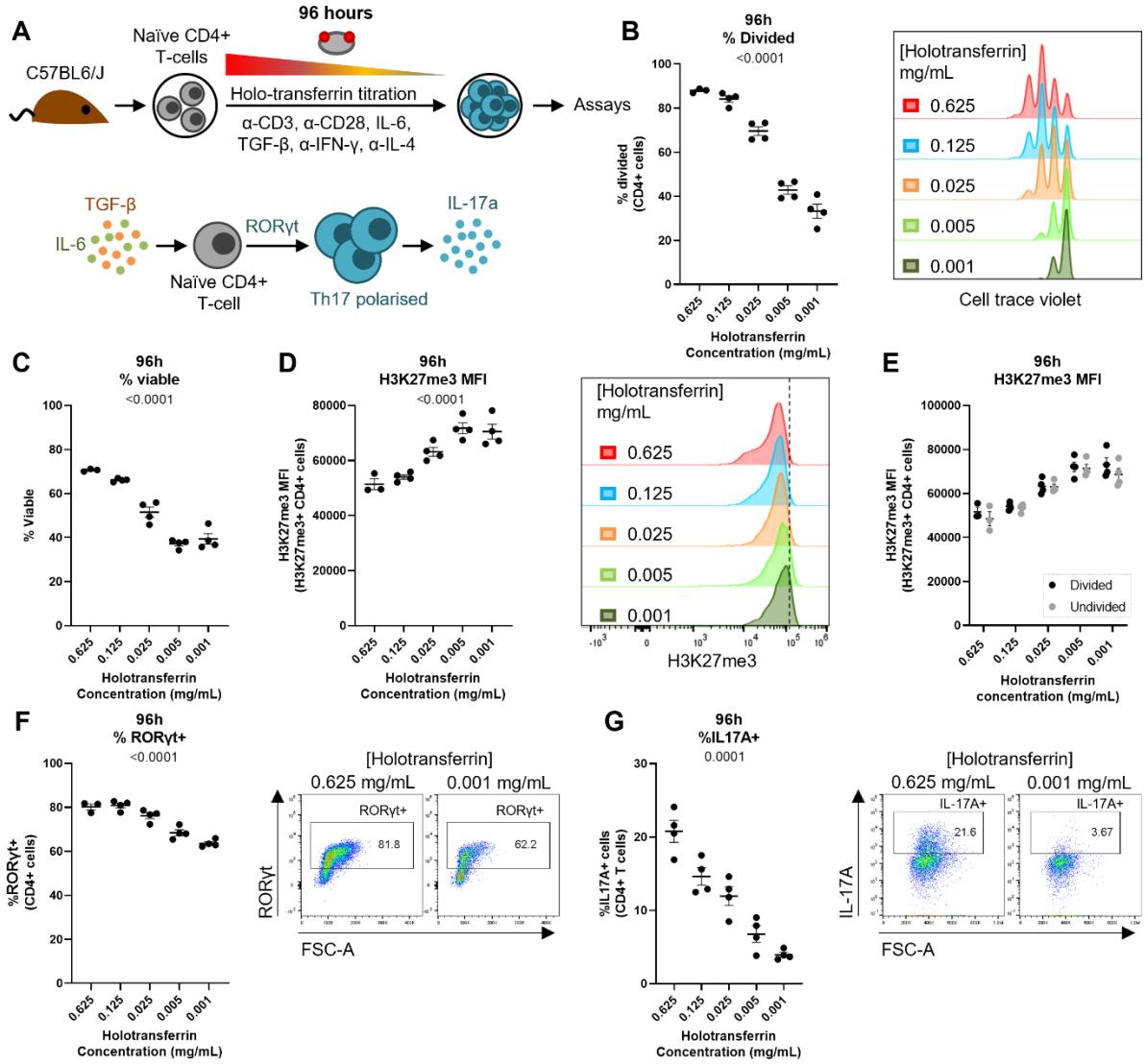

Figure 5.7. Iron deprived CD4+ T-cells in Th17-polarising conditions display impaired differentiation and epigenetic remodelling. **(A)** Naive CD4+ T-cells were cultured in Th17 polarising conditions (5 μg/mL plate bound α-CD3, 1 μg/mL α-CD28, 20 ng/mL IL-6, 5 ng/mL hTGF-β, 5 μg/mL α-IL-4, 5 μg/mL α-IFN-γ) for 96-120h with holotransferrin titrated into iron free media. IL-6 and TGF-β stimulation in the absence of IL-4 and IFN-γ induces Th17 polarisation characterised by the lineage defining transcription factor, RORγt, and cytokine, IL17a. **(B)** % divided as calculated from cell trace violet proliferation curves and **(C)** viability. H3K27me3 MFI on **(D)** all cells and **(E)** divided and undivided cells. **(F)** % RORγt+ cells and **(G)** % IL-17a+ cells. Data is mean ± SEM. Histograms are normalised to mode. Statistics for **(B-F)** are matched mixed effects analyses with the Geisser-Greenhouse correction. Statistics for **(G)** is a one-way ANOVA with the Geisser-Greenhouse correction. Data for **(B-C)** and **(D-G)** are representative of 3 and 2 experiments, respectively.

5.3 Discussion

Iron deficiency has previously been demonstrated to broadly impair T-cell metabolism. Here, we utilise a diversity of methods to further characterise iron deprivation on mitochondrial state in CD8+ T-cells. Iron deprived CD8+ T-cells showed increased mROS (Fig. 5.1A) and blockades to mitochondrial metabolism at the iron dependent enzymes, ACO2 and SDH (Fig. 5.3C). A block to metabolism at the entry point of glutamate to the TCA cycle, indicating a defect in α-KG dehydrogenase (α-KGDH) was also identified (Fig. 5.3C). Further, the combined metabolic blocks resulted in α-KG depletion. Interestingly, under iron limitation we observed accumulation of the repressive histone mark, H3K27me3, which is typically removed by the α-KG and iron dependent KDM6A/B enzymes in both CD8+ T-cells and Th17 polarised T-cells (Fig. 5.6, Fig. 5.7D-E). Simultaneously, aspartate abundance was significantly elevated suggestive of reduced usage in downstream pathways (Fig. 5.3B-C). Aspartate build up may be partially explained by backfilling of the TCA cycle via increased PC activity and the reductive TCA cycle (Fig. 5.4).

Under iron limiting conditions, CD8+ T-cells were demonstrated to increase mROS generation (Fig. 5.1A). The ETC passes electrons though a series of reactions to release the energy required to produce a proton gradient with oxygen as the terminal electron acceptor[12]. However, if electrons are prematurely passed to oxygen due to inefficient electron transfer and electron leakage, mROS are produced[32]. mROS can be produced from eight separate sites in the mitochondria, however, CI and CIII have the greatest capacity to generate mROS[36,55]. Thus, it is likely that the large increase in mROS in iron deprived CD8+ T-cells is indicative of CI and CIII dysfunction (although other sites of mROS generation are also possible). Notably, CI and CIII are highly dependent on heme and Fe-S cluster cofactors to mediate electron transfer[12] and CI and CIII subunits were also amongst the ETC proteins upregulated in iron deficient CD8+ T-cells (Fig. 4.4F). We propose that the increase in ETC proteins in iron scarcity, combined with the assumed insufficiency of iron atoms to furnish these complexes, results in inefficient electron transfer and mROS generation. Interestingly, mROS generated into the intermembrane space by CIII can play signalling roles, with studies indicating that CIII-derived ROS can drive NFAT1 activation and downstream IL-2 and TNF-α production in T-cells[14,39]. If iron deficiency generated mROS are responsible for driving the NFAT1 activation and

consequent upregulation of IL-2 and TNF-α we observe (Fig. 5.1D-G), administration of the mitochondrially targeted antioxidant, mitoTEMPO, should suppress these processes. Interestingly, T-cells with excess ROS due to defects in ROS detoxification show impaired mTOR activation and MYC expression (although the mechanism has not been described)[56] suggesting that ROS may also be partly responsible for the defects in MYC and mTORC1 signalling in iron deficient CD8+ T-cells (chapter 4, Fig. 4.2, Fig. 4.4).

While to our knowledge, our work presents the first example of metabolomics of iron deprived T-cells (Fig. 5.3, Fig. 5.4), the impacts of mitochondrial dysfunction and iron restriction on cellular metabolic pathways have been extensively examined in cell lines. Colorectal carcinoma (CRC) cell lines (HCT116 and SW480) treated with the iron chelator DFO show significant suppression of oxygen consumption[57] in line with the reduced mitochondrial function observed in iron depleted T-cells. However, while CD8+ T-cells in low iron media experience aspartate accumulation and an increased NAD+/NADH ratio (Fig. 5.3B-D), DFO treated CRC cell lines show aspartate depletion and suppression of the NAD+/NADH ratio[57]. Schwartz *et al*[57] attribute their observed effects to the mechanistic models first described by Birsoy *et al*[58] and Sullivan *et al*[59] where inhibition of the ETC (originally via ETC inhibitors, but in this case by iron restriction) results in depletion of the cellular NAD+ pool due to reduced conversion of NADH to NAD+ by iron dependent CI. Lack of NAD+ in turn prohibits the activity of NAD+ dependent MDH2 which mediates the malate to oxaloacetate reaction which is required for aspartate generation (Fig. 5.8)[57-59]. Inhibition of the TCA cycle enzymes fumarate hydratase (FH) or SDH via genetic or pharmacological means similarly reduces the NAD+/NADH ratio and aspartate generation in kidney epithelial cells[60] indicating that TCA cycle blockade can cause similar downstream metabolic effects to ETC inhibition, potentially via the same mechanism. However, given that neither reduced NAD+/NADH nor aspartate deprivation were observed under iron limitation in CD8+ T-cells (Fig. 5.3B-D), this mechanism is unlikely to be operating in our setting.

Interestingly, HEK293 cells with mutations in the crucial Fe-S cluster synthesis protein, ISCU2, more closely recapitulates our metabolic findings in iron deprived CD8+ T-cells (Fig. 5.3B-D). HEK293 cells carrying the $ISCU2^{D71A}$ mutation have impaired activity of Fe-S cluster proteins including ACO2, SDH (CII) and CI[61]. Similar to iron restricted CD8+ T-cells, $ISCU2^{D71A}$ HEK293 cells show reduced α-KG, fumarate and malate

abundance downstream of iron dependent ACO2 and SDH, while succinate shows some accumulation upstream of SDH[61]. Notably, aspartate also accumulates in ISCU2^{D71A} HEK293 cells similar to iron deficient CD8+ T-cells[61]. However, while no significant change in citrate abundance was observed in iron depleted CD8+ T-cells, ISCU2^{D71A} mutant HEK293 cells show massive accumulation of citrate which is proposed to drive lipid droplet formation due to citrate feeding into fatty acid synthesis[61], a phenomenon which also occurs in ACO2 deficient LoVo cells[62] and deferiprone (DFP) iron chelator treated macrophages[63]. While we have not specifically measured fatty acid loads of iron restricted CD8+ T-cells, an upregulation of fatty acid β-oxidation proteins was observed (chapter 4, Fig. 4.2, Fig. 4.4F) which could potentially be upregulated to handle aberrant fatty acid synthesis. Measurements of cellular fatty acids could be completed using BODIPY dyes or metabolite-MS.

The metabolic dysfunction in ISCU^{D71A} HEK293 cells and iron deprived CD8+ T-cells largely resembles each other but offers a phenotype in direct opposition to the generally accepted model where ETC and TCA cycle inhibition blocks aspartate production via reduced NAD+ availability[57-60]. Notably, ACO2 suppression in isolation has not yet been demonstrated to replicate the canonical model laid out by Birsoy *et al*[58] and Sullivan *et al*[59]. This is interesting because both ISCU^{D71A} HEK293 cells and iron deprived CD8+ T-cells have proposed defects in the Fe-S cluster protein, ACO2. ACO2 lies relatively upstream within the TCA cycle, immediately before the two NAD+ consuming steps mediated by isocitrate dehydrogenase (IDH) and α-KGDH. Decreased flux through IDH and α-KGDH due to reduced ACO2 generated isocitrate would be proposed to decrease NAD+ consumption resulting in an increased NAD+/NADH ratio in agreement with what we observe (Fig. 5.3D). In contrast, inhibition later in the TCA cycle, for instance at SDH or FH, would still permit flux through IDH and α-KGDH, thus consuming NAD+ and decreasing the NAD+/NADH ratio. This could be further exacerbated by decreased CI consumption of NADH which is known to occur during FH (and possibly SDH) inhibition[64]. It is proposed here that the location of TCA cycle blockade may differentially impact the NAD+/NADH ratio which in turn will affect whether aspartate can be generated downstream. Genetic or pharmacological inhibition of the various TCA cycle enzymes and the resulting metabolic profile should be evaluated to determine if the established model of aspartate depletion during ETC or TCA inhibition is only applicable at certain nodes of the cycle.

It should however be noted, that the aspartate depleted phenotype observed by Schwartz *et al*[57] in DFO iron chelator treated CRC cells does not support our suggested mechanism, as DFO should impair ACO2. However, as discussed in chapter 4, iron chelator treatment can be extremely harsh and result in substantial alterations in cellular state. Notably, only 4 hours of ciclopirox olamine (CPX) iron chelator treatment of Th1 T-cells was extreme enough to alter the expression of >3000 genes and impaired canonical TFRC upregulation which should occur during iron limitation (chapter 4)[65] together suggesting a highly stressed cell state. Meanwhile, our model of 48 hours of iron depleted media (which is much more physiological) only induced differential expression of around 200 genes in CD8+ T-cells (chapter 4). Thus, it is possible that DFO treatment of CRC cell lines is impairing cellular processes far beyond what might be expected from more physiological iron deficiency with unpredicted outcomes on metabolism.

Aspartate accumulation during CD8+ T-cell iron restriction (Fig. 5.3B-D) likely occurs due to both reduced usage (Fig. 5.4A) and backfilling from glucose via increased PC activity and the reductive TCA cycle (Fig. 5.4C-E). However, this is surprising given that activated T-cells have large requirements for aspartate in downstream metabolic pathways including nucleotide synthesis[46], asparagine generation[47] and protein translation. Preclusion of aspartate utilisation due to suppression of downstream pathways is potentially suggested by decreased ASNS and PPAT protein expression (Fig. 5.4F-H), critical enzymes in asparagine and purine synthesis respectively. Crucially, for aspartate to be consumed by these downstream pathways, aspartate must be cytosolically located. Thus, an alternative explanation for reduced aspartate usage could be inappropriate retention of aspartate in the mitochondria. Mitochondrial aspartate is shunted into the cytosol via the malate-aspartate shuttle (Fig. 5.8). Interestingly, knockout of various machinery critical for the malate-aspartate shuttle (SLC25A11, MDH1, MDH2) results in suppression of IFN-γ in Th1 polarised CD4+ T-cells[15], indicating the importance of this shuttle for T-cell function. In the malate-aspartate shuttle, aspartate is transported into the cytosol by SLC25A12/13 in exchange for glutamate[66]. Crucially, this transporter requires a proton gradient to mediate transport[66] and iron depleted CD8+ T-cells were previously shown to have a reduced mitochondrial membrane potential relative to iron replete controls[6]. Therefore, it is hypothesised that a reduction in ETC chain activity due to iron deficiency may reduce the mitochondrial

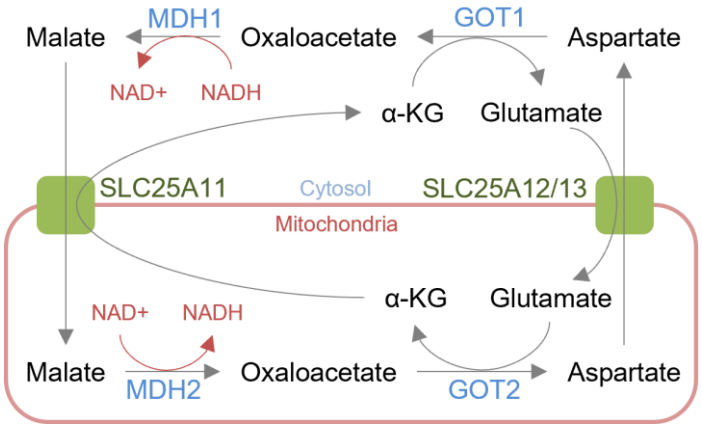

Figure 5.8. Malate-aspartate shuttle. Aspartate is generated in the mitochondria via the TCA cycle. MDH2 uses NAD+ to convert malate to oxaloacetate. GOT2 converts oxaloacetate and glutamate to aspartate and α-KG. Aspartate is transported into the cytosol in exchange for glutamate via SLC25A12/13. Aspartate can be converted back into malate via GOT1 and MDH2 which mediate the reverse reactions to their mitochondrial counterparts. Malate is transported back into the mitochondria by SLC25A11 in exchange for α-KG.

protein gradient, in turn inhibiting SLC25A12/13 and sequestering aspartate in the mitochondria. Inhibition of aspartate export to the cytosol may also alter the localisation of other metabolites of the malate-aspartate shuttle (glutamate, α-KG and malate). For instance, mitochondrial glutamate entry may be restricted by reduced SLC25A12/13 function as well as reduced function of the mitochondrial glutamate carrier (SLC25A18/22) which is also proton dependent[66]. Malate and α-KG may experience some degree of mis-localisation, however, these effects are likely attenuated by the fact that the malate/α-KG transporter is proton independent, as well as the presence of alternative proton-independent mitochondrial transporters for malate and α-KG[66]. Measurements of aspartate, glutamate, α-KG and malate in the cytosolic and mitochondrial compartments will be completed in the near future using emerging protocols. Cytosolic metabolites can be released from cells into supernatants via digitonin treatment that permeabilises plasma membranes but not mitochondrial membranes[67]. Meanwhile, a recent protocol demonstrated that metabolite-MS can be completed on hemagglutinin (HA) tagged mitochondria isolated via binding to HA-specific antibodies[68]. Such methods could be used to test how iron deficiency influences cellular compartmentalisation of metabolism, including aspartate.

Using experimental methods, it was shown that iron deprivation likely impairs chromatin remodelling in CD8+ T-cells and Th17 cells with elevated expression of the KDM6A/B target, H3K27me3 (Fig. 5.6, Fig. 5.7D-E). While we cannot be certain that the increase in H3K27me3 is due to reduced demethylation by KDM6A/B rather than increased methylation, previous studies have indicated that inhibition of KDM6A/B does impair Th17 differentiation and CD8+ T-cell proliferation and memory formation[28,29]. Notably, KDM6A/B inhibition using the drug GSK-J4 also results in metabolic remodelling in *in vitro* Th17 polarised CD4+ T-cells[29]. GSK-J4 treated Th17s show increased glycolytic metabolites but a reduction in TCA cycle metabolites which coincides with corresponding changes to glycolytic and TCA cycle enzymes[29]. These metabolic alterations may be partially explained by an increase in H3K27me3 at the loci encoding the metabolic regulators *MYC*, *PPRC1* and *PPARGC1a* in KDM6A/B inhibited Th17 cells[29]. Together, this suggests that a positive feedback loop may be in place where metabolic dysfunction drives epigenetic defects which can further alter metabolism via differential expression of metabolic regulators and enzymes. To identify if the accumulation of H3K27me3 may be driving some of the observed metabolic dysfunction in iron deprived T-cells for instance via dampening mTORC1 and MYC signalling as observed by RNA-seq and protein-MS (chapter 4), chromatin immunoprecipitation (ChIP)-seq with pull down of H3K27me3 associated DNA should be completed. This would also allow us to identify if other transcriptionally downregulated pathways in iron deficient CD8+ T-cells such as the IFN response are similarly suppressed by inappropriate H3K27me3 build up.

Increased H3K27me3 in iron deficient T-cells (Fig. 5.6, Fig. 5.7D-E) is suggestive of KDM6A/B dysfunction. This indicates that the reduced levels of α-KG (Fig. 5.5B) and/or iron depletion in our model may be capable of inhibiting 2-OGDD enzymes more generally. This is particularly relevant as most of the 2-OGDD KMDs experience upregulation during T-cell activation as observed in the Howden *et al*[7] dataset. Thus, it would be interesting to evaluate whether other histone methyl groups similarly accumulate, resulting in dysregulated chromatin. Removal of repressive DNA methylation from the promoters of effector gene loci by iron dependent TET enzymes is also required during T-cell activation[69] making evaluation of DNA methylation during iron scarcity also worthwhile. Critically, T-cell activation and memory formation is highly dependent on appropriate DNA and histone methylation remodelling[69]. The linear model of T-cell differentiation suggests a trajectory where naïve T-cells differentiate through a

memory-type state before becoming effector T-cells[69]. In this case, memory T-cell chromatin is believed to occupy an intermediate state where epigenetic changes are only partially complete[69]. In iron depleted CD8+ T-cells, H3K27me3 levels are intermediate between the naïve and iron replete conditions. While acute iron deficiency is clearly detrimental to immediate T-cell effector function, whether holding T-cells in this partial demethylated state could prevent T-cell terminal differentiation and in turn be potentially beneficial in generating memory T-cells is unknown. It is plausible that upon secondary antigen exposure upon return to iron replete conditions, T-cells could engage their demethylation enzymes and remove the remaining H3K27me3 marks located on effector gene loci. To evaluate if short term iron deficiency could potentially provide long term benefit to memory T-cell responses, OT-I T-cells should be adoptively transferred to primary hypoferremic (mediated using the hepcidin analogue, mini-hepcidin (mHep)) recipient mice and activated using an immunisation platform such as OVA and adjuvant (α-CD40/MPLA) (further described in chapter 6). Equal numbers of memory OT-I T-cells should be sorted from primary recipients and transferred to secondary iron replete recipients and the magnitude of the memory T-cell response should be quantified following secondary stimulation.

The suppression of Th17 polarisation in iron deficient media (Fig. 5.7) is in agreement with literature demonstrating that iron restriction via iron chelators or α-CD71 antibodies impairs Th17 polarisation and IL-17A production *in vitro*. However, our work further suggests that defects in chromatin remodelling due to reduced H3K27me3 removal may be responsible. Given that Th17 cells are known to mediate autoimmunity, it is also notable that iron restriction has also been shown to reduced disease severity in mouse models of autoimmunity[10,11,38,70]. Whether iron depletion also impairs Th17 responses in more beneficial settings such as gut maintenance or responses to pathogens such as *Candida albicans* or group A *streptococcus* remains unknown. Further work should also be completed to identify if similar defects occur in other CD4+ T-cell subsets, perhaps with a particular emphasis on Th2 cells which have so far been poorly characterised in the context of iron deficiency but similarly to Th17s must proliferate and remodel their chromatin to enable expression of the Th2 program[71].

5.3.1 Limitations

As discussed in chapter 4, *in vitro* culture conditions do not replicate the complex *in vivo* environment. Our *in vitro* culture setup activates T-cells at atmospheric oxygen, with non-physiological media and lacking the three-dimensional tissue context of the lymph node. Notably, recent literature has indicated that the metabolic profiles of *in vitro* activated T-cells are different than those of *in vivo* activated T-cells[72]. For instance, CD8+ T-cells activated *in vivo* show much greater usage of OXPHOS than those activated *in vitro*[72]. Further, entry of glucose into the TCA cycle via PC and reductive TCA cycling was much higher in *in vitro* activated CD8+ T-cells relative to their *in vivo* activated counterparts[72]. The discrepancy between *in vitro* and *in vivo* T-cell metabolism means that caution should be employed in over-extrapolating *in vitro* observations. However, it remains likely that the locations of metabolic blocks caused by perturbations such as iron deficiency are broadly maintained even if the usage of different metabolic pathways may differ. For instance, one might hypothesise that ACO2 and SDH activity will remain impaired *in vivo* during iron deficiency, but perhaps the capacity of PC to compensate by backfilling the TCA cycle may be altered. This may mean that the relative contributions of certain metabolic impairments to the overall state of iron deficiency induced dysfunction may be different between *in vitro* and *in vivo* cells.

Up until recently, metabolite-MS of immune cells taken directly *ex vivo* has been limited by detection sensitivity, since the method requires millions of cells and is typically not feasible without *in vitro* culture. However, methodological advancements are now permitting measurements of metabolites from much smaller cell numbers. A recent study has demonstrated proof of principle that metabolite-MS can be conducted on as few as 10,000 flow cytometry sorted cells with detection of 160 metabolites[73]. *In vivo* ^{13}C tracing via slow infusion of ^{13}C metabolites into the circulation has also been recently pioneered[72]. Together, these progressions, provide a platform through which the metabolism of *in vivo* activated T-cells could be assessed. For instance, OT-I T-cells could be transferred to recipient mice and activated via immunisation with the OVA peptide in the presence or absence of mHep to suppress serum iron. At the peak of T-cell expansion, mice could be infused with ^{13}C-glutamine for two hours prior to cull and OVA-specific T-cells could be sorted and metabolite-MS completed. Similarly, the epigenetic outcomes

of iron deprivation could also be evaluated *in vivo* using this model by completing ChIP-seq on *ex vivo* sorted OT-I T-cells.

5.3.2 Conclusion

In summary, iron depletion dramatically impairs CD8+ T-cell mitochondrial metabolism at multiple nodes including suppression of the iron dependent enzymes ACO2 and SDH, promotion of mROS generation most likely via CI and CIII dysfunction and suppression of α-KG. While not conclusive, reduced α-KG combined with low iron may be responsible for the reduced H3K27me3 levels observed in iron restricted CD8+ T-cells and Th17 polarised CD4+ T-cells. Overall, indicating that T-cell iron scarcity results in profound alterations in metabolic and epigenetic remodelling with likely consequences for cellular differentiation.

5.4 References

1 Pearce, E. L., Poffenberger, M. C., Chang, C. H. & Jones, R. G. Fueling immunity: insights into metabolism and lymphocyte function. *Science* **342**, 1242454 (2013). https://doi.org:10.1126/science.1242454

2 Brand, K., Williams, J. F. & Weidemann, M. J. Glucose and glutamine metabolism in rat thymocytes. *Biochem J* **221**, 471-475 (1984). https://doi.org:10.1042/bj2210471

3 Wang, R. *et al.* The transcription factor Myc controls metabolic reprogramming upon T lymphocyte activation. *Immunity* **35**, 871-882 (2011). https://doi.org:10.1016/j.immuni.2011.09.021

4 Shyer, J. A., Flavell, R. A. & Bailis, W. Metabolic signaling in T cells. *Cell Res* **30**, 649-659 (2020). https://doi.org:10.1038/s41422-020-0379-5

5 O'Donnell, K. A. *et al.* Activation of transferrin receptor 1 by c-Myc enhances cellular proliferation and tumorigenesis. *Mol Cell Biol* **26**, 2373-2386 (2006). https://doi.org:10.1128/mcb.26.6.2373-2386.2006

6 Frost, J. N. *et al.* Hepcidin-Mediated Hypoferremia Disrupts Immune Responses to Vaccination and Infection. *Med (N Y)* **2**, 164-179.e112 (2021). https://doi.org:10.1016/j.medj.2020.10.004

7 Howden, A. J. M. *et al.* Quantitative analysis of T cell proteomes and environmental sensors during T cell differentiation. *Nat Immunol* **20**, 1542-1554 (2019). https://doi.org:10.1038/s41590-019-0495-x

8 van der Windt, G. J. *et al.* Mitochondrial respiratory capacity is a critical regulator of CD8+ T cell memory development. *Immunity* **36**, 68-78 (2012). https://doi.org:10.1016/j.immuni.2011.12.007

9 Yarosz, E. L. *et al.* Cutting Edge: Activation-Induced Iron Flux Controls CD4 T Cell Proliferation by Promoting Proper IL-2R Signaling and Mitochondrial Function. *J Immunol* **204**, 1708-1713 (2020). https://doi.org:10.4049/jimmunol.1901399

10 Voss, K. *et al.* Elevated transferrin receptor impairs T cell metabolism and function in systemic lupus erythematosus. *Sci Immunol* **8**, eabq0178 (2023). https://doi.org:10.1126/sciimmunol.abq0178

11 Lai, Y. *et al.* Iron controls T helper cell pathogenicity by promoting glucose metabolism in autoimmune myopathy. *Clin Transl Med* **12**, e999 (2022). https://doi.org:10.1002/ctm2.999

12 Paul, B. T., Manz, D. H., Torti, F. M. & Torti, S. V. Mitochondria and Iron: current questions. *Expert Rev Hematol* **10**, 65-79 (2017). https://doi.org:10.1080/17474086.2016.1268047

13 Lisci, M. *et al.* Mitochondrial translation is required for sustained killing by cytotoxic T cells. *Science* **374**, eabe9977 (2021). https://doi.org:10.1126/science.abe9977

14 Sena, L. A. *et al.* Mitochondria are required for antigen-specific T cell activation through reactive oxygen species signaling. *Immunity* **38**, 225-236 (2013). https://doi.org:10.1016/j.immuni.2012.10.020

15 Bailis, W. *et al.* Distinct modes of mitochondrial metabolism uncouple T cell differentiation and function. *Nature* **571**, 403-407 (2019). https://doi.org:10.1038/s41586-019-1311-3

16 Tarasenko, T. N. *et al.* Cytochrome c Oxidase Activity Is a Metabolic Checkpoint that Regulates Cell Fate Decisions During T Cell Activation and Differentiation. *Cell Metab* **25**, 1254-1268.e1257 (2017). https://doi.org:10.1016/j.cmet.2017.05.007
17 Chen, X. *et al.* Succinate dehydrogenase/complex II is critical for metabolic and epigenetic regulation of T cell proliferation and inflammation. *Sci Immunol* **7**, eabm8161 (2022). https://doi.org:10.1126/sciimmunol.abm8161
18 Edmonds, J. L. *et al.* The otolaryngological manifestations of mitochondrial disease and the risk of neurodegeneration with infection. *Arch Otolaryngol Head Neck Surg* **128**, 355-362 (2002). https://doi.org:10.1001/archotol.128.4.355
19 Eom, S. *et al.* Cause of Death in Children With Mitochondrial Diseases. *Pediatr Neurol* **66**, 82-88 (2017). https://doi.org:10.1016/j.pediatrneurol.2016.10.006
20 Walker, M. A. *et al.* Predisposition to infection and SIRS in mitochondrial disorders: 8 years' experience in an academic center. *J Allergy Clin Immunol Pract* **2**, 465-468, 468.e461 (2014). https://doi.org:10.1016/j.jaip.2014.02.009
21 Reichenbach, J. *et al.* Fatal neonatal-onset mitochondrial respiratory chain disease with T cell immunodeficiency. *Pediatr Res* **60**, 321-326 (2006). https://doi.org:10.1203/01.pdr.0000233252.60457.cf
22 Jabara, H. H. *et al.* A missense mutation in TFRC, encoding transferrin receptor 1, causes combined immunodeficiency. *Nat Genet* **48**, 74-78 (2016). https://doi.org:10.1038/ng.3465
23 Soriano-Baguet, L. & Brenner, D. Metabolism and epigenetics at the heart of T cell function. *Trends Immunol* **44**, 231-244 (2023). https://doi.org:10.1016/j.it.2023.01.002
24 Russ, B. E. *et al.* Distinct epigenetic signatures delineate transcriptional programs during virus-specific CD8(+) T cell differentiation. *Immunity* **41**, 853-865 (2014). https://doi.org:10.1016/j.immuni.2014.11.001
25 Bao, X. R. *et al.* Mitochondrial dysfunction remodels one-carbon metabolism in human cells. *Elife* **5** (2016). https://doi.org:10.7554/eLife.10575
26 Islam, M. S., Leissing, T. M., Chowdhury, R., Hopkinson, R. J. & Schofield, C. J. 2-Oxoglutarate-Dependent Oxygenases. *Annu Rev Biochem* **87**, 585-620 (2018). https://doi.org:10.1146/annurev-biochem-061516-044724
27 Xiao, M. *et al.* Inhibition of α-KG-dependent histone and DNA demethylases by fumarate and succinate that are accumulated in mutations of FH and SDH tumor suppressors. *Genes Dev* **26**, 1326-1338 (2012). https://doi.org:10.1101/gad.191056.112
28 Li, J. *et al.* KDM6B-dependent chromatin remodeling underpins effective virus-specific CD8(+) T cell differentiation. *Cell Rep* **34**, 108839 (2021). https://doi.org:10.1016/j.celrep.2021.108839
29 Cribbs, A. P. *et al.* Histone H3K27me3 demethylases regulate human Th17 cell development and effector functions by impacting on metabolism. *Proc Natl Acad Sci U S A* **117**, 6056-6066 (2020). https://doi.org:10.1073/pnas.1919893117
30 Invitrogen. Vol. MAN0028459 (ed Invitrogen) (2022).
31 Roelofs, B. A., Ge, S. X., Studlack, P. E. & Polster, B. M. Low micromolar concentrations of the superoxide probe MitoSOX uncouple neural mitochondria and inhibit complex IV. *Free Radic Biol Med* **86**, 250-258 (2015). https://doi.org:10.1016/j.freeradbiomed.2015.05.032
32 Turrens, J. F. Mitochondrial formation of reactive oxygen species. *J Physiol* **552**, 335-344 (2003). https://doi.org:10.1113/jphysiol.2003.049478

33 Kim, Y. S., Gupta Vallur, P., Phaëton, R., Mythreye, K. & Hempel, N. Insights into the Dichotomous Regulation of SOD2 in Cancer. *Antioxidants (Basel)* **6** (2017). https://doi.org:10.3390/antiox6040086

34 Cho, E. A. *et al.* Differential in vitro and cellular effects of iron chelators for hypoxia inducible factor hydroxylases. *J Cell Biochem* **114**, 864-873 (2013). https://doi.org:10.1002/jcb.24423

35 Muller, F. L., Liu, Y. & Van Remmen, H. Complex III releases superoxide to both sides of the inner mitochondrial membrane. *J Biol Chem* **279**, 49064-49073 (2004). https://doi.org:10.1074/jbc.M407715200

36 Sena, L. A. & Chandel, N. S. Physiological roles of mitochondrial reactive oxygen species. *Mol Cell* **48**, 158-167 (2012). https://doi.org:10.1016/j.molcel.2012.09.025

37 Berg, V. *et al.* Iron Deprivation in Human T Cells Induces Nonproliferating Accessory Helper Cells. *Immunohorizons* **4**, 165-177 (2020). https://doi.org:10.4049/immunohorizons.2000003

38 Li, L. *et al.* Iron deprivation restrains the differentiation and pathogenicity of T helper 17 cell. *J Leukoc Biol* **110**, 1057-1067 (2021). https://doi.org:10.1002/jlb.3ma0821-015r

39 Ke, Q. *et al.* Essential role of ROS-mediated NFAT activation in TNF-alpha induction by crystalline silica exposure. *Am J Physiol Lung Cell Mol Physiol* **291**, L257-264 (2006). https://doi.org:10.1152/ajplung.00007.2006

40 Stewart, J. B. & Chinnery, P. F. Extreme heterogeneity of human mitochondrial DNA from organelles to populations. *Nat Rev Genet* **22**, 106-118 (2021). https://doi.org:10.1038/s41576-020-00284-x

41 Castellani, C. A., Longchamps, R. J., Sun, J., Guallar, E. & Arking, D. E. Thinking outside the nucleus: Mitochondrial DNA copy number in health and disease. *Mitochondrion* **53**, 214-223 (2020). https://doi.org:10.1016/j.mito.2020.06.004

42 D'Souza, A. D., Parikh, N., Kaech, S. M. & Shadel, G. S. Convergence of multiple signaling pathways is required to coordinately up-regulate mtDNA and mitochondrial biogenesis during T cell activation. *Mitochondrion* **7**, 374-385 (2007). https://doi.org:10.1016/j.mito.2007.08.001

43 Lee, H. C. & Wei, Y. H. Mitochondrial biogenesis and mitochondrial DNA maintenance of mammalian cells under oxidative stress. *Int J Biochem Cell Biol* **37**, 822-834 (2005). https://doi.org:10.1016/j.biocel.2004.09.010

44 Teh, M. R., Frost, J. N., Armitage, A. E. & Drakesmith, H. Analysis of Iron and Iron-Interacting Protein Dynamics During T-Cell Activation. *Front Immunol* **12**, 714613 (2021). https://doi.org:10.3389/fimmu.2021.714613

45 Shimomura, Y. *et al.* Novel Physiological Functions of Branched-Chain Amino Acids. *J Nutr Sci Vitaminol (Tokyo)* **61 Suppl**, S112-114 (2015). https://doi.org:10.3177/jnsv.61.S112

46 Villa, E., Ali, E. S., Sahu, U. & Ben-Sahra, I. Cancer Cells Tune the Signaling Pathways to Empower de Novo Synthesis of Nucleotides. *Cancers (Basel)* **11** (2019). https://doi.org:10.3390/cancers11050688

47 Hope, H. C. *et al.* Coordination of asparagine uptake and asparagine synthetase expression modulates CD8+ T cell activation. *JCI Insight* **6** (2021). https://doi.org:10.1172/jci.insight.137761

48 Leone, R. D. *et al.* Glutamine blockade induces divergent metabolic programs to overcome tumor immune evasion. *Science* **366**, 1013-1021 (2019). https://doi.org:10.1126/science.aav2588

49 Elia, I. *et al.* Tumor cells dictate anti-tumor immune responses by altering pyruvate utilization and succinate signaling in CD8(+) T cells. *Cell Metab* **34**, 1137-1150.e1136 (2022). https://doi.org:10.1016/j.cmet.2022.06.008

50 Loenarz, C. & Schofield, C. J. Physiological and biochemical aspects of hydroxylations and demethylations catalyzed by human 2-oxoglutarate oxygenases. *Trends Biochem Sci* **36**, 7-18 (2011). https://doi.org:10.1016/j.tibs.2010.07.002

51 Markolovic, S., Wilkins, S. E. & Schofield, C. J. Protein Hydroxylation Catalyzed by 2-Oxoglutarate-dependent Oxygenases. *J Biol Chem* **290**, 20712-20722 (2015). https://doi.org:10.1074/jbc.R115.662627

52 Tesmer, L. A., Lundy, S. K., Sarkar, S. & Fox, D. A. Th17 cells in human disease. *Immunol Rev* **223**, 87-113 (2008). https://doi.org:10.1111/j.1600-065X.2008.00628.x

53 Geginat, J. *et al.* Plasticity of human CD4 T cell subsets. *Front Immunol* **5**, 630 (2014). https://doi.org:10.3389/fimmu.2014.00630

54 Xu, S. & Cao, X. Interleukin-17 and its expanding biological functions. *Cell Mol Immunol* **7**, 164-174 (2010). https://doi.org:10.1038/cmi.2010.21

55 Brand, M. D. The sites and topology of mitochondrial superoxide production. *Exp Gerontol* **45**, 466-472 (2010). https://doi.org:10.1016/j.exger.2010.01.003

56 Mak, T. W. *et al.* Glutathione Primes T Cell Metabolism for Inflammation. *Immunity* **46**, 675-689 (2017). https://doi.org:10.1016/j.immuni.2017.03.019

57 Schwartz, A. J. *et al.* Hepcidin sequesters iron to sustain nucleotide metabolism and mitochondrial function in colorectal cancer epithelial cells. *Nature Metabolism* **3**, 969-982 (2021). https://doi.org:10.1038/s42255-021-00406-7

58 Birsoy, K. *et al.* An Essential Role of the Mitochondrial Electron Transport Chain in Cell Proliferation Is to Enable Aspartate Synthesis. *Cell* **162**, 540-551 (2015). https://doi.org:10.1016/j.cell.2015.07.016

59 Sullivan, L. B. *et al.* Supporting Aspartate Biosynthesis Is an Essential Function of Respiration in Proliferating Cells. *Cell* **162**, 552-563 (2015). https://doi.org:10.1016/j.cell.2015.07.017

60 Ryan, D. G. *et al.* Disruption of the TCA cycle reveals an ATF4-dependent integration of redox and amino acid metabolism. *Elife* **10** (2021). https://doi.org:10.7554/eLife.72593

61 Crooks, D. R. *et al.* Acute loss of iron-sulfur clusters results in metabolic reprogramming and generation of lipid droplets in mammalian cells. *J Biol Chem* **293**, 8297-8311 (2018). https://doi.org:10.1074/jbc.RA118.001885

62 You, X. *et al.* Loss of mitochondrial aconitase promotes colorectal cancer progression via SCD1-mediated lipid remodeling. *Mol Metab* **48**, 101203 (2021). https://doi.org:10.1016/j.molmet.2021.101203

63 Pereira, M. *et al.* Acute Iron Deprivation Reprograms Human Macrophage Metabolism and Reduces Inflammation In Vivo. *Cell Rep* **28**, 498-511.e495 (2019). https://doi.org:10.1016/j.celrep.2019.06.039

64 Tyrakis, P. A. *et al.* Fumarate Hydratase Loss Causes Combined Respiratory Chain Defects. *Cell Rep* **21**, 1036-1047 (2017). https://doi.org:10.1016/j.celrep.2017.09.092

65 Wang, Z. *et al.* Iron Drives T Helper Cell Pathogenicity by Promoting RNA-Binding Protein PCBP1-Mediated Proinflammatory Cytokine Production. *Immunity* **49**, 80-92.e87 (2018). https://doi.org:10.1016/j.immuni.2018.05.008

66 Ruprecht, J. J. & Kunji, E. R. S. The SLC25 Mitochondrial Carrier Family: Structure and Mechanism. *Trends Biochem Sci* **45**, 244-258 (2020). https://doi.org:10.1016/j.tibs.2019.11.001

67 Nonnenmacher, Y., Palorini, R. & Hiller, K. Determining Compartment-Specific Metabolic Fluxes. *Methods Mol Biol* **1862**, 137-149 (2019). https://doi.org:10.1007/978-1-4939-8769-6_10

68 Chen, W. W., Freinkman, E., Wang, T., Birsoy, K. & Sabatini, D. M. Absolute Quantification of Matrix Metabolites Reveals the Dynamics of Mitochondrial Metabolism. *Cell* **166**, 1324-1337.e1311 (2016). https://doi.org:10.1016/j.cell.2016.07.040

69 Henning, A. N., Roychoudhuri, R. & Restifo, N. P. Epigenetic control of CD8(+) T cell differentiation. *Nat Rev Immunol* **18**, 340-356 (2018). https://doi.org:10.1038/nri.2017.146

70 Gao, X. *et al.* Iron-dependent epigenetic modulation promotes pathogenic T cell differentiation in lupus. *J Clin Invest* **132** (2022). https://doi.org:10.1172/jci152345

71 Fields, P. E., Lee, G. R., Kim, S. T., Bartsevich, V. V. & Flavell, R. A. Th2-specific chromatin remodeling and enhancer activity in the Th2 cytokine locus control region. *Immunity* **21**, 865-876 (2004). https://doi.org:10.1016/j.immuni.2004.10.015

72 Ma, E. H. *et al.* Metabolic Profiling Using Stable Isotope Tracing Reveals Distinct Patterns of Glucose Utilization by Physiologically Activated CD8(+) T Cells. *Immunity* **51**, 856-870.e855 (2019). https://doi.org:10.1016/j.immuni.2019.09.003

73 DeVilbiss, A. W. *et al.* Metabolomic profiling of rare cell populations isolated by flow cytometry from tissues. *Elife* **10** (2021). https://doi.org:10.7554/eLife.61980

Chapter 6

6 Nutritional, pharmacologic and genetic rescue of iron deficient T-cells

6.1 Introduction

Activated T-cells require biochemical substrates to produce ATP, proteins, lipids and DNA which are necessary to support rapid proliferation and acquisition of effector functions including cytokine and cytolytic protein production[1]. While activated T-cells express many enzymes which allow for the endogenous generation of metabolic intermediates, uptake of some environmental nutrients is also necessary[1]. For instance, increased glucose import via upregulation of the glucose transporter, GLUT1, occurs following T-cell activation downstream of CD28 stimulation[2]. Glucose limitation suppresses T-cell proliferation and the production of IL-2 and IFN-γ[2]. Similarly, T-cells rapidly upregulate the iron uptake protein, TFRC, post-activation[3,4] and iron deprivation profoundly suppresses T-cell proliferation, activation and effector function[4-14] (critically, iron cannot be synthesised by cells). Notably, exogenous sources of many non-essential amino acids are necessary for T-cell function despite theoretical intracellular capacity to produce them[15-21]. Further, the requirements for extracellular nutrients including amino acids can be context dependent. For instance, rotenone treated Th1 T-cells become auxotrophic for aspartate and require exogenous aspartate sources to support proliferation[15]. Meanwhile, extracellular asparagine is required for early (first 48 hours) T-cell activation including for LCK phosphorylation and TCR signalling[16], proliferation and effector functions (GZMB and IL-2 production)[17]. However, exogenous asparagine becomes dispensable at later timepoints (72 hours) as cells gain the ability to produce asparagine *in situ* from aspartate via asparagine synthetase (ASNS)[17]. Given the iron dependency of many metabolic processes, we propose that iron restricted CD8+ T-cells may become auxotrophic for metabolites downstream of iron dependent processes which can not be produced to sufficiently high levels to support cellular function.

The context dependency of cells for certain nutrients could be particularly relevant in nutritionally depleted environments such as the tumour microenvironment or infectious niches such as tuberculosis granulomas[22,23]. Due to the high metabolic dependencies of both tumour cells and pathogens, multiple nutrients including iron may be depleted in the surrounding environment resulting in impairment of infiltrating immune cells[23,24]. The scarcity of multiple nutrients has the potential to synergistically impair immunity, especially if depletion of one nutrient (such as iron) results in auxotrophy for other nutrients.

Iron deficiency severely impairs CD8+ T-cell metabolism at multiple nodes and levels of metabolic control. For instance, iron restriction suppresses CD8+ T-cell MYC and mTORC1 signalling indicative of altered metabolic rewiring (chapter 4, Fig. 4.2, Fig. 4.4), reduces mitochondrial ATP generation[4], increases mROS production suggestive of electron transport chain (ETC) dysfunction (chapter 5, Fig. 5.1A) and alters redox status characterised by an increased NAD+/NADH ratio (chapter 5, Fig. 5.3D). At a pathway level, iron starved CD8+ T-cells feature metabolic blockades at aconitase 2 (ACO2) and succinate dehydrogenase (SDH, complex II (CII)) resulting in depletion of the downstream metabolites α-ketoglutarate (α-KG), fumarate and malate (chapter 5, Fig. 5.3B-C). Simultaneously we observed the accumulation of glutamate which enters the tricarboxylic acid (TCA) cycle via α-KG suggestive of a defect in glutamate dehydrogenase (GDH) (chapter 5, Fig. 5.3B-C). Aspartate abundance was also significantly increased in iron restricted CD8+ T-cells (chapter 5, Fig. 5.3B-C), which is likely partly driven by increased carbon flux from pyruvate to oxaloacetate via pyruvate carboxylase (PC) and by reduced aspartate usage (chapter 5, Fig. 5.4), theorised to be due to mitochondrial aspartate trapping. If alterations in cellular metabolite levels and/or localisation are responsible for driving the low iron phenotype, restoring nutrient levels with exogenous sources or by pharmacological modification of enzymes could provide significant benefit to cellular function. This principle has been demonstrated as nutritional supplementation of deferoxamine (DFO) iron chelator treated colorectal carcinoma (CRC) cell lines with aspartate or nucleosides significantly rescues proliferation[22]. Meanwhile, additional isocitrate can partially recover impaired erythropoiesis during iron restriction including the promotion of hemoglobinisation[25].

Identification of compounds with the capacity to rescue T-cells during iron limitation provides two benefits. Firstly, the capacity of a nutrient to rescue iron deficiency suggests that upstream biochemical pathways are likely impaired by reduced iron availability, thus providing an additional method to identify iron dependent nodes in metabolism. Secondly, the ability to nutritionally or pharmacologically rescue iron starvation suppressed immunity could be useful in translational contexts where individuals are iron deficient, but iron supplementation is ill-advised. For instance, iron supplementation has been demonstrated to increase malaria susceptibility in children living in malaria endemic regions[26] and the risk of infection in hospitalised patients[27].

The aim of this chapter was to screen and characterise nutritional, pharmacological and genetic interventions for their ability to rescue CD8+ T-cells during iron deficiency. Aspartate was identified as a compound which could significantly rescue the proliferative defect of iron limited CD8+ T-cells. Aspartate supplementation also induced increased expression of CD25, perforin, and IFN-γ. Conversely, TNF-α production was reduced by aspartate. RNA-seq data indicated that aspartate suppressed the expression of genes involved in the interferon response regardless of iron availability but that transcriptional changes did not significantly contribute to the observed rescue in low iron conditions. In contrast, aspartate did improve metabolic parameters in the low iron condition including boosted mTORC1 activity, increased ATP production and partial normalisation of the elevated NAD+/NADH ratio. Knockout of the dNTP degrading enzyme, SAMHD1, resulting in predicted endogenous dNTP accumulation similarly rescued iron deprived CD8+ T-cell proliferation. Despite, profound proliferative benefits of aspartate *in vitro*, neither systemic aspartate administration nor CD8+ T-cell aspartate pre-treatment was able to rescue the suppressive effect of *in vivo* hypoferremia mediated via the drug mini-hepcidin (mHep) on immunisation induced antigen specific CD8+ T-cell expansion.

6.1.1 Aims

This chapter aims to:

1. Screen nutritional, pharmacological and genetic interventions for their capacity to alter CD8+ T-cell responses to iron deficiency
2. Characterise the impacts of positive hits identified by our screen during CD8+ T-cell iron scarcity

3. Evaluate positive hits for the capacity to rescue CD8+ T-cell responses to immunisation in the context of *in vivo* hypoferremia

6.2 Results

6.2.1 Screening of nutrients and pharmacological agents for capacity to rescue iron deficient CD8+ T-cell proliferation

We screened various compounds for the ability to counteract the effects of iron scarcity on CD8+ T-cells. Our screen is based on a simple principle: if a biochemical reaction A→B is iron dependent (e.g. it requires an iron-utilising enzyme) and is necessary for downstream processes B→C/D/E, then supplementation of a downstream product of the iron deficiency inhibited reaction (B) should rescue the cellular functions that arise from the downstream processes (Fig. 6.1A). Division was used as the primary readout as proliferative suppression is the most reproducible and dramatic effect of iron restriction on CD8+ T-cells, providing plenty of dynamic range to observe signal shifts upon compound addition. CD8+ T-cells were activated *in vitro* using α-CD3, α-CD28 and IL-2 and cultured for 48 hours in media supplemented with either high (0.625 mg/mL) or low (0.001 mg/mL) holotransferrin with the addition of a variety of molecules (Fig. 6.1B). Compounds were selected in a hypothesis-driven manner and are summarised in figure 6.2C. It should be noted that compound screening was carried out in parallel to the metabolic experiments carried out in chapter 5 and therefore the hypotheses stated for each nutrient here may not be aligned with the metabolic picture that eventually emerged. Further, due to large variations in the proliferative rate between experiments (in the high (0.625 mg/mL) holotransferrin conditions, varying from 40% to >90% divided), data could not be merged between experiments and is instead presented as five independent experiments, each with their own control condition. Where more than one concentration of a compound was used, only the highest concentration which did not significantly impair viability is presented.

Due to the iron dependence of ACO2 and SDH in the TCA cycle and CI-CIV in the ETC, we predicted that these processes may be impaired in low iron conditions. TCA and ETC dysfunction including in DFO iron chelator treated CRC cell lines has previously been demonstrated to drive a reduced NAD+/NADH ratio, resulting in suppressed aspartate production and consequent impairment of downstream asparagine and nucleotide

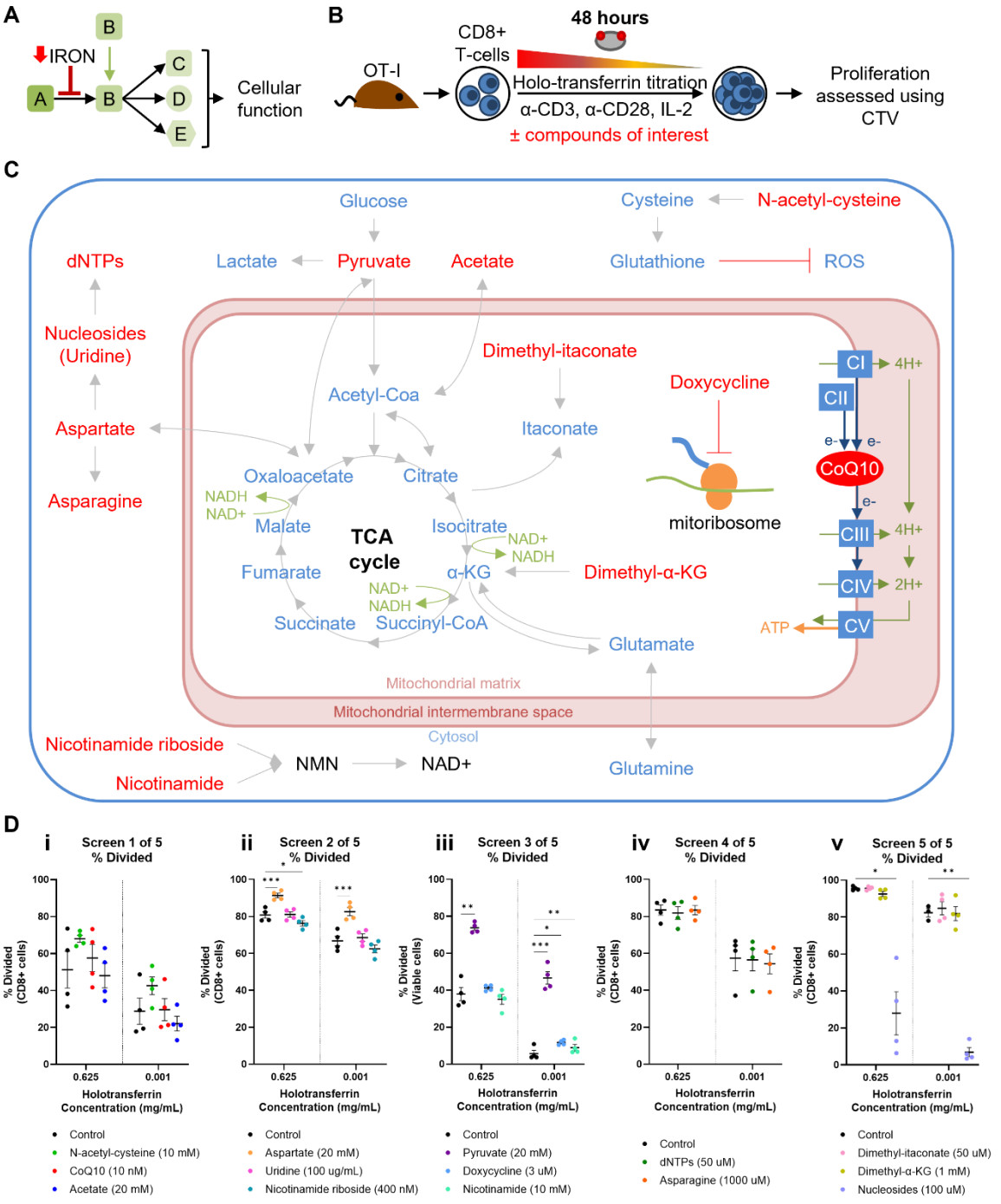

Figure 6.1. Screening for compounds which rescue proliferation in iron deprived CD8+ T-cells. **(A)** If a reaction A→B is iron dependent, supplementation of B should allow generation of the downstream products C/D/E necessary for cellular function. **(B)** Murine CD8+ T-cells were activated using 5 µg/mL plate bound α-CD3, 1 µg/mL α-CD28 and 50 U/mL IL-2 in either high (0.625 mg/mL) or low (0.001 mg/mL) holotransferrin concentrations for 48 hours. Compounds were added at the stated concentrations in each graph. **(C)** Compounds denoted in red were screened for the capacity to rescue iron deficiency impaired proliferation. **(D)** % Divided for screens 1 to 5. Division was measured using cell trace violet (CTV). Data is mean ± SEM. Statistics for **(D)** are sample matched two-way ANOVAs with the Geisser-Greenhouse correction and Sidak's test for multiple comparisons. *p < 0.05, **p < 0.01, ***p < 0.001.

synthesis[22,28-30]. To attempt to restore the hypothesised NAD+/NADH imbalance (low NAD+, high NADH), supplementation with the NAD+ precursors, nicotinamide and nicotinamide riboside, were added to culture. Nicotinamide appeared to provide slight proliferative benefit in low iron conditions (Fig. 6.1Diii) but due to the relatively small fold change was not thought to be as biologically important compared to effects of other nutrients. Meanwhile, nicotinamide riboside did not enhance CD8+ T-cell proliferation (Fig. 6.1Dii). The absence of benefit of NAD+ restoring compounds is likely because iron scarcity surprisingly drives an increased NAD+/NADH ratio (chapter 5, Fig. 5.3D). Pyruvate can similarly increase NAD+/NADH ratios via acting as an electron acceptor in the conversion of NADH to NAD+ in the production of lactate[29]. However, pyruvate can also enter various other metabolic pathways including the TCA cycle, alanine generation and gluconeogenesis[31]. Pyruvate provided significant proliferative advantages to CD8+ T-cells, with a slightly greater fold change in the low iron conditions suggesting increased benefit under iron depletion (Fig. 6.1Diii). This indicates that pyruvate is likely supporting metabolic processes impaired by iron restriction. The general proliferative benefits of pyruvate has previously been demonstrated in cancer cell lines[32] while several studies have shown T-cell dependency on pyruvate for function[33-35].

Aspartate and its downstream products, asparagine, nucleosides (pooled thymidine, adenosine, cytidine and guanosine or uridine alone), and dNTPs (dATP, dCTP, cGTP, dTTP) were also assessed for ability to rescue cellular proliferation. Similar to pyruvate, addition of aspartate significantly enhanced CD8+ T-cell division in both high and low iron concentrations with a greater fold-change benefit in low iron conditions (Fig. 6.1Dii). This suggests that aspartate is rescuing pathways inhibited by iron deficiency. In contrast, aspartate's downstream products, asparagine, nucleosides, uridine alone or dNTPs provided no proliferative advantage (Fig. 6.1ii, iv-v). In fact, nucleosides caused significant cell death (data not shown) and suppressed expansion (Fig. 6.1Dv). This is possibly due to effects mediated by extracellular adenosine which has been demonstrated to interfere with TCR signalling and can suppress proliferation[36]. Nucleoside imbalance has also been reported to suppress proliferation and thus supplementing non-adenosine nucleosides (thymidine, cytidine and guanosine) is hypothesised to be similarly detrimental[37].

Reduced TCA cycling was also predicted to drive suppressed α-KG and potentially decreased itaconate branching off of citrate. Suppression of α-KG was later observed via metabolite-MS in low iron conditions providing further rationale for attempting supplementation. Itaconate was also thought to rewire T-cell metabolism as previously described with potential benefit[38]. Cell permeable dimethyl-α-KG and dimethyl-itaconate were assayed for their capacity to rescue iron deficiency, however, neither compound provided benefit to cellular division at either iron concentration (Fig. 6.1Dv). Acetate was also proposed to alleviate strain on an inhibited TCA cycle by reducing the necessity of using citrate for acetyl-CoA production and acetylation which is critical for T-cell epigenetic programming and IFN-γ production[39,40]. Acetate, however, did not provide any enhancement to cellular proliferation in CD8+ T-cells (Fig. 6.1Di).

Due to the excess of mROS we previously observed (chapter 5, Fig. 5.1A), it was proposed that N-acetyl-cysteine (NAC) may alleviate ROS mediated proliferative suppression. NAC supplementation resulted in a trend towards increased cell division in high and low iron concentrations (Fig. 6.1Di) but this was not significant, and the effect size appeared too small to be biologically meaningful.

Given that iron deficiency is proposed in this thesis to act as a mitochondrial disorder in immune cells, we attempted to rescue iron scarcity impaired proliferation in CD8+ T-cells using therapies demonstrated to have benefit in mitochondrial disease models or patients. Mitochondria were evolutionarily acquired via the engulfment of bacterial endosymbionts[41]. Interestingly, the mitochondrial and bacterial ribosome have retained sufficient homology such that tetracycline antibiotics including doxycycline that inhibit bacterial ribosomes can have off-target suppression of mitochondrial translation[42]. A recent publication found that inhibition of mitochondrial translation using tetracyclines reduced the severity of mitochondrial disease mutations in cell lines and in *in vivo* mouse models[43]. Tetracyclines were hypothesised to reduce the translation of dysfunctional ETC proteins which cause excessive toxicity upon accumulation[43]. Doxycycline appeared to have slight but significant proliferative benefits to iron depleted T-cells, suggesting that a similar buildup of dysfunctional ETC proteins may occur in iron deficient CD8+ T-cells (Fig. 6.1Diii). However, this effect was too small to warrant following up. Meanwhile, supplementation with the mitochondrial electron carrier, coenzyme Q10 (CoQ10), which shuttles electrons between CI/II and CIII has been shown

to have therapeutic benefits to patients with mitochondrial disorders[44]. However, CoQ10 showed no effect on cellular proliferation at high or low iron concentrations (Fig. 6.1Di).

Our screen identified aspartate and pyruvate as candidate molecules capable of providing significant proliferative benefits to iron deprived CD8+ T-cells (Fig. 6.1Dii, iii). We identified aspartate first; thus, our work has focused predominantly on aspartate supplementation. However, the specific effects of pyruvate supplementation will be assessed in the future. Our data suggests that aspartate is essential during iron deprivation. Whether aspartate's downstream products including asparagine[17] and nucleotides[45] are also essential is still not clear (Fig. 6.2A).

6.2.2 Aspartate provides CD8+ T-cells significant resistance to *in vitro* iron limitation

To solidify whether aspartate provides a proliferative advantage to iron deprived CD8+ T-cells, we assessed absolute cell counts over time and proliferation across a larger iron titration. Aspartate concentrations were increased to 40 mM to further amplify the effect size. While CD8+ T-cells in low iron conditions showed almost no population expansion over 72 hours of culture (due to the balancing contributions of division and death), the addition of 40 mM of aspartate was capable of significantly pushing the carrying capacity of the low iron cell culture by approximately 10^4 additional cells (Fig. 6.2B). While a similar absolute benefit (approximately 10^4 cells) was observed at the high iron concentrations, the fold change benefit is much higher at low iron concentrations (x1.9) relative to high iron concentrations (x1.3). Similarly, when assessing division at 48 hours using cell trace violet (CTV), aspartate was able to increase the percentage of divided cells from approximately 20% in the lowest iron condition (0.0002 mg/mL holotransferrin) to around 60% with just the addition of 40 mM of aspartate (Fig. 6.2C). At 72 hours, the difference in the fraction of cells which could undergo three or more divisions in low iron conditions was profoundly increased with aspartate supplementation (Fig. 6.2D). Together indicating that aspartate can partially overcome the cell cycle impairment induced by iron scarcity.

While clonal expansion is critical for effective CD8+ T-cell effector responses, other aspects of CD8+ T-cell biology such as surface molecule expression, cytolytic protein and cytokine production are also important indicators of function. Regardless of aspartate, *Tfrc* mRNA expression was increased in low iron concentrations indicative of cellular iron

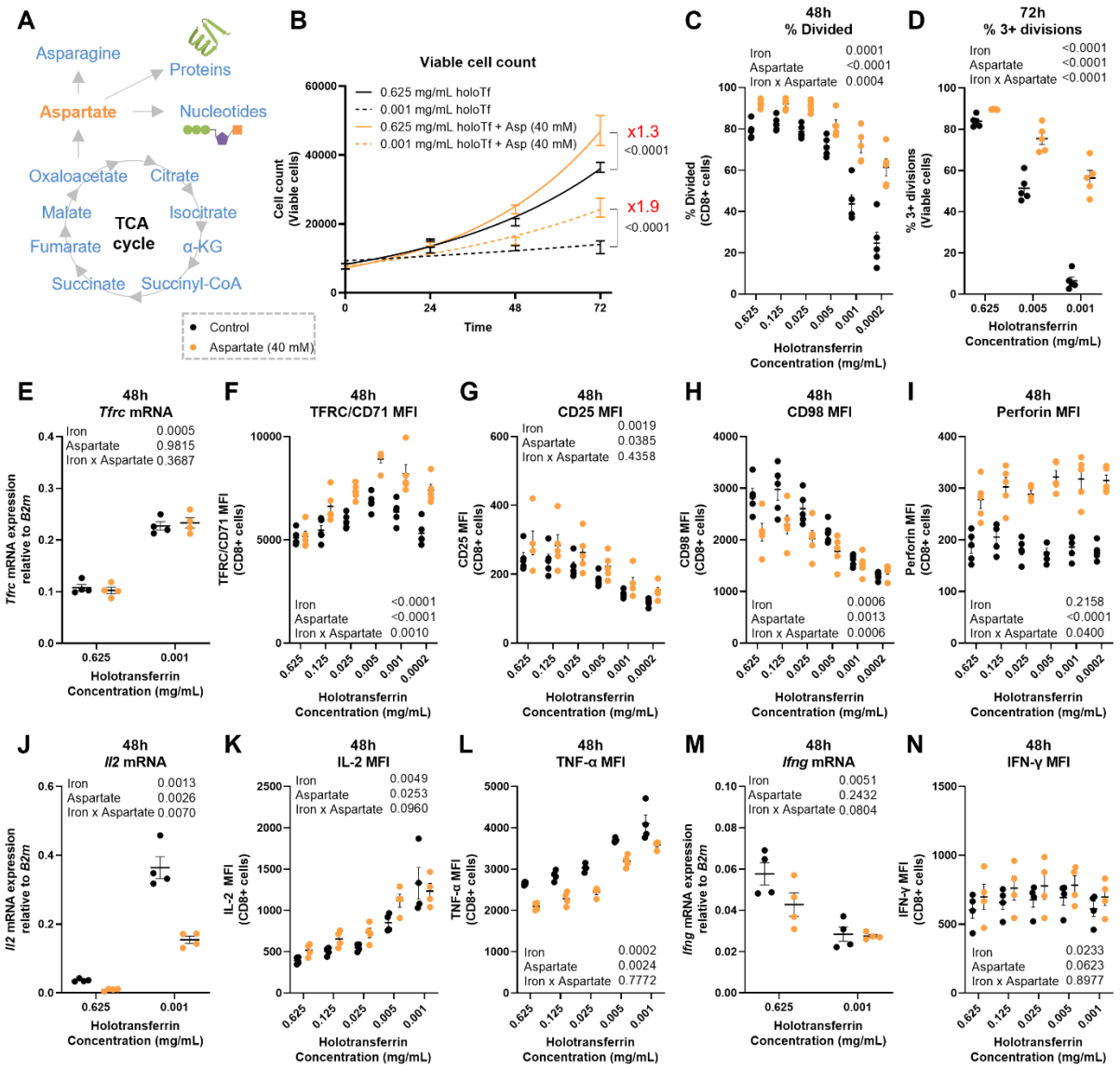

Figure 6.2. Aspartate increases the carrying capacity of iron deprived CD8+ T-cell cultures. T-cells were activated as described in figure 6.1B with or without the addition of 40 mM aspartate in a titration of holotransferrin concentrations. **(A)** Aspartate is produced downstream of the TCA cycle and is necessary for downstream processes including protein translation, nucleotide production and asparagine synthesis. **(B)** Viable cell counts at 0, 24, 48 and 72 hours post-activation. **(C)** Percentage divided cells at 48h and **(D)** percentage of cells undergoing 3+ divisions at 72h assessed using cell trace violet. *Tfrc*/CD71 **(E)** mRNA expression and **(F)** surface protein mean fluorescence intensity (MFI). **(G)** CD25, **(H)** CD98 and **(I)** perforin MFI. *Il2* **(J)** mRNA expression and **(K)** MFI. **(L)** TNF-α MFI. *Ifng* **(M)** mRNA expression and **(N)** MFI. Data is mean ± SEM. Statistics for **(B)** are non-linear regressions using exponential growth equations with an extra sum-of-squares F test applied for either high or low holotransferrin concentrations between aspartate treated and untreated. Statistics for **(C-N)** are two-way ANOVAs with the Geisser-Greenhouse correction.

scarcity (Fig. 6.2E). However, aspartate supplementation helped CD8+ T-cells to maintain high TFRC/CD71 expression in the lowest iron concentrations when expression typically begins to drop in control conditions (Fig. 6.2E). The retention of high TFRC/CD71 expression suggests that aspartate may partially provide benefit via promoting increased iron uptake during iron starvation. Aspartate interestingly has opposing effects on a variety of other readouts of CD8+ T-cell function (Fig. 6.2G-N). The activation marker, CD25, and cytolytic molecule, perforin, increased with aspartate regardless of iron concentration (Fig. 6.2G, I). IFN-γ protein expression was similarly boosted with aspartate, but this effect appears post-transcriptional as *Ifng* mRNA levels were comparable to controls (Fig. 6.2M-N). In contrast, the amino acid transporter CD98 (LAT1, SLC3A2/SLC7A5) was suppressed by aspartate at the highest iron concentrations (Fig. 6.2H) indicating that cells may induce an integrated response to increased cellular amino acids by reducing uptake. CD98 expression was not different at low iron concentrations but CD98 appeared to have reached a lower threshold of possible repression. TNF-α was suppressed while IL-2 showed no expression difference at the protein level but was clearly repressed at the mRNA level (Fig. 6.2J-L). While aspartate has clear proliferative benefits, aspartate's impact on immunological pathways shows both pro and anti-inflammatory effects.

6.2.3 Aspartate does not substantially alter the CD8+ T-cell transcriptome

To understand if aspartate may be providing benefit to iron depleted CD8+ T-cells by inducing a shift in gene expression, we conducted RNA-seq of CD8+ T-cells in iron replete (0.625 mg/mL holotransferrin) and iron deficient (0.001 mg/mL holotransferrin) conditions, with or without 40 mM aspartate. The thresholds of $\log_2|\text{fold change}| > 1.5$ and a false discovery rate (FDR) <0.05 were used (as with the RNA-seq in chapter 4 and in line with previous T-cell RNA-seq studies[46,47]).

Using principal components analysis (PCA), samples segregated largely based on iron concentrations rather than aspartate treatment (Fig. 6.3A) suggesting that aspartate supplementation is not driving broad alterations in transcriptional profile relative to their matched iron concentration controls. Aspartate supplementation induced relatively few transcriptional changes with only 76 differentially expressed genes in high iron conditions and 41 differentially expressed genes in low iron conditions. Notably, the transcriptional changes induced by aspartate in low iron conditions correlate with the

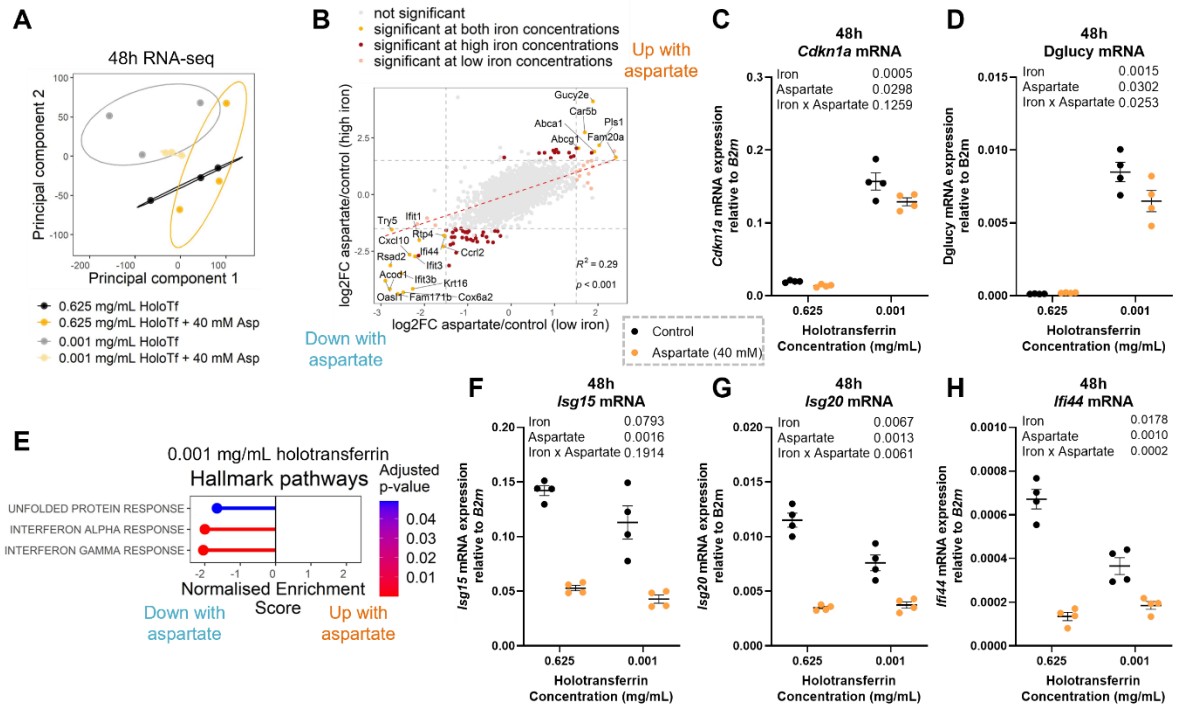

Figure 6.3. Aspartate suppresses interferon responses but does not appear to rescue the iron deficiency transcriptional response. CD8+ T-cells were activated as described in figure 6.1B with either high (0.625 mg/mL) or low (0.001 mg/mL) holotransferrin concentrations and with or without 40 mM aspartate for 48 hours before RNA-sequencing. **(A)** Principal components analysis (PCA). **(B)** Correlation plot comparing the log_2FC between aspartate and control conditions at either low iron or high iron conditions. Significance thresholds of $|log_2FC| > 1.5$ and an FDR < 0.05 were applied. **(C)** *Cdkn1a* and **(D)** *Dglucy* mRNA expression. **(E)** Gene set enrichment analysis of aspartate treated CD8+ T-cells versus control in low iron conditions. **(F)** *Isg15*, **(G)** *Isg20*, and **(H)** *Ifi44* mRNA expression. Data is mean ± SEM. For **(B)** a Pearson correlation R^2 value was calculated. Statistics for **(C-D, F-H)** are two-way ANOVAs with the Geisser-Greenhouse correction.

changes mediated by aspartate in high iron conditions (Fig. 6.3B) indicating that aspartate has similar, albeit small effects regardless of iron availability.

Given that CDKN1A was profoundly upregulated during iron limitation in CD8+ T-cells and aspartate drives increased CD8+ T-cell expansion, we assessed whether aspartate may repress *Cdkn1a* expression. Aspartate supplementation only marginally reduced *Cdkn1a* expression in low iron conditions (Fig. 6.3C) indicating that the proliferative advantage conferred by aspartate is capable of overcoming P53 mediated cell cycle inhibition despite elevated *Cdkn1a*. *Dglucy* was again upregulated in low iron conditions and similar to *Cdkn1a* experienced slight suppression by aspartate (Fig. 6.3D).

We conducted gene set enrichment analysis (GSEA) on samples from low iron conditions in either aspartate or control treated conditions. This revealed that the dominant aspartate effect is suppression of interferon (IFN) response pathways (Fig. 6.3E) and was particularly driven by reduced interferon stimulated gene (ISG) expression including *Isg15*, *Isg20* and *Ifi44*. Iron restriction also suppresses IFN pathway genes but not to the extent as aspartate supplementation (chapter 4, Fig. 4.2, Fig. 4.5J-K). Similar effects were observed for aspartate treatment at high iron concentrations (data not shown). However, this is unsurprising given that aspartate supplementation induced many of the same transcriptional changes regardless of iron concentration. Aspartate mediated ISG suppression has not previously been described for any cell type. Interestingly, IFN-α was historically used to treat chronic myeloid leukaemia (CML) as many antiproliferative and proapoptotic genes including *Cdkn1a* are IFN-α responsive[48]. While aspartate may be hypothesised to induce proliferation by antagonising IFN signalling and downstream cell cycle related ISGs, this may only partially account for the large proliferative benefit of aspartate given the limited effect on *Cdkn1a* expression.

6.2.4 Aspartate promotes enhanced CD8+ T-cell metabolism

While aspartate does not rescue most of the transcriptional profile of iron deprived CD8+ T-cells, given that aspartate is involved in biochemical pathways such as nucleotide[45] and asparagine synthesis[17], we proposed that aspartate may be providing benefit via altering cellular metabolism. Aspartate did not alter mROS generation (Fig. 6.4A), suggesting that aspartate is unable to attenuate the mitochondrial dysfunction likely occurring at CI and CIII in iron deprived CD8+ T-cells. However, aspartate did slightly suppress the iron deficiency mediated increase in the NAD+/NADH ratio (Fig. 6.4B) and increased mTORC1 activity measured via the expression of the downstream target, phospho-S6 (pS6) (Fig. 6.4C). Aspartate treated CD8+ T-cells also displayed increased glycolytic and total ATP production and a trend towards increased mitochondrial ATP production* (Fig. 6.4D-F). Together this suggests that aspartate can metabolically boost CD8+ T-cells, potentially via restoring iron deficiency impaired metabolic functions.

* The seahorse ATP rate assay described here (6.2.4) was conducted in collaboration with Barbara Kronsteiner-Dobramysl at the Centre for Tropical Medicine and Global Health at the University of Oxford

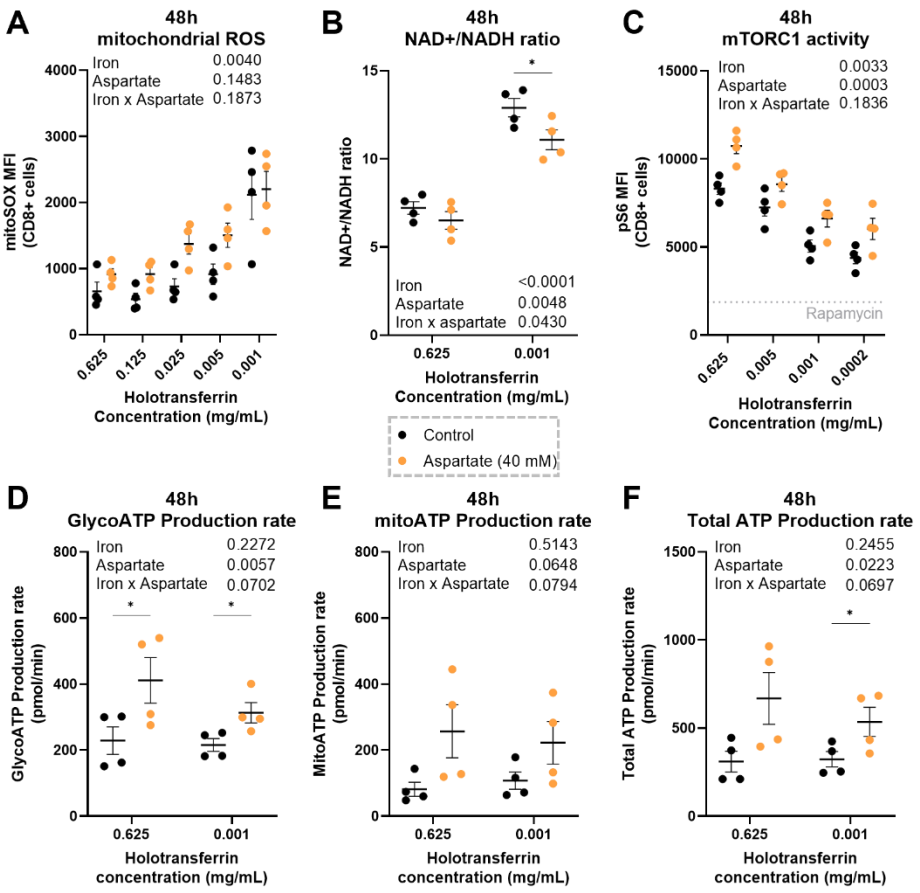

Figure 6.4. Aspartate supplementation boosts CD8+ T-cell metabolism. Activation of CD8+ T-cells was conducted as described in figure 6.1B in a variety of holotransferrin concentrations, with aspartate or control treatment. **(A)** Mitochondrial reactive oxygen species (mROS), **(B)** NAD+/NADH ratio, **(C)** and mTORC1 activity measured via phosphorylation of its downstream target S6. Overnight treatment with the mTORC1 inhibitor, rapamycin at 1 μM, was used as a control. **(D)** Glycolytic, **(E)** mitochondrial and **(F)** total ATP production rate. Data is mean ± SEM. Statistics for **(A-F)** are two-way ANOVAs with the Geisser-Greenhouse correction and Sidak's test for multiple comparisons. *p < 0.05.

6.2.5 Endogenous nucleotide accumulation provides resistance to iron depletion in SAMHD1 knockout CD8+ T-cells*

Aspartate supplementation provides significant proliferative advantages to iron deprived CD8+ T-cells, potentially via augmented metabolism. Aspartate filters into downstream pathways including protein translation, asparagine synthesis[17], nucleotide production[45], the urea cycle[49] and TCA cycle replenishment[50]. Notably, additional exogenous asparagine provided no benefit to iron depleted T-cells (Fig. 6.4D). However,

* SAMHD1 knockout mice were initially acquired from Jan Rehwinkel at the Weatherall Institute of Molecular Medicine at the University of Oxford

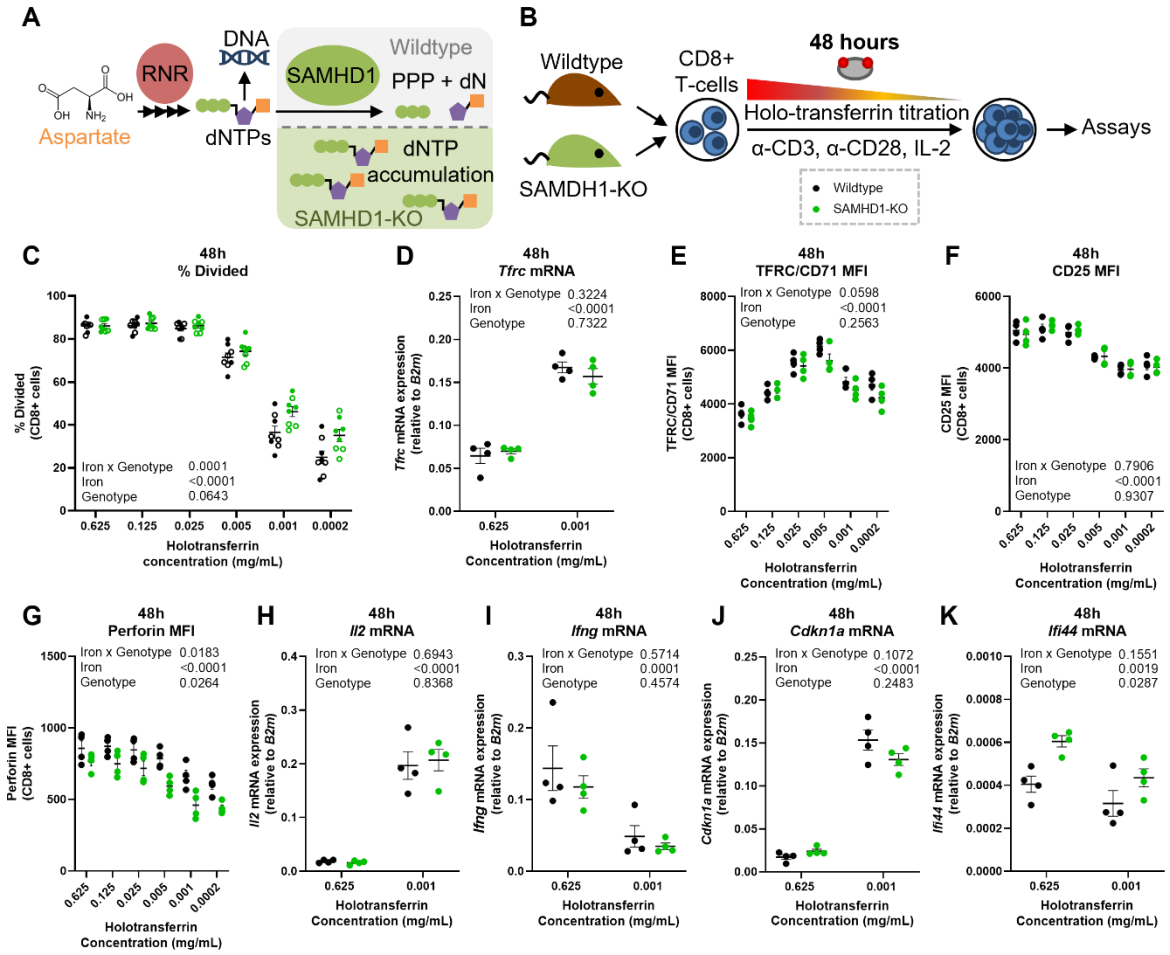

Figure 6.5. SAMHD1-KO T-cells show resistance to iron deficiency suppressed proliferation. **(A)** SAMHD1 and RNR maintain the dNTP balance in the cell. RNR enables dNTP production whereas SAMHD1 degrades dNTPs. SAMHD1-KO should result in dNTP accumulation. **(B)** T-cells isolated from SAMHD1-KO mice and wildtype littermate controls were activated with 5 μg/mL plate bound α-CD3, 1 μg/mL α-CD28 and 50 U/mL IL-2 for 48h in a titration of iron concentrations. **(C)** Cell division was measured using cell trace violet and (CTV). Data has been pooled from 2 experiments. Filled in and empty circles denote separate experiments. *Tfrc* **(D)** mRNA and **(E)** surface protein MFI. **(F)** CD25 and **(G)** perforin MFI. **(H)** *Il2*, **(I)** *Ifng*, **(J)** *Cdkn1a* and **(K)** *Ifi44* mRNA expression. Data is mean ± SEM. Statistics for **(C-K)** are sample matched two-way ANOVAs with the Geisser-Greenhouse correction applied for **(C, E-G)**.

this is perhaps not surprising as extracellular rather than endogenously produced asparagine is typically required at 48 hours post-T-cell activation[17]. Thus, iron deficiency is unlikely to be mediating its anti-proliferative effects via blocking asparagine synthesis which is not active at this time point. Meanwhile, exogenous nucleosides caused cell death (data not shown) and suppression of proliferation (Fig. 6.1D) which is proposed to be due to the suppressive effects of extracellular adenosine[36].

To circumnavigate the toxicity issues of exogenous nucleotides, we turned to a model of endogenous nucleotide accumulation. Cellular nucleotide balance is maintained via the activity of two enzymes, iron dependent ribonucleotide reductase (RNR) and SAMHD1[51] (Fig. 6.5A). While RNR enables production of dNTPs, SAMDH1 degrades dNTPs[51]. Crucially, SAMHD1 knockdown and knockout have been demonstrated to result in dNTP accumulation in lung fibroblasts[52] and bone marrow derived DCs (BMDCs)[53] respectively and is assumed to occur similarly in other cell types. We isolated CD8+ T-cells from SAMHD1 knockout (KO) or wildtype littermates and activated them with 5 μg/mL plate bound α-CD3, 1 μg/mL α-CD28 and 50 U/mL IL-2 for 48h (Fig. 6.5B). The proliferation of SAMHD1-KO CD8+ T-cells was not impaired by iron scarcity to the same extent as in wildtype controls (Fig. 6.5C) showing similarity to aspartate treated CD8+ T-cells. However, while SAMHD1-KO CD8+ T-cells showed appropriate upregulation of *Tfrc* mRNA expression in low iron concentrations (Fig. 6.5D), they showed no capacity to maintain high TFRC/CD71 surface expression at the lowest iron concentrations, unlike cells supplemented with aspartate (Fig. 6.5E). SAMHD1-KO CD8+ T-cells also failed to upregulate CD25, and perforin expression compared to control CD8+ T-cells (Fig. 6.5F-G), as observed with aspartate supplementation. Comparable expression of *Il2*, *Ifng* and *Cdkn1a* was observed in SAMHD1-KO and control CD8+ T-cells (Fig. 6.5H-J). Similar to aspartate supplementation, the increase in observed proliferation in SAMHD1-KO CD8+ T-cells likely occurs despite strong P53 mediated cell cycle suppression via CDKN1A. Interestingly, SAMHD1-KO resulted in augmentation rather than suppression of the canonical ISG, *Ifi44* (Fig. 6.5K). Together this suggests that increasing nucleotide pools may provide benefit to iron depleted CD8+ T-cells by overcoming a potential defect in nucleotide production. However, since aspartate-supplemented and SAMHD1-KO CD8+ T-cells have different immunological phenotypes, it seems likely that aspartate mediates its effects by means beyond simply providing a substrate for nucleotide production.

6.2.6 Systemic aspartate administration fails to rescue hypoferremia induced suppression of antigen specific CD8+ T-cells

Given that *in vitro* aspartate supplementation provided significant benefits to iron deficient CD8+ T-cells, we hypothesised that aspartate would provide similar benefits to iron deprived antigen specific responses *in vivo*. For these experiments we utilised a combined toll like receptor (TLR)/CD40 stimulation immunisation platform[54-57] which

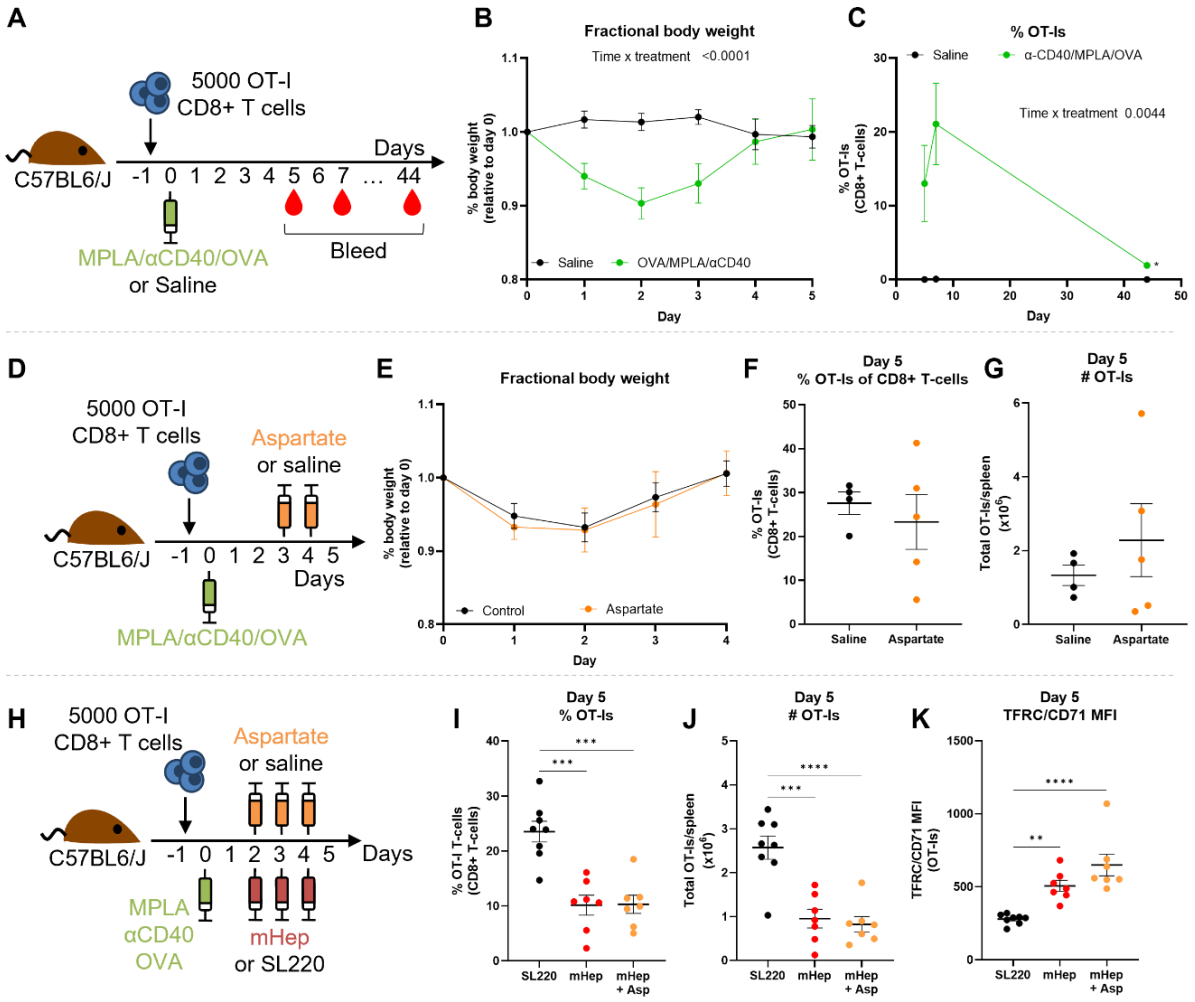

Figure 6.6. Systemic aspartate supplementation is not sufficient to rescue hypoferremia mediated suppression of antigen specific T-cells *in vivo*. **(A)** 5000 OT-I/CD45.1+ T-cells were adoptively transferred intravenously (i.v.) to CD45.2+ C57BL6/J mice a day prior to intraperitoneal (i.v.) immunisation with MPLA (25 µg), α-CD40 (50 µg) and OVA (200 µg) or saline. Mice were bled at days 5, 7 and 44 post-immunisation to evaluate OT-I expansion. **(B)** Fractional body weight post-immunisation. **(C)** OT-I frequency at days 5, 7 and 44. **(D)** ~5000 OT-I/CD45.1+ T-cells were adoptively transferred i.v. to CD45.2+ C57BL6/J mice 1 day prior to i.p. immunisation with MPLA (12.5 µg), α-CD40 (25 µg) and OVA (200 µg) or saline. Aspartate (47 nmoles) was administered i.p. on days 3-4 and mice were culled at day 5. **(E)** Fractional body weight, **(F)** OT-I frequency at day 5 and **(G)** total number of OT-Is per spleen. **(H)** 5000 OT-I/CD45.1+ T-cells were adoptively transferred i.v. to CD45.2+ C57BL6/J mice a day prior to i.p. immunisation with MPLA (12.5 µg), α-CD40 (25 µg) and OVA (200 µg) or saline. MiniHepcidin (mHep; 100 nmoles) or SL220 (control) was i.p. injected on days 2-4 in the morning. Aspartate (250 nmoles) or saline was administered i.p. on days 2-4 approximately 4 hours post-mHep injection. Mice were culled on day 5. **(I)** Percentage of OT-Is of total CD8+ T-cells, **(J)** total number of OT-Is per spleen and **(K)** OT-I CD71 MFI. Data is mean ± SEM. Statistics for **(B-C, E)** are time matched two-way ANOVAs using the Geisser-Greenhouse correction. Statistics for **(F-G)** are unpaired t-tests with Welch's correction. Statistics for **(I-K)** are ordinary one-way ANOVAs and Tukey's correction for multiple comparisons. *p < 0.05, **p < 0.01, ***p < 0.001, ****p < 0.0001.

has not previously been used by our lab. Notably, combined TLR ligand/α-CD40 results in a synergistically stronger adjuvant than either treatment alone[54,57].

We initially piloted the immunisation method to evaluate its utility. 5000 OT-I CD45.1+ CD8+ T-cells which recognise the ovalbumin peptide, SIINFEKL, were adoptively transferred to CD45.2+ C57BL6/J recipient mice (Fig. 6.6A). Recipient mice were subsequently immunised with OVA protein (200 μg/mouse) adjuvanted with the lipopolysaccharide (LPS) derivative, monophosphoryl lipid A (MPLA; TLR agonist; 25 μg/mouse) and α-CD40 (50 μg/mouse). Immunised mice lost approximately 10% body weight two days post-immunisation and regained weight by day 4 (Fig. 6.6B), suggesting that the OVA/MPLA/α-CD40 platform induces significant inflammation. OVA adjuvanted with MPLA/α-CD40 induced expansion of the OT-I CD8+ T-cell pool, comprising 10-20% of CD8+ T-cells at days 5 and 7 post-immunisation and remaining detectable at 44 days post-immunisation (Fig. 6.6C). Together, this illustrates that the OVA/MPLA/α-CD40 platform can robustly induce an antigen specific CD8+ T-cell response in our hands. For all subsequent immunisations we reduced the adjuvant doses to 12.5 μg MPLA/mouse and 25 μg α-CD40/mouse to decrease adjuvant associated adverse effects.

Using this model, we assessed antigen specific CD8+ T-cell sensitivity to systemic aspartate administration (Fig. 6.6D). Mice were treated with 47 nmoles aspartate/mouse at days 3 and 4 post- immunisation. Aspartate did not significantly alter the weight loss trajectory (Fig. 6.6E) or expansion of OT-I antigen specific T-cells (Fig. 6.6F-G) indicating aspartate at the given dose has no strong proliferative effects on CD8+ T-cells *in vivo*.

However, the absence of an aspartate effect on CD8+ T-cells does not preclude the possibility that aspartate only provides benefit to CD8+ T-cells in the context of iron scarcity. To evaluate this, we used the same OVA/MPLA/α-CD40 immunisation protocol and induced hypoferremia on days 2-4 using the hepcidin analogue, mHep (Fig. 6.6H). A matched number of aspartate doses (increased to 250 nmoles/mouse) were administered 4 hours after mHep. As previously described with other immunisation models[4], mHep significantly suppressed the expansion of OT-I CD8+ T-cells relative to mice administered the carrier drug control, SL220 (Fig. 6.6 I-J). mHep induced higher surface expression of the iron uptake receptor, TFRC/CD71, indicating that OT-I CD8+ T-cells are likely experiencing intracellular iron restriction as expected (Fig. 6.6K). However, OT-I CD8+ T-cells from aspartate/mHep treated mice showed similar OT-I

CD8+ T-cell abundance to mice treated with mHep alone indicating that exogenous aspartate failed to rescue mHep-mediated impairment of OT-I CD8+ T-cell expansion.

6.2.7 *In vitro* aspartate pre-treatment of antigenic specific T-cells fails to provide resistance to mHep suppression *in vivo*

Unlike *in vitro*, systemic *in vivo* aspartate administration did not rescue antigen specific OT-I CD8+ T-cell expansion during iron limitation. However, while certain nutrients like glucose or iron are strongly regulated by hormones (insulin[58] and hepcidin[59] respectively), many serum metabolites are regulated via a process known as mass action[58]. Mass action is a process where increased metabolite availability proportionally increases metabolite consumption driving normalisation of serum metabolite concentrations[58]. Mass action has been described for the amino acids valine, methionine, phenylalanine, lysine, alanine and serine, however, it is likely that other amino acids including aspartate are similarly controlled[58]. Aspartate administered systemically may thus be rapidly cleared by organs such as the liver to maintain homeostatic serum concentrations, but simultaneously preventing CD8+ T-cell access to aspartate thus potentially blocking aspartate mediated benefit.

To assess if aspartate supplementation to CD8+ T-cells specifically could provide resistance to iron deficiency, we established a model where OT-I CD8+ T-cell could be pre-treated with compounds *in vitro* prior to adoptive transfer and immunisation. OT-I CD8+ T-cells were isolated from spleen and lymph nodes and activated in R10 media using α-CD3/α-CD28/IL-2 (Fig. 6.7A). One day after immunisation with the OVA/MPLA/α-CD40 platform, $1x10^6$ 48 hour activated OT-I CD8+ T-cells were adoptively transferred to C57BL6/J mice. We observed substantial expansion of OT-I CD8+ T-cells at days 4 and 6 post-immunisation, making up approximately 10% of the CD8+ T-cell population (Fig. 6.7B). Pre-activated OT-I CD8+ T-cells were also still sensitive to mHep induced iron deficiency (Fig. 6.7C) showing elevated TFRC (CD71) surface expression and a trend towards suppression (Fig. 6.7D-E) with mice treated with five doses of mHep showing stronger suppression than those given three doses. Using this model, we pre-treated OT-I CD8+ T-cells with 40 mM aspartate or control media for 48 hours prior to adoptive transfer into immunised mice with or without mHep induced hypoferremia (Fig. 6.7F). While mHep treatment clearly suppressed OT-I CD8+ T-cell expansion in response to immunisation, aspartate pre-treated OT-I CD8+ T-cells show no additional resistance

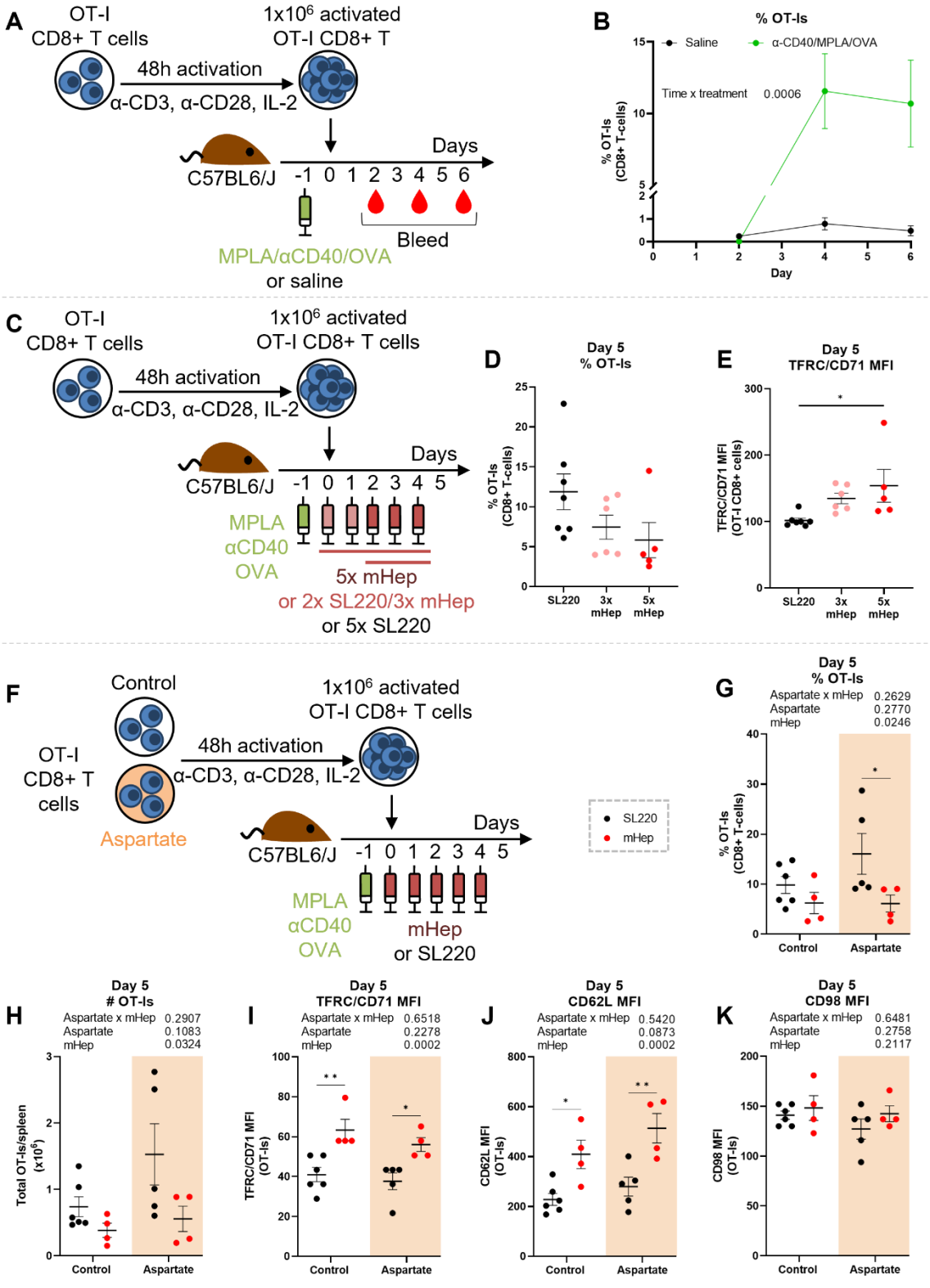

Figure 6.7. Aspartate pre-treatment of antigen specific CD8+ T-cells does not provide resistance to mHep induced hypoferremia during *in vivo* immunisation. **(A)** OT-I/CD45.1+ CD8+ T-cells were activated with 5μg/mL of plate bound α-CD3, 50 U/mL IL-2, 2 μg/mL α-CD28 and 50 μM β-mercaptoethanol in R10 media for 48h. CD45.2+ C57BL6/J mice were immunised with MPLA (12.5 μg), α-CD40 (*continued on next page*)

(*continued from last page*) (25 μg) and OVA (200 μg) or saline 24h prior to intravenous adoptive transfer of $1x10^6$ activated OT-I/CD45.1+ CD8+ T-cells were adoptively transferred intravenously to mice. **(B)** Mice were bled at days 2, 4, and 6 to track the percentage of OVA specific OT-I T-cells of total CD8+ T-cells. **(C)** Mice were treated similarly to **(A)**, but also with either 3 doses of mHep (100 nmoles) on days 2-4 or 5 doses of mHep on days 0-4. On days mHep was not administered, SL220 was given instead. Mice were culled on day 5 and the **(D)** percentage of OT-Is of total CD8+ T-cells and their **(E)** CD71 MFI were evaluated. **(F)** Experimental setup was the same as for **(C)**, however, OT-I/CD45.1+ CD8+ T-cells were cultured for 48h with or without 40 mM of aspartate supplementation. **(G)** Percentage of OT-Is of total CD8+ T-cells and **(H)** total OT-I T-cells. OT-I **(I)** CD71 MFI, **(J)** CD62L MFI and **(K)** CD98 MFI. Data is mean ± SEM. Two-way ANOVAs with the Geisser-Greenhouse correction and Sidak's correction for multiple comparisons were used for **(B, G-K)**. Statistics for **(D-E)** are ordinary one-way ANOVAs with Tukey's correction for multiple comparisons. *p < 0.05, **p < 0.01, ***p < 0.001.

to hypoferremia impaired proliferation (Fig. 6.7G-H). OT-I CD8+ T-cells with or without mHep treatment show similarly high TFRC/CD71 expression relative to SL220 control treated mice (Fig. 6.7I) and retention of the naïve T-cell marker, CD62L (Fig. 6.7J) but no change in the activation marker CD98 (Fig. 6.7K). We suspect that CD8+ T-cells fail to maintain aspartate mediated resistance to iron deficiency *in vivo* due to the rapid intracellular catabolism of aspartate and lack of a continuous exogenous supply.

6.3 Discussion

Screening of various nutrients and pharmacological agents identified aspartate as providing significant proliferative advantages to iron depleted CD8+ T-cells (Fig. 6.1Dii, Fig. 6.2B-D). Aspartate also boosted expression of the activation marker, CD25, and the effector molecule, perforin, while simultaneously repressing TNF-α and ISG expression, suggesting both pro and anti-inflammatory effects (Fig. 6.2, Fig. 6.3E-H). Aspartate did not broadly rescue the transcriptional profile of iron deficient CD8+ T-cells (Fig. 6.3), but instead appeared to mediate benefit by boosting cellular metabolism including via increased ATP production and mTORC1 activation (Fig. 6.4C-F, summarised in table 6.1). Decreasing degradation of endogenous nucleotide pools via SAMHD1-KO similarly benefited CD8+ T-cell proliferation under iron limitation but did not phenocopy other effects of aspartate (Fig. 6.5, summarised in table 6.1). However, despite aspartate providing significant proliferative advantages *in vitro*, systemic aspartate treatment or pre-treatment of CD8+ T-cells with aspartate, failed to rescue immunisation induced antigen specific CD8+ T-cell responses during *in vivo* hypoferremia (Fig. 6.6, Fig. 6.7).

Parameter	Effect of iron deficiency	Effect relative to iron deficiency	
		Aspartate	SAMHD1-KO
Proliferation	↓	↑↑	↑
Tfrc mRNA	↑	-	-
TFRC/CD71 protein	↑	↑↑	-
CD25 MFI	↓	↑	-
CD98 MFI	↓	↓	-
Perforin MFI	-	↑	↓
Il2 mRNA	↑	↓	-
Il2 MFI	↑	-	
TNF-α MFI	↑	↓	
Ifng mRNA	↓	-	-
IFN-γ MFI	-	↑	
Cdkn1a mRNA	↑	↓	-
Dglucy mRNA	↑	↓	
ISG (e.g. *Ifi44*, *Isg15*, *Isg20*) mRNA	↓	↓↓	↑
mROS MFI	↑	-	
NAD+/NADH ratio	↑	↓	
mTORC1 activity	↓	↑	
ATP production	-	↑	

Table 6.1. Summary of effects of aspartate supplementation and SAMHD1-KO. Green up arrows denote increases, red down arrows denote decreases, - denote no effect. Grey shaded boxes are used where data was not collected. Yellow shaded boxes show where "rescue" was observed.

However, these *in vivo* experiments must be interpreted cautiously as we are uncertain whether CD8+ T-cells experienced extended exposure to elevated intracellular aspartate which is likely necessary for aspartate to mediate its beneficial proliferative effects.

The benefits conferred by exogenous aspartate under iron limiting conditions (Fig. 6.2B-D), despite accumulation of endogenous aspartate (chapter 5, 5.3B-C), is consistent with the notion of mitochondrial aspartate trapping introduced in chapter 5. The concept

is that aspartate may accumulate in the mitochondria of iron deprived CD8+ T-cells despite TCA cycle inhibition due to a reduction in aspartate transport to the cytosol for use in downstream processes. This hypothesis relies on the observation that iron restriction impairs the mitochondrial membrane potential in CD8+ T-cells[4] and a proton gradient is essential for mitochondrial aspartate transport via SLC25A12/13[60]. Aspartate supplemented into the media will be taken up directly into the cytosol, theoretically restoring cytosolic aspartate levels for use in pathways such as asparagine synthesis[17], nucleotide production[45] and protein translation. This is consistent with the observed proliferative benefits conferred by extracellular aspartate to CD8+ T-cells during iron scarcity (Fig. 6.2B-D). To verify if cytosolic aspartate levels are indeed increased with aspartate supplementation, measurements of cytosolic metabolites could be completed using cytosolic compartment metabolite-MS[61]. Aspartate has also been shown to provide proliferative rescue in DFO treated CRC cell lines[22]. However, given that DFO treated CRC cell lines show depletion of total aspartate[22] (in contrast to the aspartate accumulation observed in iron starved CD8+ T-cells (chapter 5, Fig. 5.3B-C)), aspartate supplementation in this context is unlikely to be overcoming a defect in mitochondrial aspartate export but rather simply replenishing exhausted pools. Further, the general benefit of exogenous aspartate to proliferation in iron replete CD8+ T-cells is likely due to the presence of a dedicated carbon source for downstream products of aspartate such as nucleotides rather that having to share carbon derived from canonical sources (glutamine/glucose) between many cellular pathways.

Unlike aspartate, asparagine was not capable of providing benefit to iron deficient CD8+ T-cells at the concentrations used (Fig. 6.1Div). It is possible that asparagine levels were not sufficiently high to provide effect. However, at 1 mM, our dose is several fold higher than concentrations shown to hold benefit in other studies[16,17]. Further, CD8+ T-cells should be capable of efficient asparagine uptake as the asparagine transporter, SLC1A5, is upregulated upon activation[3,62] suggesting that this is unlikely to be the case. Instead, given that asparagine synthesis has been demonstrated by us (chapter 5, Fig. 5.3C) and others[17] to be inactive at the 48 hour timepoint, aspartate limitation is unlikely to suppress CD8+ T-cell function via this pathway and exogenous asparagine availability in RPMI media should remain sufficient.

In contrast, the endogenous dNTP accumulation that we presume occurs in SAMHD1-KO CD8+ T-cells provided resistance to iron deficiency (Fig. 6.5C) (in contrast with exogenous nucleosides which resulted in cell death and growth suppression (Fig. 6.1Dv). This suggests that nucleotide levels are likely depressed in iron deficient CD8+ T-cells potentially due to reduced cytosolic aspartate availability, however, this needs to be verified using metabolite-MS. This is also in line with previous data showing DFO treated CRC cell lines have reduced nucleotide levels and that DFO inhibited proliferation is nucleoside rescuable[22]. However, despite observing a rescue effect to proliferation during iron scarcity in SAMHD1-KO CD8+ T-cells relative to wildtype controls, the effect size is still relatively small compared to aspartate treatment. This is proposed to be due to the fact that while SAMHD1-KO prevents dNTP breakdown resulting in dNTP accumulation at homeostasis[52], SAMHD1-KO cannot rescue impaired dNTP production. Thus, when SAMHD1-KO CD8+ T-cells are rapidly proliferating and have high dNTP demands to support DNA synthesis, the increased initial dNTP pool is likely to still become depleted during iron deficiency without a means to replenish it, however, this effect is proposed to be delayed. To assess if this is the case, dNTPs could be measured via metabolite-MS both pre- and post-activation. While dNTP pools should be higher at day 0 in SAMHD1-KO CD8+ T-cells relative to controls, differences in dNTP levels should be smaller after 48 hours of activation in low iron conditions. Additionally, while the resistance of SAMHD1-KO CD8+ T-cells to iron scarcity may be suggestive of aspartate mediated benefit via production of nucleotides, it is possible that aspartate and endogenous dNTP accumulation may be acting via completely separate mechanisms. This is interesting as beyond proliferation, aspartate treatment and SAMHD1-KO result in different downstream effects in terms of activation markers, effector molecules and gene expression indicating that aspartate and endogenous dNTP accumulation do have non-overlapping effects. Most critically, aspartate suppresses ISG responses (Fig. 6.3E-H), while SAMHD1-KO induced the expression of the ISG, *Ifi44* (Fig. 6.5K). While SAMHD1 is utilised in this study due to its metabolic functions, SAMHD1 is better known as an ISG important for protection against viruses such as HIV[63]. In the context of viral infection, SAMHD1 upregulation mediates dNTP breakdown, preventing efficient viral DNA replication[63]. Human loss of function mutations in SAMHD1 are known to be one genetic cause of the encephalopathic autoimmune disease, Aicardi-Goutières syndrome[63]. This is because the loss of SAMHD1 activity results in an increased dNTP pool[53,63]. Consequent

dNTP sensing via the cGAS/STING DNA sensing pathway drives pathogenic levels of type I IFNs and induction of ISGs including *Ifi44*[53,63]. Thus, the increased ISG expression we observed in SAMHD1-KO CD8+ T-cells is in agreement with previous literature.

The observation that aspartate severely represses ISG responses (Fig. 6.3E-H) is in opposition to what is observed in SAMHD1-KO CD8+ T-cells, indicating that aspartate mediated ISG suppression is acting independently of the proposed upregulation of dNTPs with aspartate supplementation. Suppression of ISGs by aspartate has not been described, however, aspartate has been shown to suppress the production of the inflammatory cytokines IFN-γ, IL-17, IL-6 and TNF-α in a mouse model of rheumatoid arthritis[64]. In the context of rheumatoid arthritis, aspartate is proposed to restore suppressed NAD+/NADH ratios in pathogenic T-cells, promoting ER homeostasis and preventing inflammation[64]. However, given that we observe suppression rather than augmentation of the NAD+/NADH ratio with aspartate, this mechanism is unlikely to be occurring in our cells. The mechanism by which aspartate suppresses ISG expression is unclear. However, aspartate could act at one or more of several points within the ISG induction pathway. ISGs are induced upon infection to mediate cellular host defence and between them suppress all steps of viral life cycles[65]. Cytosolic DNA or RNA molecules (canonically derived from viral genomes) are sensed by pathogen recognition receptors (PRRs) such as cGAS, RIG-I and MDA5[65]. These nucleic acid sensing PRRs signal to STING or MAVS which induce transcription factors including IRF7, IRF3 and NF-κB to drive the production of type I IFNs (IFN-α/β)[65]. Type I IFNs can bind to their receptors on the same or adjacent cells, activating a complex comprised of STAT1, STAT2 and IRF9 to drive the downstream transcription of ISGs such as SAMHD1. Theoretically, any one of these steps could be suppressed by aspartate itself or one of aspartate's downstream products. Lactate has recently been shown to suppress IFN-β production vie interfering with RIG-I/MAVs signalling[66]. Lactate generated from aspartate (aspartate → oxaloacetate → pyruvate → lactate) could potentially drive this mechanism, however, whether aspartate can produce high levels of lactate should be evaluated via ^{13}C4-aspartate tracing. Meanwhile, loss of the TCA cycle enzyme fumarate hydratase (FH) and consequent fumarate accumulation results in mitochondrial DNA (mtDNA) and mitochondrial RNA (mtRNA) release to the cytosol where they induce the cGAS/STING and RIG-I/MDA5/MAVS pathways respectively and downstream ISG production[67,68]. Given aspartate supports mitochondrial metabolism, it is possible that aspartate may prevent

mitochondrial stress, such that less mtDNA and mtRNA are released into the cytosol. The localisation of mtRNA and mtDNA could be assessed during aspartate supplementation via fluorescence *in situ* hybridisation (FISH) with probes specific for mtRNA and mtDNA sequences. The location of aspartate mediated suppression of ISGs could also be assessed via employment of cells featuring over-expression or knockouts of key proteins upstream of ISG expression such as cGAS, STING, RIG-I, MAVS and the IFN-α receptor, IFNAR. For instance, if aspartate is capable of suppressing ISGs during over-expression of MAVS, it indicates that aspartate is acting downstream of MAVS. Meanwhile, failure of aspartate to suppress ISGs during MAVS over-expression would suggest aspartate acting upstream of MAVS. Whether aspartate mediates suppression of ISGs in alternative cell types should also be evaluated to assess the generalisability of this observation.

While we have completed extensive characterisation of aspartate supplementation during iron limitation in *in vitro* CD8+ T-cells, we have not yet completed the same characterisation for pyruvate which was observed to similarly provide proliferative advantages to iron depleted CD8+ T-cells. Pyruvate was previously shown to rescue the proliferation of respiration incompetent cell lines lacking mtDNA (denoted as ρ0). However, in the case of ρ0 cell lines, pyruvate was proposed to act via replenishment of depleted NAD+ pools which is not the case in iron deficient CD8+ T-cells which actually show augmented NAD+/NADH ratios (chapter 5, Fig. 5.3D). Instead, pyruvate may provide benefit via entering the TCA cycle via PC and the reductive TCA cycle[69] which was shown to be induced in low iron conditions (chapter 5, Fig. 5.4B-D). If this were the case, pyruvate could potentially aid in replenishment of fumarate and malate while circumnavigating the necessity for the iron dependent enzymes ACO2 and SDH. If this hypothesis is correct, inhibition of PC using the drug ZY-444[70] should abrogate the beneficial effects of pyruvate supplementation in iron restricted CD8+ T-cells. Restoration of malate and fumarate should also be assessed during pyruvate supplementation using metabolite-MS.

6.3.1 Limitations

It should be noted that aspartate must be administered at supraphysiological concentrations (40 mM) *in vitro* in order to show significant benefit to iron deprived CD8+ T-cells. However, how aspartate enters T-cells is poorly understood. Aspartate is known to be transported across the plasma membrane by the aspartate/glutamate

transporters SLC1A1 (described to be neuron specific), and SLC1A2 and SLC1A3 (predominantly expressed by astrocytes[71]). Notably, expression of these three transporters is extremely low or potentially absent on CD8+ T-cells according to transcriptional data from the immunological genome project[72]. Despite the low expression of aspartate transporters, it is evident that aspartate is having biological effects. It is possible that low levels of SLC1A1/2/3 combined with excessively high concentrations of aspartate may permit adequate uptake of aspartate to provide benefit. However, given that as many as one third of solute carrier (SLCs) transporters are still functionally orphaned[73] and some transporters display substrate promiscuity[74], it is possible that transporters other than SLC1A1/2/3 are importing aspartate into CD8+ T-cells. Alternatively, one could propose that aspartate may be acting on cell surface proteins or could be changing the extracellular environment. Crucially, while aspartate is an acidic amino acid, the pH of aspartate supplemented media is pH matched to control media and thus pH changes are unlikely to be responsible for the observed biochemical effects. Similarly, osmotic pressure changes upon excessive aspartate supplementation are unlikely as supplementation of other nutrients at similar molarities (e.g. 20 mM acetate) do not provide proliferative benefits (Fig. 6.1Dii, iv).

While exogenous aspartate provided significant proliferative benefits to *in vitro* iron depleted CD8+ T-cells, we were unable to rescue antigen specific CD8+ T-cells suppressed by hypoferremia *in vivo* using systemic aspartate administration (Fig. 6.6H-K). The availability of nutrients in the plasma (and likely the lymph) is largely regulated by the liver (glucose regulation by pancreatic insulin being a notable exception)[75]. Interestingly, the plasma concentrations of amino acids from individuals with different dietary habits (meat eaters, fish eaters, vegetarians and vegans) vary significantly less than would be expected when looking at dietary amino acid intake[76] indicating that the body maintains relatively stable plasma amino acid concentrations. A recent study suggested that maintenance of steady blood amino acid concentrations is largely due to a mechanism known as mass action where elevated amino acid levels are handled simply by increasing amino acid consumption by organs including the liver[58]. Thus, administering aspartate systemically as a bolus dose likely drives increased aspartate consumption by metabolic organs and high aspartate transporter (SLC1A1/2/3) expressing tissues such as neurons, thus preventing aspartate concentrations reaching the supraphysiological levels required to provide benefit to CD8+ T-cells which poorly

express SLC1A1/2/3[72]. It should be mentioned that intraperitoneal administration of aspartate at substantially lower doses (5 mg/kg relative to our 1676 mg/kg dose) was reported to significantly reduce inflammation in a mouse model of rheumatoid arthritis[64]. Whether low dose aspartate may provide unexpected benefits over high dose aspartate has not been assessed in our model. *In vitro* aspartate pre-treatment of antigen specific CD8+ T-cells also failed to overcome hypoferremia mediated suppression of antigen induced immune responses post-adoptive transfer (Fig. 6.7F-K). This is likely due to an inability of cells to store amino acids (except within synthesised proteins) resulting in rapid depletion of supplemented aspartate once cells are removed from high aspartate conditions. With both bolus aspartate injection and *in vitro* aspartate pre-treatment, elevated aspartate is likely transient and suggests that more continuous aspartate dosing may be required to provide benefit. This could be achieved via providing aspartate into drinking water. However, it should be noted that aspartate has been shown to elicit a similar taste response in rats as monosodium glutamate (MSG)[77]. Given that MSG is known to have a distinctive savoury taste[77], it is possible that aspartate supplementation in water may alter total fluid consumption in animals which could have confounding effects, especially if mice are averse to the taste of aspartate and avoid consuming aspartate supplemented water. Alternatively, continuous aspartate administration could be mediated by osmotic minipumps or by engineered bacteria in the local tissue niche as was recently done with arginine[20]. Over interpretation of the *in vivo* studies performed here should be avoided as we do not know if CD8+ T-cells were experiencing high aspartate during their expansive phase. Serum aspartate and intracellular aspartate in sorted CD8+ T-cells should be evaluated by metabolite-MS in future experiments to evaluate extracellular and intracellular aspartate levels at the time of cull.

6.3.2 Conclusion

Our data suggests that iron depleted CD8+ T-cells become auxotrophic for aspartate, pyruvate, and nucleotides. Aspartate supplementation provided general proliferative benefits and perforin upregulation. Interestingly, aspartate also suppressed TNF-α and ISG expression. Aspartate conferred relatively few transcriptional changes to CD8+ T-cells but induced increased metabolic activity as measured by mTORC1 activity and glycolytic and mitochondrial ATP production rate. Meanwhile, endogenous dNTP augmentation via SAMHD-KO similarly provided a proliferative advantage to iron

depleted CD8+ T-cells but had non-overlapping effects on gene expression suggesting that aspartate must have broader benefit than simply funnelling into nucleotide production. Despite profound *in vitro* benefit, aspartate administration *in vivo* failed to provide benefit to antigen specific CD8+ T-cells under hypoferremic conditions, likely due to inability to maintain plasma aspartate levels at sufficiently high concentrations for effect.

6.4 References

1 Kedia-Mehta, N. & Finlay, D. K. Competition for nutrients and its role in controlling immune responses. *Nat Commun* **10**, 2123 (2019). https://doi.org:10.1038/s41467-019-10015-4

2 Jacobs, S. R. *et al.* Glucose uptake is limiting in T cell activation and requires CD28-mediated Akt-dependent and independent pathways. *J Immunol* **180**, 4476-4486 (2008). https://doi.org:10.4049/jimmunol.180.7.4476

3 Howden, A. J. M. *et al.* Quantitative analysis of T cell proteomes and environmental sensors during T cell differentiation. *Nat Immunol* **20**, 1542-1554 (2019). https://doi.org:10.1038/s41590-019-0495-x

4 Frost, J. N. *et al.* Hepcidin-Mediated Hypoferremia Disrupts Immune Responses to Vaccination and Infection. *Med (N Y)* **2**, 164-179.e112 (2021). https://doi.org:10.1016/j.medj.2020.10.004

5 Wang, Z. *et al.* Iron Drives T Helper Cell Pathogenicity by Promoting RNA-Binding Protein PCBP1-Mediated Proinflammatory Cytokine Production. *Immunity* **49**, 80-92.e87 (2018). https://doi.org:10.1016/j.immuni.2018.05.008

6 Voss, K. *et al.* Elevated transferrin receptor impairs T cell metabolism and function in systemic lupus erythematosus. *Sci Immunol* **8**, eabq0178 (2023). https://doi.org:10.1126/sciimmunol.abq0178

7 Lai, Y. *et al.* Iron controls T helper cell pathogenicity by promoting glucose metabolism in autoimmune myopathy. *Clin Transl Med* **12**, e999 (2022). https://doi.org:10.1002/ctm2.999

8 Li, L. *et al.* Iron deprivation restrains the differentiation and pathogenicity of T helper 17 cell. *J Leukoc Biol* **110**, 1057-1067 (2021). https://doi.org:10.1002/jlb.3ma0821-015r

9 Gao, X. *et al.* Iron-dependent epigenetic modulation promotes pathogenic T cell differentiation in lupus. *J Clin Invest* **132** (2022). https://doi.org:10.1172/jci152345

10 Yarosz, E. L. *et al.* Cutting Edge: Activation-Induced Iron Flux Controls CD4 T Cell Proliferation by Promoting Proper IL-2R Signaling and Mitochondrial Function. *J Immunol* **204**, 1708-1713 (2020). https://doi.org:10.4049/jimmunol.1901399

11 Jabara, H. H. *et al.* A missense mutation in TFRC, encoding transferrin receptor 1, causes combined immunodeficiency. *Nature Genetics* **48**, 74-78 (2016). https://doi.org:10.1038/ng.3465

12 Kemp, J. D. *et al.* Inhibition of lymphocyte activation with anti-transferrin receptor Mabs: a comparison of three reagents and further studies of their range of effects and mechanism of action. *Cell Immunol* **122**, 218-230 (1989). https://doi.org:10.1016/0008-8749(89)90162-7

13 Kemp, J. D. *et al.* Role of the transferrin receptor in lymphocyte growth: a rat IgG monoclonal antibody against the murine transferrin receptor produces highly selective inhibition of T and B cell activation protocols. *J Immunol* **138**, 2422-2426 (1987).

14 Takei, F. Inhibition of mixed lymphocyte response by a rat monoclonal antibody to a novel murine lymphocyte activation antigen (MALA-2). *J Immunol* **134**, 1403-1407 (1985).

15 Bailis, W. *et al.* Distinct modes of mitochondrial metabolism uncouple T cell differentiation and function. *Nature* **571**, 403-407 (2019). https://doi.org:10.1038/s41586-019-1311-3

16 Wu, J. *et al.* Asparagine enhances LCK signalling to potentiate CD8(+) T-cell activation and anti-tumour responses. *Nat Cell Biol* **23**, 75-86 (2021). https://doi.org:10.1038/s41556-020-00615-4

17 Hope, H. C. *et al.* Coordination of asparagine uptake and asparagine synthetase expression modulates CD8+ T cell activation. *JCI Insight* **6** (2021). https://doi.org:10.1172/jci.insight.137761

18 Ron-Harel, N. *et al.* T Cell Activation Depends on Extracellular Alanine. *Cell Rep* **28**, 3011-3021.e3014 (2019). https://doi.org:10.1016/j.celrep.2019.08.034

19 Geiger, R. *et al.* L-Arginine Modulates T Cell Metabolism and Enhances Survival and Anti-tumor Activity. *Cell* **167**, 829-842.e813 (2016). https://doi.org:10.1016/j.cell.2016.09.031

20 Canale, F. P. *et al.* Metabolic modulation of tumours with engineered bacteria for immunotherapy. *Nature* **598**, 662-666 (2021). https://doi.org:10.1038/s41586-021-04003-2

21 Ma, E. H. *et al.* Serine Is an Essential Metabolite for Effector T Cell Expansion. *Cell Metab* **25**, 345-357 (2017). https://doi.org:10.1016/j.cmet.2016.12.011

22 Schwartz, A. J. *et al.* Hepcidin sequesters iron to sustain nucleotide metabolism and mitochondrial function in colorectal cancer epithelial cells. *Nature Metabolism* **3**, 969-982 (2021). https://doi.org:10.1038/s42255-021-00406-7

23 Qualls, J. E. & Murray, P. J. Immunometabolism within the tuberculosis granuloma: amino acids, hypoxia, and cellular respiration. *Semin Immunopathol* **38**, 139-152 (2016). https://doi.org:10.1007/s00281-015-0534-0

24 Zhao, S., Peralta, R. M., Avina-Ochoa, N., Delgoffe, G. M. & Kaech, S. M. Metabolic regulation of T cells in the tumor microenvironment by nutrient availability and diet. *Semin Immunol* **52**, 101485 (2021). https://doi.org:10.1016/j.smim.2021.101485

25 Bullock, G. C. *et al.* Iron control of erythroid development by a novel aconitase-associated regulatory pathway. *Blood* **116**, 97-108 (2010). https://doi.org:10.1182/blood-2009-10-251496

26 Sazawal, S. *et al.* Effects of routine prophylactic supplementation with iron and folic acid on admission to hospital and mortality in preschool children in a high malaria transmission setting: community-based, randomised, placebo-controlled trial. *Lancet* **367**, 133-143 (2006). https://doi.org:10.1016/s0140-6736(06)67962-2

27 Shah, A. A. *et al.* Risk of Infection Associated With Administration of Intravenous Iron: A Systematic Review and Meta-analysis. *JAMA Netw Open* **4**, e2133935 (2021). https://doi.org:10.1001/jamanetworkopen.2021.33935

28 Birsoy, K. *et al.* An Essential Role of the Mitochondrial Electron Transport Chain in Cell Proliferation Is to Enable Aspartate Synthesis. *Cell* **162**, 540-551 (2015). https://doi.org:10.1016/j.cell.2015.07.016

29 Sullivan, L. B. *et al.* Supporting Aspartate Biosynthesis Is an Essential Function of Respiration in Proliferating Cells. *Cell* **162**, 552-563 (2015). https://doi.org:10.1016/j.cell.2015.07.017

30 Ryan, D. G. *et al.* Disruption of the TCA cycle reveals an ATF4-dependent integration of redox and amino acid metabolism. *Elife* **10** (2021). https://doi.org:10.7554/eLife.72593

31 Zangari, J., Petrelli, F., Maillot, B. & Martinou, J. C. The Multifaceted Pyruvate Metabolism: Role of the Mitochondrial Pyruvate Carrier. *Biomolecules* **10** (2020). https://doi.org:10.3390/biom10071068

32 Diers, A. R., Broniowska, K. A., Chang, C. F. & Hogg, N. Pyruvate fuels mitochondrial respiration and proliferation of breast cancer cells: effect of monocarboxylate transporter inhibition. *Biochem J* **444**, 561-571 (2012). https://doi.org:10.1042/bj20120294

33 Elia, I. *et al.* Tumor cells dictate anti-tumor immune responses by altering pyruvate utilization and succinate signaling in CD8(+) T cells. *Cell Metab* **34**, 1137-1150.e1136 (2022). https://doi.org:10.1016/j.cmet.2022.06.008

34 Wenes, M. *et al.* The mitochondrial pyruvate carrier regulates memory T cell differentiation and antitumor function. *Cell Metab* **34**, 731-746.e739 (2022). https://doi.org:10.1016/j.cmet.2022.03.013

35 Mocholi, E. *et al.* Pyruvate metabolism controls chromatin remodeling during CD4(+) T cell activation. *Cell Rep* **42**, 112583 (2023). https://doi.org:10.1016/j.celrep.2023.112583

36 Linnemann, C. *et al.* Adenosine regulates CD8 T-cell priming by inhibition of membrane-proximal T-cell receptor signalling. *Immunology* **128**, e728-737 (2009). https://doi.org:10.1111/j.1365-2567.2009.03075.x

37 Diehl, F. F. *et al.* Nucleotide imbalance decouples cell growth from cell proliferation. *Nat Cell Biol* **24**, 1252-1264 (2022). https://doi.org:10.1038/s41556-022-00965-1

38 Zhao, H. *et al.* Myeloid-derived itaconate suppresses cytotoxic CD8(+) T cells and promotes tumour growth. *Nat Metab* **4**, 1660-1673 (2022). https://doi.org:10.1038/s42255-022-00676-9

39 Peng, M. *et al.* Aerobic glycolysis promotes T helper 1 cell differentiation through an epigenetic mechanism. *Science* **354**, 481-484 (2016). https://doi.org:10.1126/science.aaf6284

40 Qiu, J. *et al.* Acetate Promotes T Cell Effector Function during Glucose Restriction. *Cell Rep* **27**, 2063-2074.e2065 (2019). https://doi.org:10.1016/j.celrep.2019.04.022

41 Chatzispyrou, I. A., Held, N. M., Mouchiroud, L., Auwerx, J. & Houtkooper, R. H. Tetracycline antibiotics impair mitochondrial function and its experimental use confounds research. *Cancer Res* **75**, 4446-4449 (2015). https://doi.org:10.1158/0008-5472.Can-15-1626

42 Moullan, N. *et al.* Tetracyclines Disturb Mitochondrial Function across Eukaryotic Models: A Call for Caution in Biomedical Research. *Cell Rep* **10**, 1681-1691 (2015). https://doi.org:10.1016/j.celrep.2015.02.034

43 Perry, E. A. *et al.* Tetracyclines promote survival and fitness in mitochondrial disease models. *Nat Metab* **3**, 33-42 (2021). https://doi.org:10.1038/s42255-020-00334-y

44 Hargreaves, I. P. Coenzyme Q10 as a therapy for mitochondrial disease. *Int J Biochem Cell Biol* **49**, 105-111 (2014). https://doi.org:10.1016/j.biocel.2014.01.020

45 Villa, E., Ali, E. S., Sahu, U. & Ben-Sahra, I. Cancer Cells Tune the Signaling Pathways to Empower de Novo Synthesis of Nucleotides. *Cancers (Basel)* **11** (2019). https://doi.org:10.3390/cancers11050688

46 Scharping, N. E. *et al.* Mitochondrial stress induced by continuous stimulation under hypoxia rapidly drives T cell exhaustion. *Nat Immunol* **22**, 205-215 (2021). https://doi.org:10.1038/s41590-020-00834-9

47 Wang, X. *et al.* Febrile Temperature Critically Controls the Differentiation and Pathogenicity of T Helper 17 Cells. *Immunity* **52**, 328-341.e325 (2020). https://doi.org:10.1016/j.immuni.2020.01.006

48 Talpaz, M., Mercer, J. & Hehlmann, R. The interferon-alpha revival in CML. *Ann Hematol* **94 Suppl 2**, S195-207 (2015). https://doi.org:10.1007/s00277-015-2326-y

49 Keshet, R., Szlosarek, P., Carracedo, A. & Erez, A. Rewiring urea cycle metabolism in cancer to support anabolism. *Nat Rev Cancer* **18**, 634-645 (2018). https://doi.org:10.1038/s41568-018-0054-z

50 Owen, O. E., Kalhan, S. C. & Hanson, R. W. The key role of anaplerosis and cataplerosis for citric acid cycle function. *J Biol Chem* **277**, 30409-30412 (2002). https://doi.org:10.1074/jbc.R200006200

51 Davenne, T. *et al.* SAMHD1 Limits the Efficacy of Forodesine in Leukemia by Protecting Cells against the Cytotoxicity of dGTP. *Cell Rep* **31**, 107640 (2020). https://doi.org:10.1016/j.celrep.2020.107640

52 Franzolin, E. *et al.* The deoxynucleotide triphosphohydrolase SAMHD1 is a major regulator of DNA precursor pools in mammalian cells. *Proc Natl Acad Sci U S A* **110**, 14272-14277 (2013). https://doi.org:10.1073/pnas.1312033110

53 Rehwinkel, J. *et al.* SAMHD1-dependent retroviral control and escape in mice. *Embo j* **32**, 2454-2462 (2013). https://doi.org:10.1038/emboj.2013.163

54 Ahonen, C. L. *et al.* Combined TLR and CD40 triggering induces potent CD8+ T cell expansion with variable dependence on type I IFN. *J Exp Med* **199**, 775-784 (2004). https://doi.org:10.1084/jem.20031591

55 Klarquist, J. *et al.* Clonal expansion of vaccine-elicited T cells is independent of aerobic glycolysis. *Sci Immunol* **3** (2018). https://doi.org:10.1126/sciimmunol.aas9822

56 Pennock, N. D., Gapin, L. & Kedl, R. M. IL-27 is required for shaping the magnitude, affinity distribution, and memory of T cells responding to subunit immunization. *Proc Natl Acad Sci U S A* **111**, 16472-16477 (2014). https://doi.org:10.1073/pnas.1407393111

57 Sanchez, P. J., McWilliams, J. A., Haluszczak, C., Yagita, H. & Kedl, R. M. Combined TLR/CD40 stimulation mediates potent cellular immunity by regulating dendritic cell expression of CD70 in vivo. *J Immunol* **178**, 1564-1572 (2007). https://doi.org:10.4049/jimmunol.178.3.1564

58 Li, X. *et al.* Circulating metabolite homeostasis achieved through mass action. *Nat Metab* **4**, 141-152 (2022). https://doi.org:10.1038/s42255-021-00517-1

59 Ganz, T. Systemic iron homeostasis. *Physiol Rev* **93**, 1721-1741 (2013). https://doi.org:10.1152/physrev.00008.2013

60 Ruprecht, J. J. & Kunji, E. R. S. The SLC25 Mitochondrial Carrier Family: Structure and Mechanism. *Trends Biochem Sci* **45**, 244-258 (2020). https://doi.org:10.1016/j.tibs.2019.11.001

61 Nonnenmacher, Y., Palorini, R. & Hiller, K. Determining Compartment-Specific Metabolic Fluxes. *Methods Mol Biol* **1862**, 137-149 (2019). https://doi.org:10.1007/978-1-4939-8769-6_10

62 Sharma, D., Yu, Y., Shen, L., Zhang, G. F. & Karner, C. M. SLC1A5 provides glutamine and asparagine necessary for bone development in mice. *Elife* **10** (2021). https://doi.org:10.7554/eLife.71595

63 Antonucci, J. M., St Gelais, C. & Wu, L. The Dynamic Interplay between HIV-1, SAMHD1, and the Innate Antiviral Response. *Front Immunol* **8**, 1541 (2017). https://doi.org:10.3389/fimmu.2017.01541

64 Wu, B. *et al.* Mitochondrial aspartate regulates TNF biogenesis and autoimmune tissue inflammation. *Nat Immunol* **22**, 1551-1562 (2021). https://doi.org:10.1038/s41590-021-01065-2

65 Schneider, W. M., Chevillotte, M. D. & Rice, C. M. Interferon-stimulated genes: a complex web of host defenses. *Annu Rev Immunol* **32**, 513-545 (2014). https://doi.org:10.1146/annurev-immunol-032713-120231

66 Zhang, W. *et al.* Lactate Is a Natural Suppressor of RLR Signaling by Targeting MAVS. *Cell* **178**, 176-189.e115 (2019). https://doi.org:10.1016/j.cell.2019.05.003

67 Hooftman, A. *et al.* Macrophage fumarate hydratase restrains mtRNA-mediated interferon production. *Nature* **615**, 490-498 (2023). https://doi.org:10.1038/s41586-023-05720-6

68 Zecchini, V. *et al.* Fumarate induces vesicular release of mtDNA to drive innate immunity. *Nature* **615**, 499-506 (2023). https://doi.org:10.1038/s41586-023-05770-w

69 Leone, R. D. *et al.* Glutamine blockade induces divergent metabolic programs to overcome tumor immune evasion. *Science* **366**, 1013-1021 (2019). https://doi.org:10.1126/science.aav2588

70 Lin, Q. *et al.* Targeting Pyruvate Carboxylase by a Small Molecule Suppresses Breast Cancer Progression. *Adv Sci (Weinh)* **7**, 1903483 (2020). https://doi.org:10.1002/advs.201903483

71 Parkin, G. M., Udawela, M., Gibbons, A. & Dean, B. Glutamate transporters, EAAT1 and EAAT2, are potentially important in the pathophysiology and treatment of schizophrenia and affective disorders. *World J Psychiatry* **8**, 51-63 (2018). https://doi.org:10.5498/wjp.v8.i2.51

72 Heng, T. S. & Painter, M. W. The Immunological Genome Project: networks of gene expression in immune cells. *Nat Immunol* **9**, 1091-1094 (2008). https://doi.org:10.1038/ni1008-1091

73 Meixner, E. *et al.* A substrate-based ontology for human solute carriers. *Mol Syst Biol* **16**, e9652 (2020). https://doi.org:10.15252/msb.20209652

74 Pizzagalli, M. D., Bensimon, A. & Superti-Furga, G. A guide to plasma membrane solute carrier proteins. *Febs j* **288**, 2784-2835 (2021). https://doi.org:10.1111/febs.15531

75 Paulusma, C. C., Lamers, W. H., Broer, S. & van de Graaf, S. F. J. Amino acid metabolism, transport and signalling in the liver revisited. *Biochem Pharmacol* **201**, 115074 (2022). https://doi.org:10.1016/j.bcp.2022.115074

76 Schmidt, J. A. *et al.* Plasma concentrations and intakes of amino acids in male meat-eaters, fish-eaters, vegetarians and vegans: a cross-sectional analysis in the EPIC-Oxford cohort. *Eur J Clin Nutr* **70**, 306-312 (2016). https://doi.org:10.1038/ejcn.2015.144

77 Stapleton, J. R., Roper, S. D. & Delay, E. R. The taste of monosodium glutamate (MSG), L-aspartic acid, and N-methyl-D-aspartate (NMDA) in rats: are NMDA receptors involved in MSG taste? *Chem Senses* **24**, 449-457 (1999). https://doi.org:10.1093/chemse/24.4.449

Chapter 7

7 Discussion

Iron is an essential nutrient for life (with the rare exceptions of *Borrelia burgdorferi* and *Lactobacilli*)[1-3]. In humans, iron interacts with approximately 400 cellular proteins, many of which operate in pathways common to most cells including mitochondrial metabolism, DNA replication and epigenetic regulation[4]. Given the breadth and conserved nature of pathways involving iron interacting proteins it conceptually follows that iron deprivation would likely have broad implications on cell biochemistry, health and function with potential knock-on effects at the tissue or systemic levels. While anaemia resulting from impaired erythropoiesis is the most commonly recognised consequence of iron deficiency[5], impacts on other body cells are increasingly being acknowledged. For instance, recent publications have clearly demonstrated that iron restriction mediated by iron chelation, miniHepcidin (mHep) or α-TFRC antibodies impairs T-cell responses in pre-clinical models[6-10]. However, while impairment of T-cells by iron restriction must be occurring at the cellular level, the specific mechanisms of iron deprivation beyond broad readouts of cellular metabolism have not been explored in depth. In this thesis, the biochemical landscape of the iron depleted T-cell was extensively explored using *in silico*, *in vitro* and *in vivo* methods using both hypothesis-free and hypothesis-driven approaches.

7.1 Thesis summary and working model

In this thesis, it was found that iron deprivation induced significant perturbations in T-cells at the epigenetic, transcriptomic, proteomic and metabolomic levels with particular disruption observed in the mitochondrial compartment. Here we summarise these findings and place them within the context of a larger working model (Fig. 7.1).

Using an *in silico* approach and existing datasets, T-cells were predicted to increase their iron demands post-activation, with particularly high iron requirements estimated for pathways including DNA synthesis, oxidative phosphorylation (OXPHOS) and histone

demethylation (chapter 3, Fig. 3.2C, F, Fig. 3.4F-G). This predictive and data-derived method was subsequently applied across the proteomes of a diversity of human immune subsets at homeostasis and predicted a particular dependency of neutrophils for iron relative to other cell types. However, unlike T-cells, neutrophils were predicted to use iron for neutrophil degranulation proteins (chapter 3, Fig. 3.6). The iron dependency of neutropoiesis was experimentally confirmed by Frost *et al*[11] and Bonadonna *et al*[12]. Further, mathematical modelling suggested that physiologically possible levels of serum iron deprivation (transferrin saturation (TSAT) < 10-20%) would be sufficient to prevent adequate iron uptake for T-cells to meet their early iron requirements (chapter 3, Fig. 3.5). Strikingly, *in vitro* assessment of iron deprived CD8+ T-cells identified multiple nodes of dysfunction relating to each of these predicted iron demanding pathways (DNA synthesis (chapter 4, Fig. 4.3), OXPHOS (chapter 4, Fig. 4.4 and chapter 5, Fig. 5.1-4), demethylation (chapter 4, Fig. 5.6-7)).

Iron scarcity induced genes involved in the P53 cell cycle arrest pathway including the G1-S phase inhibitor protein, *Cdkn1a*, at both the transcriptional and proteomic levels in CD8+ T-cells (chapter 4, Fig. 4.3). Induction of the P53 pathway is likely responsible for the proliferative suppression observed in iron deficient cells (chapter 4, Fig. 4.3), however, the mechanism through which iron scarcity induces P53 remains to be defined (discussed in chapter 4). Iron restriction also suppressed genes and proteins involved in mTORC1 and MYC signalling pathways suggestive of metabolic dysfunction (chapter 4, Fig. 4.4) and is concurrent with previous studies demonstrating mTORC1 suppression with iron limitation[6,7,13]. Interestingly, iron deficient cells also accumulated mitochondrial proteins involved in the electron transport chain (ETC) and β-oxidation (chapter 4, Fig. 4.4F), many of which are involved in iron binding respiratory complexes. We propose that the increase in iron interacting proteins combined with an assumed depletion of iron cofactors may drive inefficient electron transfer resulting in the induction of mitochondrial reactive oxygen species (mROS) (chapter 5, Fig. 5.1A). Elevated mROS are hypothesised to drive the observed induction of IL-2 and TNF-α via activation of NFAT in iron limited CD8+ T-cells (chapter 4, Fig. 5.1D-G). The mechanism of mROS inducing IL-2 via NFAT activation was previously demonstrated by Sena *et al*[14] but must be confirmed under the context of iron deficiency using mitoTEMPO to suppress mROS.

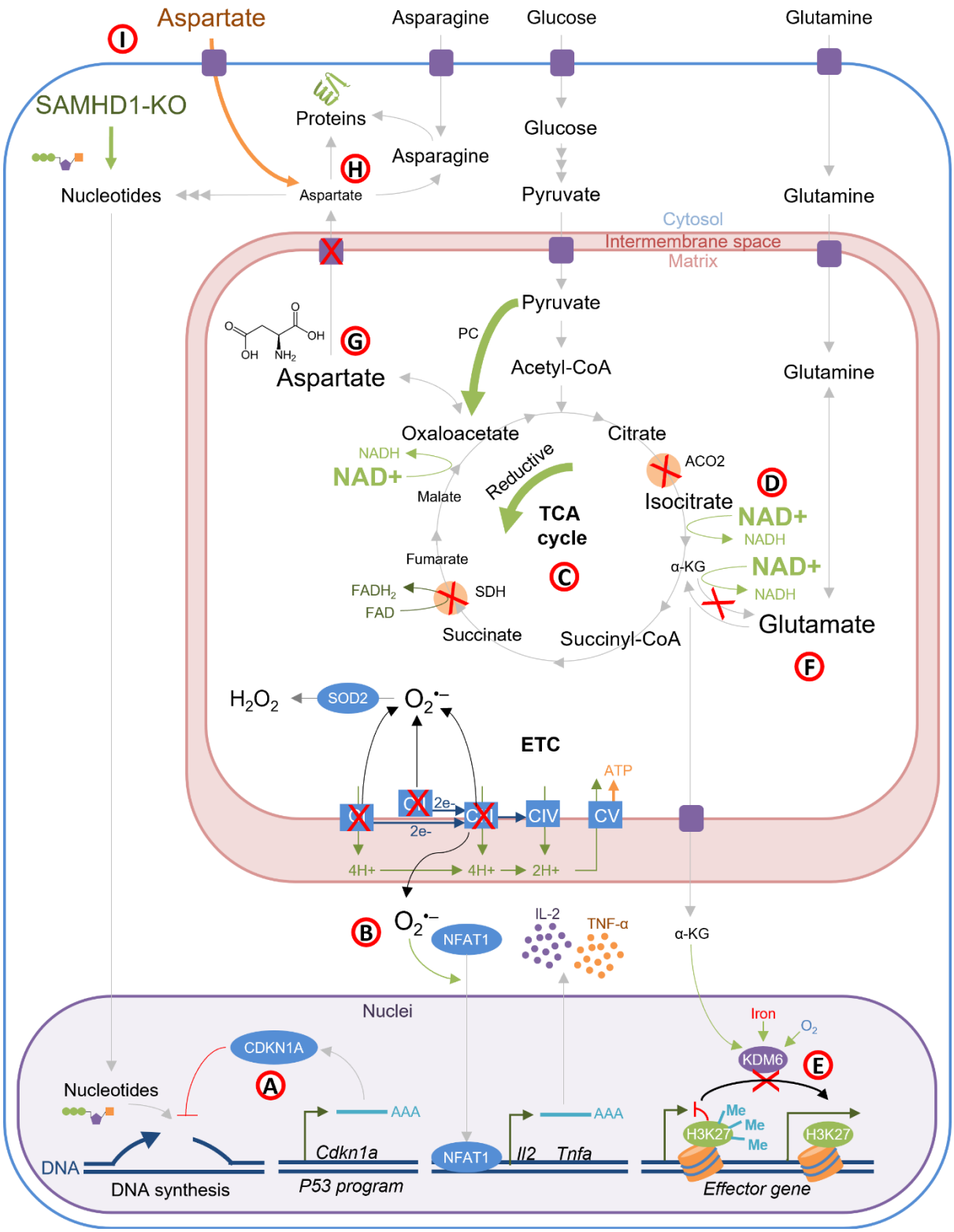

Figure 7.1. Working model for the biochemical impacts of iron deficiency in CD8+ T-cells. **(A)** Iron restriction upregulated the P53 pathway including expression of *Cdkn1a* which suppresses the G1-S phase transition[15]. **(B)** Iron scarcity drives mROS production likely due to dysfunction of iron dependent CI and CIII (although CII may also contribute). mROS produced into the matrix is detoxified by SOD2 while mROS released into the intermembrane space by CIII may play a signalling role in (*Continued on next page*)

(*Continued from last page*) NFAT1 activation and downstream production of IL-2 and TNF-α as previously described[14]. **(C)** Iron scarcity impairs carbon flux via the iron dependent enzymes, ACO2 and SDH, suggesting dysfunction of these enzymes. This results in depletion of α-KG, fumarate and malate. **(D)** Increased NAD+/NADH ratios are in line with reduced TCA cycling. **(E)** Reduction of α-KG in combination with iron deficiency is proposed to impair α-KG dependent, iron dependent histone demethylases including KDM6A/B which removes the repressive mark, H3K27me3 which is normally removed from effector gene loci during T-cell activation. **(F)** Increased glutamate derived from glutamine suggests that another unexpected blockade to metabolism exists at glutamate dehydrogenase (GDH). **(G)** Aspartate accumulates in iron deprived T-cells. This is proposed to be due to increased carbon entry via pyruvate carboxylase (PC) and the reductive TCA cycle (green arrows) as well as reduced usage. **(H)** Reduced aspartate usage during iron deficiency is proposed to be due to impaired transport via the proton dependent transporter SLC25A12/13 given iron restriction impairs the proton gradient[6]. Aspartate is used for processes such as nucleotide production[16] important for DNA synthesis, asparagine synthesis[17] and protein translation. **(I)** Aspartate supplementation and SAMHD1-KO which increases endogenous dNTP pools[18,19] provide resistance to iron deficiency presumably by replenishing these essential pathways.

Iron deficiency also suppressed the flux of carbon through the iron dependent steps of the tricarboxylic acid (TCA) cycle, mediated by aconitase 2 (ACO2) and succinate dehydrogenase (SDH, complex II (CII)), resulting in depletion of the downstream products, α-KG, fumarate and malate (chapter 5, Fig. 5.3B-C). The observed increase in the NAD+/NADH ratio is also in line with reduced TCA cycle progression (chapter 5, Fig. 5D). α-KG depletion combined with iron deprivation is proposed to be responsible for the observed impairment of H3K27me3 demethylation which is normally mediated by iron dependent and α-KG dependent KDM6A/B enzymes (chapter 5, Fig. 5.5B, Fig. 5.6, Fig. 5.7D-E). H3K27me3 demethylation is important for CD8+ T-cell and Th17 transcriptional reprogramming during activation[20,21], and thus defects in demethylation under iron restriction could account for the suppression of T-cell function. Further, changes in methylation state may also explain the observed differential expression of genes and proteins involved in pathways including the interferon response, MYC and mTORC1 signalling and the P53 pathway during iron scarcity (chapter 4, Fig. 4.2). Examination of the specific loci experiencing erroneous H3K27me3 maintenance during iron starvation will be assessed in the future via chromatin immunoprecipitation (ChIP)-seq. Further, if KDM6A/B is inhibited at the degree of iron deprivation utilised, it is likely that other iron dependent enzymes (KDMs and TETs) may be similarly impaired. Therefore, methylation of DNA and of other histone residues should also be assessed *via* either flow cytometric or ChIP-seq methods. It would be particularly interesting to

examine these changes in CD4+ T-cells where cells not only differentiate towards an effector state but must also differentiate down a cell lineage (Th1, Th2, Th17, Treg). This is especially relevant as iron-deficient Th17 polarised CD4+ T-cells showed defects in proliferation and differentiation characterised by reduced expression of RORγt and IL-17A (chapter 5, Fig. 5.7).

In contrast to α-KG depletion, iron deficient CD8+ T-cells accumulated aspartate despite suppression of flux through the TCA cycle that produces it (chapter 5, Fig. 5.3B-C). Aspartate accumulation is proposed to occur due to both increased carbon entry to the TCA cycle via pyruvate carboxylase (PC) and the reductive TCA cycle as well as reduced aspartate usage (chapter 5, Fig. 5.4). Notably, mitochondrially produced aspartate requires transport to the cytosol for use in pathways including nucleotide synthesis[16], asparagine synthesis[17] and protein translation. However, the mitochondrial aspartate transporter, SLC25A12/13 requires a proton gradient[22] and iron limited CD8+ T-cells were previously shown to have a disrupted mitochondrial membrane potential implying a reduced proton gradient[6]. Thus, we propose a scenario where iron deficiency inhibits mitochondrial aspartate export by inhibition of SLC25A12/13 resulting in cytosolic aspartate depletion and suppression of downstream aspartate-utilising pathways including nucleotide production necessary for DNA synthesis. Notably, exogenous aspartate supplementation as well as endogenous enrichment of the dNTP pool using SAMHD1-KO, partially rescued iron deficiency mediated suppression of proliferation (chapter 6, Fig. 6.2B-D, Fig. 6.5C). Together this suggests that cytosolic

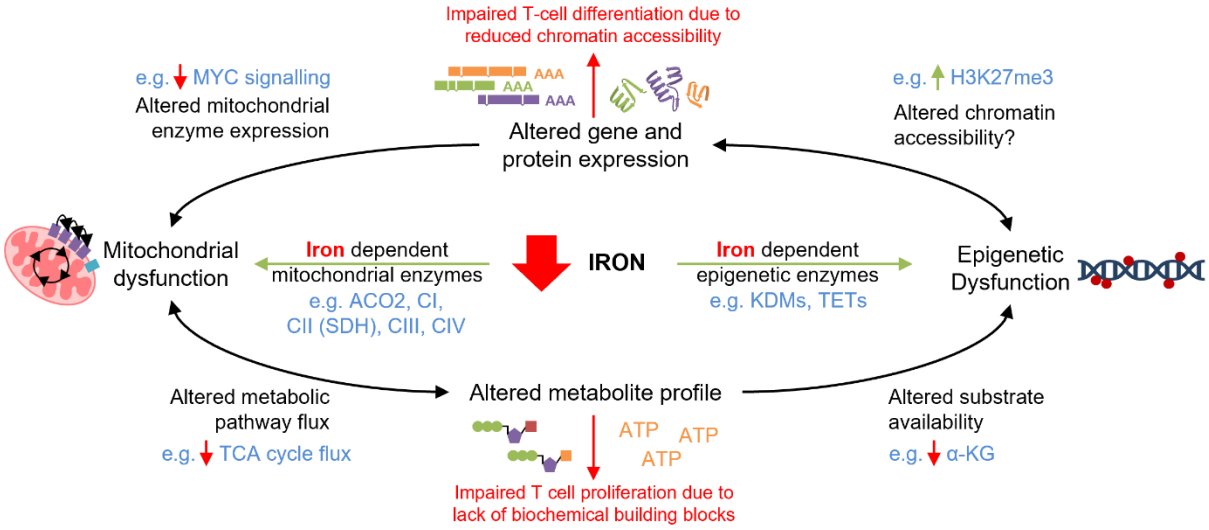

Figure 7.2. Interaction model during iron deficiency between metabolic and epigenetic function.

aspartate and dNTPs likely become limiting under iron depleted conditions. Verification of nucleotide depletion and cytosolic aspartate depletion under iron scarcity will be conducted via standard and cytosolic metabolite-MS respectively. Inadequate aspartate and dNTP pools could in turn impair T-cell proliferation by preventing efficient translation and DNA synthesis.

Using the data collected in this thesis, we propose a model (Fig. 7.2) wherein iron scarcity inhibits iron dependent enzymes involved in both mitochondrial function (e.g. ACO2, SDH, ETC) and epigenetic remodelling (e.g. histone demethylases, KDM6A/B). However, due to the intrinsic interactions between metabolism and epigenetics[23], the impacts of iron starvation on the mitochondria and chromatin remodelling are likely interdependent. Mitochondrial dysfunction will result in altered metabolic pathway flux (e.g. impaired TCA cycle progression) and alterations in the cellular metabolite profile. The modified metabolite profile is proposed to subsequently impair T-cell proliferation due to a lack of biochemical substrates (e.g. aspartate and dNTPs) to support the biosynthesis of molecules such as proteins and DNA necessary for growth and DNA replication prior to division. However, altered substrates for chromatin remodelling (e.g. reduced α-KG) may also result in epigenetic dysfunction (e.g. reduced H3K27me3 demethylation), in turn effecting chromatin accessibility and gene expression. Changes in gene expression will impact T-cell differentiation but may also consequently drive metabolic rewiring via altering transcriptional programs coordinated by transcription factors such as MYC. In sum, iron deficiency targets various enzymes in diverse pathways, crippling T-cell function from multiple angles using both direct and indirect mechanisms.

7.2 Future directions

7.2.1 *In vitro* to *in vivo*

While we believe that our low iron media provides a more physiological model of serum iron deficiency relative to iron chelators and α-CD71 antibodies, our *in vitro* system still fails to recapitulate the *in vivo* metabolic environment. Crucially, studies have shown that *in vitro* and *in vivo* activated T-cells have different pathway contributions to their metabolic state[24]. While use of physiological media which aims to resemble the nutritional environment of human[25] or mouse[26] plasma are increasingly being used to address this issue (and do induce different metabolic signatures in T-cells relative to

standard culture media), *in vivo* validation of metabolic signatures discovered *in vitro* should ideally be completed.

In vivo metabolic analysis has largely been precluded by us and others due to the necessity of substantial starting material for metabolic methods such as metabolite-MS which requires millions of cells typically expanded *in vitro*. Even the current gold standard method for metabolic analysis of immune cells, Seahorse extracellular flux analysis, requires approximately 10^6 purified cells[27]. This makes Seahorse analysis unsuitable for *ex vivo* assessment of low frequency cell types including antigen specific CD8+ T-cells induced *in vivo*. Further, despite Seahorse analysis becoming increasingly popular for studying immunometabolism, it is essentially an optimised version of the classic manometer used by Otto Warburg and Hans Krebs in the discoveries of the Warburg effect[28] and TCA cycle respectively[29]. Seahorse machines and manometers both allow for measurements of the oxygen consumption rate (OCR, proxy of OXPHOS) and the extracellular acidification rate (ECAR, proxy of glycolysis)[28] of biological samples. While Seahorse machines measure oxygen and pH using fluorescent probes[30], manometers detect changes in gas pressure as oxygen and CO_2 are consumed and produced[28]. Seahorse machines while more precise and sensitive than manometers, provide little more information. While the work completed by Warburg and Krebs in the 1920s-1950s using manometers was astounding for the time, newer protocols beyond Seahorse analysis are required to effectively study the metabolism of immune populations.

Novel protocols are now enabling more detailed analyses of *in vivo* immunometabolism beyond OCR and ECAR. Methods for metabolic analysis based off of flow cytometry and mass cytometry (also known as cytometry by time of flight (CYTOF)) are democratising the immunometabolism field. Crucially, both flow cytometry and CYTOF enable analysis of samples at a single cell resolution thus permitting evaluation of metabolism in heterogeneous samples and in rare cell types which is often the case for many immune cell populations. Flow cytometers are also relatively accessible machines for most immunology labs. Protocols for detection of metabolic enzymes involved in pathways including glycolysis, OXPHOS and β-oxidation, via flow cytometry[31,32] and CYTOF[33,34] have recently been published. One could also imagine applying the concept of antibody targeting of enzymes to CITE-seq which is a method for coupling antibody protein detection with single cell RNA-seq[35]. While measuring enzyme abundance is

proposed to give insight as to the metabolic state of the analysed cells[31-34] it should be noted that changes in amounts of metabolic enzymes are not necessarily indicative of changes in enzymatic activity. For example, we observed a striking increase in proteins involved in the ETC (chapter 4, Fig. 4.4F) despite likely dysfunction of the ETC given high mROS production (chapter 5, Fig. 5.1A). Despite this caveat, antibody-based detection of metabolic enzymes via flow cytometry, CYTOF or sc-RNA-seq presents a viable method for assessing the metabolic state of immune cells *ex vivo* from hypoferremic animals or from iron deficient patients. Comparisons could be made to the proteomic survey we produced in iron depleted CD8+ T-cells, for instance assessing whether accumulation of mitochondrial proteins (chapter 4, Fig. 4.4F) or depletion of ASNS and PPAT (chapter 5, Fig. 5.4F-H) occur in *in vivo* iron deficiency.

Meanwhile, the number of fluorescent probes for mROS, mitochondrial mass, mitophagy, mitochondrial membrane potential and many other metabolism associated processes is rapidly expanding[36]. Further, a method called SCENITH (single cell energetic metabolism by profiling translation inhibition) has recently emerged, promising a flow cytometry-based approach for measuring the contributions of glycolysis and OXPHOS to cellular metabolism[27]. SCENITH is based on the concept that translation consumes 50% of cellular ATP and assumes that the translation rate scales with ATP production[27]. Thus, the shift in the translation rate upon suppression with inhibitors of key metabolic pathways such as 2-DG (glycolysis inhibitor) and oligomycin (OXPHOS inhibitor), indicates the dependence of the cell on the inhibited pathway for ATP production[27]. Translation rate is measured by incorporation of the drug puromycin into nascent peptides and puromycin in turn is detected using a fluorescently labelled puromycin specific antibody[27]. SCENITH was demonstrated to produce results consistent with parallel Seahorse analysis and was used to characterise the metabolic signatures of a variety of cell types in murine and human samples[27]. However, while SCENITH claims to be a "single cell" method due to measurements of translation on single cells, in order to calculate the dependencies on glycolysis or OXPHOS, the translation rate must be compared between samples treated in the presence and absence of multiple inhibitors. Thus while the necessary cell counts required per condition (approximately 2000) is greatly reduced compared Seahorse, the claim of "single cell" metabolic measurements is inaccurate. Further, we and colleagues (personal correspondence) have observed that administration of the 2-DG and oligomycin inhibitors can drive rather than suppress

translation in certain cell types, potentially due to compensatory increases in the uninhibited pathways. Therefore, while SCENITH presents another accessible means to assess metabolism in *ex vivo* immune cells, results need to be analysed with caution given the potential for unexpected effects on translation with metabolic suppression.

Despite the advances in cytometry based metabolic approaches detailed here, these approaches still fail to directly measure metabolites or metabolic flux. However, as discussed in chapter 5, low cell number metabolite-MS is now emerging allowing measurements from as few as 10,000 cells[37]. Combined with *in vivo* ^{13}C-labelling via infusion of ^{13}C-glucose or ^{13}C-glutamine[24], low cell number metabolite-MS presents a technically challenging but feasible approach for measuring metabolites and pathway flux as completed here in chapter 5 but on less abundant immune populations.

Together, these methods present a means through which to validate the findings of this thesis in *in vivo* mouse models and in human samples. CD8+ T-cells could be activated *in vivo* (for instance using our α-CD40/MPLA/OVA immunisation platform) in hypoferremic mice induced using mHep. Sc-RNA-seq (or bulk analysis of sorted antigen specific CD8+ T-cells) and metabolic enzyme flow cytometry or CYTOF could be used to assess the transcriptomic and proteomic profiles. Meanwhile low cell number metabolite-MS post-^{13}C-glutamine infusion could be used to assess metabolic flux and metabolite profile of sorted antigen specific CD8+ T-cells. Antigen specific CD8+ T-cells sorted from recently vaccinated iron deficient and control patients could be also analysed via a similar approach using a combination of sc-RNA-seq, metabolic enzyme flow cytometry/CYTOF and low cell number metabolite-MS with the caveat that ^{13}C-labelling would have to be conducted via short-term *in vitro* culture.

7.2.2 Generalisability to other cell types

In this project we have extensively characterised the biochemical phenotype of iron deprived CD8+ T-cells at the transcriptional, proteomic and metabolomic levels. Similar work has to some extent been completed in deferiprone (DFP) iron chelator treated macrophages[38] and deferoxamine (DFO) iron chelator treated colorectal cancer (CRC) cell lines[39]. However, as discussed in chapter 4, iron chelators can cause unphysiological cellular responses. For instance, ciclopirox olamine (CPX) iron chelator treatment of Th1 polarised CD4+ T-cells[8] caused dramatic shifts (> 3000 differentially expressed genes) in

transcriptional profile after only four hours of treatment (chapter 4, Fig. 4.7). This high degree of change is unlikely to occur in more physiological settings such as dietary iron deficiency, hypoferremia or even tissue iron depletion in the tumour microenvironment given that even in extremely low iron media (0.001 mg/mL holotransferrin), we observe only 193 differentially expressed genes (chapter 4). Thus, we propose that the work presented here represents the most comprehensive biochemical survey of the impacts of non-chelator iron deficiency on any cell type to date.

Crucially, many of the iron dependent processes demonstrated to be impaired in CD8+ T-cells during iron scarcity including mitochondrial metabolism (TCA cycle and the ETC) and histone demethylation are broadly utilised across cell types. While preferential usage of metabolic processes differs between cell types and states (e.g. increased relative use of OXPHOS versus glycolysis in memory T-cells versus effector T-cells)[40] it is likely that some of the observed iron deprivation mediated impairments observed in CD8+ T-cells also occur in other cell types during iron depletion. While all mammalian cells likely require iron for some aspect of function, cells which undergo rapid proliferation would be predicted to be more impacted by iron deficiency than quiescent populations. This is because in iron scarce environments, dividing cells will dilute out iron stores between daughter cells without exogenous iron pools to replenish the difference. Meanwhile, quiescent cells can furnish iron interacting proteins via internal recycling of iron cofactors. This principle is demonstrated by T-cells bearing the $TFRC^{Y20H}$ mutation which reduces iron uptake efficiency[41]. Quiescent naïve $TFRC^{Y20H}$ T-cells are not noticeably impacted by the mutation but become extremely sensitive upon activation[41].

B-cells are an obvious contender for similarities in their biochemical iron deficiency phenotype to T-cells, especially given that B-cell expansion is similarly suppressed by iron scarcity[6,42,43]. B-cells emerge from the same progenitor (the common lymphoid progenitor, CLP) as T-cells[44] and like T-cells, B-cells remain quiescent until they are activated by their cognate antigen at which point they rapidly proliferate and induce transcriptional programs necessary for effector function[45]. Activated B-cells increase glycolysis and OXPHOS to meet their energy and biosynthetic requirements and germinal centre B-cells which divide as frequently as every 4-6 hours require intact mitochondrial function for formation[45,46]. B-cells must also remodel their chromatin landscape to permit differentiation and are known to induce expression of the H3K27me3

demethylases, KDM6A/B upon activation[47]. However, unlike in T-cells where loss of KDM6A/B activity prevents differentiation and memory formation[21,48], KDM6A/B inhibition promotes B-cell expansion and differentiation[47,49]. Given similar dependencies of B-cells to T-cells on mitochondrial metabolism and epigenetic regulation for normal B-cell function, iron deficiency would be proposed to cause similar biochemical blockades in the TCA cycle and of histone demethylase activity. However, iron deficiency blockade of histone demethylases may have differential impacts on B-cells given the opposing roles of KDM6A/B demethylases in B and T-cells. *In vitro* B-cell cultures utilising a similar low iron media system could be used to verify if B-cells respond in a biochemically similar way to iron scarcity as T-cells. Alternatively, the approaches detailed in section 7.2.1 could be used to assess B-cells activated in hypoferremic animals.

Haematopoiesis is another biological process predicted to be particularly iron demanding not only due to red blood cell (RBC) requirements for iron to support hemoglobin production[50] but also due to the involvement of rapid proliferation[51]. At homeostasis, haematopoiesis continually produces RBCs and white blood cells to account for cell turnover, with the average human producing approximately $2.8x10^{11}$ hematopoietic cells per day[51]. Upon perturbations such as blood loss or infection, the hematopoietic system must also be capable of further increasing outputs to maintain RBC numbers or to increase leukocyte numbers to combat pathogens[52]. Intriguingly, while *in vivo* iron deprivation mediated by IRP1/2 knockout[12], mHep mediated hypoferremia[11] or low iron diet limits neutropoiesis and erythropoiesis[53], recent publications have noted expansion of hematopoietic stem cells within the same iron depleted animals[12,53]. *In vitro* HSC expansion is enhanced in low iron media (0.0005 mg/mL holotransferrin)[53] at similar concentrations demonstrated to be severely suppressive for CD8+ T-cells in our models (although death of HSCs ensues at ultra-low iron concentrations, 0.000005 mg/mL holotransferrin[53]). A mechanistic explanation for this phenomenon has not been described. Given that HSC proliferation is promoted at comparable iron levels to those which impair T-cell function, it would be interesting to explore if iron depleted HSCs experience similar biochemical blocks to metabolism as T-cells and if this is somehow beneficial, or if HSCs resist iron deficiency by utilising alternative and presumably more optimal pathways. Meanwhile, given the observed impairment of bone marrow neutrophil output[11,12,53], examination of iron deficiency's impacts on the metabolism of later progenitors, such as the granulocyte-monocyte progenitor (GMP) could be

examined to identify if similar biochemical blockades are causing impairment of neutropoiesis as in T-cell activation.

Other rapidly proliferating cell types such as the epithelial cells of the skin, gut and airways would also be predicted to require exogenous iron to sustain rapid turnover. In the intestinal epithelium, the crypt cells which includes the stem cell niche and which enables the maintenance of the intestinal barrier, primarily utilise glycolysis[54]. However, as intestinal epithelial cells differentiate, the dependency on OXPHOS increases[54]. Differentiation of skin keratinocytes also requires mitochondrial metabolism, with the loss of the mitochondrial transcription factor, TFAM, impairing hair follicle development and epidermal differentiation[55]. Interestingly, hair loss is a reported although debated symptom of iron deficiency[56] and *Tmprss6* knockout mice which have elevated hepcidin and consequently low serum iron display profound hair loss and disrupted hair follicle morphology[57]. Airway epithelial differentiation is also mitochondrially dependent, relying on a metabolic switch from glycolysis to mitochondrial fatty acid oxidation[58]. Across epithelial tissue sites, engagement of mitochondrial pathways appears essential for maturation. Given the defects in mitochondrial metabolism observed in CD8+ T-cells during iron deprivation, iron scarcity would also be predicted to impair epithelial tissue differentiation as they attempt to upregulate iron dependent OXPHOS. However, given the beneficial effects of iron scarcity seen in HSCs by others[53], it is also possible that iron limitation may simultaneously promote epithelial stem cell maintenance. Assessing the effects of iron deprivation on epithelial cell differentiation and metabolism could be evaluated using *in vitro* differentiation models of skin, gut and airway epithelia using our low iron media *in vitro* culture system or *in vivo* using mHep to suppress serum iron and emerging metabolic methods detailed above (section 7.2.1).

Perhaps the most obvious rapidly proliferating tissues are tumours which are extremely metabolically active and can be highly iron demanding[39]. While iron chelation impairs tumour growth in a variety of *in vitro* and *in vivo* cancer models, clinical efficacy of iron chelators in human trials is low for unexplained reasons[59]. While tumour cells, similar to T-cells, are rapidly proliferating populations, tumour cells also often have remodelled metabolic pathways and many tumours are known to develop mutations in TCA cycle enzymes[60]. Heterozygous loss-of-function mutations in iron dependent SDH (CII) increase susceptibility to hereditary paraganglioma-pheochromocytomas (cancers

of the paraganglia and adrenal glands)[60] while heterozygous mutations in fumarate hydratase (FH) result in hereditary leiomyomatosis (smooth muscle tumours) and renal cell carcinoma[61]. In both cases, spontaneous loss-of-function mutations in the remaining wildtype allele result in malignant transformation[60]. While tumours with SDH and FH loss-of-function mutations feature TCA cycle impairment[60], proliferation remains intact, likely enabled by high glycolytic rates. Interestingly, FH mutations also result in fumarate accumulation which promotes the succination of Fe-S cluster synthesis proteins and ACO2, inhibiting their activity[61,62]. Given that SDH and FH mutations actively suppress iron requiring processes, it suggests that tumours bearing these mutations may be more resistant to the mitochondrial impairments observed in iron restricted CD8+ T-cells than in tumours without these mutations. Meanwhile, gain-of-function mutations in isocitrate dehydrogenase (IDH) confer the capacity to convert α-KG to 2-hydroxyglutarate (2-HG) and are associated with a variety of cancers including acute myeloid leukaemia, chondrosarcoma (bone cancer) and angioimmunoblastic T-cell lymphoma[63]. 2-HG inhibits 2-oxoglutarate (α-KG) dependent dioxygenases[63] (2-OGDDs, chapter 1, section 1.2.3), the same class of enzymes predicted to be inhibited by iron scarcity due to the iron and α-KG dependence of these enzymes. IDH mutants may resist iron deficiency due to actively inhibiting a large class of iron dependent enzymes (the 2-OGDDs). The capacity of tumours to rewire metabolism to avoid iron dependent processes could explain the low clinical efficacy of iron chelators[59]. Screening of tumour cell lines for susceptibility to iron deficiency could provide insights into mutations and pathways which enable reduced iron usage and could inform further interventions (as explored in chapter 6) for rescue of iron deficiency in immune cells.

While only a handful of examples are given here, the potential impacts of iron deficiency across body sites is potentially large. Using our survey of iron deficiency in T-cells as a framework, other iron dependent cell types could be predicted by assessing dependencies on pathways identified here as particularly sensitive to iron scarcity.

7.3 Translational applications

Iron scarcity occurs in several contexts within humans including dietary iron deficiency[5], inflammation induced hypoferremia[64], and iron restriction within local tissue niches due to the presence of iron demanding tumours[39] or pathogens[65]. Understanding

the metabolic implications of iron restriction on T-cells provides insight into how metabolic interventions could be utilised to overcome or enhance iron scarcity mediated immune suppression in a clinical setting.

For instance, we identified that aspartate supplementation could provide profound proliferative benefits to iron restricted CD8+ T-cells *in vitro* (chapter 6, Fig. 6.2B-D). While we failed to demonstrate efficacy of systemically administered aspartate or pre-aspartate treatment prior to adoptive transfer (chapter 6, Fig. 6.6H-K, Fig. 6.7F-K), an alternative approach would be to augment the capacity of CD8+ T-cells to use exogenous aspartate sources by overexpressing an aspartate transporter (SLC1A1/2/3) on the cell surface. This could be applied therapeutically by modifying clinically approved chimeric antigen receptor T-cells (CAR-T-cells) currently used for B-cell malignancies or emerging synthetic TCR systems which have greater antigen sensitivity[66]. Manipulating adoptive T-cell therapies to overcome iron scarcity is particularly relevant in cancers which are both iron hungry[39,64] while also simultaneously capable of inducing inflammation associated hypoferremia[67]. Notably, similar approaches have previously been employed, demonstrating that metabolic manipulation of adoptive T-cell therapies is feasible with potential *in vivo* benefit. Overexpression of the enzymes argininosuccinate synthase (ASS) and ornithine transcarbamylase (OTC) helps CAR-T-cells to overcome the low arginine environment which results from arginine demanding tumours[68]. Administration of ASS/OTC overexpressing CAR-T-cells marginally but significantly increase survival in tumour bearing mice[68]. Similarly, overexpression of PRODH2 which is involved in proline metabolism in CAR-T-cells also improves mouse survival upon adoptive transfer to mice with multiple myeloma[69].

While augmenting T-cell responses is preferable in tumour therapy, treatment of pathologically overactive immune responses in autoimmunity requires T-cell suppression. Notably, iron deprivation mediated via a diversity of modalities clearly suppresses pathogenic T-cell responses in pre-clinical models of autoimmunity[7-10,13]. Whether iron deprivation mediated by hepcidin analogues, α-TFRC antibodies or iron chelators similarly suppresses autoimmune reactions in humans remains to be explored. This may be in part due to the concern that clinical applications of iron deprivation are likely to simultaneously suppress erythropoiesis which is highly reliant on serum iron availability[50]. One approach for circumventing iron deficiency's non-specific effects

would be the utilisation of well-designed bispecific antibodies against TFRC and a lineage specifying surface marker such as CD3 for T-cells. Alternatively, knowledge of the consequences of iron scarcity on T-cells could allow for better predictions of combination therapies with existing immunosuppressants.

Nucleotide production is proposed to be suppressed during CD8+ T-cell iron deficiency. This is evidenced by the increased resistance of SAMHD1-KO CD8+ T-cells which theoretically have increased endogenous dNTP pool to iron deprivation (chapter 6, Fig. 6.5C). Notably, many well-known and approved drugs for autoimmune conditions inhibit T-cells by targeting nucleotide synthesis[70]. Mycophenolate mofetil and azathioprine target purine nucleotide metabolism[71], leflunomide blocks pyrimidine nucleotide metabolism[70] and methotrexate inhibits both[72]. As with most drugs, all of these compounds display some level of toxicity[71-73]. Coupling iron restriction with nucleotide synthesis inhibiting drugs could provide synergistic benefit while also permitting lower drug dosages and consequently reduced toxicity.

Alternatively, while it is established that T-cells use exogenous asparagine in early activation, T-cells gain the capacity to produce asparagine from aspartate at later timepoints[17]. Given that iron deprivation reduced aspartate usage and suppressed expression of the enzyme, ASNS (chapter 5, Fig. 5.4F) which mediates the aspartate to asparagine reaction, we propose that asparagine synthesis would likely be impaired at later timepoints during iron limitation. Thus, another drug which may provide synergistic benefit with iron deprivation in the suppression of unwanted immunity is L-asparaginase. L-asparaginase is a drug which has been clinically used since the 1960s for the treatment of acute lymphoblastic leukaemia (ALL)[74]. ALL cells lack the capacity to synthesise sufficient asparagine endogenously and thus rely on exogenous sources[74]. L-asparaginase is an enzyme which converts asparagine back to aspartate and when administered systemically depletes serum asparagine and consequently inhibits ALL[74]. L-asparaginase would not be predicted to significantly impair activated T-cells under iron replete conditions due to the capacity of activated T-cells to generate intracellular asparagine[17]. However, if iron deficiency does prevent T-cell asparagine synthesis, reducing serum asparagine with L-asparaginase could inhibit T-cells. Further, given that T-cells poorly express aspartate importers[75], the increase in serum aspartate mediated by L-asparaginase would be predicted to be non-beneficial.

Finally, it should not be forgotten that iron deficiency is globally prevalent, impacting greater than 1.2 billion individuals worldwide[76]. While the extent to which iron deficiency impairs immunity in humans is poorly understood, the possibility that iron deficiency could impair immune responses to vaccination or infection has broad global health implications. Further, iron deficiency is unlikely to be the only nutrient deficiency affecting many individuals. The combined restriction of multiple nutrients may be particularly detrimental if limitation of one nutrient such as iron results in auxotrophy for others or if different nutrients are required for common pathways. For instance, our work suggests that iron deficiency may indirectly suppress dNTP production in CD8+ T-cells via impaired aspartate usage (chapter 5-6). For example, folate (vitamin B9) is a critical cofactor for dNTP production and folate deprivation has independently been shown to also impair lymphocytes[77]. Folate deficiency has been reported to affect >20% of women of reproductive age in some low-income countries[78], a population also frequently affected by iron deficiency. Thus, combined iron and folate deficiencies could be synergistically detrimental to T-cells – and potentially other rapidly proliferating cell types - due to a double hit on nucleotide synthesis.

Knowledge of how micronutrient deficiencies interact could help inform the formulations of micronutrient supplements to better address malnutrition. However, while science provides many solutions to health issues, the solution that should not be overlooked in the case of malnutrition and iron deficiency is the structural correction of poverty and improvement of social systems[79]. Strikingly 780 million of the approximately 795 million undernourished people reside in low- and middle-income nations[79]. While addressing social systems to correct malnutrition seems daunting, historic examples show this is possible. Global undernourishment fell from 19% (1990-2002) to 11% (2014-2016) despite global population growth and this was largely driven by interventions such as reducing poverty and improving literacy and healthcare[79].

7.4 Final thoughts

While the essentiality of iron availability for cellular biochemistry has long been assumed, and the generalisability of this work remains to be demonstrated, this thesis clearly illustrates that iron scarcity has profound implications for the biochemistry of T-cells. This work demonstrates that iron deficiency presents a complex pathophysiology,

striking cellular activities at multiple nodes to induce a dysfunctional cellular state that is unlikely to be completely rescuable by any singular intervention. Understanding these epigenetic, transcriptomic, proteomic and metabolomic impacts of iron scarcity in T-cells will inform improved approaches to overcome physiological iron restriction and the use of iron modulation to manipulate immune responses in settings such as autoimmunity, cancer and vaccination. This work also presents a foundation for understanding the importance of iron in cellular biochemistry across cell types both at homeostasis and during differentiation. For as Otto Warburg wrote in 1925[80]:

"Our assertion assumes that every living cell contains iron
and that life without iron is impossible."

7.5 References

1 Archibald, F. Lactobacillus plantarum, an organism not requiring iron. *FEMS Microbiology Letters* **19**, 29-32 (1983). https://doi.org:10.1111/j.1574-6968.1983.tb00504.x

2 Posey, J. E. & Gherardini, F. C. Lack of a role for iron in the Lyme disease pathogen. *Science* **288**, 1651-1653 (2000). https://doi.org:10.1126/science.288.5471.1651

3 Sabine, D. B. & Vaselekos, J. Trace Element Requirements of Lactobacillus acidophilus. *Nature* **214**, 520-520 (1967). https://doi.org:10.1038/214520a0

4 Andreini, C., Putignano, V., Rosato, A. & Banci, L. The human iron-proteome. *Metallomics* **10**, 1223-1231 (2018). https://doi.org:10.1039/c8mt00146d

5 Pasricha, S. R., Tye-Din, J., Muckenthaler, M. U. & Swinkels, D. W. Iron deficiency. *Lancet* **397**, 233-248 (2021). https://doi.org:10.1016/s0140-6736(20)32594-0

6 Frost, J. N. *et al.* Hepcidin-Mediated Hypoferremia Disrupts Immune Responses to Vaccination and Infection. *Med (N Y)* **2**, 164-179.e112 (2021). https://doi.org:10.1016/j.medj.2020.10.004

7 Voss, K. *et al.* Elevated transferrin receptor impairs T cell metabolism and function in systemic lupus erythematosus. *Sci Immunol* **8**, eabq0178 (2023). https://doi.org:10.1126/sciimmunol.abq0178

8 Wang, Z. *et al.* Iron Drives T Helper Cell Pathogenicity by Promoting RNA-Binding Protein PCBP1-Mediated Proinflammatory Cytokine Production. *Immunity* **49**, 80-92.e87 (2018). https://doi.org:10.1016/j.immuni.2018.05.008

9 Li, L. *et al.* Iron deprivation restrains the differentiation and pathogenicity of T helper 17 cell. *J Leukoc Biol* **110**, 1057-1067 (2021). https://doi.org:10.1002/jlb.3ma0821-015r

10 Gao, X. *et al.* Iron-dependent epigenetic modulation promotes pathogenic T cell differentiation in lupus. *J Clin Invest* **132** (2022). https://doi.org:10.1172/jci152345

11 Frost, J. N. *et al.* Plasma iron controls neutrophil production and function. *Sci Adv* **8**, eabq5384 (2022). https://doi.org:10.1126/sciadv.abq5384

12 Bonadonna, M. *et al.* Iron regulatory protein (IRP)-mediated iron homeostasis is critical for neutrophil development and differentiation in the bone marrow. *Sci Adv* **8**, eabq4469 (2022). https://doi.org:10.1126/sciadv.abq4469

13 Lai, Y. *et al.* Iron controls T helper cell pathogenicity by promoting glucose metabolism in autoimmune myopathy. *Clin Transl Med* **12**, e999 (2022). https://doi.org:10.1002/ctm2.999

14 Sena, L. A. & Chandel, N. S. Physiological roles of mitochondrial reactive oxygen species. *Mol Cell* **48**, 158-167 (2012). https://doi.org:10.1016/j.molcel.2012.09.025

15 Levine, A. J., Hu, W. & Feng, Z. The P53 pathway: what questions remain to be explored? *Cell Death Differ* **13**, 1027-1036 (2006). https://doi.org:10.1038/sj.cdd.4401910

16 Villa, E., Ali, E. S., Sahu, U. & Ben-Sahra, I. Cancer Cells Tune the Signaling Pathways to Empower de Novo Synthesis of Nucleotides. *Cancers (Basel)* **11** (2019). https://doi.org:10.3390/cancers11050688

17 Hope, H. C. *et al.* Coordination of asparagine uptake and asparagine synthetase expression modulates CD8+ T cell activation. *JCI Insight* **6** (2021). https://doi.org:10.1172/jci.insight.137761

18 Franzolin, E. *et al.* The deoxynucleotide triphosphohydrolase SAMHD1 is a major regulator of DNA precursor pools in mammalian cells. *Proc Natl Acad Sci U S A* **110**, 14272-14277 (2013). https://doi.org:10.1073/pnas.1312033110

19 Rehwinkel, J. *et al.* SAMHD1-dependent retroviral control and escape in mice. *Embo j* **32**, 2454-2462 (2013). https://doi.org:10.1038/emboj.2013.163

20 Russ, B. E. *et al.* Distinct epigenetic signatures delineate transcriptional programs during virus-specific CD8(+) T cell differentiation. *Immunity* **41**, 853-865 (2014). https://doi.org:10.1016/j.immuni.2014.11.001

21 Cribbs, A. P. *et al.* Histone H3K27me3 demethylases regulate human Th17 cell development and effector functions by impacting on metabolism. *Proc Natl Acad Sci U S A* **117**, 6056-6066 (2020). https://doi.org:10.1073/pnas.1919893117

22 Ruprecht, J. J. & Kunji, E. R. S. The SLC25 Mitochondrial Carrier Family: Structure and Mechanism. *Trends Biochem Sci* **45**, 244-258 (2020). https://doi.org:10.1016/j.tibs.2019.11.001

23 Soriano-Baguet, L. & Brenner, D. Metabolism and epigenetics at the heart of T cell function. *Trends Immunol* **44**, 231-244 (2023). https://doi.org:10.1016/j.it.2023.01.002

24 Ma, E. H. *et al.* Metabolic Profiling Using Stable Isotope Tracing Reveals Distinct Patterns of Glucose Utilization by Physiologically Activated CD8(+) T Cells. *Immunity* **51**, 856-870.e855 (2019). https://doi.org:10.1016/j.immuni.2019.09.003

25 Leney-Greene, M. A., Boddapati, A. K., Su, H. C., Cantor, J. R. & Lenardo, M. J. Human Plasma-like Medium Improves T Lymphocyte Activation. *iScience* **23**, 100759 (2020). https://doi.org:10.1016/j.isci.2019.100759

26 Kaymak, I. *et al.* Carbon source availability drives nutrient utilization in CD8(+) T cells. *Cell Metab* **34**, 1298-1311.e1296 (2022). https://doi.org:10.1016/j.cmet.2022.07.012

27 Argüello, R. J. *et al.* SCENITH: A Flow Cytometry-Based Method to Functionally Profile Energy Metabolism with Single-Cell Resolution. *Cell Metab* **32**, 1063-1075.e1067 (2020). https://doi.org:10.1016/j.cmet.2020.11.007

28 Hardie, D. G. 100 years of the Warburg effect: a historical perspective. *Endocr Relat Cancer* **29**, T1-t13 (2022). https://doi.org:10.1530/erc-22-0173

29 Leigh, F. W. Sir Hans Adolf Krebs (1900-81), pioneer of modern medicine, architect of intermediary metabolism. *J Med Biogr* **17**, 149-154 (2009). https://doi.org:10.1258/jmb.2009.009032

30 Agilent Technologies, I. (ed Inc. Agilent Technologies) 1-38 (USA, 2018).

31 Ahl, P. J. *et al.* Met-Flow, a strategy for single-cell metabolic analysis highlights dynamic changes in immune subpopulations. *Commun Biol* **3**, 305 (2020). https://doi.org:10.1038/s42003-020-1027-9

32 Thompson, E. A. *et al.* Metabolic programs define dysfunctional immune responses in severe COVID-19 patients. *Cell Rep* **34**, 108863 (2021). https://doi.org:10.1016/j.celrep.2021.108863

33 Hartmann, F. J. *et al.* Single-cell metabolic profiling of human cytotoxic T cells. *Nat Biotechnol* **39**, 186-197 (2021). https://doi.org:10.1038/s41587-020-0651-8

34 Levine, L. S. *et al.* Single-cell analysis by mass cytometry reveals metabolic states of early-activated CD8(+) T cells during the primary immune response. *Immunity* **54**, 829-844.e825 (2021). https://doi.org:10.1016/j.immuni.2021.02.018

35 Stoeckius, M. *et al.* Simultaneous epitope and transcriptome measurement in single cells. *Nat Methods* **14**, 865-868 (2017). https://doi.org:10.1038/nmeth.4380

36 Chen, H., Yu, Z., Ren, S. & Qiu, Y. Fluorescent Probes Design Strategies for Imaging Mitochondria and Lysosomes. *Front Pharmacol* **13**, 915609 (2022). https://doi.org:10.3389/fphar.2022.915609

37 DeVilbiss, A. W. *et al.* Metabolomic profiling of rare cell populations isolated by flow cytometry from tissues. *Elife* **10** (2021). https://doi.org:10.7554/eLife.61980

38 Pereira, M. *et al.* Acute Iron Deprivation Reprograms Human Macrophage Metabolism and Reduces Inflammation In Vivo. *Cell Rep* **28**, 498-511.e495 (2019). https://doi.org:10.1016/j.celrep.2019.06.039

39 Schwartz, A. J. *et al.* Hepcidin sequesters iron to sustain nucleotide metabolism and mitochondrial function in colorectal cancer epithelial cells. *Nature Metabolism* **3**, 969-982 (2021). https://doi.org:10.1038/s42255-021-00406-7

40 Pearce, E. L., Poffenberger, M. C., Chang, C. H. & Jones, R. G. Fueling immunity: insights into metabolism and lymphocyte function. *Science* **342**, 1242454 (2013). https://doi.org:10.1126/science.1242454

41 Jabara, H. H. *et al.* A missense mutation in TFRC, encoding transferrin receptor 1, causes combined immunodeficiency. *Nature Genetics* **48**, 74-78 (2016). https://doi.org:10.1038/ng.3465

42 Wideman, S. K. *et al.* Cellular iron governs the host response to malaria. *bioRxiv*, 2023.2002.2005.527208 (2023). https://doi.org:10.1101/2023.02.05.527208

43 Jiang, Y. *et al.* Iron-dependent histone 3 lysine 9 demethylation controls B cell proliferation and humoral immune responses. *Nat Commun* **10**, 2935 (2019). https://doi.org:10.1038/s41467-019-11002-5

44 Kondo, M. Lymphoid and myeloid lineage commitment in multipotent hematopoietic progenitors. *Immunol Rev* **238**, 37-46 (2010). https://doi.org:10.1111/j.1600-065X.2010.00963.x

45 Jellusova, J. Metabolic control of B cell immune responses. *Curr Opin Immunol* **63**, 21-28 (2020). https://doi.org:10.1016/j.coi.2019.11.002

46 Yazicioglu, Y. F. *et al.* Dynamic mitochondrial transcription and translation in B cells control germinal center entry and lymphomagenesis. *Nat Immunol* **24**, 991-1006 (2023). https://doi.org:10.1038/s41590-023-01484-3

47 Kania, A. K., Guo, M., Scharer, C. D. & Boss, J. M. Inhibition of H3K27me3 Demethylases Promotes Plasmablast Formation. *Immunohorizons* **5**, 918-930 (2021). https://doi.org:10.4049/immunohorizons.2000087

48 Li, J. *et al.* KDM6B-dependent chromatin remodeling underpins effective virus-specific CD8(+) T cell differentiation. *Cell Rep* **34**, 108839 (2021). https://doi.org:10.1016/j.celrep.2021.108839

49 Kania, A. K. *et al.* H3K27me3 Demethylase UTX Restrains Plasma Cell Formation. *J Immunol* **208**, 1873-1885 (2022). https://doi.org:10.4049/jimmunol.2100948

50 Ganz, T. Systemic iron homeostasis. *Physiol Rev* **93**, 1721-1741 (2013). https://doi.org:10.1152/physrev.00008.2013

51 Cosgrove, J., Hustin, L. S. P., de Boer, R. J. & Perié, L. Hematopoiesis in numbers. *Trends Immunol* **42**, 1100-1112 (2021). https://doi.org:10.1016/j.it.2021.10.006

52 Boettcher, S. & Manz, M. G. Regulation of Inflammation- and Infection-Driven Hematopoiesis. *Trends Immunol* **38**, 345-357 (2017). https://doi.org:10.1016/j.it.2017.01.004

53 Zhang, D. *et al.* The microbiota regulates hematopoietic stem cell fate decisions by controlling iron availability in bone marrow. *Cell Stem Cell* **29**, 232-247.e237 (2022). https://doi.org:10.1016/j.stem.2021.12.009

54 Rath, E. & Haller, D. Intestinal epithelial cell metabolism at the interface of microbial dysbiosis and tissue injury. *Mucosal Immunol* **15**, 595-604 (2022). https://doi.org:10.1038/s41385-022-00514-x

55 Hamanaka, R. B. *et al.* Mitochondrial reactive oxygen species promote epidermal differentiation and hair follicle development. *Sci Signal* **6**, ra8 (2013). https://doi.org:10.1126/scisignal.2003638

56 Trost, L. B., Bergfeld, W. F. & Calogeras, E. The diagnosis and treatment of iron deficiency and its potential relationship to hair loss. *J Am Acad Dermatol* **54**, 824-844 (2006). https://doi.org:10.1016/j.jaad.2005.11.1104

57 Folgueras, A. R. *et al.* Membrane-bound serine protease matriptase-2 (Tmprss6) is an essential regulator of iron homeostasis. *Blood* **112**, 2539-2545 (2008). https://doi.org:10.1182/blood-2008-04-149773

58 Crotta, S. *et al.* Repair of airway epithelia requires metabolic rewiring towards fatty acid oxidation. *Nat Commun* **14**, 721 (2023). https://doi.org:10.1038/s41467-023-36352-z

59 Ibrahim, O. & O'Sullivan, J. Iron chelators in cancer therapy. *Biometals* **33**, 201-215 (2020). https://doi.org:10.1007/s10534-020-00243-3

60 Anderson, N. M., Mucka, P., Kern, J. G. & Feng, H. The emerging role and targetability of the TCA cycle in cancer metabolism. *Protein Cell* **9**, 216-237 (2018). https://doi.org:10.1007/s13238-017-0451-1

61 Tyrakis, P. A. *et al.* Fumarate Hydratase Loss Causes Combined Respiratory Chain Defects. *Cell Rep* **21**, 1036-1047 (2017). https://doi.org:10.1016/j.celrep.2017.09.092

62 Ternette, N. *et al.* Inhibition of mitochondrial aconitase by succination in fumarate hydratase deficiency. *Cell Rep* **3**, 689-700 (2013). https://doi.org:10.1016/j.celrep.2013.02.013

63 Pirozzi, C. J. & Yan, H. The implications of IDH mutations for cancer development and therapy. *Nat Rev Clin Oncol* **18**, 645-661 (2021). https://doi.org:10.1038/s41571-021-00521-0

64 Nemeth, E. *et al.* IL-6 mediates hypoferremia of inflammation by inducing the synthesis of the iron regulatory hormone hepcidin. *J Clin Invest* **113**, 1271-1276 (2004). https://doi.org:10.1172/jci20945

65 Qualls, J. E. & Murray, P. J. Immunometabolism within the tuberculosis granuloma: amino acids, hypoxia, and cellular respiration. *Semin Immunopathol* **38**, 139-152 (2016). https://doi.org:10.1007/s00281-015-0534-0

66 Burton, J. *et al.* Inefficient exploitation of accessory receptors reduces the sensitivity of chimeric antigen receptors. *Proc Natl Acad Sci U S A* **120**, e2216352120 (2023). https://doi.org:10.1073/pnas.2216352120

67 Macciò, A. *et al.* The role of inflammation, iron, and nutritional status in cancer-related anemia: results of a large, prospective, observational study. *Haematologica* **100**, 124-132 (2015). https://doi.org:10.3324/haematol.2014.112813

68 Fultang, L. *et al.* Metabolic engineering against the arginine microenvironment enhances CAR-T cell proliferation and therapeutic activity. *Blood* **136**, 1155-1160 (2020). https://doi.org:10.1182/blood.2019004500

69 Ye, L. *et al.* A genome-scale gain-of-function CRISPR screen in CD8 T cells identifies proline metabolism as a means to enhance CAR-T therapy. *Cell Metab* **34**, 595-614.e514 (2022). https://doi.org:10.1016/j.cmet.2022.02.009

70 Scherer, S. *et al.* Pyrimidine de novo synthesis inhibition selectively blocks effector but not memory T cell development. *Nat Immunol* **24**, 501-515 (2023). https://doi.org:10.1038/s41590-023-01436-x

71 Broen, J. C. A. & van Laar, J. M. Mycophenolate mofetil, azathioprine and tacrolimus: mechanisms in rheumatology. *Nat Rev Rheumatol* **16**, 167-178 (2020). https://doi.org:10.1038/s41584-020-0374-8

72 Cronstein, B. N. & Aune, T. M. Methotrexate and its mechanisms of action in inflammatory arthritis. *Nat Rev Rheumatol* **16**, 145-154 (2020). https://doi.org:10.1038/s41584-020-0373-9

73 Charatan, F. Arthritis drug should be removed from market, says consumer group. *Bmj* **324**, 869 (2002). https://doi.org:10.1136/bmj.324.7342.869/a

74 Egler, R. A., Ahuja, S. P. & Matloub, Y. L-asparaginase in the treatment of patients with acute lymphoblastic leukemia. *J Pharmacol Pharmacother* **7**, 62-71 (2016). https://doi.org:10.4103/0976-500x.184769

75 Heng, T. S. & Painter, M. W. The Immunological Genome Project: networks of gene expression in immune cells. *Nat Immunol* **9**, 1091-1094 (2008). https://doi.org:10.1038/ni1008-1091

76 Collaborators, G. D. a. I. I. a. P. Global, regional, and national incidence, prevalence, and years lived with disability for 328 diseases and injuries for 195 countries, 1990-2016: a systematic analysis for the Global Burden of Disease Study 2016. *Lancet* **390**, 1211-1259 (2017). https://doi.org:10.1016/s0140-6736(17)32154-2

77 James, S. J., Miller, B. J., Cross, D. R., McGarrity, L. J. & Morris, S. M. The essentiality of folate for the maintenance of deoxynucleotide precursor pools, DNA synthesis, and cell cycle progression in PHA-stimulated lymphocytes. *Environ Health Perspect* **101 Suppl 5**, 173-178 (1993). https://doi.org:10.1289/ehp.93101s5173

78 Rogers, L. M. *et al.* Global folate status in women of reproductive age: a systematic review with emphasis on methodological issues. *Ann N Y Acad Sci* **1431**, 35-57 (2018). https://doi.org:10.1111/nyas.13963

79 Webb, P. *et al.* Hunger and malnutrition in the 21st century. *Bmj* **361**, k2238 (2018). https://doi.org:10.1136/bmj.k2238

80 Warburg, O. IRON, THE OXYGEN-CARRIER OF RESPIRATION-FERMENT. *Science* **61**, 575-582 (1925). https://doi.org:10.1126/science.61.1588.575

Appendix

This appendix includes the two first-author publications which contributed to this thesis. Firstly, the poem found on page 5, “Natural history of an iron atom”, which was published as Teh, 2022, American Journal of Hematology (DOI: 10.1002/ajh.26678). Secondly, the research article “Analysis of iron and iron interacting proteins in T-cells”, which contributed to chapters 3 and 5, published as Teh *et al*, Frontiers of Immunology, 2021 (DOI: 10.3389/fimmu.2021.714613).

Received: 21 July 2022 | Accepted: 1 August 2022

DOI: 10.1002/ajh.26678

EDITORIAL

Natural history of an iron atom

This story is quite elementary,
For iron is most necessary,
By this atom though small in size,
Life in fact is catalysed

Consumption of a ferric source,
(Beans or steak for your main course),
Sends iron on its merry way,
To help you live another day

Inside your duodenal intestine,
Iron uptake by absorption,
Moves this elemental species,
Into you and not your faeces,
Once inside an Enterocyte,
Iron pauses or takes flight,
Ferroportin mediated,
To serum, iron is liberated

Another quarry to be mined,
Are Red blood cells that have died,
These rotund red corpuscles,
Parcels packed with rusty metals,
Swallowed whole by Macrophages,
Releasing iron from Heme cages,
Thence once again, through Ferroportin,
Iron to blood, is transported

From blood, Transferrin tries to chelate,
Iron from its sanguineous state,
This union is most essential,
For free iron is detrimental,
Since microbes of many a kind,
Like us, for ferric ions pine,
From bids to steal the host supply,
Transferrin acts to fortify

When pathogens do invade,
And undertake an iron raid,
Another mode of self-defence,
In the liver does commence,
Hepatic Hepcidin is produced,
To keep serum iron running loose,
To Ferroportin it does bind,
Blocks iron export, locks ions inside

Transferrin with its iron crown,
Will quick become receptor bound,
Intake via endosome,
Brings iron to its brand new home,
Surplus stored in Ferritin vaults,
In case external supply ever halts,
The rest dependant on each cell's needs,
To different pathways it does feed

For what is iron used, you ask?
Well, it's put to work at many a task,
Red cell Hemoglobin claims two thirds,
And like a shepherd tries to herd,
Oxygen with all its might,
Through blood to every tissue site,
The rest is used by other cells,
In both cytosol and organelles

ONE – In DNA synthesis it plays a role,
In Primases and DNA pols,
TWO – Mitochondrial metabolism,
(But try to avoid toxic oxygen radicalism),
THREE – epigenetic regulation,
For Histone and DNA demethylation,
FOUR – other roles are rather muddy,
And definitely warrants further study

In short, I hope you've come to see,
Via this peculiar poetry,
The importance of this element,
Deems work on it, time well spent

DATA AVAILABILITY STATEMENT

Data sharing is not applicable to this article.

Megan R. Teh

MRC Human Immunology Unit, MRC Weatherall Institute of Molecular Medicine, University of Oxford, John Radcliffe Hospital, Oxford, UK

Correspondence

Megan R. Teh, MRC Human Immunology Unit, MRC Weatherall Institute of Molecular Medicine, University of Oxford, John Radcliffe Hospital, Oxford, UK.

Email: megan.teh@ccc.ox.ac.uk

ORCID

Megan R. Teh https://orcid.org/0000-0002-8095-9961

frontiers in Immunology

ORIGINAL RESEARCH
published: 12 August 2021
doi: 10.3389/fimmu.2021.714613

Analysis of Iron and Iron-Interacting Protein Dynamics During T-Cell Activation

Megan R. Teh[1], *Joe N. Frost*[1], *Andrew E. Armitage*[1] *and Hal Drakesmith*[1,2*]

[1] MRC Human Immunology Unit, MRC Weatherall Institute of Molecular Medicine, University of Oxford, John Radcliffe Hospital, Oxford, United Kingdom, [2] Haematology Theme, Oxford Biomedical Research Centre, Oxford, United Kingdom

OPEN ACCESS

Edited by:
Wilson Savino, Oswaldo Cruz Foundation (Fiocruz), Brazil

Reviewed by:
Bobby Cherayil, Massachusetts General Hospital and Harvard Medical School, United States
Laura Silvestri, San Raffaele Scientific Institute (IRCCS), Italy

***Correspondence:**
Hal Drakesmith
alexander.drakesmith@ndm.ox.ac.uk

Specialty section:
This article was submitted to Nutritional Immunology, a section of the journal Frontiers in Immunology

Received: *25 May 2021*
Accepted: *06 July 2021*
Published: *12 August 2021*

Citation:
Teh MR, Frost JN, Armitage AE and Drakesmith H (2021) Analysis of Iron and Iron-Interacting Protein Dynamics During T-Cell Activation. Front. Immunol. 12:714613. doi: 10.3389/fimmu.2021.714613

Recent findings have shown that iron is a powerful regulator of immune responses, which is of broad importance because iron deficiency is highly prevalent worldwide. However, the underlying reasons of why iron is needed by lymphocytes remain unclear. Using a combination of mathematical modelling, bioinformatic analysis and experimental work, we studied how iron influences T-cells. We identified iron-interacting proteins in CD4+ and CD8+ T-cell proteomes that were differentially expressed during activation, suggesting that pathways enriched with such proteins, including histone demethylation, may be impaired by iron deficiency. Consistent with this, iron-starved Th17 cells showed elevated expression of the repressive histone mark H3K27me3 and displayed reduced RORγt and IL-17a, highlighting a previously unappreciated role for iron in T-cell differentiation. Quantitatively, we estimated T-cell iron content and calculated that T-cell iron demand rapidly and substantially increases after activation. We modelled that these increased requirements will not be met during clinically defined iron deficiency, indicating that normalizing serum iron may benefit adaptive immunity. Conversely, modelling predicted that excess serum iron would not enhance CD8+ T-cell responses, which we confirmed by immunising inducible hepcidin knock-out mice that have very high serum iron concentrations. Therefore, iron deficiency impairs multiple aspects of T-cell responses, while iron overload likely has milder effects.

Keywords: T-cell, iron, immunometabolism, adaptive immunity, iron deficiency, demethylation, Th17 cells, iron overload

Abbreviations: apoTf, apotransferrin; diTf, diferric transferrin; Fe-S cluster, iron sulfur cluster; GO, gene ontology; GZMB, granzyme B; H3K27me3, Histone 3 lysine 27 trimethylation; holoTf, holotransferrin; IL-17a, Interleukin 17; KDM, lysine demethylase; MFI, mean fluorescence intensity; monoTf, monoferric transferrin; OVA, ovalbumin; OXPHOS, oxidative phosphorylation; RORγt, RAR related orphan receptor gamma; Tf, transferrin; TFRC, Transferrin receptor; Th17 cells, T helper 17 cells; TSAT, transferrin saturation.

INTRODUCTION

Effective adaptive immunity is critical for the clearance of many pathogens. Activation of adaptive immune responses is metabolically demanding and reliant on nutritional factors such as glucose, amino acids and lipids (1). Growing evidence also implicates iron as a critical nutrient for adaptive immune responses (2). For instance, activating T-cells adopt an iron accumulatory phenotype characterised by upregulation of the iron acquisition proteins transferrin receptor (TFRC, CD71), solute carrier family-11 member-2 (SlC11A2) and SLC39A14, and suppression of the sole known iron exporter, Slc40a1 (3, 4). Further, children bearing an amino acid change in the transferrin receptor, that impairs cellular iron uptake, display severe combined immunodeficiencies featuring hypogammaglobulinemia and defective lymphocyte proliferation (5). Induction of hypoferremia (low serum iron) in mouse models impairs B and T-cell responses to both vaccination and influenza infection, while supply of iron to iron-deficient piglets improves vaccine responses (3). Effects of iron deficiency inhibiting, and iron supplementation enhancing vaccine responses in humans have also been reported (6, 7). Mechanistically, *in vitro* T-cell studies with iron starvation mediated *via* iron depleted media or the use of iron chelators demonstrate the importance of iron for cellular proliferation, activation and the production of effector molecules such as granzyme B (GZMB), granulocyte macrophage colony stimulating factor (GM-CSF) and interferon γ (IFN-γ) (3, 5, 8–10). While a profound role for iron in T-cell activation and function has been established, the specific dynamics of iron utilisation, and the key biological processes affected within T-cells remain unclear. Understanding how iron is used by T-cells may provide insight as to how iron modulation could be used to improve or attenuate immune responses in diverse contexts such as vaccination, infection or cancer.

Iron's ability to act as an electron donor and acceptor is a characteristic often co-opted by cellular proteins for catalysis of reduction-oxidation (redox) reactions and oxygen binding (11). The central role of iron in cellular biochemistry was highlighted in a study by Andreini et al, which predicts that ~2% of human protein coding genes and ~6.5% of enzymes interact with iron (12). Protein interactions with iron can occur either directly with iron ions or *via* heme or iron-sulfur (Fe-S) cluster prosthetic groups (12). Iron ion binding proteins bind iron directly and are predominantly catalytic (12); many such proteins are 2-oxoglutarate (2-OG) dependent dioxygenases which mediate hydroxylation reactions involved in processes such as histone and DNA demethylation and collagen synthesis (12, 13). Meanwhile, heme cofactors consist of iron within larger porphyrin ring structures (14). Heme proteins, including hemoglobin are well known for oxygen binding, but are also involved in mitochondrial electron transfer and oxidative reactions involved in pathways such as prostaglandin synthesis, nitric oxide production and tryptophan metabolism (14). Finally, Fe-S clusters coordinate iron and sulfur atoms as [2Fe-2S], [3Fe-4S] or [4Fe-4S] structures in mammals (15). Fe-S cluster interacting proteins are extremely diverse and include proteins involved in Fe-S cluster synthesis itself, mitochondrial respiration and DNA synthesis (12, 15).

Using a previously published T-cell proteomics dataset from Howden et al. (4) that assesses T-cell protein content at 0h, 24h and 6 days post activation, and a list of iron interacting proteins derived from Andreini et al. (12), we aimed to understand how iron interacting proteins are differentially expressed during T-cell activation and differentiation. We identified processes enriched for iron interacting proteins in T-cells including demethylation, oxidative phosphorylation (OXPHOS), DNA synthesis and Fe-S cluster biogenesis and predict that T-cell iron requirements increase substantially post-activation. Using computational and experimental models we suggest that while iron deficiency may impair T-cell iron uptake, excess iron is unlikely to provide significant benefit to activating T-cells. Our analysis provides a unique approach to "immunometallomics" and provides insight as to the importance of iron in T-cell function.

METHODS

Deriving a List of Iron Interacting Mouse Protein Homologues

Using the Uniprot IDs of human iron interacting proteins provided by Andreini *et al*, corresponding standard human gene names were identified using the Uniprot mapping tool (https://www.uniprot.org/uploadlists/) (16). To curate an equivalent list of mouse iron interacting protein homologues, the list of human iron interacting genes was input into the Ensembl BioMart tool (http://useast.ensembl.org/biomart/martview/893cea99357a57529ab65ce92c12e306) selecting for comparison to the Ensembl Genes 100 database, Human genes (GRCh38.p13) dataset (**Supplementary File 1**) (17). Filtering was completed by gene name using an external reference ID list and selecting for the attributes: gene stable ID, gene name, mouse gene stable ID, mouse gene name and gene description. This method was able to identify mouse homologues for the majority of human iron interacting proteins (349/398, 88%). In cases where gene matches were not identified by Ensembl, manual verification was completed and several more matches were identified (8 proteins). Some human iron interacting proteins were found to have no mouse homologues (23 proteins, ex//KDM4E, SCD5, NOX5, etc.) or poor gene annotation limited the identification of matches (18 proteins, ex//CYP2C, FADS2P1, DKFZp686G0638). To obtain further cofactor information regarding protein to iron atom stoichiometry, the Uniprot database was manually searched using the cofactor terms: 4Fe-4S, 3Fe-3S, 2Fe-2S, heme, Fe2+, Fe3+. Retrieved cofactor information was manually added to the list of iron interacting information

Notably, the iron interacting protein list does not include proteins that indirectly interact with iron such as TFRC which interacts with iron *via* intermediate contact with Tf. The resulting list of mouse iron interacting proteins is relatively comprehensive but likely does not include the complete set of iron interacting proteins. For instance, mouse iron interacting proteins with no corresponding human homologue or

homologues that are poorly annotated would not be identified using this method. Alternatively, the possibility also exists that some mouse homologues of human iron interacting proteins may not themselves interact with iron.

Identifying Iron Interacting Proteins in the Howden Dataset

Using bioinformatic methods, the list of mouse iron interacting proteins was compared against the complete list of proteins detected in the Howden dataset as well as individual lists of differentially regulated proteins as copy-number or concentration by T-cell sub-type (CD4-24h, CD8-24h, Th1, CTL). Matches were extracted and can be found in **Supplementary File 2**. In the case of the gene CIAO3, it was noted that the Howden dataset uses the alternative name NARFL. To ensure that NARFL was picked up by our analysis, NARFL was added as an alternative name for CIAO3 in our list of iron interacting proteins.

Pathway Enrichment Analysis

Pathway enrichment for the genes of interest were analysed using unranked lists using the gProfiler algorithm, selecting for the gene ontology (GO) biological processes (18). Term size was limited to 3-500 genes and the significance threshold used was a Benjamini-Hochberg false discovery rate set at <0.05. Only gene intersections greater than 4 were plotted.

Estimating Iron Atom Counts per Protein Species

Copy-number values for iron interacting proteins for each of 0h, 24h and 6d post-activation CD4+ and CD8+ T-cells were extracted from the Howden et al. dataset. If available, iron atom counts per protein were obtained using the Uniprot database cofactor information for each protein. Where iron atom counts were not available on Uniprot, estimates of iron usage per protein species was assumed to be 1 atom for heme and iron ion interacting proteins and 2 atoms for Fe-S cluster interacting proteins. The iron atom estimates per protein species were multiplied by the protein copy-number to produce estimates of iron atoms required by each protein population. The total number of iron atoms required per cell was calculated as the sum of iron atoms required by each protein species, while the "iron need" per cell was calculated as the difference in iron atoms per cell between 0h and 24h post-activation.

To stratify our iron count per protein species by iron interaction we utilised the iron interaction classifications provided by Andreini et al. (12). To stratify by cellular pathway, we utilised the gene sets for the GO terms: iron ion homeostasis (GO:0055072), DNA replication (GO:0006260), iron-sulfur cluster assembly (GO:0016226), oxidative phosphorylation (GO:0006119), aerobic respiration (GO:0009060), histone demethylation (GO:0016577) and DNA demethylation (GO:0080111). We combined the GO terms for oxidative phosphorylation and aerobic respiration due to discrepancies in both GO terms. Where overlaps in genes between GO term gene sets were identified, genes were allocated to the gene set deemed most appropriate: GLRX3, ISCU, ACO1 and NUBP1 were assigned to iron-sulfur cluster assembly and IREB2 was assigned to iron ion homeostasis.

Modelling Iron Uptake Based on TSAT

TSAT values were derived from Tf and serum iron concentrations using the following equations from Yamanishi et al. (19):

$$\text{TSAT}\ (\%) = \frac{[\text{Serum Fe}]\left(\frac{\mu\text{mol}}{\text{L}}\right)}{\text{Total iron binding capacity (TIBC)}\left(\frac{\mu\text{mol}}{\text{L}}\right)} \times 100$$

$$\text{TIBC}\left(\frac{\mu\text{mol}}{\text{L}}\right) = [\text{Tf, g/L}] \times \frac{1\ \text{mol Tf}}{795710\text{g Tf}} \times \frac{10^6\mu\text{mol}}{\text{mol}} \times 2 \quad \text{Fe binding sites}$$

The following equations directly derived from Chasteen, et al. and Aisen, et al. (20, 21) were used to calculate the relative proportions of the 4 Tf forms given any TSAT value. **It should be noted that [Fe] is a RELATIVE unitless value and thus is only useful from within this set of equations.**

Relative association constants for Fe binding to the C and N termini of Tf

$$k'_{1N} = \text{1st atom N terminus binding}$$

$$k'_{2N} = \text{2nd atom N terminus binding}$$

$$k'_{2C} = \text{1st atom C terminus binding}$$

$$k'_{2C} = \text{2nd atom C terminus binding}$$

$$X_A = \text{mole fraction of apoTf} = \frac{1}{1 + (k'_{1N} + k'_{1C})[\text{Fe}] + k'_{1N}k'_{2C}[\text{Fe}]^2}$$

$$X_N = \text{mole fraction of N terminus monoTf} = \frac{1}{1 + \frac{k'_{1C}}{k'_{1N}} + \frac{1}{k'_{1N}[\text{Fe}]} + k'_{2C}[\text{Fe}]}$$

$$X_C = \text{mole fraction of C terminus monoTf} = \frac{1}{1 + \frac{k'_{1N}}{k'_{1C}} + \frac{1}{k'_{1C}[\text{Fe}]} + k'_{2N}[\text{Fe}]}$$

$$X_D = \text{mole fraction of diTf} = \frac{1}{1 + \frac{k'_{2C}+k'_{2N}}{k'_{2C}k'_{2N}[\text{Fe}]} + \frac{1}{k'_{1C}k'_{1N}[\text{Fe}]^2}}$$

$$\text{TSAT}\ (\%) = 50\ (X_N + X_C + 2X_D)$$

Each molar fraction equation was substituted into the TSAT equation as follows:

$$\text{TSAT}\ (\%) = 50\left[\frac{1}{1 + \frac{k'_{1C}}{k'_{1N}} + \frac{1}{k'_{1N}[\text{Fe}]} + k'_{2C}[\text{Fe}]} + \frac{1}{1 + \frac{k'_{1N}}{k'_{1C}} + \frac{1}{k'_{1C}[\text{Fe}]} + k'_{2N}[\text{Fe}]} + \frac{2}{1 + \frac{k'_{2C}+k'_{2N}}{k'_{2C}k'_{2N}[\text{Fe}]} + \frac{1}{k'_{1C}k'_{1N}[\text{Fe}]^2}}\right]$$

The following literature values for relative association constants of iron for Tf were substituted into the equation which was rearranged and solved for the value [Fe] (20):

$$k'_{1N} = 1.00\ k'_{1C} = 2.5 \pm 0.30\ k'_{2N} = 0.66 \pm 0.07\ k'_{2C} = 1.60 \pm 0.30$$

Using the calculated [Fe] value → the values for X_A, X_N, X_C, X_D could be determined, giving the relative molar frequencies of each Tf form. Using Tf concentration ranging from 1-4g/L, estimates of actual concentrations for each Tf form were calculated (22):

$$[\text{apoTf, mol/L}] = [\text{Tf, g/L}] \times X_A \times \frac{\text{mol}}{79570\text{g Tf}}$$

$$[\text{C terminus monoTf, mol/L}] = [\text{Tf, g/L}] \times X_C \times \frac{\text{mol}}{79570\text{g Tf}}$$

$$[\text{N terminus monoTf, mol/L}] = [\text{Tf, g/L}] \times X_N \times \frac{\text{mol}}{79570\text{g Tf}}$$

$$[\text{diTf, mol/L}] = [\text{Tf, g/L}] \times X_D \times \frac{\text{mol}}{79570\text{g Tf}}$$

To determine the relative probabilities of each Tf form binding to TFRC, literature values for association constants for Tf binding to the Tf receptor were used, substituting in the calculated concentrations for each Tf form (23).

$$k_{apo} = \frac{4.6 \times 10^6}{M}$$

$$k_{mono\,C} = \frac{2.5 \times 10^7}{M}$$

$$k_{mono\,N} = \frac{2.8 \times 10^7}{M}$$

$$k_{di} = \frac{1.1 \times 10^8}{M}$$

$$k_{apo} = \frac{4.6 \times 10^6}{M} \times [\text{apoTf, mol/L}]$$

$$k_{mono\,C} = \frac{2.5 \times 10^7}{M} \times [\text{C terminus monoTf, mol/L}]$$

$$k_{mono\,N} = \frac{2.8 \times 10^7}{M} \times [\text{N terminus monoTf, mol/L}]$$

$$k_{di} = \frac{1.1 \times 10^8}{M} \times [\text{diTf, mol/L}]$$

$$P(k_{apo}) = \frac{k_{apo}}{k_{apo} + k_{mono\,C} + k_{mono\,N} + k_{di}}$$

$$P(k_{mono\,C}) = \frac{k_{mono\,C}}{k_{apo} + k_{mono\,C} + k_{mono\,N} + k_{di}}$$

$$P(k_{mono\,N}) = \frac{k_{mono\,N}}{k_{apo} + k_{mono\,C} + k_{mono\,N} + k_{di}}$$

$$P(k_{di}) = \frac{k_{di}}{k_{apo} + k_{mono\,C} + k_{mono\,N} + k_{di}}$$

The weighted iron uptake and cycle time per TFRC protein was calculated as the probability of each Tf form binding to TFRC multiplied by the corresponding number of iron atoms or cycle time. The apoTf cycling time of 60 minutes was derived from Nuñez et al. (24). The diTf cycling time of 14.53 minutes was estimated as the average of cycling times described by 6 different methods in Nuñez et al. (24) and reviewed by Mayle et al. (25). monoTf cycling times were assumed to fall between diTf and apoTf cycling times at an intermediate 37.265 minutes as literature values could not be found.

$$\begin{aligned}\text{iron uptake} = {} & \left(0 \times P(k_{apo})\right) + \left(1 \times P(k_{mono\,C})\right) \\ & + \left(1 \times P(k_{mono\,N})\right) + \left(2 \times P(k_{di})\right)\end{aligned}$$

$$\begin{aligned}\text{cycle time} = {} & \left(60\text{ min} \times P(k_{apo})\right) \\ & + \left(37.265\text{ min} \times P(k_{mono\,C})\right) \\ & + \left(37.265\text{ min} \times P(k_{mono\,N})\right) \\ & + \left(14.53\text{ min} \times P(k_{di})\right)\end{aligned}$$

The time required to uptake the calculated "iron need" was calculated using the Howden et al. average TFRC copy-number at 24h, the iron uptake and cycle time values:

$$\begin{aligned}\text{iron acquired in 1h} = {} & \text{TFRC copy number} \\ & \times \text{iron uptake} \times \left[\tfrac{60\text{ min}}{\text{cycle time}}\right]\end{aligned}$$

$$\text{Time required to meet iron need} = \frac{\text{Iron need}}{\text{Iron acquired in 1h}}$$

Mice

Animal work was conducted under the authority of the UK Home Office project and personal licenses granted under the Animals (Scientific Procedures) Act 1986. Mice were housed in individually ventilated cages.

Inducible hepcidin knockout mice (iHampKO: *Rosa26-CreERT2 Hamp*$^{flox/flox}$) were previously produced in Armitage et al. (26) and feature a fused Cre recombinase-estrogen receptor (CreERT2) protein under the control of a Gt(ROSA)25ser promoter and exons 2 and 3 of *Hamp1* located between LoxP sites. Mice carrying the floxed *Hamp1* loci but lacking the CreERT2 fusion peptide were used as controls (iHampCtrl: *Hamp*$^{flox/flox}$). Administration of tamoxifen induces CreERT2 expression and subsequent *Hamp1* knockout in iHampKO mice but not iHampCtrl mice.

OT-I CD45.1 mice were obtained from Vincenzo Cerundolo, University of Oxford.

C57BL6/J mice were purchased from Envigo.

Immunisation Model

OT-I CD8+ T-cells were adoptively transferred to iHampKO and iHampCtrl mice one day prior to immunisation. For the adoptive transfer, spleens of OT-1 CD45.1 mice were collected, homogenised through a 40 μm filter and treated with red cell lysis buffer. Flow cytometry was used to assess the frequency of OT-I CD8+ T-cells in the suspension which was then was diluted to a concentration of 50000 CD8+ T-cells/mL in PBS. 100 μL containing 5000 OT-I cells was injected intravenously per mouse. Mice were immunised subcutaneously with 100 μL of MVA-OVA at 1 x 10^8 PFU/mL in PBS. At 2 days post-infection, 1 mg of tamoxifen (Sigma, T5648) per mouse was prepared in 90% corn oil and 10% ethanol and administered *via* intraperitoneal injection to induce iron loading in iHampKO mice. At day 7 post-immunisation, mice were euthanised using a rising concentration of CO_2. Spleen and lymph nodes were collected for flow cytometry analysis. For serum analysis blood was collected by cardiac puncture in BD microtainer SST tubes (Beckton Dickinson). Liver was collected in RNAlater (Thermofisher Scientific, AM7020) for RNA analysis.

qPCR

Sections of liver tissue (2-3 mm^3) were homogenised in 700 μL RLT+ buffer using a TissueRuptor (Qiagen). RNA was extracted from 350 μL of the resulting lysate using the Qiagen RNeasy Plus Mini Kit (Qiagen, 74136). RNA concentration and quality was measured using a Nanodrop One machine (Thermofisher Scientific) and cDNA was generated *via* reverse transcription using the High capacity RNA-to-cDNA kit (Applied Biosystems/Thermofisher Scientific, 4388950). qPCR was conducted using the Taqman gene expression master mix (Applied Biosystems/Thermofisher Scientific, 4369016) and the TaqMan Gene Expression Assays for *Hamp1* (Applied Biosystems/Thermofisher Scientific, Mm04231240_s1) and the housekeeping gene *Hprt1* (Applied Biosystems/Thermofisher Scientific, Mm01545399_m1).

Serum Biochemistry

Blood was collected in BD microtainer SST tubes (Beckton Dickinson), allowed to clot and then centrifuged at 8000 g for 5 minutes. Serum was stored at -80°C. Serum measurements were conducted with the MULTIGENT iron kit and the John Radcliffe Hospital, Oxford, UK on an Abbott Architect c16000 automated analyser (Abbott Laboratories).

Th17 Cell Culture

Iron free media was prepared using RPMI-1640 media, 5% pannexin NTS iron free serum substitute (Pan biotech, P04-95080), 1% penicillin/streptomycin and 1% glutamine. Media was supplemented with defined concentrations of human holoTf (R&D systems, 2914-HT-001G/Sigma-Aldrich, T0665) ranging from 0.001-0.625 mg/mL. Additional human apoTf (R&D systems, 3188-AT-001G/Sigma-Aldrich, T1147) was added to maintain a constant total Tf concentration of 1.2 mg/mL.

Murine spleen and lymph nodes were sterilely dissected and homogenised through 40 μm filters using EasySep buffer (Stem cell technologies, 20144). Naïve CD4+ T-cells were isolated using the EasySep Mouse Naïve CD4+ T-cell isolation kit (Stem cell technologies, 19765) and the EasyPlate EasySep magnet (Stem cell technologies, 18102) with the manufacturers protocols. Cells were stained with cell trace violet (Invitrogen, C34557) prior to culture. Cells were plated at a density of 0.5 x 10^6 cells/mL in iron free media with defined holoTf supplementation, 50 μM β-mercaptoethanol and 1 μg/mL α-CD28 (Biolegend, 102115) in 96 well plates pre-coated with 5 μg/mL α-CD3 (Biolegend, 100239) in PBS for 2-3 hours at 37°C. To induce Th17 polarisation, cultures were supplemented with 20 ng/mL IL-6 (Biolegend, 575702), 5 ng/mL hTGF-β1 (Biolegend, 781802), 5 μg/mL α-IFN-γ (Biolegend, 505802) and 5 μg/mL α-IL-4 (Biolegend, 504102). T-cells were cultured for 96-120h at 37°C, 5% CO_2.

Flow Cytometry

For analysis of leukocytes from the immunisation model, spleen or lymph nodes were macerated through 40 μm filters and treated with tris ammonium chloride red blood lysis buffer. Cells were transferred to 96 round bottom plates and washed with PBS.

For analysis of *in vitro* cultured Th17 cells, cell were transferred to round bottom plates. For intracellular cytokine staining, cells were stimulated with cell activation cocktail (1:500) (Biolegend, 423301), brefeldin A (5 μg/mL) (Biolegend, 420601) and monensin (2 μM) (Biolegend, 420701) for 5 hours prior to staining.

The cells were stained with 30 μL of surface stain prepared in PBS and incubated for 20 minutes on ice. Cells were fixed a using fixation buffer (Biolegend, 420801) for 20 minutes on ice or for nuclear staining, cell were fixed with FoxP3 transcription factor fixation buffer (eBioscience, 00-5523-00) for 1 hour on ice. Prior to intracellular staining, cells were permeabilised using perm/wash buffer (Biolegend, 421002) for 20 minutes on ice and then stained with 20-30 μL of intracellular stain in perm buffer. Samples were analysed on an Attune NxT flow cytometer (Thermofisher Scientific) or a BD Fortessa flow cytometer (BD biosciences).

Gating schemes can be found in **Figures S2F** and **S5E**.

Data Analysis

Analysis was completed using Excel (Microsoft) and Prism software (GraphPad), Ensembl (17), Uniprot (16) and gProfiler (18) online programs as well as custom code written using the R programming language.

RESULTS

Identifying Iron Interacting Proteins Differentially Expressed During T-Cell Activation and Differentiation

Our analysis utilised the Howden et al. dataset which consists of quantitative protein mass spectrometry (MS) data for murine CD4+ and CD8+ T-cells at 0 hours, 24 hours and 6 days post-activation. CD4+ and CD8+ T-cells cultured for 6 days were differentiated towards Th1 and cytotoxic T-lymphocytes (CTLs)

respectively and protein expression data at all timepoints was reported by both copy-number and concentration (4). Notably, total cellular protein concentration increases by two to three-fold within 24h post-activation and continues to increase at 6 days (4). Howden et al. considered proteins with fold change values greater than 1.5 and p-values less than 0.05 as significantly differentially regulated; we also utilised these threshold values (4). In contrast to the Howden et al. dataset, the list of iron interacting proteins provided by Andreini et al. focused on human proteins (12). To cross reference the datasets, we compiled a corresponding list of mouse iron interacting proteins *via* searching for homologous proteins (see *Methods*).

Using a computational approach, the list of murine iron interacting proteins was cross compared against the T-cell proteomic profiles provided by Howden et al. Of the 9436 proteins detected in the Howden et al. dataset, 204 were identified as iron interacting proteins (**Supplementary File 2**). This corresponds to a frequency of iron interacting proteins of 2.16% (**Table 1**) which is approximately the frequency expected by chance alone (12). This suggests that there is no apparent detection bias for or against iron interacting proteins in this dataset. However, when stratifying proteins by iron interaction type (Fe-S cluster, heme group or iron ion), heme proteins were underrepresented as assessed by a chi-squared test. While the composition of the original Andreini et al. iron interacting protein list was 48%, 35% and 18% respectively for heme, iron ion and Fe-S clusters (**Table 1**), the Howden data set only contained 28% heme interacting proteins (12).

Iron interacting proteins were also identified amongst proteins considered differentially expressed by copy-number or concentration during T-cell activation (0h *vs* 24h) or differentiation (0h *vs* 6 days) for CD4+ and CD8+ T-cells (**Supplementary File 2**). In all cases, approximately 2% of differentially expressed proteins were identified as iron interacting. When further broken down into heme, iron ion or Fe-S cluster interacting proteins, the frequencies did not deviate significantly from the frequencies observed amongst all detected iron interacting proteins (**Table 1**).

Ribonucleoside-diphosphate reductase subunit M2 (RRM2) was the most highly differentially upregulated iron interacting protein in CD4+ and CD8+ T-cells at both 24h and 6 days (**Figure 1A**). RRM2 is also amongst the top 10 highest expressed iron interacting proteins by absolute copy-number at 6 days post-activation in CD4+ and CD8+ T-cells (**Table 2**). RRM2 is a protein subunit of the ribonucleotide reductase (RNR) which catalyses the reduction step of deoxyribonucleotide synthesis and is essential for downstream DNA synthesis (27, 28). The di-iron centre of RRM2 is critical for RNR catalytic activity and iron chelation with desferrioxamine inhibits RNR activity in leukocytes (28, 29). Given the essentiality of nucleotide synthesis for DNA replication and proliferation, RRM2 appears to be a critical target for iron usage in T-cells.

DNA replication ATP-dependent helicase/nuclease (DNA2), Deoxyhypusine hydroxylase (DOHH) and Prolyl 4-Hydroxylase Subunit Alpha 1 (P4HA1) were also amongst the most highly upregulated iron interacting proteins and were the only other upregulated iron interacting proteins with fold changes greater than 15 in all subsets (**Figures 1B–D**). Similar to RRM2, DNA2 is involved in DNA replication and uses its Fe-S cluster to enable efficient DNA binding and mediation of helicase and nuclease activities (30). DOHH catalyses eIF5A hypusination from polyamines, a process critical for translational efficiency (31). eIF5A hypusination has been implicated in B cell function while polyamine availability and generation is critical for T-cell proliferation and viability (32, 33). P4HA1 is a proline hydroxylase most well-known for its role in collagen synthesis but is also known to hydroxylate other protein targets; the importance of P4H1 in T-cell function is unknown (34). The significant upregulation of these 4 diverse enzymes is testament to the widespread utilisation of iron in cellular function and indicates that iron deficiency may result in complex disruption of cellular activity.

Many of the iron interacting proteins identified by our analysis were differentially regulated in both CD4+ and CD8+ T-cells, highlighting a requirement for similar iron dependent processes.

TABLE 1 | Frequency of iron interacting proteins in the Howden dataset.

			Iron interacting proteins	Heme interacting proteins	Iron ion interacting proteins	Fe-S cluster interacting proteins	p-value
Andreini et al. (12) (human)			~2%	192/398 (48.24%)	139/398 (34.92%)	70/398 (17.59%)	-
All proteins detected by Howden et al. (4)			204/9436 (2.16%)	57/204 (27.94%)	90/204 (44.12%)	60/204 (29.41%)	<0.0001 †
DIFFERENTIALLY EXPRESSED (VS NAÏVE)	CD4+	copy-number	161/6842 (2.35%)	43/161 (26.71%)	71/161(44.10%)	50/161 (31.06%)	0.8764 ‡
	24h	concentration	154/6248 (2.46%)	39/154 (25.32%)	72/154 (46.75%)	45/154 (29.22%)	0.7241 ‡
	Th1	copy-number	175/8032 (2.18%)	46/175 (26.29%)	78/175 (44.57%)	51/175 (29.14%)	0.9122 ‡
	6 days	concentration	146/6503 (2.25%)	44/146 (30.14%)	61/146 (41.78%)	44/146 (30.14%)	0.7877 ‡
	CD8+	copy-number	174/7440 (2.34%)	44/174 (25.29%)	77/174 (44.25%)	56/174 (32.18%)	0.6327 ‡
	24h	concentration	143/6305 (2.27%)	42/143 (29.37%)	60/143 (41.96%)	44/143 (30.77%)	0.8333 ‡
	CTL	copy-number	181/8169 (2.22%)	47/181 (25.97%)	79/181 (43.65%)	58/181 (32.04%)	0.6991 ‡
	6 days	concentration	151/6457 (2.34%)	44/151 (29.14%)	68/151 (45.03%)	42/151 (27.81%)	0.8776 ‡

Frequencies for iron interacting proteins are calculated as a fraction of total proteins detected, frequencies of individual iron interactions (heme, iron ion and Fe-S clusters) are calculated as a fraction of iron interacting proteins. Statistics are chi-square tests for goodness of fit for the distribution of iron ion, heme and Fe-S cluster iron interacting proteins. † The chi-square test was calculated relative to the Andreini dataset (12). ‡ Chi-square tests are calculated relative to the complete set of iron interacting proteins detected in the Howden dataset (4).

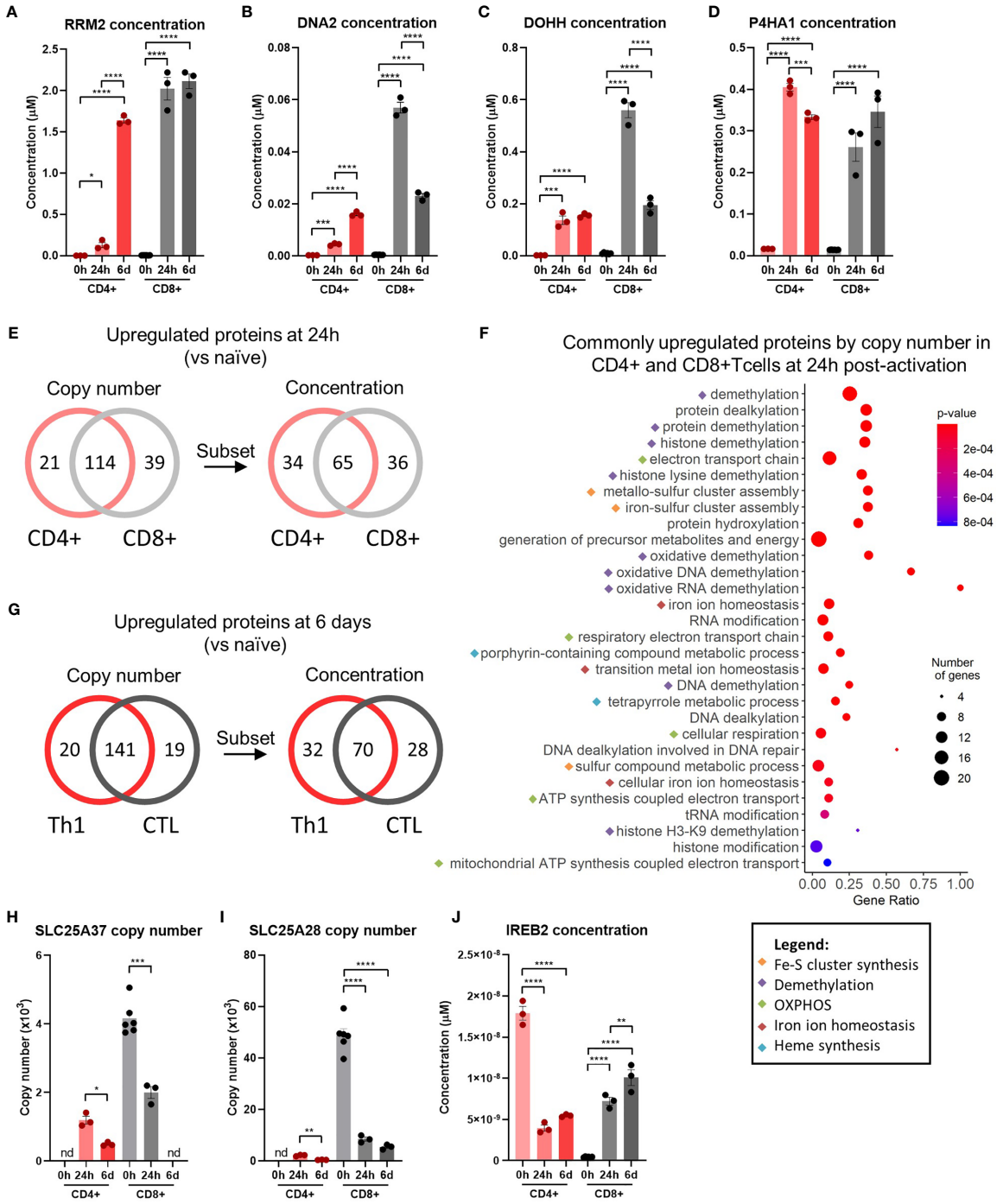

FIGURE 1 | Iron interacting proteins are involved in diverse pathways during T-cell activation. An iron interacting protein list derived from Andreini et al. (12) was cross compared against the Howden dataset (4) consisting of protein-MS data for 0h, 24h and 6 day activated CD4+ and CD8+ T-cells. Protein concentrations for **(A)** RRM2, **(B)** DNA2, **(C)** DOHH and **(D)** P4HA1. **(E)** Number of differentially upregulated iron interacting proteins by copy-number and concentration between 0h and 24h for activated CD4+ and CD8+ T-cells and **(F)** GO term analysis of the 114 commonly upregulated iron interacting proteins by copy-number at 24h. Gene ratios indicate the percentage of gene hits within each GO term set. **(G)** Number of differentially increased iron interacting proteins by copy-number and concentration between 0h to 6 days for activated CD4+ and CD8+ T-cells. Protein copy number for **(H)** SLC25A37 and **(I)** SLC25A28 and protein concentration for **(J)** IREB2. Copy-number and concentration data is derived from the Howden et al. dataset (4). Data is mean ± SEM. Statistics for **(A–D, H–J)** are ordinary one-way ANOVAs with multiple comparisons using Tukey's correction within CD4+ or CD8+ T-cells or in cases where absence of protein detection prevented use of one-way ANOVAs, unpaired t-tests with Welch's correct were used. *$p < 0.05$; **$p < 0.01$; ***$p < 0.001$; ****$p < 0.0001$.

TABLE 2 | Top ten iron interacting proteins ranked by absolute copy-number.

RANK	CD4+ 0h	CD4+ 24h	Th1 6 days	CD8+ 0h	CD8+ 24h	CTL 6 days
1	CYCS	ACO2	PPP1CA	HBB	PPP1CA	CYB5A
2	PPP1CA	GSTP1/2	CYB5A	GSTP1/2	GSTP1/2	PPP1CA
3	ACO2	PPP1CA	GSTP1/2	PPP1CA	CYCS	CYCS
4	CISD1	FTL1/2	CYCS	ACO2	ACO2	GSTP1/2
5	ABCE1	ADI1	BOLA2	FTL1/2	RRM2	ACO2
6	NDUFS1	CYB5A	ACO2	CYCS	FTL1/2	GLRX3
7	CISD2	GLRX3	CYB5B	CYB5A	BOLA2	BOLA2
8	SDHB	ABCE1	RRM2	CYC1	GLRX3	RRM2
9	GSTP1/2	NDUFS1	COPA	UQCRFS1	ABCE1	CYB5B
10	COPA	HBB	GLRX3	NDUFS1	PPAT	COX5A
Cumulative proportion of predicted total cellular iron content	67%	51%	41%	51%	37%	38%

Colours highlight proteins commonly found in the top 10 expressed iron interacting proteins between conditions.

Of the iron interacting proteins that were significantly upregulated 24h post-activation, 114 proteins were found to be commonly upregulated in terms of copy-number in CD4+ and CD8+ T-cells (**Figure 1E**). 65 of these iron interacting proteins were also commonly upregulated in terms of concentration. Since the total protein content of T-cells increases upon activation and differentiation, for the concentration of these proteins to be significantly upregulated, the copy-number value must be experiencing a fold change increase greater than the fold change of total protein content. Thus, the proteins upregulated by concentration are a subset of proteins upregulated by copy-number and represent the most highly upregulated proteins. To understand if specific pathways may be particularly reliant on iron dependent proteins at 24h post T-cell activation, unranked pathway analysis using gProfiler (18) was completed on the sets of 114 iron interacting proteins upregulated by both CD4+ and CD8+ T-cells by copy-number at 24h post-activation (**Figure 1F**). The list of upregulated iron interacting proteins was enriched for GO terms relating to demethylation, Fe-S cluster synthesis, cellular respiration and unsurprisingly, iron homeostasis. The high enrichment of these pathways with iron interacting proteins, suggests that iron scarcity may disproportionately disrupt these processes.

At 6 days post activation, 141 proteins were commonly upregulated (from 0h) in both CD4+ and CD8+ T-cells by copy-number, of which 70 were also increased in concentration (**Figure 1G**). Pathway analysis for the 141 upregulated iron interacting proteins by copy-number produced a very similar list of iron interacting proteins to the enrichment at 24h (**Figure S1A**), indicating the continued necessity of iron dependent processes such as demethylation, OXPHOS and Fe-S clusters throughout T-cell activation and differentiation.

Downregulated iron interacting proteins were far less common (**Figure S1B, C**) but included iron interacting proteins such as albumin (ALB), hemopexin (HPX) and lysine demethylase 7a (KDM7A). Due to the low number of downregulated iron interacting proteins, pathway analysis on these proteins was not performed. However, we were also interested in identifying iron interacting proteins that displayed extreme differences in regulation upon activation between CD4+ and CD8+ T-cells. To do so, we filtered for proteins that showed significant differences in expression upon activation in CD4+ and CD8+ T-cells but in opposite directions. Using this method we identified three iron homeostasis proteins of interest (**Figures 1H–J**). Prior to activation, CD4+ T-cells showed no expression of either SLC25A37 and SLC23A28 (mitoferrins 1 and 2 respectively) which govern mitochondrial iron import (35, 36). In contrast, naïve CD8+ T-cells displayed detectable expression of both importers. Upon activation, CD4+ T-cells marginally but significantly upregulated both SLC25A28 and SLC25A37, while CD8+ T-cells dramatically downregulated both mitochondrial iron import proteins.

Iron response element binding protein 2 (IREB2) also showed divergent regulation in CD4+ and CD8+ T-cells (**Figure 1J**). IREB2 and aconitase 1 (ACO1) are proteins that post-transcriptionally regulate iron homeostasis (37). During cellular iron deficiency, IREB2 and ACO1 induce iron acquisition and retention by stabilising mRNAs that encode iron uptake proteins such as TFRC while blocking translation of mRNAs that encode proteins involved in iron sequestration and egress (37). While CD8+ T-cells increase IREB2 expression upon activation, CD4+ T-cells show downregulation of IREB2. Taken alone, this data may suggest that CD4+ T-cells have a reduced ability to respond to environmental iron signals relative to CD8+ T-cells. However, it should be noted that the significant downregulation of IREB2 in CD4+ T-cells may be partially or completely compensated by ACO1, whose concentration remains relatively constant in CD4+ T-cells at all time points (**Figure S1E**).

Iron Scarcity Impairs Differentiation and Epigenetic Remodelling in Th17 CD4+ T-Cells

Our computational analysis revealed that demethylation is a process highly enriched for iron interacting proteins during

T-cell activation. The dependency of jumonji C domain lysine demethylases (KDMs) and ten-eleven translocation enzymes (TETs) on iron ion co-factors, suggests that iron-deficiency may unduly impair epigenetic remodelling (13, 38). Crucially, activating T-cells dramatically remodel their epigenetic landscapes to suppress expression of genes characteristic of naïve T-cells while permitting transcription of genes required for effector function (39, 40). Iron dependent KDMs showed dramatic changes upon activation in the Howden dataset (**Figure S2A**). KDM6b showed the greatest expression fold-change of all KDMs in CD4+ T-cells and the second greatest fold-change in CD8+ T-cells between 0h and 24h post-activation (**Figure 2A**). KDM6b is responsible for the removal of the repressive histone mark H3K27me3, a process critical for effector function acquisition and CD4+ T cell differentiation (39, 40). Notably, pharmacological inhibition of KDM6b was previously shown to attenuate Th17 CD4+ T-cell responses (39).

Given the importance of KDM6b for Th17 differentiation and the necessity of iron for KDM6b enzymatic activity, we hypothesised that iron starvation may alter T-cell epigenetic remodelling and in consequence Th17 differentiation. To assess the impact of iron deficiency on Th17 CD4+ T-cells we used an *in vitro* iron deficiency model of Th17 polarisation (**Figure 2B**) in which iron is titrated into iron depleted media in the form of

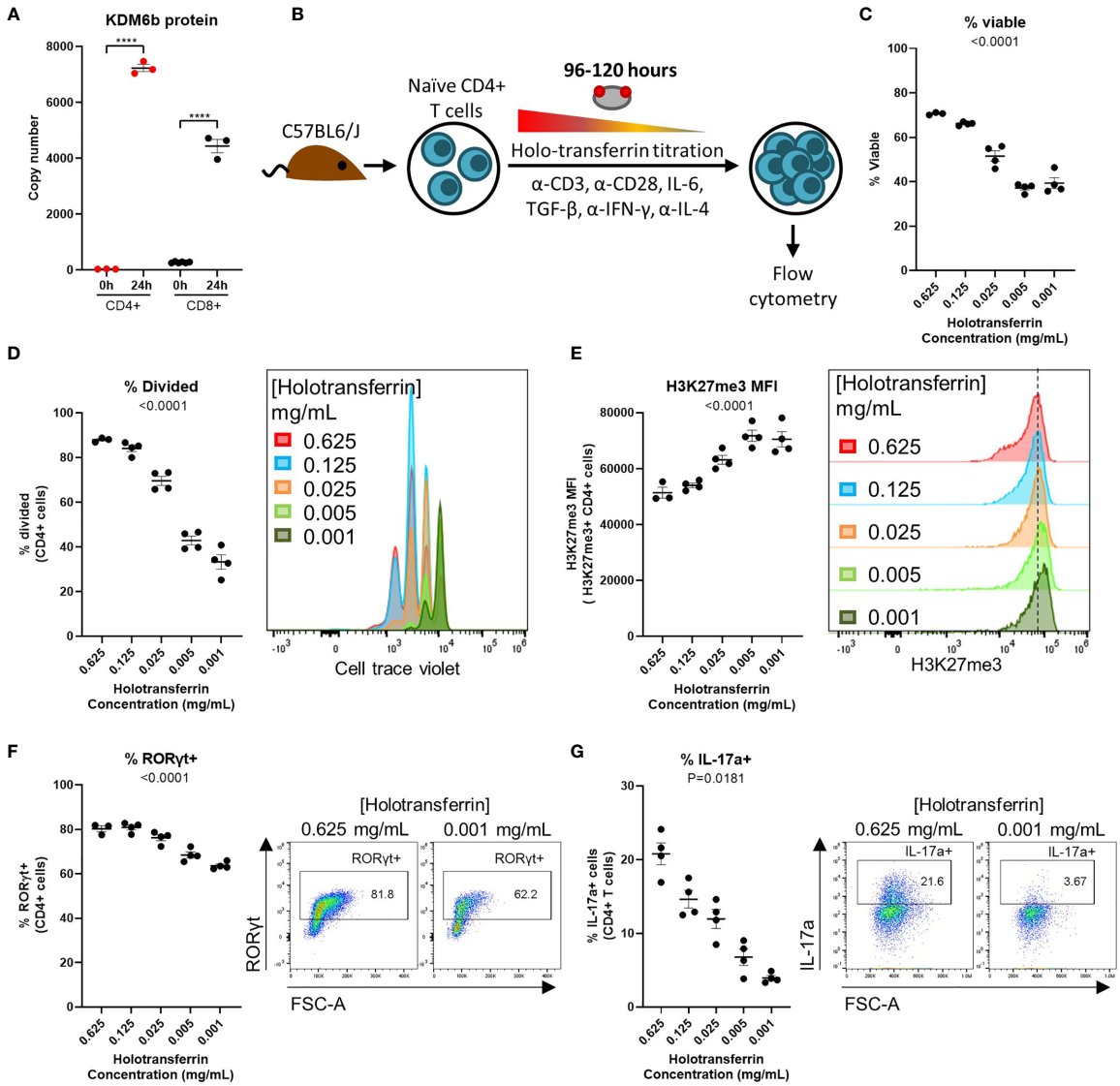

FIGURE 2 | Iron deprived CD4+ T-cells in Th17-polarising conditions display impaired differentiation and epigenetic remodelling. **(A)** KDM6b protein copy number from the Howden et al. dataset (4). **(B)** Th17 iron deficiency model. Naive CD4+ T-cells were cultured in Th17 polarising conditions for 96-120h with holoTf titrated into iron free media at known concentrations. **(C)** Viability, **(D)** proliferation, **(E)** H3K27me3 MFI, **(F)** % RORγt+ cells, and **(G)** % IL-17a+ T-cells for cells cultured in Th17-polarising conditions. Graphs show mean ± SEM. An unpaired t-test was used for **(A)**, mixed effects analysis with repeated measures were used for **(C–F)** and a 1-way ANOVA was used for **(G)**. Data for **(C, D)** and **(E–G)** are representative of 3 and 2 experiments respectively. ****p < 0.0001.

iron-saturated transferrin (Tf), known as holotransferrin (holoTf). As iron availability decreased, CD4+ T-cells in Th17 polarising conditions showed significantly reduced viability and proliferation (**Figures 2C, D**). During iron deficiency, Th17 cells demonstrated elevated H3K27me3 expression (**Figure 2E**) indicating alterations in global chromatin remodelling. Elevated H3K27me3 expression in iron starved Th17 cells could be due to reduced passive loss of methylation by division dilution. However, we found that H3K27me3 levels were also increased in iron deprived T-cells that had not undergone division (**Figures S2B, C**), supporting our hypothesis that high H3K27me3 levels may be attributed to impaired active demethylation by KDM6 enzymes during iron deficiency. A concurrent decrease in the percentage of cells expressing the Th17 lineage defining transcription factor, RORγt, and cytokine, IL-17a, was also observed during iron starvation (**Figures 2F, G**). Cells that manage to divide at least once have some degree of differentiation advantage, as divided cells showed no difference in RORγt expression relative to iron replete controls (**Figures S2D, E**). This data shows that iron availability influences epigenetic regulation and differentiation of Th17 cells.

Estimating T-Cell Iron Content Using Iron Interacting Protein Data

To better comprehend how alterations in iron availability may impact T-cell function, it is useful to assess the cellular iron requirements during activation and differentiation. Using protein copy-number data from the Howden dataset we estimated the average iron requirement of CD4+ and CD8+ T-cells at 0h, 24h and 6d post-activation given the assumption that all iron interacting protein iron binding sites are actively occupied. Where possible, known values of iron atoms per protein species were used based on searching the Uniprot database for iron cofactors (45% of iron interacting proteins in the Howden dataset, **Figure S3A**). In cases where exact values were not readily available, deliberate underestimations of 1 iron atom for heme or iron ion interactions or 2 iron atoms for Fe-S cluster interactions were used, to bias our estimates conservatively.

Naïve CD4+ and CD8+ T-cells had average iron atom estimates of ~$10x10^6$ and $16x10^6$ respectively (**Figure 3A**). Estimates for iron requirements increase by ~2 fold for CD4+ T-cells and ~3 fold for CD8+ T-cells within the first 24h of activation and continue to increase at 6d post-activation. Howden et al. report a very large increase in the expression of the iron import protein, TFRC, throughout T-cell differentiation (3, 4). TFRC likely mediates the uptake of iron required to supply newly synthesised iron interacting proteins with their necessary iron cofactors.

To identify protein species which may collectively bind high amounts of iron due to a combination of high protein expression and/or high iron interacting protein:iron atom stoichiometry and thus act as "iron sinks", we ranked iron interacting proteins by the predicted iron atoms bound by each protein species (**Table 3**). Amongst the protein species predicted to bind the most iron are ACO2, NDUFS1, SDHB and PPP1CA which were expressed at high levels in both CD4+ and CD8+ T-cells at all time points (**Table 3**). Strikingly, the top 10 proteins in each cell type and differentiation state are predicted to contain 48%-73% of all cellular iron.

When iron atom requirements are subdivided by iron interaction, iron atoms utilised in all iron interaction types (Fe-S clusters, ions and heme groups), increase upon activation (**Figure 3B**). At all stages of activation, over 60% of iron atoms in CD4+ and CD8+ T-cells are predicted to be involved in Fe-S clusters (**Figure S3B**). This is largely due to the nature of mammalian Fe-S clusters to contain two to four iron atoms per cluster (4Fe-4S, 3Fe-4S, 2Fe-2S) meaning that Fe-S cluster interacting proteins tend to have greater iron atom stoichiometry relative to heme or iron ion interacting proteins. We also

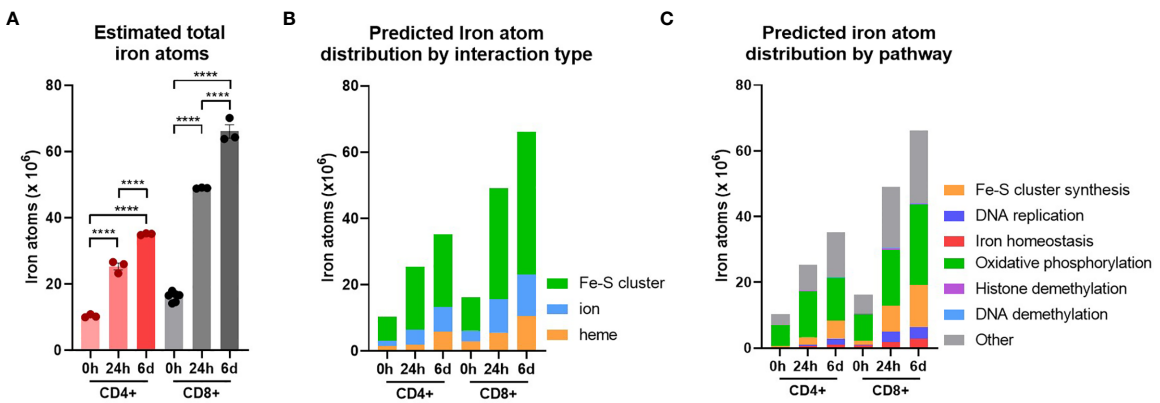

FIGURE 3 | T-cells are predicted to increase total iron content upon activation. Cellular iron atom content was estimated by assuming complete saturation of all iron binding sites by iron interacting proteins. Where possible known values of iron atom:protein stoichiometry were used. If unknown, values were assumed to be 2 for Fe-S clusters, 1 for iron ions and 1 for heme groups. **(A)** Estimates for iron atom counts per cell. Estimates for iron atom distribution by **(B)** interaction type (Fe-S cluster, iron ion, heme group) and **(C)** pathway. Iron interaction information was derived from Andreini et al. (12). Pathways were defined using GO terms (see *Methods*). Data is mean ± SEM. Statistics for **(A)** are ordinary one-way ANOVAs with multiple comparisons using Tukey's correction within CD4+ or CD8+ T-cells. ****$p < 0.0001$.

TABLE 3 | Top 10 iron interacting proteins ranked by predicted iron atoms per protein species.

RANK	CD4+ 0h	CD4+ 24h	Th1 6 days	CD8+ 0h	CD8+ 24h	CTL 6 days
1	ACO2	ACO2	ACO2	ACO2	ACO2	ACO2
2	NDUFS1	NDUFS1	SDHB	NDUFS1	NDUFS1	NDUFS1
3	SDHB	SDHB	PPP1CA	SDHB	SDHB	SDHB
4	CYCS	GSTP1	BOLA2	HBB-BS	PPP1CA	HBB-BS
5	PPP1CA	NDUFS8	NDUFS1	GSTP1	PPAT	GSTP1
6	CISD1	PPP1CA	CYB5A	PPP1CA	NUBP2	PPP1CA
7	NDUFV1	PPAT	GSTP1	NDUFS8	BOLA2	NDUFS8
8	NDUFS2	NDUFV1	NUBP2	NDUFV1	GSTP1	NDUFV1
9	ABCE1	NUBP2	CYCS	FTL1	CYCS	FTL1
10	CISD2	GLRX3	NUBP1	CYCS	GLRX3	CYCS
Cumulative proportion of predicted total cellular iron content	73%	64%	52%	61%	48%	48%

Colours indicate iron interacting proteins commonly predicted to be amongst the top 10 that sequester iron between conditions.

observed the enrichment of Fe-S cluster synthesis proteins detected *via* GO term enrichment at 24h and 6d of activation (**Figures 1F** and **S1A**). Upregulation of Fe-S cluster synthesis machinery is required to facilitate the predicted high Fe-S cluster demand (**Figure 3B**).

While the GO term analysis enabled us to identify the most commonly differentially regulated pathways between T-cell subsets, it did not provide information as to the pathways that are most iron demanding. Using the gene set enrichment data, we identified GO terms of 6 different major iron requiring pathways. Using the gene sets for each term, we stratified our estimated iron counts per protein species by pathway. This analysis predicts that the largest proportion of iron atoms per T-cell are being utilised within OXPHOS (**Figure 3C**). In naïve T-cells, approximately 60% of iron atoms are localised in OXPHOS proteins. Following activation, the proportion of iron atoms in OXPHOS proteins, while still being the largest iron utilising pathway of the 6 we analysed, drops to approximately 40%. However, it should be noted that the absolute number of iron atoms in the OXPHOS pathway does increase with activation (**Figures 3C** and **S3C**). Notably, OXPHOS contains a high number of iron interacting proteins with relatively high stoichiometry of iron atoms per protein. For instance, NDUFS1 of CI contains 3 Fe-S clusters alone, corresponding to a total of 10 iron atoms. The majority of the iron interactions in the electron transport chain are with Fe-S clusters which partially accounts for the predicted high number of Fe-S cluster interactions within the cell (**Figure 3B**). Given the high demand for Fe-S clusters, Fe-S cluster synthesis was unsurprisingly predicted to have the second highest proportion of iron atoms. Moreover, the proportion of iron atoms in this pathway increases upon activation, again indicating the importance of Fe-S cluster synthesis during T-cell activation.

DNA replication was also a major hub of iron utilisation in 24h and 6d stimulated T-cells (**Figure 3C**). This is in agreement with the observation that RRM2, DNA2 and other iron requiring DNA replication enzymes (POLE, POLA1, PRIM2) were amongst the most upregulated iron interacting proteins post-activation. In contrast, while methylation was a top hit in gene enrichment analysis, both histone and DNA methylation make minor contributions of iron atoms to total predicted cellular iron content (**Figure 3C**). This discrepancy may be partially explained by the nature of demethylase iron interactions. While many of the enzymes involved in OXPHOS and DNA synthesis interact with Fe-S clusters containing two or more iron atoms, the JmjC KDM demethylases interact with singular iron atoms. Nevertheless, the prominence of JmjC KDM enzymes in our pathway analysis of commonly upregulated proteins is consistent with our *in vitro* data indicating the importance of iron for T-cell methylation remodelling (**Figure 2E**).

Modelling T-Cell Iron Uptake Dynamics

The iron import protein, TFRC, is critical for immunological function and is upregulated upon T-cell activation (3–5). TFRC iron uptake is facilitated *via* binding to the serum iron binding protein transferrin which induces receptor mediated endocytosis (41). Once internalised, acidification of the endosome promotes iron release from Tf allowing for cellular use (41). TFRC is subsequently recycled back to the cell surface to complete an endocytic cycle (41).

Tf has two asymmetric iron binding sites located at the C and N termini of the protein with different iron binding affinities (20). Therefore, Tf can exist in 4 different forms depending on iron occupancy; apotransferrin (apoTf), C or N terminus monoferric Tf (monoTf), and diferric Tf (diTf), which bind to 0, 1 and 2 iron atoms respectively (20). Notably, all 4 forms are capable of binding and inducing endocytosis of TFRC, albeit with different affinities and with different endocytic cycling periods (23, 24). Since apoTf is also capable of binding and inducing endocytosis of TFRC, high levels of apoTf can effectively inhibit iron uptake *via* accumulation of TFRC within endosomes (24). Using equations developed by Aisen *et al*, the relative proportions of each Tf form can be calculated given the overall Tf saturation (TSAT) level (20, 21). Using

known association constant values for TFRC binding to each Tf form we calculated the relative probabilities of TFRC binding to each Tf form (22, 23). With the calculated relative probabilities for TFRC-Tf binding, we estimated the average iron uptake and cycling time per TFRC protein for any given TSAT value.

Using this model, the time required to obtain the calculated 24h "iron need" was determined. "Iron need" was calculated as the difference in estimated iron atoms between 0h and 24h post activation (**Figure 4A**). It should be noted that our "iron need" predictions do not take into account intracellularly stored ferritin bound iron that may be released following activation. Ferritin levels are observed to increase in T-cells post-activation (**Figures S4A, B**) but how this influences access to cellular iron in T-cells is unknown. In our model, the rate at which T-cells are capable of taking up iron is a factor of TFRC expression. While CD4+ T-cells show reduced "iron need" relative to CD8+ T-cells, since CD4+ T-cells express lower levels of TFRC, this results in an increased "iron need":TFRC ratio which is reflected in the slower iron uptake by CD4+ T-cells observed in our model (**Figures 4B, C**). The reduced rate of iron uptake by CD4+ T-cells in this model may indicate that CD4+ T-cells may be more sensitive to iron deprivation. Given that TFRC expression is at least partially driven by iron response proteins (IREB2 and ACO1) during T-cell activation (3), the lower ability to upregulate TFRC relative to predicted "iron need" in CD4+ T-cells may be due to the observed suppression of IREB2 in activated CD4+ T-cells relative to CD8+ T-cells.

In humans, TSAT values between 25-45% are considered normal, with TSAT values <16% defined as iron deficient by the World Health Organization (22, 42). In the context of inflammation, TSAT values <20% are often considered iron deficient (43). Our model predicts that T-cells will no longer be able to meet their iron requirements (over 24 hours) at TSAT values of ~10-20% (**Figure 4C**). This supports the idea that clinically defined iron deficiency is likely to impact on T-cell mediated immunity. Notably, our model demonstrates that the T-cells of individuals with TSAT values within the normal range should be able to easily meet iron requirements and it is unclear that there is any iron-acquisition benefit to T-cells with TSAT values greater than ~45%, for example as occurs in haemochromatosis and thalassaemia.

Given TSAT is derivable from Tf and serum iron concentrations, we were also able to model the rate of iron uptake based on these factors (**Figures 4D, E**). As Tf concentrations drop (as occurs

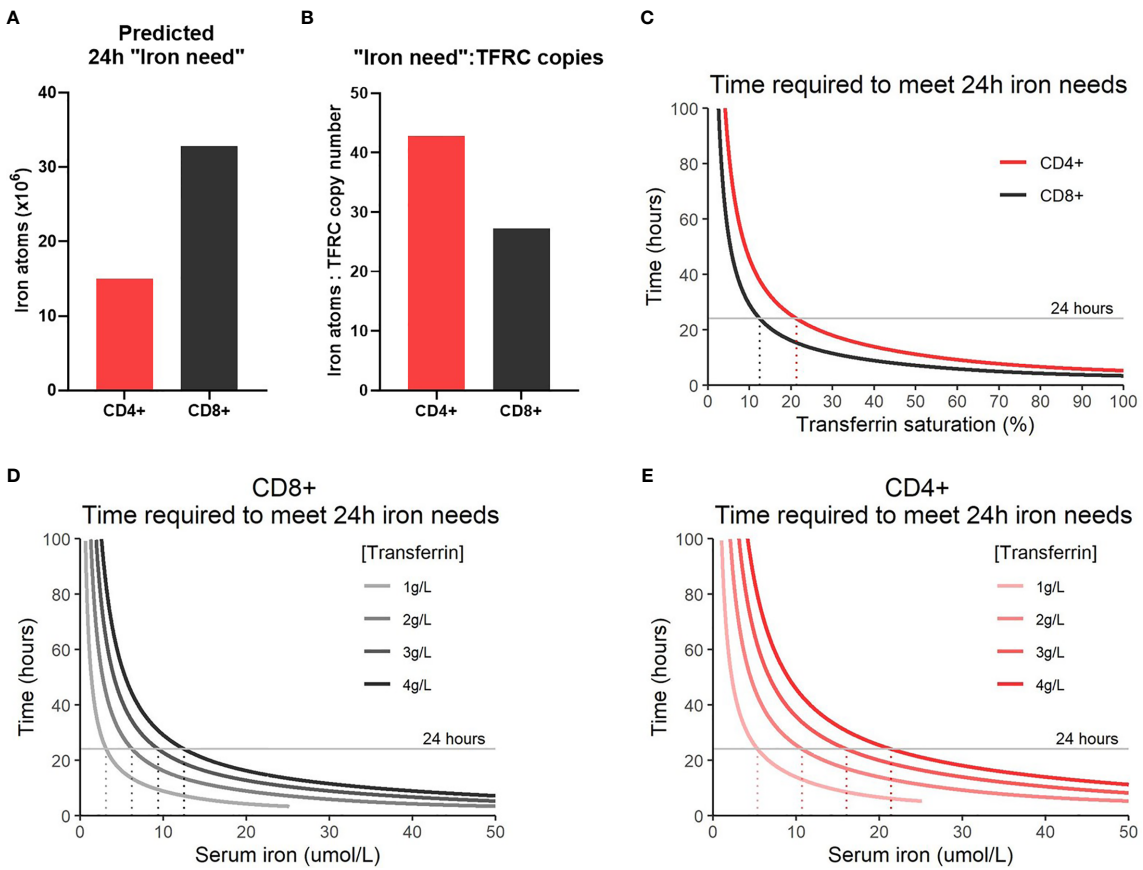

FIGURE 4 | Modelling iron atom acquisition in the first 24h post-activation. **(A)** 24h "iron-need" and the **(B)** 24 "iron-need":TFRC copy ratio. 24h "iron-need" is the difference in iron atom estimates between 0h and 24h. **(C)** Model of the time required for T-cells to acquire their 24h "iron need" *vs* TSAT. TSAT is a function of serum iron and Tf concentration. Models of the time required for **(D)** CD8+ and **(E)** CD4+ T-cells to acquire their 24h "iron need" at different serum iron concentrations.

physiologically during inflammation), our model predicts that the time required to meet cellular "iron need" also falls regardless of serum iron concentration. This is because suppression of Tf expression while iron concentrations remain constant effectively drives up the TSAT value and increases the probability of diTf : TFRC binding. Generally, our model indicates that suppression of serum iron levels may prevent T-cells from acquiring sufficient iron for activation needs, but that sensitivity of activated T-cells to low iron may be more pronounced in nutritional iron deficiency (in which transferrin levels are high-normal) compared to inflammatory hypoferremia (in which transferrin is low).

Iron Overload Does Not Provide Significant Benefits to CD8+ T-Cells During Activation

Our mathematical model predicts that iron levels above the normal physiological range are unlikely to provide significant quantitative benefit to activating T-cells. To evaluate the impact of excess iron on T-cell immune responses and function, we utilised an inducible hepcidin knockout mouse [iHampKO: *Rosa26-CreERT2 Hamp*$^{flox/flox}$, described previously (26)], which displays rapid serum iron loading following tamoxifen treatment. Hepcidin is a liver produced hormone that regulates systemic blood iron by inhibiting macrophage mediated iron recycling and dietary iron absorption (44); consequently, when its deletion is induced, iron is released to serum from macrophages and dietary iron absorption is enhanced leading to iron loading.

Ovalbumin (OVA) specific OT-I CD8+ T-cells were adoptively transferred to iHampKO or iHampCtrl (*Hamp*$^{flox/flox}$) mice which were subsequently immunised with modified vaccinia virus Ankara-OVA (MVA-OVA) (**Figure 5A**) to induce a proliferative anti-OVA specific CD8+ T-cell response. Tamoxifen treatment was given at 2 days post-immunisation to induce *Hamp1* knockout resulting in elevated serum iron during the period of T-cell activation (**Figures 5B, C**). We then analysed the response of functionally wild type antigen specific T-cells in the context of systemic hepcidin deficiency and consequent iron loading. Consistent with our mathematical model, elevation of serum iron did not confer a proliferative benefit to T-cells. Comparable frequencies of OVA-specific T-cells were observed between iHampCtrl and iHampKO mice in both lymph nodes and spleen (**Figures 5D** and **S5A**). A higher frequency of OT-I cells expressing GZMB (a key mediator of cytolytic activity) was observed in lymph nodes (but not spleen) of iron loaded animals; the expression level [median fluorescent intensity (MFI)] of GZMB was not affected by iron loading (**Figures 5E, F** and **S5B, C**). TFRC expression is inversely proportional to cellular iron (45). Expression of TFRC by splenic and lymph node OT-I cells was slightly but significantly lower in iHampKO mice, consistent with activated OT-I cells acquiring more iron from a high serum iron environment (**Figures 5G** and **S5D**).

DISCUSSION

Using a combination of data mining from publicly available datasets and experimental methods, we investigated the dynamics of iron and iron interacting proteins during T-cell activation and differentiation. Our analysis indicates that T-cells rapidly and substantially increase iron demands post-activation for use in diverse cellular pathways including OXPHOS, demethylation and DNA synthesis. As evidence for the potential impact of iron deficiency on T-cell biochemistry, we show that iron depletion impairs removal of a key suppressive histone methylation mark and differentiation in an *in vitro* model of Th17 polarisation. In contrast, excess iron was shown to have no significant quantitative benefit for T-cell responses *in vivo* in comparison to control iron replete animals.

T-cell pathways enriched for iron interacting proteins such as DNA synthesis, OXPHOS, demethylation and Fe-S cluster biogenesis may be particularly susceptible to dysfunction during iron deficiency. Iron atoms in Fe-S clusters seem especially important as they make up the majority of predicted iron atoms per cell. Fe-S cluster biogenesis appeared as a top hit in pathway enrichment and showed an increase in the proportion of iron atoms in that pathway during T-cell activation. Further, Fe-S cluster synthesis feeds into many pathways including OXPHOS which was predicted to be the pathway with the highest concentration of iron atoms. *In vitro* iron deprived T-cells have been shown to suppress mitochondrial ATP generation, further reinforcing the necessity of iron for T-cell OXPHOS (3).

Using our computational analysis alone, it is difficult to evaluate the degree of impairment of iron deficiency on independent processes. For instance, histone and DNA demethylation were identified as critical iron dependent processes due to the high number of individual iron interacting proteins in these pathways. But, the absolute number of iron atoms attributed to DNA and histone demethylases is relatively low compared to OXPHOS and Fe-S cluster synthesis. However, using the computational analysis as a foundation, we predicted that KDM6b may be a major iron-demanding epigenetic regulator. Using experimental methods we show that iron deprivation impairs chromatin remodelling in Th17 cells with elevated expression of the KDM6b target, H3K27me3. While we cannot be certain that the increase in H3K27me3 is due to reduced demethylation by KDM6A/B rather than increased methylation, previous studies have indicated that inhibition of KDM6A/B does impair Th17 differentiation and CD8+ T-cell proliferation and memory formation (39, 46). In contrast, while DNA synthesis did not score amongst the highest enrichment terms in pathway analysis, two critical enzymes involved in DNA synthesis, RRM2 and DNA2, were amongst the most highly differentially regulated iron interacting proteins in activated T-cells, indicating that iron dependent DNA synthesis proteins are likely critical for T-cell activation. This is in agreement with previous data showing that *in vitro* iron deprivation impairs DNA synthesis and cell-cycle progression in CD8+ T-cells (3).

It is still unclear how iron depletion affects intracellular iron distribution. Data from the Howden dataset showed that Mitoferrins 1 and 2, which mediate mitochondrial iron transport, have different expression kinetics in CD4+ and CD8+ T-cells. Given that pathway analysis highlighted that

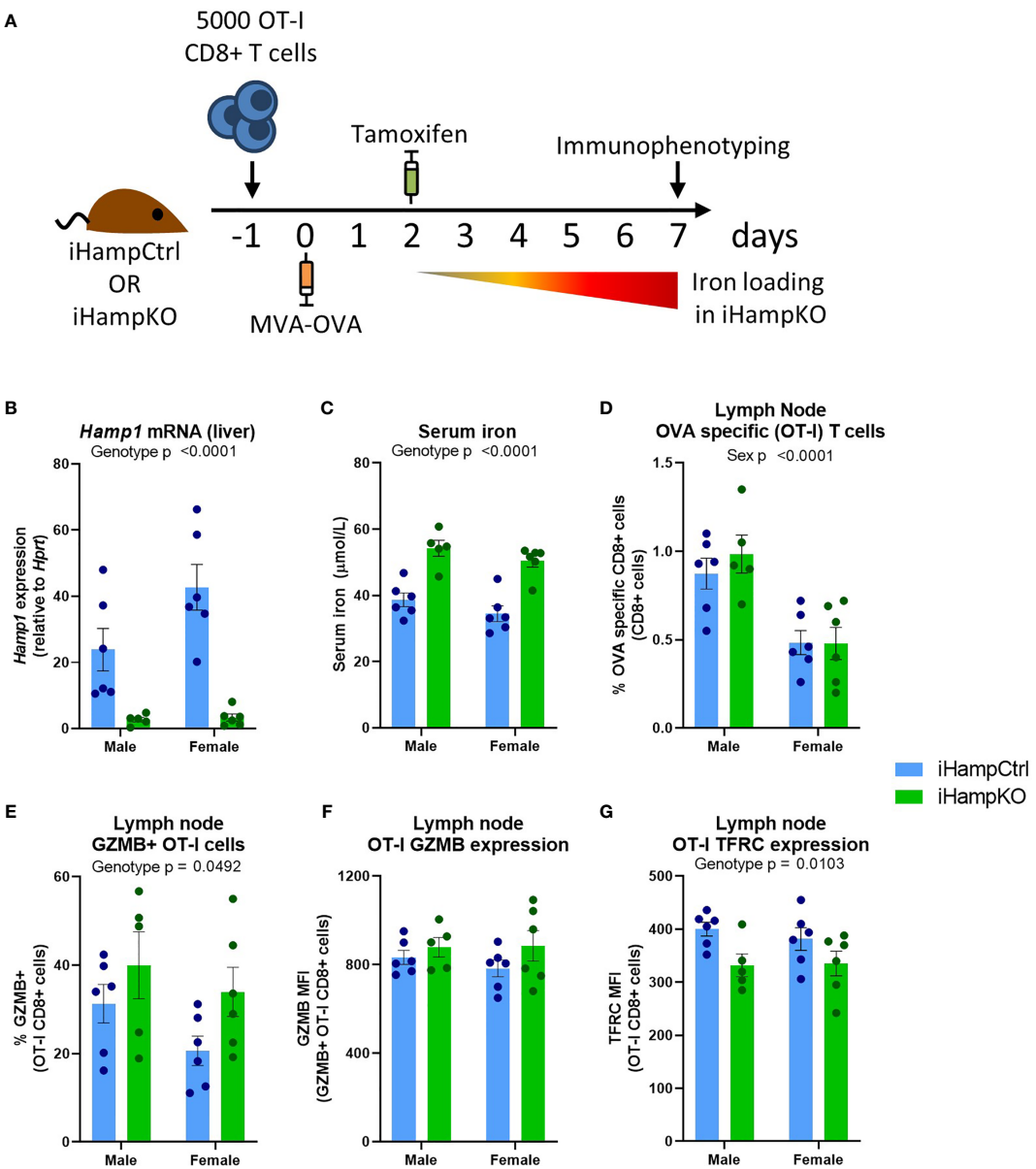

FIGURE 5 | Induction of elevated serum iron does not significantly benefit activating T-cells. **(A)** Experimental setup. On day -1, 5000 OT-I CD8+ T-cells were adoptively transferred to iHampCtrl and iHampKO mice followed by immunisation with MVA-OVA at day 0. Iron loading was induced in iHampKO mice with tamoxifen on day 2 post-immunisation. **(B)** Liver *Hamp1* mRNA expression and **(C)** serum iron. Flow cytometry of lymph nodes was conducted at day 7 post-immunisation. Lymph node **(D)** OT-I frequency, **(E)** frequency of GZMB+ OT-Is, **(F)** GZMB MFI of GZMB+ OT-I cells and **(G)** OT-I TFRC median fluorescence index (MFI). Graphs shown mean ± SEM. Statistics for **(B–G)** are 2 way ANOVAs.

iron dependent mitochondrial pathways such as OXPHOS, Fe-S cluster synthesis and heme synthesis are commonly upregulated in both CD4+ and CD8+ T-cells, it seems counterintuitive that mitochondrial iron transporters show different kinetics of expression in these two cell types. One may speculate that CD4+ and CD8+ T-cells may differentially store and re-distribute iron throughout the cell prior and during activation. The ability of different T-cell subsets to move iron into the mitochondria could profoundly affect the nature of iron interactions in the cell as the flux of iron into mitochondrial heme and Fe-S cluster biosynthetic pathways could present a major bottleneck for cellular iron usage.

Using protein copy-number values we estimated the total number of iron atoms per cell at various stages of activation and predicted that T-cell iron content increases 2-3 fold post-activation. The dramatic transition from quiescent naïve cells with relatively low estimated iron content to rapidly proliferating activated cells with elevated predicted iron content provides a

rationale as to why cellular iron deficiency appears to more significantly impair activated versus naïve cells. Humans and mice carrying a TFRC mutation which impairs iron uptake have normal percentages of circulating naïve CD4+ and CD8+ T-cells, however, TFRC mutant T-cells fail to proliferate upon activation stimuli both *in vitro* and *in vivo* (3, 5). The quiescent state of naïve T-cells likely means that once adequate cellular iron is acquired, supply of iron to iron-dependent proteins can be maintained through internal turnover of iron binding proteins.

Measures of naïve T-cell iron have previously been evaluated using inductively coupled plasma mass spectrometry (ICP-MS) where iron measures for bulk T-cells were divided by the number of input cells (47). Our predicted iron content for naïve T-cells was approximately the same as the 75 percentile value for CD8+ T-cells and 1.5 fold higher than the 75 percentile value for CD4+ T-cells as measured by Konz et al. (47). While our values are on the high end of the values reported by Konz *et al*, they are of a similar magnitude giving us confidence in our methods of estimation.

Using the estimated iron counts per cell and existing kinetic data for Tf-TFRC endocytic cycling kinetics, we constructed a model to simulate T-cell iron uptake at various TSAT values. Our model predicts that at TSAT values between 10-20%, T-cells would no longer be able to acquire the iron they need to maintain occupancy of all iron binding sites. Low TSAT can occur either due to nutritional iron deficiency or due to inflammatory hypoferraemia caused by severe infections and/or chronic inflammation. For example, in SARS-CoV2 infection, several studies of hospitalised COVID-19 patients report average TSAT values of well below 15% with some patients with severe disease having TSAT values as low as 5% (48–51). Our model suggests that at such very low TSATs, T-cells are unlikely to be able to acquire sufficient iron for effective activation and differentiation. Suppression of Tf concentration from normal levels (2-3.5g/L) (22) has been observed during COVID-19 infection as well as other inflammatory states such as sepsis (48, 50–52). Suppression of Tf may be a compensatory mechanism to attempt to maintain TSAT homeostasis levels to preserve a constant rate of iron availability to the host immune system during hypoferremia.

Our model suggests that the economic theory of diminishing returns may be applicable to cellular iron nutrition: beyond a critical threshold, additional iron is unlikely to provide additional benefit. Once all iron binding proteins become saturated and are operating at peak rates, additional iron supply likely holds no advantage and may eventually become detrimental given the inherent toxicity of unchelated iron. The observation that T-cells activated in iron loaded conditions downregulate TFRC suggests that T-cells have an upper limit of desired cellular iron. In support of the non-linearity of our mathematical model, previous work from our group shows that serum iron restriction mediated *via* administration of a mini-hepcidin analogue significantly impairs both CD8+ and CD4+ T-cell proliferation and functionality in the context of diverse vaccination models and influenza infection (3). In contrast, we demonstrate that increasing serum iron beyond physiological levels *via* an inducible hepcidin knockout mouse model, does not enhance CD8+ T-cell proliferation or GZMB expression compared to iron replete control mice. Similarly, injection of wild-type mice on a standard diet with iron dextran, which increases serum iron, does not induce CD8+ T-cell proliferation beyond normal levels after immunisation (3). Recently, it has been reported that high iron concentrations may suppress CD4+ T-cell proliferation and Th1 differentiation (53), indicating that there may be complex context-dependent effects of excess iron on CD4+ T-cells. These data indicate that while iron supplementation may be able to boost immunity in individuals with existing iron deficiency, supplementing iron in iron replete individuals may provide little benefit.

Limitations

One limitation to our bioinformatic approach relates to the input data. For instance, it was noted that the iron interacting protein SDHD was not detected in the Howden dataset. Given that SDHD is an essential component of complex II (CII) of the electron transport chain and all other CII proteins (SDHA, SDHB, SDHC) were detected, the absence of SDHD points to incomplete protein detection in the Howden dataset. Unfortunately, in most cases it is difficult to know whether lack of detection is due to biological or technical reasons limiting our capacity to account for undetected proteins when calculating T-cell iron content. Whether differences in the proportions of proteins involved in different types of iron interactions (heme, Fe-S cluster or iron ions) are inherent to the T-cell proteomic profiles or are due to a detection bias in the protein-MS method also remains to be determined.

When estimating T-cell iron content, we used known iron atom:protein stoichiometry values where possible. However, in cases where values were not readily available, we assumed low values of 1, 1, and 2 iron atoms for each of iron ion, heme and Fe-S cluster interactions respectively to minimise the probability of overestimating iron content. While known or cautious estimates for iron content can be made for most proteins, approximations for iron bound in ferritin complexes is difficult to assess given that ferritin cages can contain anywhere from 0 to ~4300 iron atoms (54). Ferritin levels do increase upon T-cell activation (**Figures S5A, B**), however, whether the iron content of ferritin cages changes with activation is also unknown. In our analysis, ferritin light and heavy chains (FTL1/2 and FTH1) were treated similarly to all other iron ion binding proteins and were assumed to bind one iron atom per protein. Thus, each ferritin complex is assumed to contain 24 iron atoms. Again, this is likely to result in a conservatively low approximation of T-cell iron content. It should be noted that the inability to properly assess ferritin iron content also impacts the predicted T-cell "iron need" as ferritin is likely to supply at least a fraction of the cellular iron requirements during activation. If naïve T-cells contain variable amounts of ferritin iron as a function of underlying iron status of the individual, this could influence the subsequent sensitivity of T-cells to extracellular iron sources following activation. Nevertheless, other evidence strongly supports a likely general dominant dependence of T-cell responses on extracellular iron. TFRC expression is upregulated over 200-fold following T-cell activation, and decreasing extracellular iron availability profoundly suppresses T-cell responses to

immunization even in iron-replete animals (3, 4). Furthermore, a mutation in TFRC that reduces efficiency of extracellular iron uptake by ~50% causes severe immunodeficiency in children (5). While many of our assumptions aimed to bias our estimates conservatively, we also assume complete saturation of iron binding sites, likely overestimating iron binding per protein species. Perhaps as a result of these balancing assumptions we produced iron content estimates which are of a similar magnitude to experimentally observed values (47).

When building our model for T-cell iron uptake, we assumed that TFRC values increase instantaneously from 0h levels to 24h levels, whereas this process, although very rapid, will take longer. Neither does the model account for the increased TFRC expression that would occur in response to iron deficiency at low TSAT values. While the absolute relationship between TSAT and time required to meet T-cell iron needs may be inaccurate due to the reported limitations, the shape of the relationship is likely correct as evidenced by experimental data indicating that while low serum iron severely impairs T-cell responses (3), elevated serum iron has negligible beneficial effects (**Figure 5**).

In summary, using computational and experimental methods we have demonstrated the diverse nature of iron-interacting proteins in T-cell biology. We show evidence for effects of iron deficiency on epigenetic remodelling and T-cell differentiation, and describe the distinct impacts of iron scarcity and overload on T-cell responses.

DATA AVAILABILITY STATEMENT

The original contributions presented in the study are included in the article/**Supplementary Material**. Further inquiries can be directed to the corresponding author.

ETHICS STATEMENT

Animal procedures were performed under the authority of UK Home Office project and personal licenses in accordance with the Animals (Scientific Procedures) Act 1986, and were approved by the University of Oxford ethical review committee.

AUTHOR CONTRIBUTIONS

MT designed the computational analysis. MT and JF designed and executed the experiments and analysed the resulting data. MT wrote the manuscript. AA and HD provided scientific guidance and supervised the project. All authors contributed to the article and approved the submitted version.

FUNDING

This work was supported by the UK Medical Research Council (MRC Human Immunology Unit core funding to HD, award no. MC_UU_12010/10) and with the support of the Clarendon Fund and the Corpus Christi College A. E. Haigh graduate scholarship to MT.

ACKNOWLEDGMENTS

The authors thank the staff of the Department of Biomedical Services, University of Oxford for animal husbandry, Alireza Morovat (Clinical Biochemistry, Oxford University Hospitals NHS Foundation Trust) for assistance with biochemical measurements, the Weatherall Institute of Molecular Medicine flow cytometry facility and members of the Cantrell Lab, University of Dundee, for many helpful discussions.

SUPPLEMENTARY MATERIAL

The Supplementary Material for this article can be found online at: https://www.frontiersin.org/articles/10.3389/fimmu.2021.714613/full#supplementary-material

REFERENCES

1. Wei J, Raynor J, Nguyen T-LM, Chi H. Nutrient and Metabolic Sensing in T Cell Responses. *Front Immunol* (2017) 8:247. doi: 10.3389/fimmu.2017.00247
2. Preston AE, Drakesmith H, Frost JN. Adaptive Immunity and Vaccination – Iron in the Spotlight. *Immunother Adv* (2021) 1(1):1–11. doi: 10.1093/immadv/ltab007
3. Frost JN, Tan TK, Abbas M, Wideman SK, Bonadonna M, Stoffel NU, et al. Hepcidin-Mediated Hypoferremia Disrupts Immune Responses to Vaccination and Infection. *Med (NY)* (2021) 2(2):164–79.e12. doi: 10.1016/j.medj.2020.10.004
4. Howden AJM, Hukelmann JL, Brenes A, Spinelli L, Sinclair LV, Lamond AI, et al. Quantitative Analysis of T Cell Proteomes and Environmental Sensors During T Cell Differentiation. *Nat Immunol* (2019) 20(11):1542–54. doi: 10.1038/s41590-019-0495-x
5. Jabara HH, Boyden SE, Chou J, Ramesh N, Massaad MJ, Benson H, et al. A Missense Mutation in TFRC, Encoding Transferrin Receptor 1, Causes Combined Immunodeficiency. *Nat Genet* (2016) 48(1):74–8. doi: 10.1038/ng.3465
6. Stoffel NU, Uyoga MA, Mutuku FM, Frost JN, Mwasi E, Paganini D, et al. Iron Deficiency Anemia at Time of Vaccination Predicts Decreased Vaccine Response and Iron Supplementation at Time of Vaccination Increases Humoral Vaccine Response: A Birth Cohort Study and a Randomized Trial Follow-Up Study in Kenyan Infants. *Front Immunol* (2020) 11(1313):1–16. doi: 10.3389/fimmu.2020.01313
7. Fülöp TJr., Wagner JR, Khalil A, Weber J, Trottier L, Payette H. Relationship Between the Response to Influenza Vaccination and the Nutritional Status in Institutionalized Elderly Subjects. *J Gerontol A Biol Sci Med Sci* (1999) 54(2):M59–64. doi: 10.1093/gerona/54.2.M59
8. Leung S, Holbrook A, King B, Lu HT, Evans V, Miyamoto N, et al. Differential Inhibition of Inducible T Cell Cytokine Secretion by Potent Iron Chelators. *J Biomol Screen* (2005) 10(2):157–67. doi: 10.1177/1087057104272394
9. Yarosz EL, Ye C, Kumar A, Black C, Choi EK, Seo YA, et al. Cutting Edge: Activation-Induced Iron Flux Controls Cd4 T Cell Proliferation by

Promoting Proper IL-2R Signaling and Mitochondrial Function. *J Immunol* (2020) 204(7):1708–13. doi: 10.4049/jimmunol.1901399
10. Wang Z, Yin W, Zhu L, Li J, Yao Y, Chen F, et al. Iron Drives T Helper Cell Pathogenicity by Promoting Rna-Binding Protein Pcbp1-Mediated Proinflammatory Cytokine Production. *Immunity* (2018) 49(1):80–92.e7. doi: 10.1016/j.immuni.2018.05.008
11. Coffey R, Ganz T. Iron Homeostasis: An Anthropocentric Perspective. *J Biol Chem* (2017) 292(31):12727–34. doi: 10.1074/jbc.R117.781823
12. Andreini C, Putignano V, Rosato A, Banci L. The Human Iron-Proteome. *Metallomics* (2018) 10(9):1223–31. doi: 10.1039/c8mt00146d
13. Markolovic S, Wilkins SE, Schofield CJ. Protein Hydroxylation Catalyzed by 2-Oxoglutarate-dependent Oxygenases. *J Biol Chem* (2015) 290(34):20712–22. doi: 10.1074/jbc.R115.662627
14. Poulos TL. Heme Enzyme Structure and Function. *Chem Rev* (2014) 114 (7):3919–62. doi: 10.1021/cr400415k
15. Johnson DC, Dean DR, Smith AD, Johnson MK. Structure, Function, and Formation of Biological Iron-Sulfur Clusters. *Annu Rev Biochem* (2005) 74:247–81. doi: 10.1146/annurev.biochem.74.082803.133518
16. UniProt Consortium. UniProt: A Worldwide Hub of Protein Knowledge. *Nucleic Acids Res* (2019) 47(D1):D506–d15. doi: 10.1093/nar/gky1049
17. Yates AD, Achuthan P, Akanni W, Allen J, Allen J, Alvarez-Jarreta J, et al. Ensembl 2020. *Nucleic Acids Res* (2020) 48(D1):D682–8. doi: 10.1093/nar/gkz966
18. Raudvere U, Kolberg L, Kuzmin I, Arak T, Adler P, Peterson H, et al. G: Profiler: A Web Server for Functional Enrichment Analysis and Conversions of Gene Lists (2019 Update). *Nucleic Acids Res* (2019) 47(W1):W191–8. doi: 10.1093/nar/gkz369
19. Yamanishi H, Iyama S, Yamaguchi Y, Kanakura Y, Iwatani Y. Total Iron-Binding Capacity Calculated From Serum Transferrin Concentration or Serum Iron Concentration and Unsaturated Iron-Binding Capacity. *Clin Chem* (2003) 49(1):175–8. doi: 10.1373/49.1.175
20. Chasteen ND, Williams J. The Influence of Ph on the Equilibrium Distribution of Iron Between the Metal-Binding Sites of Human Transferrin. *Biochem J* (1981) 193(3):717–27. doi: 10.1042/bj1930717
21. Aisen P, Leibman A, Zweier J. Stoichiometric and Site Characteristics of the Binding of Iron to Human Transferrin. *J Biol Chem* (1978) 253(6):1930–7. doi: 10.1016/S0021-9258(19)62337-9
22. Kelly AU, McSorley ST, Patel P, Talwar D. Interpreting Iron Studies. *Bmj* (2017) 357:j2513. doi: 10.1136/bmj.j2513
23. Young SP, Bomford A, Williams R. The Effect of the Iron Saturation of Transferrin on Its Binding and Uptake by Rabbit Reticulocytes. *Biochem J* (1984) 219(2):505–10. doi: 10.1042/bj2190505
24. Núñez MT, Núñez-Millacura C, Beltrán M, Tapia V, Alvarez-Hernandez X. Apotransferrin and Holotransferrin Undergo Different Endocytic Cycles in Intestinal Epithelia (Caco-2) Cells. *J Biol Chem* (1997) 272(31):19425–8. doi: 10.1074/jbc.272.31.19425
25. Mayle KM, Le AM, Kamei DT. The Intracellular Trafficking Pathway of Transferrin. *Biochim Biophys Acta* (2012) 1820(3):264–81. doi: 10.1016/j.bbagen.2011.09.009
26. Armitage AE, Lim PJ, Frost JN, Pasricha SR, Soilleux EJ, Evans E, et al. Induced Disruption of the Iron-Regulatory Hormone Hepcidin Inhibits Acute Inflammatory Hypoferraemia. *J Innate Immun* (2016) 8(5):517–28. doi: 10.1159/000447713
27. Stubbe J. Di-Iron-Tyrosyl Radical Ribonucleotide Reductases. *Curr Opin Chem Biol* (2003) 7(2):183–8. doi: 10.1016/S1367-5931(03)00025-5
28. Kolberg M, Strand KR, Graff P, Andersson KK. Structure, Function, and Mechanism of Ribonucleotide Reductases. *Biochim Biophys Acta* (2004) 1699 (1-2):1–34. doi: 10.1016/S1570-9639(04)00054-8
29. Hoffbrand AV, Ganeshaguru K, Hooton JW, Tattersall MH. Effect of Iron Deficiency and Desferrioxamine on DNA Synthesis in Human Cells. *Br J Haematol* (1976) 33(4):517–26. doi: 10.1111/j.1365-2141.1976.tb03570.x
30. Mariotti L, Wild S, Brunoldi G, Piceni A, Ceppi I, Kummer S, et al. The Iron-Sulphur Cluster in Human DNA2 Is Required for All Biochemical Activities of DNA2. *Commun Biol* (2020) 3(1):322. doi: 10.1038/s42003-020-1048-4
31. Dever TE, Gutierrez E, Shin B-S. The Hypusine-Containing Translation Factor Eif5a. *Crit Rev Biochem Mol Biol* (2014) 49(5):413–25. doi: 10.3109/10409238.2014.939608
32. Zhang H, Alsaleh G, Feltham J, Sun Y, Napolitano G, Riffelmacher T, et al. Polyamines Control Eif5a Hypusination, Tfeb Translation, and Autophagy to Reverse B Cell Senescence. *Mol Cell* (2019) 76(1):110–25.e9. doi: 10.1016/j.molcel.2019.08.005
33. Wu R, Chen X, Kang S, Wang T, Gnanaprakasam JNR, Yao Y, et al. De Novo Synthesis and Salvage Pathway Coordinately Regulate Polyamine Homeostasis and Determine T Cell Proliferation and Function. *Sci Adv* (2020) 6(51):eabc4275. doi: 10.1126/sciadv.abc4275
34. Gorres KL, Raines RT. Prolyl 4-Hydroxylase. *Crit Rev Biochem Mol Biol* (2010) 45(2):106–24. doi: 10.3109/10409231003627991
35. Paradkar PN, Zumbrennen KB, Paw BH, Ward DM, Kaplan J. Regulation of Mitochondrial Iron Import Through Differential Turnover of Mitoferrin 1 and Mitoferrin 2. *Mol Cell Biol* (2009) 29(4):1007. doi: 10.1128/MCB.01685-08
36. Shaw GC, Cope JJ, Li L, Corson K, Hersey C, Ackermann GE, et al. Mitoferrin Is Essential for Erythroid Iron Assimilation. *Nature* (2006) 440(7080):96–100. doi: 10.1038/nature04512
37. Wilkinson N, Pantopoulos K. The IRP/IRE System *In Vivo*: Insights From Mouse Models. *Front Pharmacol* (2014) 5:176. doi: 10.3389/fphar.2014.00176
38. Loenarz C, Schofield CJ. Physiological and Biochemical Aspects of Hydroxylations and Demethylations Catalyzed by Human 2-Oxoglutarate Oxygenases. *Trends Biochem Sci* (2011) 36(1):7–18. doi: 10.1016/j.tibs.2010.07.002
39. Cribbs AP, Terlecki-Zaniewicz S, Philpott M, Baardman J, Ahern D, Lindow M, et al. Histone H3K27me3 Demethylases Regulate Human Th17 Cell Development and Effector Functions by Impacting on Metabolism. *Proc Natl Acad Sci USA* (2020) 117(11):6056–66. doi: 10.1073/pnas.1919893117
40. Russ BE, Olshanksy M, Smallwood HS, Li J, Denton AE, Prier JE, et al. Distinct Epigenetic Signatures Delineate Transcriptional Programs During Virus-Specific CD8(+) T Cell Differentiation. *Immunity* (2014) 41(5):853–65. doi: 10.1016/j.immuni.2014.11.001
41. Dautry-Varsat A, Ciechanover A, Lodish HF. Ph and the Recycling of Transferrin During Receptor-Mediated Endocytosis. *Proc Natl Acad Sci USA* (1983) 80(8):2258–62. doi: 10.1073/pnas.80.8.2258
42. WHO. *Iron Deficiency Anaemia: Assessment, Prevention, and Control: A Guide for Programme Managers*. World Health Organization (2001).
43. Lopez A, Cacoub P, Macdougall IC, Peyrin-Biroulet L. Iron Deficiency Anaemia. *Lancet* (2016) 387(10021):907–16. doi: 10.1016/S0140-6736(15)60865-0
44. Nemeth E, Tuttle MS, Powelson J, Vaughn MB, Donovan A, Ward DM, et al. Hepcidin Regulates Cellular Iron Efflux by Binding to Ferroportin and Inducing Its Internalization. *Science* (2004) 306(5704):2090–3. doi: 10.1126/science.1104742
45. Muckenthaler MU, Rivella S, Hentze MW, Galy B. A Red Carpet for Iron Metabolism. *Cell* (2017) 168(3):344–61. doi: 10.1016/j.cell.2016.12.034
46. Li J, Hardy K, Olshansky M, Barugahare A, Gearing LJ, Prier JE, et al. KDM6B-Dependent Chromatin Remodeling Underpins Effective Virus-Specific CD8(+) T Cell Differentiation. *Cell Rep* (2021) 34(11):108839. doi: 10.1016/j.celrep.2021.108839
47. Konz T, Monnard C, Restrepo MR, Laval J, Sizzano F, Girotra M, et al. Multielemental Analysis of Low-Volume Samples Reveals Cancer-Specific Profile in Serum and Sorted Immune Cells. *Anal Chem* (2020) 92(13):8750–8. doi: 10.1021/acs.analchem.9b05643
48. Shah A, Frost JN, Aaron L, Donovan K, Drakesmith H, McKechnie SR, et al. Systemic Hypoferremia and Severity of Hypoxemic Respiratory Failure in COVID-19. *Crit Care* (2020) 24(1):320. doi: 10.1186/s13054-020-03051-w
49. Bolondi G, Russo E, Gamberini E, Circelli A, Meca MCC, Brogi E, et al. Iron Metabolism and Lymphocyte Characterisation During Covid-19 Infection in ICU Patients: An Observational Cohort Study. *World J Emerg Surg* (2020) 15 (1):41. doi: 10.1186/s13017-020-00323-2
50. Bellmann-Weiler R, Lanser L, Barket R, Rangger L, Schapfl A, Schaber M, et al. Prevalence and Predictive Value of Anemia and Dysregulated Iron Homeostasis in Patients With COVID-19 Infection. *J Clin Med* (2020) 9(8):1–11. doi: 10.3390/jcm9082429
51. Hippchen T, Altamura S, Muckenthaler MU, Merle U. Hypoferremia Is Associated With Increased Hospitalization and Oxygen Demand in COVID-19 Patients. *Hemasphere* (2020) 4(6):e492. doi: 10.1097/HS9.0000000000000492
52. Brandtner A, Tymoszuk P, Nairz M, Lehner GF, Fritsche G, Vales A, et al. Linkage of Alterations in Systemic Iron Homeostasis to Patients' Outcome in

Sepsis: A Prospective Study. *J Intensive Care* (2020) 8(1):76. doi: 10.1186/s40560-020-00495-8
53. Pfeifhofer-Obermair C, Tymoszuk P, Nairz M, Schroll A, Klais G, Demetz E, et al. Regulation of Th1 T Cell Differentiation by Iron *Via* Upregulation of T Cell Immunoglobulin and Mucin Containing Protein-3 (Tim-3). *Front Immunol* (1856) 2021:12. doi: 10.3389/fimmu.2021.637809
54. Fischbach FA, Anderegg JW. An X-Ray Scattering Study of Ferritin and Apoferritin. *J Mol Biol* (1965) 14(2):458–73. doi: 10.1016/S0022-2836(65)80196-6

Conflict of Interest: The authors declare that the research was conducted in the absence of any commercial or financial relationships that could be construed as a potential conflict of interest.

Publisher's Note: All claims expressed in this article are solely those of the authors and do not necessarily represent those of their affiliated organizations, or those of the publisher, the editors and the reviewers. Any product that may be evaluated in this article, or claim that may be made by its manufacturer, is not guaranteed or endorsed by the publisher.